

Analysis of microtubule-severing enzymes in the nervous system of *Mus musculus* (Linnaeus, 1758)

Dissertation
zur Erlangung der Würde des Doktors der Naturwissenschaften
des Fachbereichs Biologie der Fakultät für Mathematik, Informatik und
Naturwissenschaften der Universität Hamburg

vorgelegt von

Laura Ruschkies
aus Klaipėda

Hamburg, 2018

1st reviewer: Prof. Dr. Matthias Kneussel
2nd reviewer: Prof. Dr. Christian Lohr

Day of oral defense: 27 May 2019

TABLE OF CONTENTS

| | | |
|----------|--|-----------|
| 1 | ABSTRACT | 1 |
| 2 | INTRODUCTION | 2 |
| 2.1 | THE MAMMALIAN NERVOUS SYSTEM | 2 |
| 2.1.1 | <i>Neurons</i> | 2 |
| 2.1.2 | <i>Synaptic plasticity, learning and memory</i> | 4 |
| 2.2 | THE MICROTUBULE CYTOSKELETON | 9 |
| 2.2.1 | <i>Intrinsic properties of microtubules</i> | 10 |
| 2.2.2 | <i>Cellular functions of microtubules</i> | 10 |
| 2.2.3 | <i>Extrinsic regulators of the microtubule cytoskeleton</i> | 13 |
| 2.3 | MICROTUBULE-SEVERING ENZYMES | 16 |
| 2.3.1 | <i>AAA ATPases</i> | 16 |
| 2.3.2 | <i>Spastin</i> | 17 |
| 2.3.3 | <i>Katanin</i> | 20 |
| 2.3.4 | <i>Fidgetin</i> | 21 |
| 2.3.5 | <i>Mechanism and regulation of microtubule-severing</i> | 21 |
| 2.3.6 | <i>Physiological functions of microtubule-severing enzymes</i> | 23 |
| 2.4 | GENE TARGETING | 29 |
| 2.4.1 | <i>Model organisms</i> | 29 |
| 2.4.2 | <i>Mouse mutagenesis</i> | 30 |
| 2.4.3 | <i>Homologous recombination</i> | 30 |
| 2.4.4 | <i>Conditional mutagenesis</i> | 30 |
| 2.4.5 | <i>Spatiotemporal control of Cre and FLP recombinases</i> | 31 |
| 2.4.6 | <i>Genome engineering: new approaches in mutagenesis</i> | 32 |
| 2.5 | AIM OF THIS STUDY | 33 |
| 3 | MATERIAL AND METHODS | 34 |
| 3.1 | MATERIAL | 34 |
| 3.1.1 | <i>Chemicals</i> | 34 |
| 3.1.2 | <i>Enzymes</i> | 34 |
| 3.1.3 | <i>Other Material</i> | 34 |
| 3.1.4 | <i>Software</i> | 34 |
| 3.1.5 | <i>Kits</i> | 35 |
| 3.1.6 | <i>Molecular weight markers</i> | 35 |
| 3.1.7 | <i>Antibodies</i> | 36 |
| 3.1.8 | <i>Vectors and constructs</i> | 37 |
| 3.1.9 | <i>Bacterial strains</i> | 37 |
| 3.1.10 | <i>Cell lines</i> | 37 |
| 3.1.11 | <i>Buffers and media</i> | 38 |

| | | |
|--------|--|----|
| 3.1.12 | <i>Machines</i> | 40 |
| 3.1.13 | <i>Oligonucleotides</i> | 42 |
| 3.2 | CELL BIOLOGY | 42 |
| 3.2.1 | <i>Primary hippocampal cell culture</i> | 42 |
| 3.2.2 | <i>HEK293-TN-cell culture</i> | 43 |
| 3.2.3 | <i>Immunocytochemistry</i> | 43 |
| 3.2.4 | <i>Immunohistochemistry</i> | 43 |
| 3.2.5 | <i>Transfection HEK 293TN-cells</i> | 44 |
| 3.2.6 | <i>Transfection of neurons</i> | 44 |
| 3.2.7 | <i>LacZ staining</i> | 44 |
| 3.2.8 | <i>Nissl staining</i> | 45 |
| 3.2.9 | <i>Confocal laser scanning microscopy</i> | 45 |
| 3.2.10 | <i>Live cell imaging</i> | 46 |
| 3.2.11 | <i>Electron microscopy</i> | 46 |
| 3.3 | MOLECULAR BIOLOGY | 46 |
| 3.3.1 | <i>Polymerase chain reaction</i> | 46 |
| 3.3.2 | <i>Genotyping of mouse-tail-tip biopsies</i> | 47 |
| 3.3.3 | <i>Cloning of DNA fragments</i> | 48 |
| 3.3.4 | <i>Isolation of plasmid-DNA from bacteria</i> | 48 |
| 3.3.5 | <i>Determination of DNA-concentration and purity</i> | 48 |
| 3.3.6 | <i>Restriction digestion</i> | 49 |
| 3.3.7 | <i>Dephosphorylation of DNA fragments</i> | 49 |
| 3.3.8 | <i>Phosphorylation of DNA fragments</i> | 49 |
| 3.3.9 | <i>Agarose gel electrophoresis</i> | 49 |
| 3.3.10 | <i>Purification of DNA fragments from agarose gels</i> | 50 |
| 3.3.11 | <i>Ligation of DNA fragments</i> | 50 |
| 3.3.12 | <i>Transformation of chemically competent E. coli strains</i> | 50 |
| 3.3.13 | <i>Colony-PCR</i> | 50 |
| 3.3.14 | <i>Sequencing of DNA</i> | 51 |
| 3.3.15 | <i>Ethanol precipitation of DNA</i> | 51 |
| 3.3.16 | <i>Quantitative linearization of the targeting vector for spastin</i> | 51 |
| 3.3.17 | <i>Phenol/chloroform extraction of DNA</i> | 51 |
| 3.3.18 | <i>Electroporation of mouse embryonic stem cells</i> | 52 |
| 3.3.19 | <i>Generation of radiolabeled probes for Southern Blotting</i> | 52 |
| 3.3.20 | <i>Southern Blotting (alkaline method)</i> | 53 |
| 3.3.21 | <i>Long-range-PCR</i> | 54 |
| 3.4 | BIOCHEMISTRY | 54 |
| 3.4.1 | <i>Protein extraction from HEK293-TN (or neuronal cell) lysates</i> | 54 |
| 3.4.2 | <i>Preparation of cellular fractions from brain lysates by differential centrifugation</i> | 55 |

| | | |
|----------|---|-----------|
| 3.4.3 | <i>Preparation of synaptosomal fractions</i> | 56 |
| 3.4.4 | <i>Co-immunoprecipitation</i> | 56 |
| 3.4.5 | <i>Determination of protein concentration (BCA Assay)</i> | 57 |
| 3.4.6 | <i>SDS-PAGE</i> | 57 |
| 3.4.7 | <i>Western Blotting</i> | 58 |
| 3.5 | BEHAVIOR ANALYSIS | 59 |
| 3.5.1 | <i>Experimental animals and housing conditions</i> | 59 |
| 3.5.2 | <i>Exploration and anxiety behavior</i> | 59 |
| 3.5.3 | <i>Learning and memory</i> | 60 |
| 3.6 | QUANTIFICATION AND STATISTICS..... | 61 |
| 4 | RESULTS | 62 |
| 4.1 | GENE TARGETING AND BREEDING STRATEGIES..... | 62 |
| 4.1.1 | <i>Knockout-first-allele targeting strategy</i> | 62 |
| 4.1.2 | <i>Breeding strategy for katanin and spastin knockout mouse lines</i> | 63 |
| 4.1.3 | <i>Forebrain-specific Cre-driver lines</i> | 63 |
| 4.2 | SPASTIN..... | 66 |
| 4.2.1 | <i>Spastin targeting strategy and confirmation</i> | 66 |
| 4.2.2 | <i>General health of spastin depleted animals & reproduction</i> | 71 |
| 4.2.3 | <i>Spastin expression pattern</i> | 75 |
| 4.2.4 | <i>Gross brain morphology of spastin KO-1st mice</i> | 78 |
| 4.2.5 | <i>Microtubule modifications and AMPAR distribution in the hippocampus of spastin KO mice</i> | 79 |
| 4.2.6 | <i>EB3 dynamics in dendritic spines of spastin knockout mice</i> | 81 |
| 4.3 | KATANIN | 82 |
| 4.3.1 | <i>Katanin targeting strategy and confirmation</i> | 82 |
| 4.3.2 | <i>General health of katanin depleted animals & reproduction</i> | 87 |
| 4.3.3 | <i>Katanin expression pattern</i> | 89 |
| 4.3.3.1 | <i>Endogenous katanin promoter activity</i> | 89 |
| 4.3.3.2 | <i>Subcellular location of ectopically expressed katanin</i> | 90 |
| 4.3.4 | <i>Gross brain morphology of katanin knockout mice</i> | 91 |
| 4.3.4.1 | <i>Nissl staining of conditional katanin knockout using the Nestin-Cre promoter</i> | 91 |
| 4.3.5 | <i>Behavioral phenotyping of forebrain-specific katanin knockout mice</i> | 92 |
| 4.3.5.1 | <i>Exploration and anxiety behavior</i> | 93 |
| 4.3.5.2 | <i>Learning and memory</i> | 95 |
| 5 | DISCUSSION | 98 |
| 5.1 | GENERATION OF SPASTIN AND KATANIN KNOCKOUTS | 98 |
| 5.1.1 | <i>Spastin</i> | 98 |
| 5.1.1.1 | <i>The pEGFP-ΔM1-spastin construct and 6C6 anti spastin antibodies</i> | 99 |
| 5.1.2 | <i>Katanin</i> | 100 |

| | | |
|----------|--|------------|
| 5.1.3 | <i>Targeting and breeding strategy</i> | 102 |
| 5.1.4 | <i>Usage of conditional Cre-driver lines</i> | 103 |
| 5.2 | EXPRESSION ANALYSIS OF SPASTIN AND KATANIN IN MICE..... | 104 |
| 5.2.1 | <i>Expression analysis of spastin and katanin using gene-trap reporter alleles</i> | 104 |
| 5.2.2 | <i>Expression analysis of spastin and katanin in wild type mice</i> | 105 |
| 5.2.3 | <i>Subcellular expression analysis of spastin and katanin</i> | 106 |
| 5.3 | GENERAL HEALTH OF SPASTIN DEPLETED ANIMALS..... | 106 |
| 5.3.1 | <i>Reduced body weight of spastin KO mice</i> | 106 |
| 5.3.2 | <i>Altered gait parameters in spastin KO mice</i> | 107 |
| 5.3.3 | <i>Sterility of homozygous spastin knockouts</i> | 108 |
| 5.4 | GENERAL HEALTH OF KATANIN DEPLETED ANIMALS..... | 109 |
| 5.4.1 | <i>Embryonic lethality of homozygous katanin knockout mice</i> | 109 |
| 5.4.2 | <i>Reduced body weight of Nestin-Cre conditional katanin knockouts</i> | 110 |
| 5.5 | HIPPOCAMPAL CA1 CELL LOSS IN SPASTIN KO MICE | 110 |
| 5.6 | MICROTUBULE-SEVERING AND EB3 DYNAMICS..... | 112 |
| 5.7 | BEHAVIOR CHARACTERIZATION OF FOREBRAIN-SPECIFIC KATANIN KNOCKOUTS..... | 113 |
| 5.7.1 | <i>Choice of the control group for behavioral analyses</i> | 114 |
| 5.8 | CONCLUSION AND OUTLOOK..... | 115 |
| 6 | REFERENCES | 118 |
| 7 | APPENDIX | 141 |
| 7.1 | ABBREVIATIONS..... | 141 |
| 7.2 | FIGURES | 142 |
| 7.3 | TABLES..... | 145 |
| 7.4 | SUPPLIERS..... | 146 |
| 7.5 | SEQUENCES..... | 148 |
| 7.5.1 | <i>Katna1 p60 amino acid sequence</i> | 148 |
| 7.5.2 | <i>Spastin amino acid sequence</i> | 149 |
| 7.5.3 | <i>Sequence of the 5' southern probe for spastin</i> | 150 |
| 7.6 | ACKNOWLEDGEMENTS | 151 |
| 7.7 | CURRICULUM VITAE..... | 152 |
| 7.8 | PUBLICATIONS..... | 152 |
| 7.9 | STATEMENT OF CONTRIBUTION..... | 152 |
| 7.10 | ERKLÄRUNG..... | 153 |

1 ABSTRACT

Microtubules are dynamic, polymeric structures of the eukaryotic cytoskeleton with diverse physiological functions. In recent years there has been increasing evidence of their essential role in the synaptic plasticity of the nervous system. Severing by microtubule-severing enzymes is a mechanism to cleave microtubules internally, thus contributing to their dynamics. However, the contribution of severing to synaptic plasticity is still mainly hypothetical, which is also due to the lack of suitable *in vivo* models.

In the present work general and conditional "loss-of-function" mutants of the genes for the two microtubule-cutting enzymes spastin and katanin were generated in the mouse model. Using homologous recombination and by applying the "knockout-first" strategy, critical exons were flanked by loxP sites, so that by using Cre-recombinase a frameshift could arise.

Using the gene-trap LacZ reporter in heterozygous knockout animals, the endogenous expression of the two genes spastin and katanin has been studied during the development of the mouse in different tissues. A strikingly weak promoter activity was observed for both genes, which further decreased with increasing age. The expression of the two genes was also analyzed by Western blotting in different tissues.

For spastin, both brain-specific, as well as general knockouts could be produced. A general homozygous katanin knockout was embryonic lethal and only a conditional knockout could be achieved with the use of a tissue-specific promoter in the brain.

An initial characterization of the general mutants for spastin showed evidence of a potential role of the gene in the CA1 region of the hippocampus. Furthermore, the animals displayed a reduced body weight, an impaired motor function and were sterile. In the first instance, no affectation of microtubule spine entry could be observed using EB3 live-cell imaging in cultured hippocampal neurons.

Using the CamKII α promoter, postnatal and forebrain-specific katanin knockouts could be generated and initially analyzed biochemically, and in the biology of behavior. Here, a possible role for katanin on long-term memory was found.

2 INTRODUCTION

2.1 The mammalian nervous system

The appearance of nervous tissue opened a new ecological niche, which enabled organisms to perceive and to respond to external and internal stimuli with appropriate behavior. With exception of sponges, placozoans and mesozoans, nervous systems are a hallmark of multicellular animals. Nervous systems vary strongly in complexity and size, ranging from diffuse net-like structures of a few hundreds cells in simple organisms to highly organized systems exceeding 100 billion cells in some mammals. At the fundamental level, the nervous system connects one part of the body to others by sending signals from one cell to others (Kandel, Schwartz et al. 2000).

In mammals and most other organisms, the nervous system comprises two main parts, the central nervous system (CNS) and the peripheral nervous system (PNS). The CNS can be considered as the main control center and includes the brain and the spinal cord. It processes the sensory input from the environment through its afferent pathways, and sends executive commands through its efferents, thereby coordinating the voluntary and involuntary actions of an animal. The PNS consists mainly of nerves, which connect the CNS to other parts of the body (Kandel, Schwartz et al. 2000).

Being a highly complex organ, the nervous system is susceptible to malfunction as a result of genetic defects, physical damage, infection, or aging. Thus, the study of nervous systems is of high relevance and beneficial to cure and prevent disease.

2.1.1 Neurons

The major cell types in the CNS are neurons and the numerically superior glial cells. Besides their supportive function to neurons, the latter ones seem to fulfill a growing number of physiological functions such as neuronal guidance during development, the regulation of synaptic neurotransmitter release and active modulation of synaptic strength in a composition that has been termed “tripartite synapse” (Araque, Parpura et al. 1999). Nevertheless, the main part of the information transfer in the nervous system is realised by neurons.

Being connected to each other, neurons form networks consisting of three specialized main types. Information from sensory receptors in the body is collected by afferent sensory neurons and transmitted to the brain. Interneurons interpret the information from sensory neurons and communicate it to motor neurons. Efferent motor neurons innervate muscles and enable the body to react to intrinsic or extrinsic stimuli.

Morphologically, neurons can be subdivided into three major compartments with highly specialized functions (Figure 1). Multiple branched dendrites of hundreds of micrometers in length form the dendritic tree, which is responsible for the signal detection originating from other cells.

The incoming signals are further passed on to the cell soma, where all information originating from different dendrites is collected and subsequently integrated and processed at the axon hillock. The axon extends from the latter one for distances of up to 1 m in humans or even longer in other species. Its task is to transmit electrical or chemical information from a neuron's cell interior to other cells through intercellular connections called synapses. One neuron is thought to form around 1,000 to 10,000 of these connections with other neurons (Herculano-Houzel 2012).

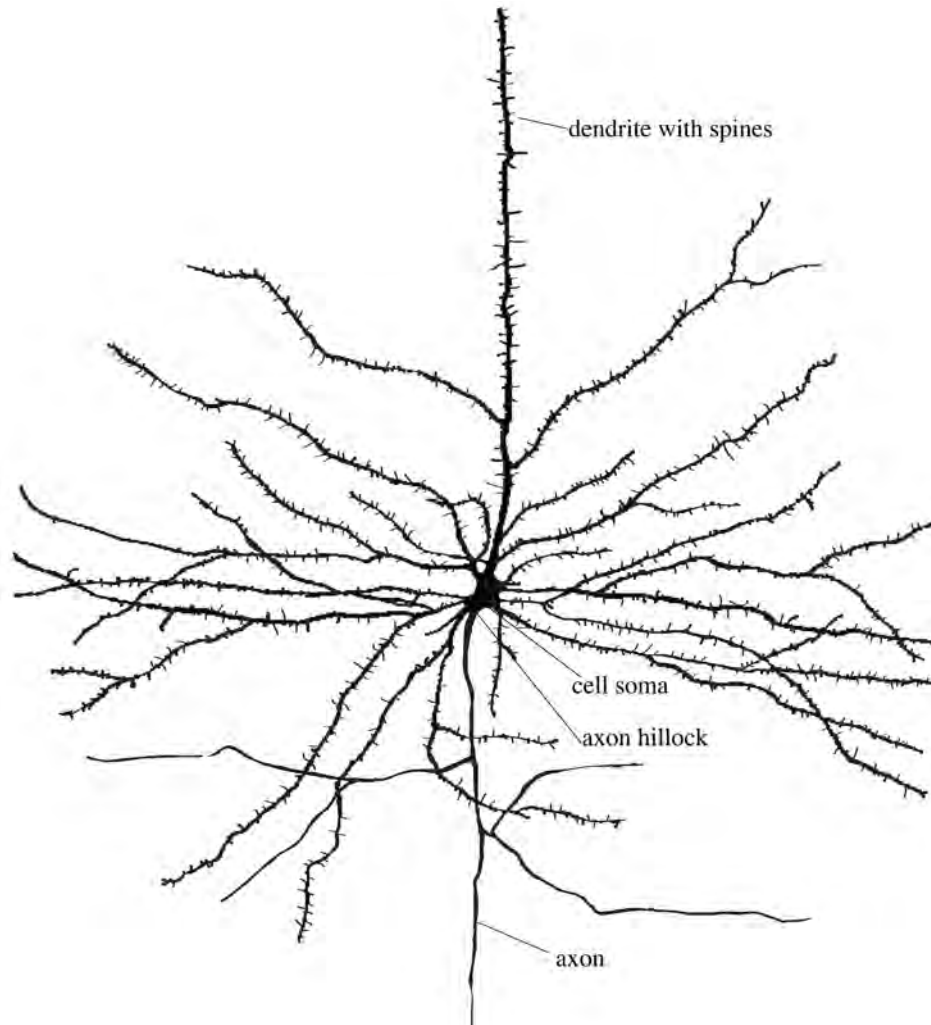


Figure 1: Model of a neuron. Several dendrites and one axon arise from the cell soma. While the dendrites can have spines and form a branched network, the axon is spineless and can reach greater lengths. After signals are received at dendritic sites or at the cell soma, the intracellular information is integrated at the axon hillock, which extends from the cell body and subsequently transferred onto target cells by the axon. The picture was modified after a drawing from Santiago Felipe Ramón y Cajal (1852-1934).

The maintenance of this polarized neuronal subcompartmentalization is a key requirement for the successful transmission of information.

The unique ability of neurons to receive and to propagate information is due to their electrical excitability. The latter one is due to the characteristic membrane properties of a neuron allowing it to switch from a resting to an action potential condition.

Under resting conditions, a neuron's ion composition between the intracellular and the extracellular fluids differs. As a consequence of the presence of intracellular proteins, there is a

differential distribution of sodium (Na^+), potassium (K^+), chloride (Cl^-), and calcium (Ca^{2+}) ions at both sides of the plasma membrane. In addition, differential permeabilities across the neuronal plasma membrane mainly caused by selective ion channels and ion pumps lead to an excess of negative charges intracellularly and positive charges extracellularly, leading to a negative resting membrane potential of approximately -70 mV (Storm 1987, Staff, Jung et al. 2000).

In response to an external or internal signal/stimulus and neuronal activation at synaptic sites, the opening of ion channels mainly allows the entrance of positively charged ions into the postsynaptic cell and leads to local depolarization of its membrane. Signals from several synaptic sites can be propagated to and integrated at the cell soma. In case a threshold depolarization is reached at the axon hillock, an action potential with peak depolarization values of +50 mV will be generated (Armstrong and Hille 1998).

Because the axonal membrane comprises differently regulated ion channels and pumps, the directionality of an action potential is predetermined. The action potential propagates down the axon in an all-or-nothing fashion, leading to a rapid and transient change in polarity across the membrane. At the axon terminal, the action potential usually provokes the release of neurotransmitters from presynaptic vesicles, which can modify the potential and activity of postsynaptic neurons. Repolarization occurs when positive ion exit outbalances their entry into the cell and the resting potential is reached again.

Examples for channels and receptors mainly responsible for neurotransmitter detection and ion conductance across the postsynaptic plasma membrane include receptors for the neurotransmitters glutamate, GABA (gamma amino butyric acid), acetylcholine, glycine, serotonin, dopamine, epinephrine or histamine.

2.1.2 Synaptic plasticity, learning and memory

One of the fascinating properties of nervous systems is their capability to enable the organism not only to react to current stimuli, but also to recall previous experiences and, using this information, to predict future events and to behave accordingly. On the other hand, irrelevant information and memories have to be filtered out in order to permit the organism to adapt to changing environmental circumstances. While some memories last for a lifetime, others vanish after short periods.

Theoretically, the plasticity of nervous systems can be explained by several mechanisms: The genesis of new neurons (Lledo and Gheusi 2006), the formation of new neuronal circuits and connections also known as rewiring (Holtmaat and Svoboda 2009) or the strengthening or weakening of already existing synaptic contacts (Yuste and Bonhoeffer 2001). Since neurogenesis is mainly limited to very young brains and few postnatal brain regions, and the formation of neuronal circuits predominates during early development, synapses and their plasticity are assumed to be fundamental for complex neuronal functions such as learning and

memory formation (Bliss and Collingridge 1993, Hyman and Malenka 2001, Malenka and Bear 2004, Whitlock, Heynen et al. 2006, Mayford, Siegelbaum et al. 2012).

Synapses form by the connection of an axonal terminus from one cell, called the presynapse and a postsynaptic contact region originating from another cell.

The morphology, size and type of synapses vary strongly. A major distinction is made between electrical and chemical synapses (Kandel, Schwartz et al. 2000). The characteristic of electrical synapses is a direct connection of two neurons via gap junctions made up of connexins. Six of the latter ones form a pore allowing fast and direct transfer of the signal (< 0.1 ms). In the case of chemical synapses (see Figure 2), the presynaptic axon terminus of an activated neuron releases neurotransmitters (e. g. glutamate or glycine) from neurotransmitter vesicles into the synaptic cleft. After binding to their corresponding receptors at the postsynaptic membrane, the neurotransmitters lead to an altered ion conductance and a change in postsynaptic membrane potential.

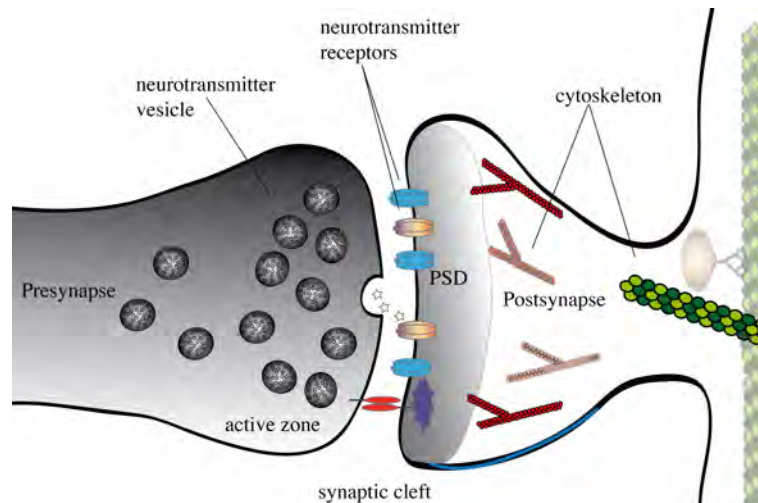


Figure 2: Schematic representation of an excitatory chemical synapse. The presynaptic axon bouton is separated from the postsynaptic membrane by the synaptic cleft, which contains the extracellular matrix and the extracellular domains of adhesion proteins. An action potential in the presynaptic neuron results in the fusion of neurotransmitter-containing vesicles with the presynaptic membrane and the release of their content into the synaptic cleft. The neurotransmitters bind to their corresponding receptors at the postsynaptic membrane. The opening of ion channels leads to an altered postsynaptic potential. The presynaptic active zone, that is rich in neurotransmitter-containing vesicles and the postsynaptic density (PSD), rich in postsynaptic scaffolding molecules, as well as the cytoskeleton (actin in red and microtubules in green) are indicated.

A postsynaptic neuron's reaction to a presynaptic stimulus can differ depending on previous experience, a phenomenon known as synaptic plasticity (Kandel, Schwartz et al. 2000, Citri and Malenka 2008). Dependent on the duration, strength and timing of the stimulus, the synaptic contact and transmission can either be strengthened (potentiated) or weakened (depressed) in size and efficacy.

Very strong presynaptic stimuli lead to strong postsynaptic responses. In case of induction of long-term potentiation (LTP), following weaker stimuli will still evoke increased postsynaptic responses similar to those induced by the initial strong stimulus (Bliss and Gardner-Medwin 1973,

Bliss and Lomo 1973). In contrast to that, weak presynaptic stimulation changes the postsynaptic neuron's potential only weakly, resulting in the induction of long-term depression (LTD) and the weakening of synaptic contacts in size and efficacy (Stent 1973).

On the morphological level, LTP and LTD are accompanied by changes in size, shape and amount of synapses and spines (Lee, Schottler et al. 1980, Chang and Greenough 1984, Alvarez and Sabatini 2007, Feldman 2009). On the structural level, synaptic plasticity also involves changes in the physiology of the pre- and postsynapse including protein composition and their activation status.

At excitatory synapses, postsynaptic scaffold proteins such as post-synaptic-density 95 (PSD-95) anchor and regulate glutamate receptors, which are mainly responsible for synaptic transmission. Under basal conditions, the glutamate receptors, which can be activated by its selective agonist AMPA (α -amino-3-hydroxy-5-methyl-4-isoxazolepropionic acid), are constantly exchanged at the postsynaptic membrane. Depending on their activation status, the AMPA-receptors (AMPA receptors or GRIAs) are removed from the postsynaptic membrane and can either be sorted into recycling endosomes for reinsertion into the plasma membrane or into late endosomes for lysosomal degradation (Derkach, Oh et al. 2007, Citri and Malenka 2008).

After neurotransmitter binding, the AMPAR pore opens, leading to the flow of monovalent cations (mainly sodium and potassium), ultimately enabling the depolarization of a neuron (Figure 3a).

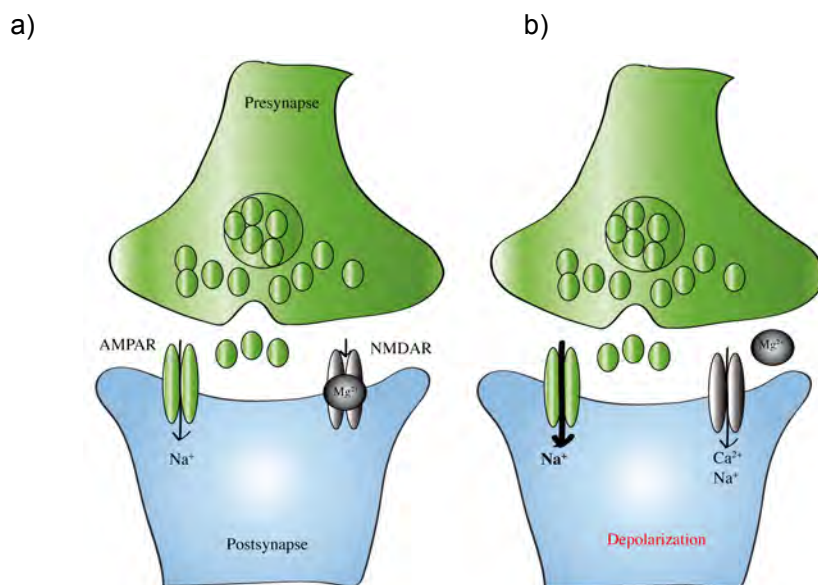


Figure 3: Magnesium blockade of the NMDA receptor. a) A weak stimulation of the postsynapse via AMPA receptors (green) is not sufficient to activate NMDA receptors (grey). b) In contrast, a strong presynaptic stimulus leads to a strong Na⁺-influx (arrow) and depolarization of the postsynapse. The voltage-dependent abrogation of a pore-blocking Mg²⁺ cation is followed by additional influx of Na⁺ and Ca²⁺ ions into the postsynapse. The figure was modified from Citri and Malenka 2008.

To induce both LTP and LTD, the intracellular concentration of Ca^{2+} -ions in the dendrite in addition to neuronal depolarization is critical (Lynch, Larson et al. 1983, Malenka 1991, Malenka, Lancaster et al. 1992, Malenka and Nicoll 1993). In contrast to AMPARs, the glutamate receptor channels of NMDA-type (which can be activated by the selective agonist N-methyl-D-aspartate) allow Ca^{2+} as well as Na^+ ions to enter the postsynaptic spine. Their inhibition using the selective NMDA-receptor antagonist APV ((2R)-amino-5-phosphonovaleric acid; (2R)-amino-5-phosphonopentanoate) blocks the induction of both LTP and LTD (Malenka and Bear 2004). Because the binding of glutamate alone is not sufficient to open their channel, the NMDA-receptors are also called coincidence detectors. Only when the simultaneous AMPAR-mediated depolarization of the neuron is strong enough, a pore-blocking magnesium-ion from the NMDA receptor is abrogated and enables Ca^{2+} conductance (see Figure 3b) (Mayer, Westbrook et al. 1984, Nowak, Bregestovski et al. 1984).

Intracellularly, Ca^{2+} is a key regulator of downstream targets and effectors, such as CamKII (Ca^{2+} /calmodulin-dependent protein kinase II), PKA, PKC and PKM ζ (protein kinases A, C and M ζ , respectively), Src and MAPK (mitogen activated protein kinase), which themselves regulate the course of LTP or LTD (reviewed by Citri and Malenka 2008).

One possibility of regulation is given at the posttranslational level by activity-dependent kinases (such as CamKII, PKA or PKC) and phosphatases (such as the protein phosphatase PP1 or calcineurin), that regulate a receptor's phosphorylation status at specific sites, leading to modulated receptor density, conductance, stability and location (Lee, Barbarosie et al. 2000, Soderling and Derkach 2000, Derkach, Oh et al. 2007, Citri and Malenka 2008).

When LTP is induced initially, the reinsertion of AMPA receptors from recycling pools outbalances the removal and lysosomal degradation, resulting in increased receptor density at extrasynaptic sites. The subsequent lateral diffusion leads to their anchoring into the post-synaptic density (Derkach, Oh et al. 2007), followed by stronger synaptic transmission (see Figure 4).

In order to establish and maintain long-lasting changes in synaptic structure and strength, several other processes such as gene expression, local dendritic protein synthesis and targeted protein transport and the composition of the post synaptic density have to be modulated (Reymann and Frey 2007, Citri and Malenka 2008). In fact, both LTP and long-term memory formation are impaired when protein translation is inhibited (Squire and Barondes 1972, Krug, Lossner et al. 1984, Stanton and Sarvey 1984, Deadwyler, Dunwiddie et al. 1987, Karachot, Shirai et al. 2001).

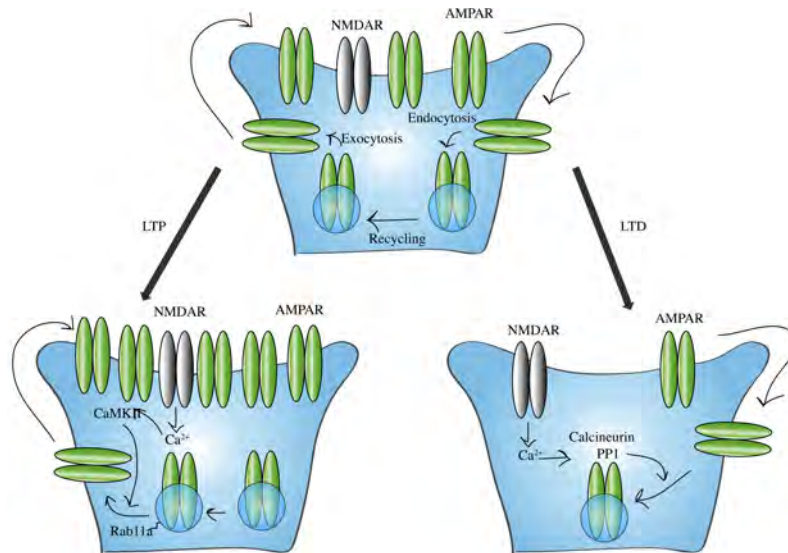


Figure 4: Synaptic plasticity is NMDA-receptor dependent. Under basal conditions, AMPA receptors are constantly removed from and inserted to perisynaptic sites by endo- and exocytosis. Strong depolarization and voltage dependent activation of NMDA receptors leads to strong Ca^{2+} influx followed by net exocytosis of AMPA receptors at perisynaptic sites via CamKII dependent activation of the small GTPase Rab11a. Subsequent lateral diffusion to synaptic sites leads to stronger synaptic transmission (LTP). Weak activation of the NMDA receptor leads to low Ca^{2+} influx and results in the net endocytosis of AMPA receptors via the activation of the phosphatases calcineurin and PP1. In this case, the synaptic transmission is weakened (LTD). The figure was modified after Citri and Malenka 2008.

Although synaptic plasticity has been described in several brain regions (hippocampus, amygdala, cortex, cerebellum), the most studied form of LTP is the NMDA-receptor dependent form at the synapses of the Schaffer collaterals and pyramidal neurons in the CA1 (cornu ammonis 1) region of the hippocampus. The hippocampus is a brain structure in the medial temporal lobe and resembles a seahorse. It has been demonstrated to have a critical role in memory formation since the observation of severe amnesia after temporal lobe resection in patient M. H. (Scoville and Milner 1957) and by the observation of severe learning deficits in humans with damages to this region (Milner and Taylor 1970, Zola-Morgan, Squire et al. 1986, Cipolotti, Shallice et al. 2001). To date, the hippocampus has been shown to play important roles in several types of memory, like cognitive mapping, declarative memory, explicit memory, recollection, and relational memory (Konkel and Cohen 2009). The hippocampus is composed of the DG (dentate gyrus), the CA1-3 regions and the subiculum. The so-called hippocampal formation additionally includes the perirhinal and entorhinal cortices and is thought to process information in the so-called trisynaptic pathway (see Figure 5).

Granule cell dendrites in the dentate gyrus receive information input from layer II of the entorhinal cortex via the so-called perforant path and send it to the pyramidal neurons of the CA3 region via mossy fiber axon bundles. The axons originating from the CA3 region project into the CA1 pyramidal neuron dendritic field from where the information leaves the hippocampus and is passed on to the layer V of the entorhinal cortex (Amaral and Witter 1989, Yeckel and Berger 1990).

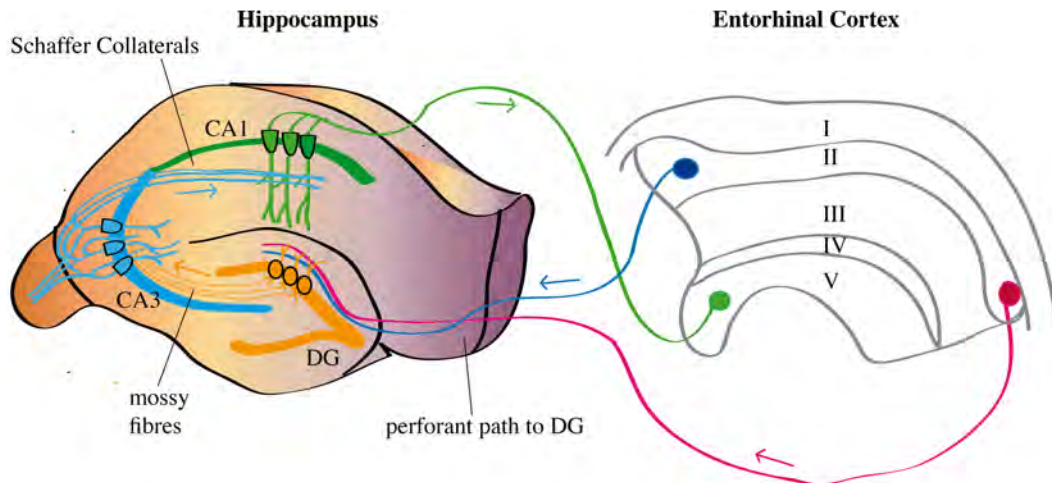


Figure 5: Schematic representation of the information flow in the hippocampal formation. The main information flow of the trisynaptic loop is depicted by arrows. Information from the layer II in the entorhinal cortex is passed to the dentate gyrus via the perforant path. From there information is passed on to the CA3 region via the mossy fibres and to the CA1 via Schaffer collaterals. The information then flows back into the layer V of the entorhinal cortex. CA: cornu ammonis. Modified from (Neves, Cooke et al. 2008).

Experimentally, the phenomena of LTP and LTD can be induced by applying electrical stimulation protocols of different strength and frequency or by using chemical stimulation of acute or cultured brain slices or neurons. A widely used technique is the repetitive, high frequency stimulation of the Schaffer collateral projections from CA3 to CA1 followed by recordings from the CA1 region.

2.2 The microtubule cytoskeleton

As it becomes evident from sections 4.1.1 and 4.1.2, the nervous system requires structures that confer stability to the complex neuronal morphology on the one hand and flexibility to enable synaptic plasticity on the other hand. This challenging task has to be fulfilled by the neuronal cytoskeleton. The polymeric cytoskeletal scaffolding molecules are major organizers of the cell interior, which are subcategorized into microfilaments (or actin filaments), intermediary filaments and the microtubules (MTs) (Berg, Tymoczko et al. 2006).

Neurofilaments and vimentins are examples for neuronal intermediary filaments. They build rope-like polymers of about 10 nm in diameter, which seem to be mainly important for the stabilization of the neuronal shape (Ishikawa, Bischoff et al. 1968, Perrot, Berges et al. 2008).

The microfilaments are the cytoskeletal polymers with the smallest diameter of roughly 8 nm, with actin as their building unit. Their major role in neurons lies in the mantling and regulation of dynamic structures such as dendritic spines and neurite tips, thus determining their morphology and function (Matus 2000, Dent and Gertler 2003, Tada and Sheng 2006, Cingolani and Goda 2008).

The MTs' main role is thought to serve as railways for cargo delivery. There is an increasing body of evidence that in addition to actin, dynamic microtubules might play an important regulatory role in dendritic spine plasticity (Penzes, Srivastava et al. 2009, Hoogenraad and Akhmanova 2010), thus the following section will focus on MT properties and their functions in neurons.

2.2.1 Intrinsic properties of microtubules

The smallest building units of the microtubules, the α - and β -tubulins, are globular GTPases with a molecular mass of about 50 kDa and an amino acid identity of approximately 50 % (Burns 1991, Desai and Mitchison 1997, Nogales 2001). After folding, α - and β -tubulins heterodimerize noncovalently and can then undergo a head-to-tail oligomerization into protofilaments (Nogales, Wolf et al. 1998). 13 of the latter ones then form a tubulus by lateral assembly, in which the neighboring protomers are shifted lengthwise by approximately 0.9 nm leaving the individual heterodimers in a helical composition around the central axis. The hollow cylinders (see Figure 6) formed have an outer diameter of about 25 nm (Westermann and Weber 2003).

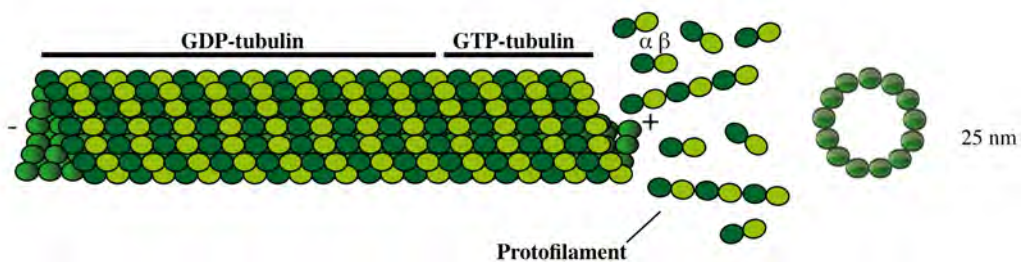


Figure 6: Schematic representation of microtubules. The smallest building blocks of MTs are the $\alpha\beta$ -tubulin heterodimers, which form a hollow cylindrical tubulus with a diameter of approximately 25 nm. The microtubule grows from the GDP-rich minus-end (-) by the addition of new protomers or heterodimers at the GTP-rich plus-end (+).

The addition of each new protomer is followed by the hydrolysis of GTP to GDP (guanosine triphosphate and guanosine diphosphate, respectively) by β -tubulin, which negatively influences the stability of the newly formed MT. This leads to a polarized structure of the MTs with one fastly depolymerizing so-called minus-end and a growing plus-end, which has a not-yet-hydrolyzed GTP-cap, a MT property known as dynamic instability (Mitchison and Kirschner 1984). In addition, a mechanism known as “microtubule catastrophe” leads to the rapid depolymerization of a MT from the plus-ends, when the GTP hydrolysis reaches the tip of the MT. In contrast, “microtubule rescue” describes the addition of GTP-rich tubulin dimers, leading to the inhibition of depolymerization and thus the stabilization of the MTs (Inoue and Salmon 1995). The intrinsic properties of MTs are also influenced by the multiple genetically encoded α - and β - tubulin isoforms they are made up of (Luduena 1998, Nogales 2001).

In most interphase cells, the nucleation and organization of MTs are thought to happen at the centrosome, also known as the microtubule-organizing center (MTOC). Binding to the latter one via their minus-ends, the MTs irradiate into the cell periphery with their plus-ends.

Summarizing their intrinsic properties, microtubules are polar and highly dynamic structures, predetermined for the engagement in multiple dynamic, transient-state processes, which require directionality.

2.2.2 Cellular functions of microtubules

MTs are needed to fulfill an enormous amount of physiological functions. As the main components of the highly organized axonemal structures found in cilia and flagella, they are required for cell motility (Scholey 2003). During cell division, MTs form the so-called mitotic spindle, and regulate chromosome migration towards the cell poles (Karsenti and Vernos 2001).

Interphase MTs are thought to be the major organizers of cell morphogenesis. As essential determinants of cell shape and motility, they are required for the assembly of the Golgi apparatus and the endoplasmic reticulum, and used as tracks for organelle and cargo transport by motor proteins (Hirokawa 1998, Hirokawa and Takemura 2005). During neuronal development, they seem to be key factors responsible for the outgrowth, branching and the maintenance of the neurites (Baas 2002).

Being highly polarized and large cells, neurons are particularly dependent on active transport of pre- and postsynaptic proteins and cargoes either to the axon or to dendrites and to synaptic sites. Depending on the permanently changing demands of the neuron, organelles, vesicles and newly synthesized proteins need to be transported to and removed from different cellular compartments. For specific cargo delivery, the cytoskeleton is used by motor proteins; several adaptor proteins like GRIP1 (glutamate receptor interacting protein 1), JIP1 and 2 (c-Jun N-terminal kinase (JNK) interacting protein 1 and 2), gephyrin, TRAK1/2 (trafficking kinesin-binding protein 1/2) mediate specific binding to multiple cargoes (e. g. vesicles, organelles or proteins) (Setou, Nakagawa et al. 2000, Kanai, Dohmae et al. 2004, Glater, Megeath et al. 2006). While Myosins use actin filaments as tracks at the neuronal cortex, dynein and kinesins use the MT cytoskeleton, especially for long-distance transport (see Figure 7) (Ross, Ali et al. 2008, Hirokawa, Niwa et al. 2010).

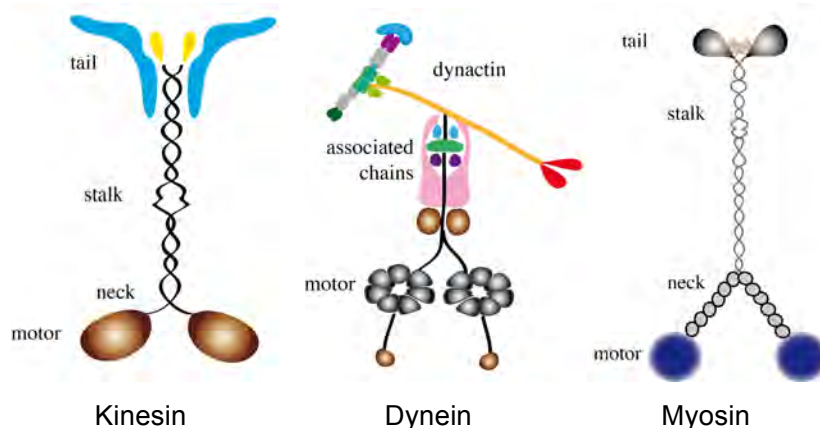


Figure 7: Schematic representation of cytoskeletal associated motor proteins. Motor proteins form homodimers through the association of the stalk-regions of their heavy chains via coiled-coil domains. The binding to the cytoskeleton occurs via globular motor domains of the heavy chains. The neck-regions translate the free enthalpy generated through ATP hydrolysis in the head domains to mechanical work and the movement along MTs. Cargo binding occurs via the tail domain and other associated proteins (e. g. the dynactin complex in

the case of dynein). Myosins mediate actin-dependent transport of cargo. Kinesins and cytoplasmic dynein are MT dependent motor proteins. Modified after (Hirokawa, Niwa et al. 2010).

Because MTs are mainly oriented with their plus-ends towards the cell periphery, the mostly plus-end-directed motor proteins from the kinesin family are considered anterograde motors while dyneins mediate retrograde transport (Vale 2003, Welte 2004, Kapitein and Hoogenraad 2011).

Interestingly, proximal dendritic MTs have a mixed polarity (Baas, Deitch et al. 1988, Baas and Lin 2011). It is assumed, that this enables minus-end directed dyneins to sort cargo for transport into dendrites, thus enabling specific sorting of cargo between axonal and dendritic compartments (Baas, Black et al. 1989). Defects in parts of the neuronal intracellular trafficking machinery are associated with several neurodegenerative or psychiatric disorders (e. g. hereditary spastic paraplegias, Alzheimer's, Huntington's and Parkinson's disease and schizophrenia) (Li, Orr et al. 2010, Atkin, MacAskill et al. 2011, Baloyannis 2014, Agostinho, Pliassova et al. 2015, Hunn, Cragg et al. 2015, Schreij, Fon et al. 2016).

There is growing evidence that besides the actin cytoskeleton, MTs play an important role at synaptic sites, too. Although there were occasional studies reporting the presence of MTs in spines (Chicurel and Harris 1992, Fiala, Kirov et al. 2003), it was not clear whether these observations were due to technical circumstances and most scientists saw their role at extrasynaptic sites. In fact, because MTs are densely packed in neurites, it was not possible to visualize individual fluorescence-labeled polymers in living neurons using conventional microscopy until recently. With the discovery and fluorescence labeling of MT end-binding proteins (see also section 2.2.3), dynamic MTs could be successfully imaged and were shown to regularly enter spines, and to regulate dendritic spine morphology and synaptic plasticity (Stepanova, Slemmer et al. 2003, Jaworski, Kapitein et al. 2009, Kapitein, Yau et al. 2011, Merriam, Lombard et al. 2011) (Figure 8). On the one hand, MTs entering spines are supposed to facilitate cargo delivery and removal to and from spines (Jaworski, Kapitein et al. 2009), on the other hand, the +TIPs at the plus-end of MTs are known to interact with a large number of proteins residing within the cell's actin cortex (Akhmanova and Steinmetz 2008). During their disassembly MTs are known to release factors that had been bound to their lattice, including kinases and small G proteins, with important roles in signaling pathways of the actin cytoskeleton (Wittmann and Waterman-Storer 2001, Kapitein, Yau et al. 2011). Due to these discoveries, neuronal MTs are increasingly seen as information carriers (Dent and Baas 2014).

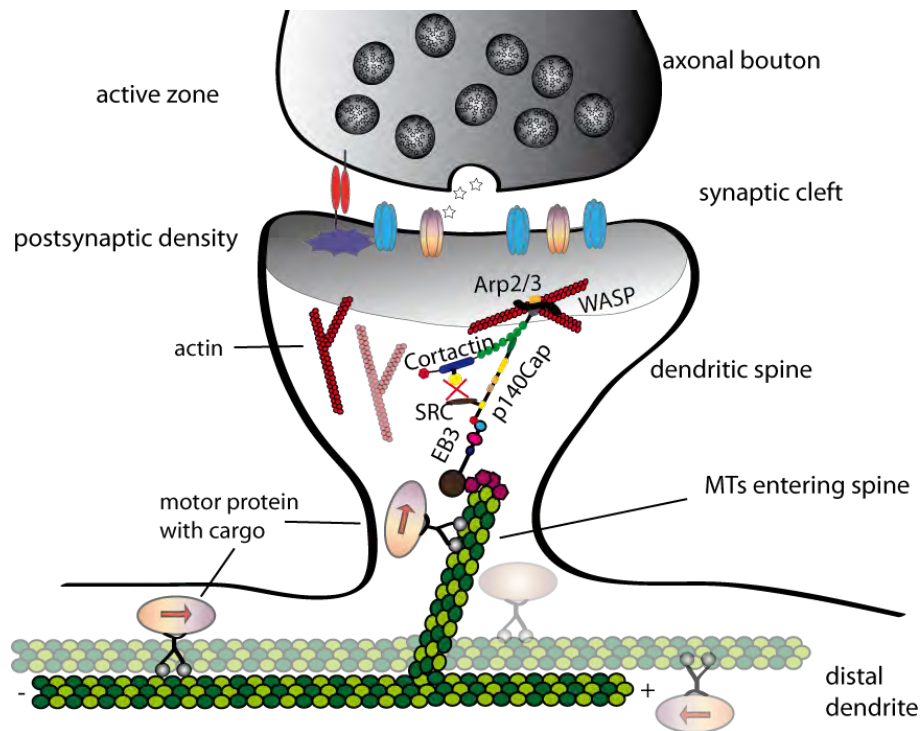


Figure 8: Proposed functions of dynamic MT entrance into spines. On the one hand, MTs could mediate delivery of cargo to individual spines. On the other hand, dynamic MTs could influence the actin structure and spine morphology via the concentration of MT binding proteins (in this case EB3) and actin regulatory proteins (in this case p140Cap, a negative regulator of src kinase, cortactin, a src kinase substrate and an F-actin binding protein). The figure was made on the basis of (Penzes, Srivastava et al. 2010 and Jaworski, Kapitein et al. 2009).

2.2.3 Extrinsic regulators of the microtubule cytoskeleton

In addition to their intrinsic dynamic instability, microtubular properties are strongly determined by extrinsic factors, such as MT-associated proteins and post-translational modifications and importantly, also by their interplay. MTs are able to interact with a large number of proteins and various regulatory proteins are responsible for their dynamic reconstruction. Among them, microtubule associated proteins (MAPs) are proteins, which directly bind to MTs and mainly regulate their stability, dynamics, structure and function. Stabilizing MAPs exert their function by supporting and promoting the polymerization of the MT itself, or by favoring the “rescue” and inhibiting the “catastrophic” events.

MAP1, MAP2, MAP4 and tau are classical examples of microtubule-associated proteins that are believed to have mainly stabilizing functions (Vallee 1982, Tokuraku, Matsushima et al. 2003). Whereas MAP1 and MAP4 bind to MTs in several cell types, MAP2 and tau are exclusively found on dendritic and axonal MTs of neurons, respectively (Matus 1994). Their stabilizing function stems from conferring mechanical stability to the polymer and by preventing access for destabilizing proteins. In addition, the γ -tubulin ring complex (γ -TuRC) promotes the nucleation of MTs, which is a prerequisite for the initiation of tubulin polymerization (Moritz, Braunfeld et al. 2000, Wiese and Zheng 2000).

At the growing tips of MTs, plus-end-binding (EB) proteins like EB1, EB3 and CLIP170 (cytoplasmic linker protein 170) have been shown to additionally promote MT growth at the plus-

ends (+TIPs) (Schuyler and Pellman 2001, Komarova, De Groot et al. 2009, Gouveia and Akhmanova 2010). Furthermore, the +TIP proteins are involved in the binding of a myriad of other proteins present at the cell cortex. For instance, the end-binding protein EB3 binds to the postsynaptic scaffold protein PSD-95, suggesting its role to linking MT dynamics to synaptic function (Sweet, Previtiera et al. 2011).

Examples for MAPs with destabilizing function are Stathmin/Oncoprotein 18, Kin-13, and the MT-severing enzymes spastin, katanin and fidgetin. Stathmin/Oncoprotein 18 inhibits the integration of free tubulin dimers into the MT by complexing them (Jourdain, Curmi et al. 1997, Cassimeris 2002, Grenningloh, Soehrman et al. 2004). The M-type kinesin Kin-13/KIF2a is a motor protein without cargo delivery function and promotes the „catastrophic events“ by depolymerizing MTs from their plus-ends (Desai, Verma et al. 1999, Hirokawa, Niwa et al. 2010). The MT-severing enzymes (see section 2.3) can remove tubulin dimers from the MT polymers, leading to their internal fracturation, which is primarily believed to destabilize the MT cytoskeleton (Vale 1991, Roll-Mecak and Vale 2005).

As the C-terminal tails of tubulin become exposed to the outer surface of the MTs after polymerization (Nogales, Wolf et al. 1998), these are the sites where microtubule associated proteins (MAPs) and motor proteins can bind (Wang and Sheetz 2000, Lakamper and Meyhofer 2005). The tubulin tails are subjected to numerous posttranslational modifications (PTMs), generating a functional diversity of the MT track (Figure 9). Consequently, such PTMs influence the binding of MAPs and motor proteins and function as molecular “traffic signs” for specific cargo transport (Westermann and Weber 2003, Schlager and Hoogenraad 2009, Janke and Kneussel 2010).

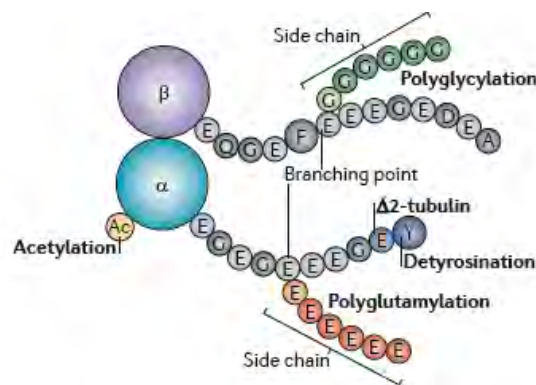


Figure 9: Schematic representation of the $\alpha\beta$ -tubulin dimer and its associated modifications. The carboxy-terminal tails of both tubulins are represented as amino acid sequences (which correspond to mouse α 1A-tubulin (from residue 441 to the end) and β 2B-tubulin (from 432 to the end)). Both α -tubulin and β -tubulin can be modified by polyglutamylation and polyglycylation on different Glu residues within those tails. Together with detyrosination at the C terminus and the follow-up removal of the penultimate Glu residue (which generates Δ 2-tubulin), these modifications are specific to the C-terminal tails of tubulin. Acetylation (Ac) of Lys40 is localized at the amino-terminal domain of α -tubulin. The figure adapted from (Janke and Bulinski 2011).

Newly polymerized MTs are comprised of α -tubulin with a carboxy-terminal tyrosine residue. The removal of that tyrosine from α -tubulin is called detyrosination (Barra, Rodriguez et al. 1973) and

the subsequent irreversible removal of a glutamate residue results in the so-called $\Delta 2$ -tubulin (Paturle, Wehland et al. 1989, Paturle-Lafanechere, Edde et al. 1991). Both PTMs increase microtubule stability by decreasing depolymerization by depolymerizing kinesins (Schulze, Asai et al. 1987, Khawaja, Gundersen et al. 1988, Peris, Wagenbach et al. 2009). Detyrosination of tubulin is thought to be important for neuronal polarization because this modification is specifically recognized by the motor protein KIF5 during axon specification and leads to KIF5-mediated accumulation of axonal cargoes. The retyrosination of monodetyrosinated tubulin (Ersfeld, Wehland et al. 1993) is thought to favor dynamic MT functions, e. g. in the axon growth cone (Janke and Kneussel 2010). In fact, mice lacking the tubulin tyrosine ligase (TTL) catalyzing this modification show a perinatal lethality due to premature axonal differentiation (Erck, Peris et al. 2005).

Acetylation of α -tubulin is generally found on detyrosinated tubulin (Cambray-Deakin and Burgoyne 1987) and is equally associated with stable and long-lived microtubules, but does not seem to be causal for their stabilization (Palazzo, Ackerman et al. 2003). This PTM seems to enhance the processivity of the motor protein KIF5 (Cai, McEwen et al. 2009).

Both α - and β -tubulin can be subjected to polyglutamylation, a reversible reaction comprising an initial addition of a glutamyl chain to a protein coded glutamate followed by further elongation to a polyglutamyl chain (Edde, Rossier et al. 1990, van Dijk, Miro et al. 2008). The enzymes catalyzing this reaction belong to the TTL (tubulin tyrosine ligase-like) family (Regnard, Audebert et al. 1998, Regnard, Desbruyeres et al. 1999). Polyglutamylated MTs have a negatively charged surface and are specifically enriched on the MTs of neurons, centrioles, cilia and of the mitotic spindle. A study using mice with defects in polyglutamylation showed an altered distribution of KIF1A and impaired localization of synaptic vesicles, representing their cargo (Okada, Yamazaki et al. 1995, Ikegami, Heier et al. 2007). Additionally, this study suggested that neuronal activity could be influenced by polyglutamylation through regulation of synaptic vesicle transport. In neurons, activity-induced polyglutamylation enhances the binding of MAP2 to MTs and leads to inhibition of transport processes mediated by the motor protein KIF5 (Maas, Belgardt et al. 2009). Polyglutamylation was also shown to enhance MT fragmentation via the MT-severing enzyme spastin (Lacroix, van Dijk et al. 2010). The reverse reaction of polyglutamylation is carried out by cytosolic carboxypeptidases (CCPs); mice lacking CCP1 show increased MT polyglutamylation and Purkinje cell degeneration (Kimura, Kurabe et al. 2010, Rogowski, van Dijk et al. 2010).

From the chemical point of view, polyamination of MTs might represent the opposite reaction to polyglutamylation. Polyaminated tubulin has recently been found on very stable MTs present in neuronal axons (Brady, Tytell et al. 1984, Song, Kirkpatrick et al. 2013). This PTM involves the addition of a positive charge to the outer surface of MTs and might increase their stability, eventually by decreasing access for MT-destabilizing and severing proteins. In general, this class of MTs is considered to be nondynamic (Baas 2013).

The polyglycylation involves the addition of multiple glycine residues to the C-termini of both α - and β -tubulin (Redeker, Levilliers et al. 1994). This PTM has been described on MTs from motile axonemal and flagellar structures (Verhey and Gaertig 2007).

In vitro experiments suggest the existence of palmitoylation of MTs, which involves the addition of a fatty acid chain to tubulin. This PTM is believed to be important for hydrophobic interactions while targeting MTs to membranous compartments (Caron 1997, Ozols and Caron 1997, Zambito and Wolff 1997).

The phosphorylation of a serine residue within the carboxy-terminal tail of a tubulin class has also been described and seems to accompany neurite outgrowth during neuronal differentiation (Eipper 1974, Gard and Kirschner 1985).

2.3 Microtubule-severing enzymes

Besides the dynamic instability whereby MTs polymerize and depolymerize from their ends, MT-severing is another mechanism that leads to their internal breakage without impacting primary protein structure. The MT-severing enzymes exert their function as “molecular scissors” by cutting MTs into smaller fragments (Vale 1991, Roll-Mecak and Vale 2005, Mukherjee, Diaz Valencia et al. 2012). Because the capacity of a MT to move is directly related to its length (Dent, Callaway et al. 1999, Baas, Vidya Nadar et al. 2006), MT-severing is thought to be a key mechanism for the generation of short and mobile MTs (Wang and Brown 2002). The latter ones can then polymerize to long MTs and can be either transported by motor proteins or by a mechanism known as treadmilling (Wegner 1976).

In humans, seven genes are known so far to code for a subclass of AAA ATPases with MT-severing activity and can be grouped as follows: katanin and katanin-like (KATNA1, KATNAL1, KATNAL2), spastin (SPAST or SPG4) and the fidgetin and fidgetin-like (FIGN, FIGNL1, FIGNL2) proteins (Roll-Mecak and McNally 2010). The phylogenetically highly related vacuolar protein sorting 4 VPS4 (VPS4A and VPS4B) is not believed to sever MTs (Babst, Wendland et al. 1998, Bishop and Woodman 2000, Yoshimori, Yamagata et al. 2000). In addition, *KATNB1* and *KATNBL1* seem to be genes involved in the regulation of MT-severing (Roll-Mecak and McNally 2010). Among the mentioned ones, the two related proteins spastin (SPG4) and katanin (KATNA1) are the most extensively studied (Frickey and Lupas 2004).

2.3.1 AAA ATPases

MT-severing enzymes belong to the large family of ATPases associated with various cellular activities (AAA ATPases), which are highly conserved from prokaryotes to mammals. They represent a subgroup of P-loop ATPases, which share a strong homology in their ATP binding domains. As mechanochemical enzymes, AAA ATPases use the free enthalpy from ATP hydrolysis to induce conformational changes in their target molecules, which is required for

processes such as protein unfolding and degradation, membrane fusion or DNA-replication (Hanson and Whiteheart 2005).

While mostly having nonconserved N-terminal regions, which are important for their individual functions, all AAA ATPses share a highly conserved ATPase domain of about 200-250 amino acids (White and Lauring 2007).

AAA proteins oligomerize to form hexameric rings with a central cavity in their quaternary structure. AAA ATPases, containing tandem-AAA domains (e. g. N-ethylmaleimide-sensitive factor) have additionally been shown to associate to dodecamers via stacking of two hexameric rings on top of each other (Whiteheart, Schraw et al. 2001).

The part of the ATPase domain directly involved in ATP-binding and hydrolysis is formed by highly conserved motifs of the large AAA subdomain (Walker A P-loop, the Walker B motif, the sensor-1 and sensor-2 regions as well as an arginine-finger) which are folded in a Rossman-fold and a small α -helical AAA subdomain (Iyer, Leipe et al. 2004).

In addition to the highly conserved structural motifs essential for the ATPase activity, the N-linker domain translates the energy from ATP hydrolysis to the rest of the protein, while loops mantle the inner of the central pore of the AAA oligomer (Yamada-Inagawa, Okuno et al. 2003, Siddiqui, Sauer et al. 2004, Hanson and Whiteheart 2005).

2.3.2 Spastin

Spastin has been studied long before it has been demonstrated to be a MT-severing enzyme due to its strong association with the neurodegenerative disease hereditary spastic paraplegia (HSP). Only later it has been shown to act as a MT-severing enzyme (Errico, Ballabio et al. 2002, Evans, Gomes et al. 2005, Roll-Mecak and Vale 2005, Salinas, Carazo-Salas et al. 2005).

In humans, the 90 kb spanning *SPG4* gene is composed of 17 exons and coded on chromosome 2 (32.29 – 32.38 Mb). Its mouse orthologue *Spg4* is coded on chromosome 17 (74.34 – 74.39 Mb) (Hazan, Fonknechten et al. 1999).

Full-length spastin has 616 amino acids (aa) in humans and 614 aa in mice (Figure 10) with a sequence identity of 94 % (see section 7.5.2). Depending on different usage of two AUG codons in the first exon (M1/M87 in humans and M1/M85 in mice), and alternative splicing of exon 4, four spastin isoforms can be detected (Svenson, Ashley-Koch et al. 2001, Claudiani, Riano et al. 2005, Mancuso and Rugarli 2008, Solowska, Morfini et al. 2008). The most abundant isoform in tissues is the one retaining exon 4 and starting from the second methionine (Salinas, Carazo-Salas et al. 2005). The function of the 32 aa stretch encoded by exon 4 is unknown. Characteristic for most AAA ATPases, the carboxy-terminal end of spastin contains the ATPase domain, whereas the amino terminus confers the individual interaction with specific target molecules.

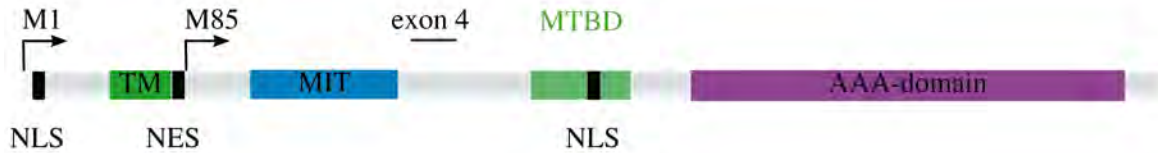


Figure 10: Schematic representation of the murine spastin protein sequence. Spastin translation can either start from methionine 1 or 85 (M1 or M85) because the mRNA has two start codons. The protein has two nuclear localization sequences (NLS), one nuclear export sequence (NES), one MT interacting and trafficking domain (MIT) and one additional MT binding domain (MTBD). The AAA ATPase domain is located at the carboxy terminus. A transmembrane domain (TM) and a PEST-Sequence are predicted to be present in the amino-terminal region. Exon 4 of the spastin mRNA is alternatively spliced, leading to 4 possible spastin isoforms at the protein level (1st ATG+Exon 4: 68 kDa; 1st ATG without Exon 4: 64 kDa; 2nd ATG+ Exon 4: 58 kDa and 2nd ATG without Exon 4: 55 kDa).

The full-length protein contains an atlastin-binding domain (Evans, Keller et al. 2006), a microtubule interacting and trafficking (MIT) domain thought to be important for endosomal trafficking processes (Ciccarelli, Proukakis et al. 2003) and a second MT binding domain (MTBD) (White, Evans et al. 2007). Spastin uses these two different MT-binding domains—one on the outside of the hexameric ring and one on the loop domains inside the ring—to lock onto tubulin and cause severing.

Human spastin has been shown to contain two nuclear localization sequences (NLS) (Beetz, Brodhun et al. 2004), two nuclear export sequences (NES) (Claudiani, Riano et al. 2005) and a transmembrane domain (TMD), which has been suggested not to span the lipid bilayer completely, but to plunge into the membrane in a wedge-like fashion (Blackstone 2012). In addition, a PEST-sequence that is rich in proline, glutamate, serine, and threonine and which is associated with proteins that have a short intracellular half-life is supposed to be present at least in human spastin (Schickel, Pamminger et al. 2007). It is hypothesized that the PEST sequence acts as a signal peptide for protein degradation (Rogers, Wells et al. 1986).

The shorter spastin isoform starting from the second start codon lacks the NES sequence, one NLS sequence, the TMD and the PEST sequence. Consequently, the longer isoform is primarily found in the cytoplasm, whereas the shorter isoform can be found both in the nucleus and the cytoplasm (Beetz, Brodhun et al. 2004, Claudiani, Riano et al. 2005). It is assumed that nuclear spastin is required for transcriptional regulation, as it was shown to function as a corepressor of the homeobox gene *HOXA10* (Daftary, Tetrault et al. 2011).

Spastin is enriched in the centrosome in interphase and during mitosis, in the cytokinesis structure midbody, and in the growth cones and branching points of neurons (Errico, Claudiani et al. 2004, Yu, Qiang et al. 2008). In *Drosophila melanogaster*, D-spastin could also be detected in axons and synaptic sites (Trotta, Orso et al. 2004).

Given the multiple domains contained in the spastin protein and the existence of the four different isoforms already suggests that it has many functions and can be found at multiple subcellular locations. In humans and mice, spastin is ubiquitously expressed and especially enriched in the

brain region (Ma, Chia et al. 2006). As revealed by immunohistochemistry on postmortem brains, spastin is mainly a neuronal protein found in the hippocampus, the spinal motoneurons as well as in the cortical and hippocampal pyramidal cells (Wharton, McDermott et al. 2003).

2.3.2.1 Spastin's role in hereditary spastic paraplegia

Spastin was initially discovered as a gene mutated in the autosomal dominant form of hereditary spastic paraplegia (HSP) with a prevalence ranging from 1.3 to 9.6 in 100,000 (McMonagle, Webb et al. 2002, Sedel, Fontaine et al. 2007). In a majority of cases, this disease is caused by various loss-of-function mutations within one allele of the *SPG4* gene (Hazan, Fonknechten et al. 1999). HSP is a dying-back axonopathy characterized by progressive lower limb weakness and spasticity due to degeneration of the long central motor axons from corticospinal tracts which can reach the length of 1 m in an adult (Fink 2006).

To date, approximately 150 different mutations of various types have been found in HSP patients, including missense, nonsense or splice-site mutations, as well as deletions and insertions causing frameshifts and thus the loss-of protein function (Depienne, Stevanin et al. 2007). The mean age of onset ranges around 34 years but varies strongly between the different types of mutation (McDermott, Burness et al. 2006). Several modes of action are discussed for the development of HSP through spastin mutations. Besides the most favored haploinsufficiency-model supported by genetic analysis, also a dominant-negative- and a threshold-effect-model are described for some spastin mutations (Errico, Ballabio et al. 2002, Chinnery, Keers et al. 2004, Klimpe, Zibat et al. 2011).

Three loss-of-function mouse models for spastin have been published to date. In two studies exons 5-7 and 7 were targeted, leading to the loss of spastin expression; a third knock-in mouse model bears a N386K missense mutation, which leads to the expression of an ATP-hydrolysis-defective spastin (Tarrade, Fassier et al. 2006, Kasher, De Vos et al. 2009, Connell, Allison et al. 2016). Each of these mouse models developed gait abnormalities at different ages ranging from 4 to 7 and 22 months. Spastin null mutants and knockdowns in *Drosophila* were also shown to display impaired locomotor behavior (Sherwood, Sun et al. 2004, Trotta, Orso et al. 2004).

On the cellular level, it is believed that HSP arises through disturbed MT dynamics in the long central motor axons in patients with mutated *SPG4*. Containing more than 99 % of the cytoplasm of the cell, these axons are dependent on efficient transport of organelles, cytoskeletal components, and lipid constituents synthesized in the cell body. In line with this hypothesis, cultivated cortical neurons derived from the spastin loss-of-function mice developed axonal swellings, containing trapped cytoskeletal components and organelles. These phenotypes could in part be rescued by the application of low-dosage MT targeting drugs (Tarrade, Fassier et al. 2006, Fassier, Tarrade et al. 2013, Fan, Wali et al. 2014). A naturally occurring spastin mutation in cattle with a severe and early onset of spinal demyelination also displayed axonal swellings with trapped organelles and disorganized MTs (Thomsen, Nissen et al. 2010).

2.3.3 Katanin

Katanin (derived from the Japanese word “Katana” for sword) was the first MT-severing enzyme to be described (Vale 1991). It was initially isolated from sea urchin eggs and shown to be composed of a 60 kDa catalytic AAA subunit (p60, KATNA1) and a 80 kDa regulatory subunit (p80, KATNB1) (McNally and Vale 1993, Hartman, Mahr et al. 1998). Katanin p60 is highly conserved throughout the animal, higher plant and protozoan kingdoms having orthologues in *Drosophila melanogaster*, *Caenorhabditis elegans* and *Arabidopsis thaliana* (ATKN1). In Humans and in mice, KATNA1 p60 is a 491 amino acid protein with 93 % sequence identity (see also section 7.5.1). It contains a 230 amino acid AAA ATPase module. In addition, 2 katanin-p60-like proteins (KATNAL1 and KATNAL2) and one katanin-p80-like protein (KATNBL1) have been described (Figure 11) (Roll-Mecak and McNally 2010). Human KATNA1 and KATNAL1 have similar domain architectures with an N-terminal microtubule interacting and trafficking domain (MIT) followed by a coiled-coil domain (CC), an AAA ATPase domain (AAA) and a C-terminal VPS4 domain (VPS4) (Iwaya, Akiyama et al. 2012). In contrast, KATNAL2 only contains the AAA domain and lacks the MIT, CC, and VPS4 domains. Additionally, it has an N-terminal LisH (LIS1 homology) domain. Its predicted MT-severing activity still has to be proven.

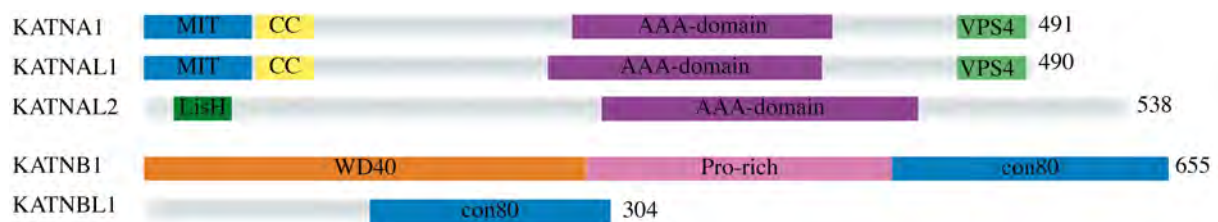


Figure 11: Domain architecture of the three KATNA1, KATNAL1, KATNAL2 catalytic subunits and the two KATNB1 and KATNBL1 regulatory subunits. Major domains within each katanin include the microtubule interacting and trafficking domain (MIT), the coiled-coil domain (CC), the AAA ATPase domain (AAA), the VPS4 C-terminal domain (VPS4), the proline-rich domain (Pro-rich) and the conserved C-terminal region that binds to the N-terminal domain of KATNA1 (con80). The number of total amino acid residues is indicated for each protein.

The role of the ubiquitously expressed p80-subunit is not fully clear yet, but it is assumed, that it has important regulatory and targeting functions, e. g. to the centrosome and to dynein, NDEL1 and LIS1 (McNally, Okawa et al. 1996, McNally, Bazirgan et al. 2000). The amino-terminal WD40-domain (repeated structural motifs of 40 aa, often terminating with tryptophane and aspartate) has been shown to target to interphase chromosomes using a GFP-fusion construct (Hartman, Mahr et al. 1998). Both p60 and p80 were demonstrated to bind to MTs in vitro, but the affinity and the severing activity was enhanced by the interaction of both subunits (McNally, Buster et al. 2002). Both KATNB1 and its conserved C-terminal con80 domain alone have been shown to stimulate KATNA1 MT-severing activity, whereas the KATNB1 WD40 domain alone inhibited MT-severing (Hartman, Mahr et al. 1998, McNally, Bazirgan et al. 2000).

Interestingly, the p60 and p80 subunits do not seem to be present at equimolar levels within cells and differ dramatically in different tissues and developmental stages (Yu, Solowska et al. 2005). To date, there is little evidence for the interaction of the different katanin subunits. One

interactome study could show that katanin and KATNAL1 can interact, suggesting that their functions might be regulated or compensated by this interaction (Cheung, Senese et al. 2016).

2.3.4 Fidgetin

Fidgetin has been detected through a spontaneous mouse mutation leading to the fidget phenotype associated with uncontrolled headshaking as its leading phenotype (Carter and Gruneberg 1950). These mice showed further pleiotropic developmental defects in their auditory, ocular and skeletal systems, and an increased occurrence of a palatine cleft (Wallace 1950, Yang, Mahaffey et al. 2006). The severing activity of fidgetin has been demonstrated using in vitro experiments (Zhang, Rogers et al. 2007, Mukherjee, Diaz Valencia et al. 2012). In addition, FIGNL1 and FIGNL2 have been detected as vertebral fidgetin-like proteins (Cox, Mahaffey et al. 2000).

2.3.5 Mechanism and regulation of microtubule-severing

As is the case for most members of the AAA ATPase family, MT-severing enzymes are active as oligomers, forming hexameric rings of 14-16 nm with a central pore (White, Evans et al. 2007, Roll-Mecak and Vale 2008). The oligomerization seems to be induced by ATP binding (Figure 12a), since an ATP-hydrolysis deficient p60 (E334Q) mutant of katanin forms stable oligomers. Additionally, MT binding seems to stimulate the oligomerization state, as well as the ATPase and the severing activities. At concentrations between 2-10 μ M, peak values of katanin ATPase activity could be detected followed by an inhibition at higher concentrations (Hartman, Mahr et al. 1998, Hartman and Vale 1999). The Walker A and Walker B motifs within the AAA domain have been shown to be responsible for ATP binding and hydrolysis (Hartman and Vale 1999, Roll-Mecak and Vale 2008).

The disassembly of the hexamer is induced after the ATP hydrolysis. Since ADP-katanin is less likely to oligomerize and has a lower affinity to tubulin, the katanin-tubulin complex is thought to dissociate (Hartman, Mahr et al. 1998, Hartman and Vale 1999). Upon new ATP binding, the severing process can restart. Thus, the ATPase activity is a prerequisite for MT-severing. Interestingly, pore-loop mutants defective in ATP hydrolysis are still able to bind to and bundle MTs without severing them (White, Evans et al. 2007).

A study suggests that MT-severing enzymes preferentially sever bent MTs, probably because then the lattice becomes more accessible to the severing enzymes or because bent MTs are more prone to breakage (Odde, Ma et al. 1999). Another study could show that bending alone is not sufficient for MT breakage (Janson and Dogterom 2004). For katanin it has been demonstrated that it preferentially severs at MT lattice defects, such as protofilament shifts and filament ends (Davis, Odde et al. 2002, Diaz-Valencia, Morelli et al. 2011). To date, it is not known whether the removal of one tubulin dimer from the lattice is sufficient to lead to severing.

With the resolution of the *Drosophila* spastin (D-spastin) crystal structure, a model has been

developed, proposing that severing enzymes recognize the negatively charged carboxy-terminal tails of tubulin and pull it through their positively charged central pore (Roll-Mecak and Vale 2008). This is thought to partially unfold tubulin, ultimately destabilizing tubulin–tubulin interactions within the lattice through mechanical force (Figure 12b). In line with this model, it has been shown, that the activity of spastin is increased by the polyglutamylation of tubulin, which further increases the negative charge on the carboxy-terminal tails of tubulin (Lacroix, van Dijk et al. 2010). In contrast, masking of that region with antibodies (Roll-Mecak and Vale 2008) and by non-specific protease treatment (Roll-Mecak and Vale 2005, White, Evans et al. 2007) abrogated spastin mediated severing. Interestingly, glutamylation of MTs seems to be a non-linear tuner of severing and becomes inhibitory beyond a threshold number of glutamyl chains attached (Valenstein and Roll-Mecak 2016). Similar to spastin, also katanin p60 has recently been shown to require the acidic C-terminal tails of α - and β -tubulin for severing (Johjima, Noi et al. 2015).

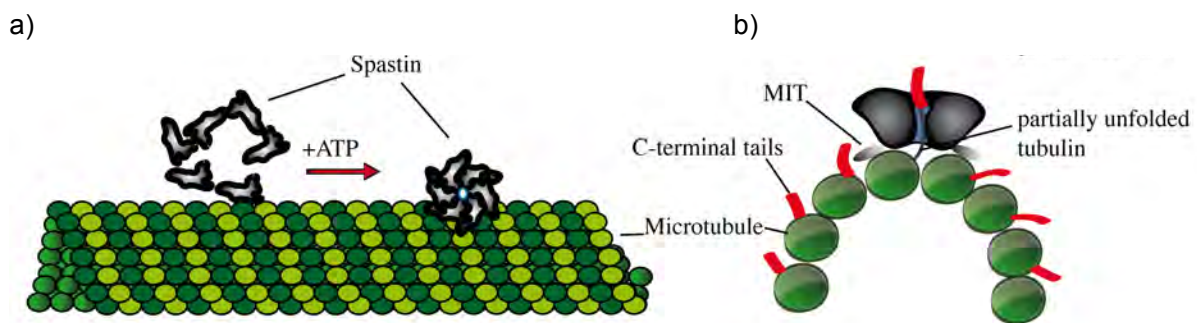


Figure 12: Proposed model of microtubule-severing by the MT-severing enzyme spastin. a) Spastin monomers can bind to MTs in an ATP-independent manner. ATP binding induces hexamerization of spastin and the formation of a central pore with positively charged pore loops 1, 2 and 3 (highlighted in blue). The MIT domains are shown as ovals on the lateral view in b). The valency of the interaction of the MIT domains with the MT is unknown. b) The hexameric spastin AAA core recognizes the C-terminal tubulin tails (shown in red), leading to partial unfolding of tubulin. Modified from (White, Evans et al. 2007) and from (Roll-Mecak and Vale 2008).

It is not yet known exactly how the hexameric rings bind to MTs. Two possible models have been proposed: The flat binding onto the MT surface (as shown in Figure 12b), or the upright standing on it, like a wheel (see Figure 12a) (Sharp and Ross 2012). Additionally, the “MAP protection model” (Baas and Qiang 2005) suggests MAPs and their conditional binding to MTs as the main protectors from severing. For katanin, there is strong evidence that its severing activity is blocked by the MT-associated proteins MAP4, tau and by the neuroprotective peptide NAP (McNally, Buster et al. 2002, Qiang, Yu et al. 2006, Sudo and Baas 2011).

In summary, the severing process is dependent on the availability of ATP, the accessibility to and modification of MTs, and the stimulation or inhibition of the catalytic subunits by regulatory proteins. A summarizing overview of the known regulators both at the expression and the activity level is given in Table 1.

Independent of their severing activities, MT-severing enzymes have also been shown to exert a function in MT-bundling (Salinas, Carazo-Salas et al. 2005).

Table 1: Summarizing overview of the known regulators of the MT-severing enzymes katanin and spastin.

| Regulation | Regulator | Mode of action | Reference |
|--------------------|--|---|--|
| Katanin inhibition | MAP2c and MAP4 | Shielding of MTs from severing | (McNally, Buster et al. 2002, Qiang, Yu et al. 2006) |
| | tau | | (Qiang, Yu et al. 2006) |
| | NAP | unknown | (Sudo and Baas 2011) |
| | LAPSER1 | Decreased affinity of p60/p80 heterodimer to MTs? | (Sudo and Maru 2008) |
| | Ca ²⁺ | ATPase inhibition by spatial rearrangement? | (Iwaya, Akiyama et al. 2012) |
| | SPN-2 | Expression level | (Li, DeBella et al. 2009) |
| bFBF | (Qiang, Yu et al. 2010) | | |
| Katanin activation | tubulin acetylation | unknown | (Sudo and Baas 2010) |
| | C-terminal tails of tubulin | protein-protein interaction | (Johjima, Noi et al. 2015) |
| Spastin inhibition | very long polyglutamyl chains on tubulin | | |
| | IGF-1 | Phosphorylation of spastin by IGFR1? | (Korulu and Karabay 2011) |
| | Dar1 | expression level | (Ye, Kim et al. 2011) |
| | miR-96 and miR-182 | | (Henson, Zhu et al. 2012) |
| | Jagged 1 | | (Ferrari-Toninelli, Bonini et al. 2008) |
| NRF1 and SOX11 | (Henson, Zhu et al. 2012) | | |
| Spastin activation | bFBF | | (Qiang, Yu et al. 2010) |
| | knot | | (Jinushi-Nakao, Arvind et al. 2007) |
| | PAK3 | genetic interaction | (Ozdowski, Gayle et al.) |
| | polyglutamylation of MTs | protein-protein interactions | (Lacroix, van Dijk et al. 2010) |

2.3.6 Physiological functions of microtubule-severing enzymes

Given the multiple cellular functions of MTs (as described in section 2.2.2), MT-severing enzymes also play an important regulatory role in these processes and further contribute to the complexity of MT dynamics. Data from *in vitro* experiments on MT-severing enzymes suggests that they rapidly sever stable MTs until their complete degradation (Vale 1991, McNally and Vale 1993). *In vivo*, they additionally seem to be involved in anabolic processes like the initiation of MT growth, the release of MTs from their nucleation sites and the transport between different compartments of the cell (Baas, Karabay et al. 2005, Roll-Mecak and McNally 2010). In other cases, severing-proteins play a crucial role in the regulation and the formation of MT ends (Diaz-Valencia, Morelli et al. 2011, Zhang, Grode et al. 2011).

To date, the main research focus was set on the severing activities of MT-severing enzymes. However, there are some reports about their functions entirely unrelated to severing as well (Du, Ozdowski et al. 2010, McNally and McNally 2011).

2.3.6.1 The role of MT-severing during the cell-division-cycle

During the cell-division cycle, the MT cytoskeleton forms the mitotic or meiotic spindles required for the segregation of chromosomes, the central spindle and the midbody during cytokinesis (Mullins and McIntosh 1982, Glotzer 2001, McIntosh, Grishchuk et al. 2002, Blagden and Glover 2003, Glotzer 2009, Douglas and Mishima 2010).

It is assumed, that MT-severing enzymes work together to coordinate chromosome segregation during mitosis and meiosis. Results from *Drosophila* indicate that MTs are severed from both their plus- and minus-ends, enabling their shortening by depolymerization, which causes poleward chromatid movement termed as “pacman-flux” (Zhang, Rogers et al. 2007). Spastin and fidgetin are mainly thought to sever the pole-focused MTs from their minus-ends, whereas the kinetochore-associated katanin was shown to primarily act as a plus-end depolymerase (Zhang, Grode et al. 2011). Because katanin's activity increases already during the mitotic prophase, it is assumed that severing is also important for the disassembly of interphase MTs and their reassembly into the mitotic spindle (McNally and Thomas 1998).

In fact, especially katanins seem to have important roles during cell division by regulating MT-dependent processes like mitotic spindle length and structure (McNally, Audhya et al. 2006) (Zhang, Rogers et al. 2007). The mutation of human katanin's regulatory subunit p80 has recently been linked to brain disorders like complex cerebral malformations, including microcephaly. These disorders seem to be caused by a disruption of the asymmetric division of neural progenitors (Mishra-Gorur, Caglayan et al. 2014).

Katanin p60 and p80 were observed in the cleavage furrow during the cell division of trypanosomes. The depletion of katanin p80 using RNA interference triggered a cytokinesis block, whereas the depletion of p60 katanin did not. In contrast, the absence of the p60 homolog in *Tetrahymena* also led to an arrest in cytokinesis (Sharma, Bryant et al. 2007). Similarly, the depletion of spastin in HeLa-cells resulted in delayed cytokinesis and a defective disruption of the intercellular bridge formed by MTs during the final abscission process after membrane invagination (Connell, Lindon et al. 2009). This suggests that spastin might be responsible for severing the stable MT bundles found in the midbody.

Before its discovery as a MT-severing enzyme in 1991, the katanin orthologues mei-1 (p60 subunit) and mei-2 (p80 subunit) were found to cause embryonal lethality in a screening study performed on the nematode *C. elegans* (Mains, Kemphues et al. 1990). Katanin has been located at meiotic chromosomes and at spindle poles and it was shown that during oocyte M-phase, the meiotic spindle MTs were not formed properly and aggregated around the chromosomes in null mutants (Clandinin and Mains 1993, Clark-Maguire and Mains 1994, Srayko, O'Toole E et al. 2006).

Additionally, hypomorphic mutants with decreased katanin activity showed a phenotype with fewer, but abnormally elongated bipolar spindle MTs and defects in the orientation and dynamics of the oocyte-cortex (McNally, Audhya et al. 2006). Thus, severing by katanin seems to increase the amount and density of MTs in the meiotic spindle in *C. elegans* by the generation of short fragments, which can further polymerize (Roll-Mecak and Vale 2006, Srayko, O'Toole E et al. 2006).

Recently, the mutation of katanin subunits has also been linked to male infertility in mice (O'Donnell, Rhodes et al. 2012, Smith, Milne et al. 2012). Katanin's regulatory p80 subunit seems to play an essential role for the assembly and dissolution of the male meiotic spindle and for the removal of midbody MTs essential for cytokinesis. This regulation is thought to happen via the interaction with the p60 subunit (O'Donnell, Rhodes et al. 2012). The mutation of *KATNAL1* also caused male infertility, but presumably not primarily due to defects in germ cell division. Here, the regulation of MT dynamics in the supportive testicular Sertoli cells (SC) was perturbed, leading to defective spermiogenesis (Smith, Milne et al. 2012). Interestingly, SCs and neuronal axons seem to share morphological, structural and functional properties of the cytoskeleton, being largely parallel in orientation and predominantly spaced one to two MT diameters apart (Neely and Boekelheide 1988). To date, no reports were published about spastin's role during meiosis with the exception of homozygous spastin null mutants, which were shown to display sterility in both sexes (Sherwood, Sun et al. 2004, Tarrade, Fassier et al. 2006).

2.3.6.2 Severing in cilia biogenesis

Axonemes are conserved organelles formed by a bundle of nine fused doublet-MTs- and two central single MTs. Their interaction enables the beating of tracheal motile cilia in order to expel particulate matter and the swimming of sperm is caused by the beating of their flagella. In contrast, immotile cilia lack the central pair of axonemal MTs.

Several models exist for the role of katanin in ciliar and flagellar dynamics in different eukaryotic organisms. A katanin-like protein was shown to be located at the flagella of trypanosomes and its ectopic expression led to a significant flagellar length reduction (Casanova, Crobu et al. 2009). Mutated katanin was shown to result in nonmotile cilia lacking the central pair of MTs (Dymek, Lefebvre et al. 2004, Sharma, Bryant et al. 2007). Additionally, in some cases, katanin was essential for deflagellation (Lohret, Zhao et al. 1999), a prerequisite to release basal bodies from axonemal MTs, which can be reutilised as the centrioles in centrosomes during mitosis (Rasi 2009).

Interestingly, Tetrahymena katanin null mutants showed altered PTMs of their axonemal MTs with increased polyglutamylolation and decreased polyglycylation, suggesting that these modifications might also be important for the regulation of MT-severing by katanin (Sharma, Bryant et al. 2007).

2.3.6.3 Role of MT-severing in neurons

Vertebrate nervous systems develop by five major stages: neural progenitor cells proliferate in an epithelium, followed by the specification of neurons and glia and their migration to their target zones, the growth and guidance of axons and dendrites, and the development and refinement of electrical and chemical synapses (Cooper 2013). In all of these stages, the cytoskeleton performs a variety of essential tasks. Thus evidence is growing that MT-severing enzymes are involved in many of these processes as well (see also Figure 13).

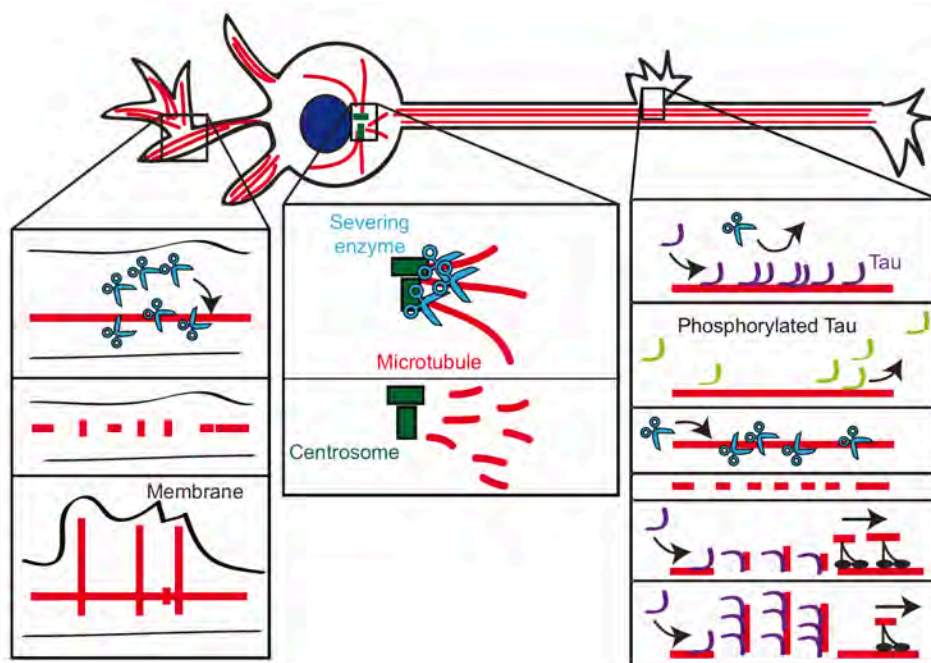


Figure 13: Summarizing overview of the multiple neuronal functions of MT-severing enzymes. MT-severing enzymes (represented by the blue scissors) are present throughout all neuronal compartments. In dendrites, severing by spastin and a katanin-like protein contributes to dendritic arborization. In the cell soma, centrosomal MTs are released by the severing activity of katanin and can be further transported into axons. In axons, severing by spastin and katanin is thought to be a key mechanism for collateral branch formation. The figure was adapted from (Sharp and Ross 2012).

The dynamic regulation of the cytoskeletal organization is thought to play a major role in the complex process of cell migration (Marin and Rubenstein 2003, Ayala, Shu et al. 2007). At the leading process of a migrating cell, the dynamic filopodia and lamellipodia resembling growth cones invade the surrounding area, followed by the invasion of the MT cytoskeleton (Watanabe, Noritake et al. 2005). Most neurons migrate with the centrosome, Golgi apparatus, and recycling endosomes in front of the nucleus (Tsai and Gleeson 2005). Severing activity may contribute to this protrusive event in different ways, either by the generation of short and mobile MTs or by the generation of free MT ends lacking the stabilizing protein cap at their tips, making them prone to depolymerization. In fact, katanin was shown to play a role in cell migratory events. It has been shown to be aberrantly expressed in metastatic cancer cells, and its overexpression in primary cancer cells enhanced their cell motility (Ye, Lee et al. 2012). Its inhibition by expressing dominant-negative katanin mutants in migrating neurons resulted in defective migration and the elongation of nuclear-centrosomal distance (Toyo-Oka, Sasaki et al. 2005). It has been shown to

interact with a protein mutated in lissencephaly, a brain morphogenesis disease with disorganized cerebral cortex layers resulting from a defect in neuronal migration (Dobyns 1987, Dobyns, Reiner et al. 1993). Additionally, an inhibition of katanin's regulatory subunit p80 resulted in slower migration of epithelial cells (Sudo and Maru 2008). Nevertheless, katanin's impact on cell migration is not straightforward. Data from *Drosophila* katanin rather point to its role as a negative regulator of cell migration, a phenotype also observed for the mammalian katanin-like protein 1 (KATNAL1) (Zhang, Grode et al. 2011). Spastin overexpression has also been linked to glioblastoma, and to be enriched in the leading edges of cells in glioblastoma cell lines (Draberova, Vinopal et al. 2011). In this study, the depletion of spastin resulted in reduced cell motility, suggesting that it also plays a role in migratory and invasion processes.

MT-severing also seems to play an important role in the outgrowth and specification of the individual neurites, where the composition of MT arrays plays a crucial role. The first and decisive event during neuronal polarization is the specification of the axon. As mentioned in section 2.2.1, MTs normally nucleate at centrosomal sites, from where they can be released by MT-severing activity. Later during neurodevelopment, the centrosome becomes deactivated, whereas levels of the MT-severing enzyme katanin increase at the tip of axons and dendrites at later developmental stages (Yu, Solowska et al. 2005). The latter two and the sites of newly developing axonal branches are characteristic for the presence of short MTs (Dent, Callaway et al. 1999). Thus, locally severed MTs are thought to serve as new seeds for MT polymer growth (Roll-Mecak and Vale 2006) and to enter the axon branches during axon specification. In fact, axons are able to extend without centrosomal MT nucleation, presumably because of the existence of MT-severing (Stiess, Maghelli et al. 2010). In contrast, *in vitro* inhibition of the MT-severing enzyme katanin revealed a strong compromise of axonal growth (Karabay, Yu et al. 2004). Similarly, a knockdown of spastin in zebrafish displayed a disorganized and sparse axonal MT array and impaired axonal outgrowth as well (Wood, Landers et al. 2006).

In axons, spastin was shown to specifically accumulate at future branch sites and its depletion *in vitro* led to a severe reduction of branching, whereas slight overexpression led to enhanced neurite branching and elongation (Yu, Qiang et al. 2008, Riano, Martignoni et al. 2009). This process requires the delivery of new membrane to the branch site. It was shown that disruption of MTs in the area of the new branch points is sufficient to promote delivery of membrane-bound cargoes that can insert membrane into the growing branch (Zakharenko and Popov 1998). It is hypothesized that this membrane required for axonal branching is derived from a specialized endosomal compartment (Hernandez-Deviez, Mackay-Sim et al. 2007). In line with these observations, spastin is also assumed to link MT dynamics to membrane trafficking (Connell, Lindon et al. 2009). Contrarily, katanin is not thought to accumulate at axonal branching sites but to be selectively active at axonal sites with local tau detachment from MTs (Qiang, Yu et al. 2006). Interestingly, the available spastin knockout (KO) mouse model did not show any

branching phenotype in cultivated hippocampal neurons, suggesting that in vivo, other mechanisms might compensate for its loss (Fassier, Tarrade et al. 2013).

In dendrites, MT-severing enzymes seem to be involved in dendritic arborization and dendritic pruning as well. Perturbation of spastin levels in *Drosophila* sensory neurons seems to result in decreased dendritic branching (Jinushi-Nakao, Arvind et al. 2007, Ye, Kim et al. 2011, Stewart, Tsubouchi et al. 2012), whereas KATNAL1 was required for the detachment of dendrites during metamorphosis (Lee, Jan et al. 2009).

Although many assumptions have been made about the possible roles of MT-severing for synaptic function and plasticity, little direct evidence is available to date. A synaptic role has been proposed for katanin, because it preferentially severs tau-deprived MTs due to its hyperphosphorylation – a condition that is associated with neurodegenerative tauopathies such as Alzheimer's disease (AD) (Sudo and Baas 2011).

Spastin has been reported to have an indirect synaptic role as well, because it severs hyperpolyglutamylated dendritic MTs due to tau-mediated TLL6 (tubulin tyrosine ligase-like 6) mislocalization with subsequent decay of MTs and mature spines, thus explaining the cognitive decline in AD patients (Zempel, Luedtke et al. 2013). However, the synaptic phenotype observed in this study seems to be a consequence of upstream pathological conditions due to the presence of amyloid-beta oligomers and hyperphosphorylated tau.

There are also some reports about cognitive impairment in HSP patients but the association between *SPG4* mutations and progressive cognitive decline is still controversial (Heinzlef, Paternotte et al. 1998, Webb, Coleman et al. 1998, White, Ince et al. 2000, Mc Monagle, Byrne et al. 2001, Tallaksen, Guichart-Gomez et al. 2003, Murphy, Gorman et al. 2009, Guthrie, Pfeffer et al. 2013). Similarly, there are controversial reports about the synaptic localization and function of the *Drosophila* orthologue of spastin (D-spastin) (Sherwood, Sun et al. 2004, Trotta, Orso et al. 2004). The AAA domains of human and *Drosophila* spastin display a 67 % aa identity, whereas the amino-terminal domains show a homology of about 40 % and less (Kammermeier, Spring et al. 2003). However, the D-spastin is a MT-severing enzyme (Roll-Mecak and Vale 2005) and overexpression of human spastin was able to rescue the defective phenotypes observed in *Drosophila* spastin null mutants (Du, Ozdowski et al. 2010). *Drosophila* is an attractive genetic model system for the study of glutamatergic synapses in the mammalian brain and spinal cord (Keshishian, Broadie et al. 1996) because their neuromuscular junctions (NMJs) use glutamate and employ ionotropic glutamate receptors homologous to vertebrate AMPA receptors (Schuster, Ultsch et al. 1991, Petersen, Fetter et al. 1997, Marrus, Portman et al. 2004). The presynaptic boutons are surrounded by a postsynaptic scaffold, and the synapses exhibit plasticity (Koh, Gramates et al. 2000).

In one of the studies, D-spastin was enriched in presynaptic boutons of NMJs and its knockdown using RNAi resulted in synaptic undergrowth, increased neurotransmission and more stable MTs

(Trotta, Orso et al. 2004). In contrast, the authors from the second study report more numerous and more clustered synaptic boutons in spastin null mutants than in wild types, a sparser MT network at synaptic sites and an impaired neurotransmitter release (Sherwood, Sun et al. 2004). *SPG4* is assumed to be a dosage-sensitive gene with pleiotropic effects caused by small changes in spastin levels, which could eventually explain these synaptic discrepancies (Riano, Martignoni et al. 2009). Interestingly, it was recently shown that the synaptic phenotype caused by spastin mutations is strongly influenced even by the surrounding temperature (Baxter, Allard et al. 2014).

In the last years increasing evidence is emerging, that dynamic MTs are important for a multitude of synaptic functions, such as spine growth (Jaworski, Kapitein et al. 2009) and memory formation (Uchida, Martel et al. 2014). In line with that, a very recent study suggests that dynamic MTs generated by MT destabilizers such as spastin play an important role during synapse remodeling in *C. elegans* (Kurup, Yan et al. 2015), which is an essential process in the development of mature neuronal circuits in many animals, including humans (Hensch 2004).

2.4 Gene targeting

The strongest evidence of a protein's function in its natural environment can be achieved through its genetic disruption in a living organism. By comparing the observed effects to an appropriate control, one can draw conclusions about the natural function of the protein (Iredale 1999). In that way, the overall impact on the organism caused by the lack of the protein can directly be observed and the cell types to which the protein is essential can be identified. Eventual compensatory effects through other proteins and cell types give direct evidence about the proteins' biological relevance. Because all clones have the same genetic background and protein disruption level, and because usually no additional external treatment is needed to induce the KO, there is no additional influence on the cellular function. In addition, directly observable consequences on vitality, fertility, morbidity or brain function do not have to be translated to a living organism. At the same time, this method is the most time and resource consuming.

2.4.1 Model organisms

Besides many established KO model organisms like the fruit fly *Drosophila melanogaster*, the nematode *C. elegans* or the zebrafish *Danio rerio*, the rodents mouse (*Mus musculus*) and rat (*Rattus norvegicus*) are among the preferred KO model organisms due to their close genetic and physiological similarities to humans (Capecchi 1994). They are useful tools to study more complex mammalian physiological systems like for instance the nervous system or the cardiovascular system.

Although neurons are a hallmark of most animals, the complexity of their organization varies strongly (see 2.1). In order to study higher brain functions such as learning, memory, empathy, anxiety and addiction, one is often restricted to use mammals as model systems. In neurobiology,

the mouse model is the preferred one because mice are easier to handle than rats, reproduce fast, and share about 99 % of genes with humans (Capecchi 1994).

2.4.2 Mouse mutagenesis

The earliest model organisms were developed by the selection and breeding of animals with specific traits. In chemical mutagenesis, DNA-damaging chemicals were used to introduce random mutations into the genome. The development of genetic technologies made it possible to produce mouse models with the desired mutations to study specific diseases and gene functions. In transgenesis a new gene randomly integrates into the genome. The DNA of interest is microinjected into the pronucleus of a zygote, which is then transferred into the uterus/oviduct of a pseudopregnant foster female. The chimeric progenitors can then directly be utilized for line expansion and testing. The relatively fast method is a good way to overexpress a gene of interest. Its disadvantage is due to the limited possibility to control the site of integration of the DNA requiring appropriate controls. The generation of loss-of-function models is possible e. g. by overexpression of dominant-negative proteins or by introducing a gene-trapping cassette.

2.4.3 Homologous recombination

In contrast to transgenesis, homologous recombination has the advantage of allowing the control of the genomic location of DNA integration. The desired DNA sequence is flanked by two large homology arms of at least 2 kb of sequence homology (Melton 2002), increasing the probability of DNA integration by homologous recombination (Lin and Sternberg 1984) and a neomycin selection cassette (Smithies, Gregg et al. 1985). The events of random DNA integration still can occur, but can partly be circumvented by introducing a negative selection cassette such as DTA (diphtheria toxin A) into the targeting vector.

The generation of genetically modified mice by homologous recombination requires the linearized targeting vector DNA to be electroporated into cultivated pluripotent embryonic stem cells (ESCs) (Evans and Kaufman 1981) and the selection for positive ESC clones with their subsequent injection into blastocysts (Bradley, Evans et al. 1984). The latter ones are then implanted into foster females by embryo transfer. Male chimeras are preferred due to the possibility of fast line expansion, leading to the fact that normally male ES cells are used. After manipulation of their genetic information the ESCs are injected into blastocysts and the chimeric offspring is used for line expansion. In contrast to transgenesis, gene targeting by using homologous recombination takes more time and expertise because it requires a more complex design of the targeting vector, the electroporation of cultivated ES cells and the selection of positive clones.

2.4.4 Conditional mutagenesis

Since about 15 % of gene KOs are developmentally lethal (www.genome.gov/12514551), spatiotemporal control of gene KO is desirable. Following the development of the Cre/loxP and the Flp/FRT technologies, it was possible to generate conditional KOs (Dymecki 1996, Sauer 1998). The 34 nt loxP (locus of X-ing over derived from bacteriophage P1) sites can be

introduced around a critical exon of a gene (Gu, Marth et al. 1994). If the two loxP sites are oriented in the same direction, the recombination results in a circular excision of the intervening sequence by Cre recombinase (Sternberg and Hamilton 1981). Thus, Cre recombinases can be used as molecular switches for the excision or inversion of a genomic sequence of interest (see Figure 14).

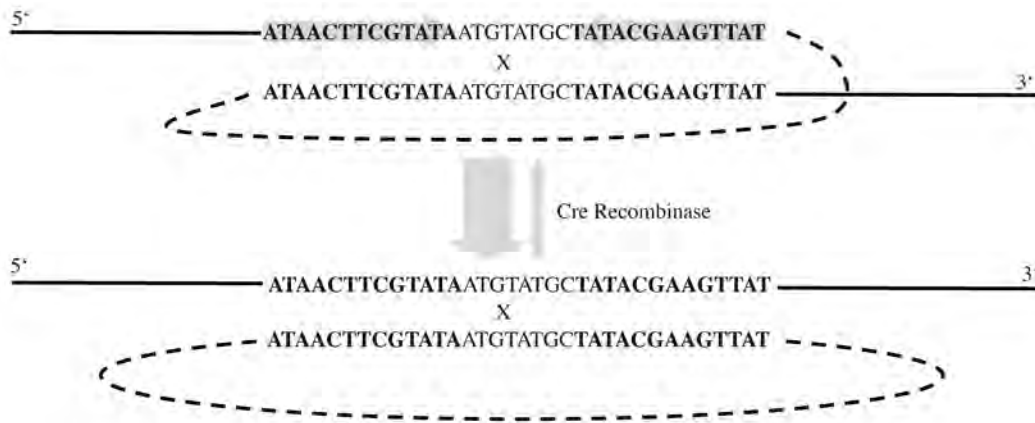


Figure 14: Mechanism of the Cre/loxP recombination system. Cre recombinase catalyzes the bidirectional recombination reaction between two palindromic loxP sites. In case of an equal orientation of the loxP sites, recombination results in the circular excision of the intervening sequence. The excision of the intervening sequence is favored over its reinsertion.

As in the Cre/loxP system, the FLP/FRT system makes use of a similar palindromic sequence (FRT) and a FLP recombinase derived from yeast. The combination of both systems allows a wide variety of possibilities in conditional mutagenesis.

2.4.5 Spatiotemporal control of Cre and FLP recombinases

The existence of the Cre/loxP and FLP/FRT systems requires conditional expression or activity of the respective recombinases in order to enable spatiotemporal control of gene KO. Several strategies were used to achieve this goal. Recombinases, which are already expressed in germ cells, lead to a recombination of loxP- or FRT-flanked genomic sequences in the whole organism. These FLP-deleter (Kranz, Fu et al. 2010) and Cre-deleter (Schwenk, Baron et al. 1995) mice are used for the generation of non-conditional, full KO progeny, for instance. In the tetracycline/doxycycline controlled transcriptional activation system, the expression of Cre can either be induced or turned off upon administration of the antibiotics tetracycline or doxycycline (Utomo, Nikitin et al. 1999).

The tamoxifen inducible system is another way to control Cre recombinase activity (Feil, Wagner et al. 1997, Hayashi and McMahon 2002). In this case, a BAC-transgene or a knock-in-allele carries Cre recombinase, which is fused to the ligand-binding domain of the estrogen receptor (ERT2). By three point mutations, the latter one is rendered unresponsive to its natural ligand estrogen. The Cre-ERT2 fusion protein is constitutively expressed but Cre activity is blocked by the binding to heat shock proteins. Upon administration of the synthetic estrogen derivative 4-OH-

tamoxifen, the heat shock proteins dissociate from the ERT2 domain and allow the activated Cre domain to cut loxP flanked DNA segments.

Another possibility to conditionally knock out genes is by the usage of a specific promoter, which is only active in the cell-type of interest and/or at certain time points to control Cre expression. The advantage of this system is the fact that no additional treatment with either tamoxifen or doxycycline/tetracycline is necessary, which might impact physiological functions (e. g. estrogen plays a role in the hippocampal memory; tetracycline influences the composition of enteric bacteria) (Woolley 1998, Silva, Mello et al. 2000).

In line with that, many promoters have been used to generate mouse models for brain-specific expression of Cre at different stages of development (Nestin-Cre, Emx-Cre, CamKII α -Cre). Nestin-Cre mice were widely used for the Cre-mediated excision of loxP-flanked genes in the central and peripheral nervous systems including neuronal and glial cell precursors (Tronche, Kellendonk et al. 1999). The EMX1-Cre knock-in mouse starts to express the Cre recombinase during the development of the forebrain. Cre is specifically expressed in progenitor cells of pyramidal neurons of the cortex, hippocampus and olfactory bulb (Iwasato, Datwani et al. 2000).

The activity of the murine CamKII α promoter has also been widely studied and the expression of the CamKII α gene has been described to be mainly restricted to the postnatal forebrain (Burgin, Waxham et al. 1990, Mayford, Bach et al. 1996). In line with that, several transgenic CamKII α -Cre mouse models were developed (Tsien, Chen et al. 1996, Minichiello, Korte et al. 1999, Casanova, Fehsenfeld et al. 2001). Nevertheless, for many of these tissue-specific promoter-driven Cre mice, a background expression has been reported in several tissues, with other phenotypes unrelated to Cre activity (Liang, Hippenmeyer et al. 2012, Zhang, Dublin et al. 2013). As an alternative, Cre can be directly introduced by injection using a viral vector (Anton and Graham 1995).

In addition to in situ hybridization and immunohistochemistry in order to visualize expression of Cre RNA or protein, useful mouse models have been developed as genetic tools to visualize Cre activity. In this case, a reporter gene/cDNA, such as LacZ (Soriano 1999) or GFP (Kawamoto, Niwa et al. 2000) is knocked-in into the ROSA26 locus and flanked by loxP sites but not expressed. Only in presence of Cre, the reporter gene is remodified such that it can be expressed and visualized either by LacZ staining or by fluorescence microscopy.

2.4.6 Genome engineering: new approaches in mutagenesis

The generation of mouse models using ES cell-based approaches is time-consuming and requires specific expertise. Genome editing is a recently discovered alternative type of genetic engineering in which genomic DNA can be modified using engineered nucleases. These methods employ endonucleases capable of inducing double-strand breaks (DSB) at desired locations in the chromosomal DNA. The induced DSBs are repaired through the two major cellular DNA

damage repair pathways nonhomologous end-joining (NHEJ) or homology-directed repair (HDR), resulting in targeted mutations.

Currently, there are four families of engineered nucleases being used: meganucleases (Epinat, Arnould et al. 2003), zinc finger nucleases (ZFNs), transcription activator-like effector-based nucleases (TALEN), and the CRISPR-Cas system (clustered regularly interspaced short palindromic repeats with the CRISPR associated (Cas) nuclease). ZFNs and TALE nucleases are chimeric proteins composed of sequence-specific DNA-binding modules, which are fused to the non-specific Fok1 nuclease (Carroll 2011, Cermak, Doyle et al. 2011). In the CRISPR-Cas system, an RNA molecule navigates the Cas nuclease to the genomic target site (Wang, Yang et al. 2013).

2.5 Aim of this study

Despite the fact that a lot of research has been conducted in the field of microtubule-severing enzymes, the knowledge about their role in adult brain is rather limited. As described above, microtubule-severing enzymes are involved in a myriad of different physiological tasks whereof one is the development of neurons. Since there is increasingly more evidence that MTs are not only confined to the dendritic compartment but can also enter spines, the question arises whether MT-severing enzymes play a role in the regulation of this phenomenon in adult neurons.

The available general spastin knockout mouse models show a developmental phenotype and a katanin p60 knockout mouse has not been described to date.

Thus, this study aimed at initiating a more systematic and comprehensive approach, which would enable to investigate the loss-of-functions of microtubule-severing enzymes in adult and normally developed neurons.

In order to achieve this aim, a conditional targeting approach for the spastin and katanin p60 genes had to be established in the mouse model, followed by the confirmation and initial characterization of the gene losses.

3 MATERIAL AND METHODS

3.1 Material

3.1.1 Chemicals

Unless stated otherwise, all chemicals used in the experiments of this work were of the highest degree of purity (pro analysi) and were obtained from the following suppliers: SIGMA, Carl Roth GmbH & Co. KG, Roche, AppliChem, LifeTechnologies, VWR and Merck. An overview list with the supplier information can be found in section 7.4.

3.1.2 Enzymes

Enzymes were purchased from suppliers listed in Table 2. The enzyme buffers were provided by the supplier.

Table 2: Enzymes used in this thesis and their suppliers.

| Enzymes | Company |
|---|---|
| DNA Polymerase I, Large (Klenow) Fragment | New England Biolabs |
| Restriction endonucleases (EcoRV, AsiSI) | Roche , LifeTechnologies, New England Biolabs |
| Phusion High Fidelity DNA Polymerase | Thermo Fisher Scientific |
| PfuTurbo-DNA-polymerase | Stratagene |
| T4 DNA Ligase | LifeTechnologies |
| FastAP | LifeTechnologies |
| T4 PNK | LifeTechnologies |
| Dreamtaq | LifeTechnologies |
| rAPid Alkaline Phosphatase | Roche |

3.1.3 Other Material

Plasticware and goods for single-use were obtained from Sarstedt, Carl Roth GmbH & Co. KG, Greiner and Thermo Fisher Scientific.

3.1.4 Software

Software used in this thesis is listed in Table 3. Images were acquired using proprietary software from Leica, Olympus, Carl Zeiss AG and Visitron Systems. ImageJ (Schneider, Rasband et al. 2012) and Fiji (Schindelin, Arganda-Carreras et al. 2012) were used for image processing and kymograph plotting. MetaMorph 7.1 was used for particle tracking and kymograph plotting. Prism (GraphPad) was used for statistical analysis. Adobe Illustrator and InDesign were used to assemble figures and Microsoft Word and Adobe InDesign were used to write this thesis. Graphs were plotted with Microsoft Excel and Prism and processed with Adobe InDesign. For planning and evaluation of molecular cloning SeqMan, EditSeq and SeqBuilder packages of DNASTAR Lasergene were used. Sequence results were evaluated using the Macintosh software 4Peaks. For sequence alignment, the ClustalW2 method was used. TierBase (TBASE) was used for mouse colony management. EndNote was used for reference management.

Table 3: Software used in this thesis.

| Software | Source Company | Purpose |
|--|-------------------------------|--|
| Proprietary software for image acquisition | Olympus | Image acquisition |
| | Visitron Systems | |
| | Leica | |
| | Metavue | |
| TierBase (TBase) | | Mouse colony management |
| Ethovision XT 6.1 | Noldus Technology | Automated analysis of animal behavior |
| ImageJ Fiji | National Institutes of Health | Image processing |
| 4Peaks | | |
| EndNote | Thomson Reuters Corp | Reference management |
| SeqMan, EditSeq and SeqBuilder packages of DNASTAR | Lasergene | Planning and evaluation of molecular cloning |
| SPSS | IBM | Statistical analysis and graph plotting |
| Prism | GraphPad | |
| Adobe Illustrator and InDesign | Adobe Systems | Figure assembly and thesis writing |
| Microsoft Word | Microsoft | Thesis writing |
| Microsoft Excel | | Graph plotting |
| MetaMorph 7.1 | Universal Imaging | Image analysis |

3.1.5 Kits

- ECL kit (Thermo Fisher Scientific)
- QuickExtract- DNA Extraction Solution (Epicentre)
- QIAprep Maxiprep kit (Qiagen)
- Megaprime DNA Labeling System (Amersham)
- T4 DNA ligation kit (Thermo Fisher Scientific)
- BCA Protein Assay kit (Thermo Fisher Scientific)
- NucleoSpin® Gel and PCR Clean-up (Machery Nagel)
- NucleoSpin® Plasmid QuickPure (Machery Nagel)

3.1.6 Molecular weight markers

- HyperLadder I and HyperLadder V from Biorad
- Precision Plus Protein™ Dual Color Standards from Biorad

3.1.7 Antibodies

Primary and secondary antibodies used in this thesis are listed in Table 4 and in Table 5, respectively. Antibodies were diluted in 1 x PBS (for WB) or permeabilization buffer (for ICC). Working dilutions were stored at 4 °C and stock solutions were stored according to manufacturer's instructions.

Table 4: Primary antibodies used for Western Blotting (WB), immunohistochemistry (IHC), immunoprecipitations (IP) and immunocytochemistry (ICC) including host species, dilution and source company.

| Antibody | Host species | Dilution | Source |
|--------------------------------|------------------------|----------------------------------|--------------------------|
| α-acetylated tubulin | mouse clone 6-11B-1 | 1:5,000 WB | SIGMA |
| α-β –actin | mouse clone AC-15 | 1:3,500 WB | SIGMA |
| α-β –actin phalloidin Atto-488 | - | 1:500 ICC | SIGMA |
| α-EB3 | rat clone K53 | 1:1,000 WB; IP | Abcam |
| α-GAPDH | mouse clone 6C5 | 1:10,000 WB | Abcam |
| α-GFP | Rabbit polyclonal | 1:5,000 WB | SIGMA |
| α-GluR2 | mouse clone 6C4 | 1:1,000 WB 1:200 IHC | Millipore |
| α-katanin M13 | goat polyclonal | 1:500 WB | Santa Cruz Biotechnology |
| α-kif2a | rabbit polyclonal | 1:10,000 WB | Abcam |
| α-MAP2 | Rabbit polyclonal | 1:2,000 ICC | Synaptic systems |
| α-NR2A | Rabbit clone epr7063 | 1:2000 WB | epitomics |
| α-NR2B | mouse monoclonal | 1:500 WB | Abcam |
| α-NSE | chicken polyclonal | 1:5,000 WB | Novus Biologicals |
| α-polyglutamylated tubulin | mouse clone B3 | 1:3,000 WB 1:200 IHC/ICC | SIGMA |
| α-PAN-cadherin | mouse clone CH-19 | 1:2,000 WB | Abcam |
| α-PSD-95 | mouse clone 7E3-1B8 | 1:2,000 WB; IP | ABR |
| α-SNAP25 | mouse clone 20/SNAP-25 | 1:3,000 WB | BD Biosciences |
| α-spastin 6C6 | mouse clone 6C6 | 1:500 WB 1:50 ICC | Abcam |
| α-spastin 6C6 | mouse clone 6C6 | 1:100 (in 1% BSA) WB 1:50 ICC | Santa Cruz Biotechnology |
| α-synaptophysin | guinea pig polyclonal | 1:1,000 WB 1: 500 IHC | Synaptic systems |
| α-tau | guinea pig polyclonal | 1:1,000 WB | Synaptic systems |

Table 5: Secondary antibodies used for Western Blotting (WB) and immunocytochemistry (ICC) experiments in this thesis including conjugation, host species, dilution and source company.

| Antibody | conjugation | Host species | Dilution | Source |
|--------------|-------------|--------------|-------------|--------------------------|
| α-goat | Alexa 488 | donkey | 1:1,000 ICC | Dianova |
| α-mouse | Alexa 488 | donkey | 1:1,000 ICC | Dianova |
| α-mouse | Cy3 | donkey | 1:500 ICC | Dianova |
| α-mouse | Cy5 | donkey | 1:500 ICC | Dianova |
| α-rabbit | Cy5 | donkey | 1:500 ICC | Dianova |
| α-chicken | HRP | donkey | 1:10,000 WB | Thermo Fisher Scientific |
| α-goat | HRP | donkey | 1:1,000 WB | Dianova |
| α-guinea pig | HRP | donkey | 1:1,000 WB | Dianova |
| α-mouse | HRP | goat | 1:10,000 WB | Dianova |

| | | | | |
|----------|-----|------|-------------|---------|
| α-rabbit | HRP | goat | 1:10,000 WB | Dianova |
|----------|-----|------|-------------|---------|

3.1.8 Vectors and constructs

The vectors and constructs used for this thesis are listed in Table 6.

Table 6: Vectors and constructs used in this study.

| Vector/construct | Usage | Sources |
|--------------------------|--|---|
| pEGFP-C-spastin (ΔM1) | transfection of HEK cells and neurons in order to test anti-spastin antibodies and to study expression pattern | Dr. Peter W. Baas (Philadelphia, USA) |
| pAcGFP-C2-katanin | transfection of HEK cells and neurons in order to test anti-Katanin antibodies and to study expression pattern | XhoI and DNA Polymerase I, Large (Klenow) Fragment were used for restriction digestion of the pEGFP-C2 vector. Ligation was made with dephosphorylated katanin PCR amplicon (using Primers P5 and P6) |
| pAcGFP-C2-dn-katanin | transfection of HEK cells and neurons | fusion PCR mutagenesis using pAcGFP-C2-katanin and primers containing the target mutation |
| pEGFP-C1-3 and pAcGFP-C2 | expression of eGFP in eukaryotic cells; source for cloning of EGFP tagged proteins | Clontech |
| pmRFP | expression of mRFP fusion proteins in eukaryotic cells, volume marker of transfected cells | Dr. R. Y. Tsien (San Diego, USA) |
| pEGFP-EB3 | live cell imaging of EGFP-EB3 comet entry into spines of wt and spastin deficient neurons | The construct was kindly provided by Dr. Matthias Kneussel (ZMNH, Hamburg) |
| pGEM-T Easy | cloning | Promega |
| pBluescript II SK (+) | cloning | Agilent |

3.1.9 Bacterial strains

The Escherichia (E.) coli strains that were used for the present work and are listed below in Table 7.

Table 7: Bacterial strains used for this study.

| Strain name | genotype | source | Purpose |
|-------------|---|------------|---------|
| DH5 α | F- Φ80lacZΔM15 Δ(lacZYA-argF) U169 recA1 endA1 hsdR17(rk-, mk+) phoA supE44 thi-1 gyrA96 relA1 λ- | Invitrogen | cloning |
| XL1-Blue | recA1 endA1 gyrA96 thi-1 hsdR17 supE44 relA1 lac [F' proAB lacIqZΔM15 Tn10 (Tetr) | Stratagene | cloning |

3.1.10 Cell lines

HEK293-TN cells Human embryonic kidney cell line CRL-11268 (ATCC)

3.1.11 Buffers and media

Water was purified by a Milli-Q-System (Millipore) to the degree of purity "aqua bidestillatus" and it was used to produce solutions, media and buffers. For the adjustment of pH values NaOH, KOH or HCl were used. For sterilization of solutions, the autoclaving method at 121° C and 2.1 bar over a time period of 20 min was used. In other cases, solutions were filtered using filter tips with a pore size of 0.22 µm (Millipore).

Media for cell culture were purchased either from LifeTechnologies or Lonza. Standard solutions were produced either according to (Sambrook, Fritsch et al. 1989) or according to the manufacturer's instructions.

| |
|--|
| Blocking Buffer (Immunocytochemistry): 1 % (w/v) Bovine serum albumin (BSA) in 1x PBS |
| Blocking Buffer (Western Blotting): 5 % (w/v) skimmed milk powder in 1x TBST |
| Detergent solution (LacZ staining): 0.1 M phosphate buffer pH 7.3, 2 mM MgCl ₂ , 0.01 % sodiumdesoxycholate, 0.02 % Nonidet (Igepal), dissolved in H ₂ O |
| 6 x DNA loading buffer: 7.5 g Ficoll, 0.125 g bromophenol blue, ad 50 mL H ₂ O; the aliquots were stored at -20 °C |
| 2 x HBS Hepes buffered saline: 1.6 g NaCl, 0.074 g KCl, 0.027 g Na ₂ HPO ₄ *2H ₂ O, 0.2 g dextrose, 1 g HEPES, ad 100 mL H ₂ O, pH 7.05 (NaOH), sterile filtration, storage of aliquots at -20 °C |
| HEK cell medium: 500 mL D-MEM (+ 4,500 mg/L glucose, + GlutaMAX™ I, - pyruvate), 5 mL penicillin/streptomycin solution (10,000 U/ml), 50 mL FBS |
| HEPES buffer (transfection): 10 mM HEPES (pH 7.4), 135 mM NaCl, 5 mM KCl, 2 mM CaCl ₂ , 2 mM MgCl ₂ , 15 mM glucose |
| IMAC buffer: 20 mM HEPES, 100 mM K-Acetate, 40 mM KCl, 5 mM EGTA, 5 mM MgCl ₂ , pH 7.2 Freshly supplemented with protease inhibitor (Roche cOmplete), 2 mM Mg-ATP, 5 mM DTT and 1 mM PMSF |
| IP-Buffer: 50 mM Tris, 150 mM NaCl, 5 mM MgCl ₂ , 1 mM PMSF, pH 7.5 |
| LB (Luria Bertani) medium: 10 g tryptone, 5 g yeast extract, 5 g NaCl, ad 1,000 mL H ₂ O, pH 7.5 (NaOH), autoclave |
| LB agar plates: LB medium, 1.5% (w/v) agar, autoclave, cool down to 50°C |

MATERIAL AND METHODS

| |
|---|
| Antibiotic supplementation: ampicillin (100 µg/mL), kanamycin (50 µg/mL) |
| Lysis buffer: 1 % Triton X-100, 1 mM PMSF, cOmplete protease inhibitor (Roche) in PBS |
| Mini prep solution I: 50 mM D-glucose, 20 mM Tris HCl (pH 8.0), 2.5 mM EDTA (pH 8.0) |
| Mini prep solution II: 1 % (w/v) SDS, 0.2 M NaOH |
| Mini prep solution III: 67.4 mL 5 M potassium acetate, 12.95 mL 100 % acetic acid, ad 100 mL H ₂ O |
| Neuronal culture medium: 500 mL Neurobasal medium (A) (LifeTechnologies), 2 mM L-glutamine, 25 µg/mL pyruvate, 5 mL penicillin/streptomycine solution (10000 U/ mL) 2 % (v/v) B27 |
| Paraformaldehyde solution: 40 g paraformaldehyde, 40 g sucrose, ad 1,000 mL 1 x PBS, pH 7.2 (NaOH); the aliquots were stored at -20 °C. |
| Phosphate buffered saline (PBS): 8 g NaCl, 0.2 g KCl, 1.44 g Na ₂ HPO ₄ , 0.24 KH ₂ PO ₄ ; ad 1,000 mL H ₂ O; pH 7,5 (autoclave) |
| 10 x SDS PAGE running buffer: 250 mM Tris, 2.5 M glycine, 1 % (w/v) SDS, pH 8.3 (HCl) |
| 4x SDS sample buffer: 220 mM Tris (pH 6.8), 40 % (v/v) glycerol; 8 % (w/v) SDS, 0.8 % (w/v) bromophenol blue; 100µL of loading buffer were supplemented with 8 µL β-mercaptoethanol before use |
| SOB buffer: 2 % (w/v) bacto tryptone, 0.5 % (w/v) yeast extract, 10 mM NaCl, 2.5 mM KCl, 10 mM MgCl ₂ , 10 mM MgSO ₄ , pH 6.7 (KOH) |
| SOC medium: 2 % (w/v) bacto tryptone, 0.5 % (w/v) yeast extract, 10 mM NaCl, 2.5 mM KCl, 10 mM MgCl ₂ , 10 mM MgSO ₄ , 200 mM glucose, pH 6.7 (KOH) |
| 20 x SSPE (Southern Blotting): 3 M NaCl, 0.2 M NaH ₂ PO ₄ , 0.02 M EDTA, pH 7.4 (adjusted with NaOH) |
| 20 x SSC (Southern Blotting): 3 M NaCl, 0.3 M Trisodium citrate (Na ₃ C ₆ H ₅ O ₇), autoclave |
| Speed hyb II (Southern Blotting): 7 % (w/v) SDS, 10 % (w/v) polyethylene glycol 6000, 1.5 x SSPE, 200 µg/mL denatured herring sperm-DNA |
| Herring sperm-DNA (Southern Blotting): 10 mg/mL in H ₂ O, boil in microwave 3 x, cool on ice, 15 min ultra sound, aliquots were frozen in 1 mL samples |

| |
|---|
| <p>Washing buffer A (Southern Blotting): 2 x SSC, 0.5 % SDS</p> <p>Washing buffer B (Southern Blotting): 0.2 x SSC, 0.1 x SDS</p> |
| <p>Staining solution for LacZ staining: 1 mg/ml X-Gal, 5 mM potassium ferricyanide $K_3[Fe(CN)_6]$, 5 mM potassiumferrocyanide, $K_4[Fe(CN)_6] \cdot 3 H_2O$ dissolved in detergent solution</p> |
| <p>Stripping Buffer (Western Blotting): 25 mM Glycine, 1 % SDS, pH 2.0</p> |
| <p>Sucrose buffer A (synaptosomal fractionation): 320 mM sucrose, 1 mM $NaHCO_3$, 1 mM $MgCl_2$, 500 μM $CaCl_2$, 5 mM EDTA pH 8, 1 μM PMSF, supplemented with cOmplete protease inhibitor (Roche, Mannheim, Germany) without EDTA</p> <p>Sucrose buffer B (synaptosomal fractionation): 320 mM sucrose, 1 mM $NaHCO_3$</p> <p>Sucrose gradient from top to bottom (synaptosomal fractionation; 10 mL each): 1.2 M sucrose and 4 μL 1 M $NaHCO_3$ 1 M sucrose and 4 μL 1 M $NaHCO_3$ 0.85 M sucrose and 4 μL 1 M $NaHCO_3$</p> |
| <p>50 x TAE buffer: 242 g Tris, 57.1 mL acetic acid, 100 mL 0.5 M EDTA (pH 8.0), ad 1,000 mL H_2O</p> |
| <p>Tail-tip lysis buffer: 0.5 % SDS, 50 mM Tris-HCl, pH 8.0, 100 mM NaCl, 50 mM EDTA</p> |
| <p>TBS (10 x): 100 mM Tris (pH 8.0), 1.5 M NaCl</p> |
| <p>TBST (10 x): 0.5 % (v/v) Tween 20, dissolved in 10 x TBS</p> |
| <p>TE buffer: 10 mM Tris-HCl (pH 8.0), 0.1 mM EDTA, in H_2O</p> |
| <p>Transfer Buffer (Western Blotting): 20 % (v/v) methanol, 48 mM Tris, 39 mM glycine, 0.037 % SDS</p> |

3.1.12 Machines

Agarose gel electrophoresis system: Owl Separation Systems B2 and B1A (Thermo Fisher)

Bacterial culture incubator: Innova 3200 Platform Shaker (New Brunswick Scientific)

Cell culture incubators: HeraCell 150/150i (Thermo Fisher Scientific)

Cell culture sterile hood: SterilGARD Class II TypA/B3 (Baker Company)

Centrifuges: Ultracentrifuge L7 (Beckman Coulter), 5417 C (Eppendorf), MC6 Minifuge (Sarstedt)

Centrifuge rotors: TLA 100.3, JA-10, JA-14, JA-25.5, SW-40Ti (Beckman Coulter)
Chemiluminescence reader: (Intas Science Imaging GmbH)
Confocal microscopes: Olympus Fluoview F1000 (Olympus), Olympus Fluoview Software Version 2.1b (Olympus), Leica DM IRBE (Leica Microsystems)
Cryostat: Leica CM3050S (Leica)
DNA gel imager: Intas Gel Imager (Intas)
Epifluorescent microscope: Zeiss Axiovert 200M (Zeiss) combined with a Sony CCD-Camera 12.0 Monochrome w/o IR-18 (Diagnostic Instruments Inc., Sterlings Heights, USA). Imaging software MetaVue (Visitron Systems, Puchheim, Germany)
Fluorescent image analyzer: FLA-3000 (Fujifilm)
Freezer (-20 °C): G 3513 Comfort (Liebherr)
Freezer (-80 °C): MDF-U74V ultra low temperature freezer (Sanyo)
Homogenizer: PotterS (Sartorius)
Laboratory scales: Sartorius LC-6201 (Sartorius), Mettler AE240 (Mettler-Toledo)
Microtiter plate reader: Infinite 200 PRO NanoQuant (Tecan)
Overhead shaker: Suspension mixer CMV-1S (Fröber Labortechnik)
PCR machines: PTC-200 Peltier Thermal Cycler (MJ Research)
pH-meter: SevenEasy (Mettler-Toledo)
Platform shaker: Promax 2020 (Heidolph Instruments), WS5 (Edmund Bühler GmbH)
Power supplies: Power Pac 200 (BioRad)
Refrigerator: G 5216 Comfort (Liebherr)
Rolling incubator: TRM5.V (IDL GmbH & Co. KG)
SDS-PAGE chambers: Mini-PROTEAN Tetra Electrophoresis System (Bio-Rad)
Semi-dry blotter: V20 SemiDry Blotter (SCIE-PLAS)
Sequencer: ABI Prism 377 DNA Sequencer (Applied Biosystems)
Spectrophotometer: NanoQuant plate for Infinite 200 PRO NanoQuant (Tecan)
Spinning disk microscope: Visitron Systems Spinning Live Cell Confocal. 4 solid-state lasers: 405, 488, 561 and 647. The microscope was combined with two charge-coupled device EM-CCD cameras (Hamamatsu Photonics) and with an optical image splitter.
Thermomixer: Thermomixer 5436 (Eppendorf)
Transmission microscope: Zeiss Axiovert 25 (Zeiss)
Vibratome: Leica VT 1000S
Vortex: REAX 2000 (Heidolph Instruments)
Water bath: GFL-1012 (GFL)
Water purification system: Milli-Q-System (Millipore)
Western Blot chemiluminescence reader: Intas ChemoCam (Intas).
Western Blotting system: Mini Trans-Blot Cell (Bio-Rad)

3.1.13 Oligonucleotides

The following unmodified desoxyoligonucleotides were obtained from MWG Biotech in high purity salt-free quality (HPSF):

Table 8: Oligonucleotides used for this thesis.

| Name | Sequence (5' – 3') | usage |
|------|--|------------------------------------|
| P5 | CCATGAGTCTTCAAATGATTGTTGAGAATGTAAAATTG | Katanin cloning |
| P6 | CTACTAGCATGATCCAAACTCAACTATCCATTTTC | |
| P9 | TGTTGGCCACCTGGCCTGGAGCGACCCTTCTAGCTAAAGC AGTTG | Katanin mutagenesis |
| P10 | CAACTGCTTTAGCTAGAAGGGTCGCTCCAGTGCCAGGTGGGC CAACCA | |
| P83 | ATGCGCTGGGCTCTATGGCTTCTG | CamKII α -Cre genotyping |
| P84 | TGCACACCTCCCTCTGCATGCACG | |
| P20 | AGCTTTACATTCCAAGAAGATACATTTTAATAGTGTCAT | Spastin 5' southern probe |
| P21 | AATAGATCCTTCCTTCATCTTTGGCCCA | |
| P93 | TCAAGGCCATTATCCTTAGAAAGTT | Katanin genotyping |
| P94 | CAAGATGGCTCATGCAGATAGATGTA | |
| P170 | ACTTTGGCTTCTGTTTATCTCCTTTCTCT | Spastin genotyping |
| P41 | AAGTCATGGCAGTCTTTCTGGCT | |
| P89 | CACATGGTGGCTCATAACCATTTA | Cre genotyping |
| P169 | ATTTGCAAAAACACTACTTGCTATTAATCC | |
| P142 | AGTTTCGTTCACTCA | Flp genotyping |
| P143 | TCGACCAGTTTAGTT | |
| P155 | GTTGCGCTAAAGAAGTATATGTGCC | Long-range PCR 5' katanin |
| P154 | GTCACTGCAGTTTAAATACAAGACG | |
| P87 | CCAAGTACCTTGGGCAAGAACAT | Long-range PCR 3' spastin |
| P123 | CAGCTGTGTTGCTGAAAATGAAGTATGGAA | |
| P23 | TCTACATCCCCTCATTAGTGCAATACAT | Long-range PCR 3' katanin |
| P61 | TACATTATACGAAGTTATGGTCT | |
| P86 | GAGATGGCGCAACGCAATTAAT | Long-range PCR 3' katanin |
| P122 | TGACAAGCAGGGCTCTAAGTGGAG | |

3.2 Cell biology

3.2.1 Primary hippocampal cell culture

Cultured hippocampal neurons were obtained from embryonic day E16 to postnatal day P2 mice. After sacrificing by decapitation, the hippocampi were collected in ice-cold PBS, supplemented with 10 mM glucose. For the separation of the cells, the neuronal tissue was incubated in a 0.05 % trypsin solution at 37 °C for 10 min. After 2 washing steps with Dulbecco's Modified Eagle Medium DMEM/F12-complete (Invitrogen), the cells were separated by trituration with fire smoothed polished Pasteur pipettes using the same medium. 140,000 cells were plated in DMEM/F12-complete on 12 mm glass coverslips.

The latter ones were previously coated with 1.5 μ g/mL poly-L-lysine in H₂O (SIGMA) o/n at 4 °C and then washed twice with H₂O.

The cultures were incubated under a vapor-saturated atmosphere at 37 °C and 5 % (v/v) CO₂ in an incubator.

In order to remove damaged cells and cell debris, the medium was exchanged after 4 to 5 hours by neurobasal medium. After 3 days in vitro (DIV3), 1.5 µM 1-β-D arabinofuranosyl-cytosine (SIGMA) was added to the cultures in order to restrict the proliferation of astrocytes. One third of the culture medium was exchanged on a weekly basis.

3.2.2 HEK293-TN-cell culture

All cell culture works were done under sterile conditions; whereby sterile hood, sterile reagents and sterile dishes were used. The HEK293-TN-cells were cultivated in 100 mm cell culture dishes (Sarstedt) at 37 °C and 5 % (v/v) CO₂ in a vapor-saturated atmosphere. Every two to three days, before the cells reached confluency, they were split in a 1:4 to 1:8 ratio. After washing once with 10 mL PBS the cells were incubated with 1 x trypsin-EDTA solution (Invitrogen) for 2 min at 37 °C and detached from the cell culture dish. After the addition of HEK293-TN-medium the proteolytic activity of trypsin was stopped. By pipetting up and down the cells were separated. Then, the required amount of cells was transferred into a cell culture dish containing the required volume of fresh and prewarmed cell culture medium.

3.2.3 Immunocytochemistry

Neurons growing on 12 mm glass slides were washed twice with 500 µL 1 x PBS and subsequently fixed in 500 µL 4 % (w/v) paraformaldehyde and 4 % (w/v) sucrose in 1 x PBS for 12 min. The cells were then rewashed 3 times with 500 µL PBS and permeabilized for 4 min using 500 µL PBS supplemented with 0.25 % (v/v) Triton-X-100. In order to reduce non-specific binding of the antibodies in the following steps, the permeabilized cells were blocked with 1 % BSA (bovine serum albumin) or a 10 % serum solution from goat or from donkey (both from SIGMA), dependent on the host species of the secondary antibodies to be used. Then the cells were incubated with the corresponding primary antibody in the same blocking solution for 2 hours at room temperature. After three 5-minute washing steps using 500 µL of 1 x PBS, the cells were incubated with a secondary fluorescent antibody that was diluted in blocking solution for 45 min in a dark humid chamber. After three additional 5-minute washing steps in 1x PBS, the glass coverslips were dipped shortly into H₂O and mounted onto glass slides using AquaPoly-Mount (Polysciences). After a drying period of 24 h at room temperature, the stained cells could be used for microscopical analysis or they were stored at 4 °C in the dark.

3.2.4 Immunohistochemistry

Brains were isolated and fixed in a 4 % PFA/PBS solution for 4 hours at 4 °C with a following cryopreservation in a 30 % sucrose solution for 2 days. 30 µm brain sections were generated using a vibratome (Leica VT 1000S) and mounted onto Superfrost Plus microscope slides (Thermo Fisher Scientific). The sections were washed three times in PBS and permeabilized with 0.4 % Triton-X-100 (v/v)/PBS for 20 min. To minimize

nonspecific antibody binding, the sections were incubated at room temperature with blocking buffer (4 % goat serum in 0.1 % Triton-X-100 in PBS) for 1 hour. After three washing steps using PBS, the sections were incubated for 2 hours with primary antibodies diluted in blocking buffer in a humid chamber at 4 °C. Next, the sections were washed three times with PBS. They were then incubated with secondary antibodies diluted in the blocking buffer in the dark at room temperature for 1 hour. After rinsing three times with PBS the sections were mounted using AquaPolyMount (Polysciences) and dried overnight. They were stored at 4 °C in the dark until further usage.

3.2.5 Transfection HEK 293TN-cells

HEK293-TN-cells were transfected using the calcium phosphate method (Chen and Okayama, 1987). One day before transfection, cells were dissociated and plated onto 100 mm cell culture dishes and were transfected at a confluency of 40 to 50 % on the next day. For a 100 mm cell culture dish, 12 µg of plasmid-DNA were diluted in 225 µL H₂O and mixed with 75 µL of 1 M CaCl₂. This solution was slowly mixed with 300 µL 2 x HBS using slow vortexing and incubated for 15 min at room temperature. Then, the transfection mixture was distributed evenly onto the HEK293-TN-Medium. After 8 to 24 h incubation at 37 °C and 5 % CO₂ (v/v) the cells could be used for analysis.

3.2.6 Transfection of neurons

Primary neuronal cultures were also transfected using the calcium phosphate transfection method, with slight modifications. After 7 to 12 days in vitro (DIV7-12), 2 µg of plasmid-DNA were diluted in 18.75 µL H₂O and mixed with 6.25 µL 1 M CaCl₂. In case of usage of more than one construct per transfection, 1 µg of plasmid-DNA per construct was used. This solution was slowly pipetted to 25 µL 2 x HBS under mild vortexing and incubated for 15 min at room temperature.

700 µL of preconditioned medium were kept aside at 37 °C, and the transfection mixture was pipetted evenly to the cells with the remaining medium. After one hour in the cell culture hood and 5 % (v/v) CO₂, the medium with the transfection mixture was discarded and the cells were washed with 500 µL of prewarmed HEPES-buffer. Then the preconditioned medium was supplemented with 300 µL fresh neurobasal medium and the mixture was added back to the transfected cells. Depending on the construct, the expression time was between 8 and 72 hours.

3.2.7 LacZ staining

Animals were anesthetized by CO₂ oxygen miscellaneous gas and then decapitated. The tissue was fixed in 1 % PFA at 4 °C overnight and then the sections were washed three times with 2 mM MgCl₂ in PBS. After a 10 min incubation in detergent solution (0,1 M phosphate buffer pH 7.3, 2 mM MgCl₂, 0.01 % sodium- desoxycholate, 0.02 % Nonidet (Igepal) in H₂O) the tissue of interest was incubated for 16 h in X-Gal-staining solution (1 mg/ml X-Gal, 5 mM potassium ferricyanide, 5 mM potassium ferrocyanide in detergent solution) at 30 °C. The tissue was postfixed for 1 hour in 4 % paraformaldehyde, then rinsed once with PBS and then mounted with

mowiol mounting medium (100 mM Tris pH 8.5, 10 % (w/v) Mowiol 4-88, 25 % glycerol). Whole embryos were postfixed in 4 % PFA overnight and stored in 50 % glycerol in PBS.

3.2.8 Nissl staining

In order to visualize neuronal cell bodies and indirectly measure the number of cells in a section of a certain brain region (e. g. CA1 or CA3 of the hippocampus), the Nissl staining was used as a fast and reliable method (Nissl 1984).

After transcardial perfusion of the mice using PBS and a 4 % PFA/PBS solution, the brains were isolated and post-fixed in the latter solution for 4 hours and 4 °C, followed by cryopreservation in a 30 % sucrose solution for 2 days.

In order to stain the regions of interest, 30 µm coronal or sagittal brain cryosections were generated using a cryostat (Leica), mounted on Superfrost™ Plus microscope slides (Thermo Fisher Scientific) and air-dried for two hours. Then, the brain sections were submerged sequentially in a series of bath solutions, summarized in Table 9:

Table 9: sequence of bath solutions used for Nissl staining.

| Step | Reagent/solution | Time (min) |
|------|---|------------|
| 1 | 95 % ethanol | 15 |
| 2 | 70 % ethanol | 1 |
| 3 | 50 % ethanol | 1 |
| 4 | H ₂ O | 2 |
| 5 | H ₂ O | 1 |
| 6 | cresyl violet staining solution | 2 |
| 7 | H ₂ O | 1 |
| 8 | 50 % ethanol | 1 |
| 9 | 70 % acid ethanol (1 mL anhydrous acetic acid in 100 mL of 70 % ethanol) | 2 |
| 10 | 95 % ethanol | 2 |
| 11 | 95 % ethanol | 0.1 |
| 12 | 100 % ethanol | 1 |
| 13 | Histo-Clear | 5 |

In the first five steps, the tissue was hydrated. To prepare the cresyl violet staining solution for step six, 1.25 g of cresyl-violet and 0.75 mL glacial acetic acid were mixed with 250 mL warm water (50 °C) and filtered after cooling down. In steps seven to twelve, the stained sections were dried in a series of bath solutions with increasing ethanol concentrations. Finally, the brain sections were cleared with Histo-clear (Biozym) and mounted with Di-n-butyl-phthalate.

3.2.9 Confocal laser scanning microscopy

Confocal laser scanning microscopy was performed with a Leica Leica DM IRBE microscope (Leica Microsystems), using proprietary imaging software. A 40 x objective (N/A 1.25) was used. The pinhole was set at 118 µm and sequential line scans were performed. The laser power and computational gain were adjusted depending on the intensity of the fluorescent signals and kept constant within one group of experiments.

3.2.10 Live cell imaging

To study the motility of GFP-EB3 comets, primary hippocampal or primary cortical neurons were grown on glass coverslips and transfected with pmRFP and pEGFP-EB3 after seven days in vitro. For live cell imaging, the coverslips were transferred into coverslip chambers (Bioscience Tools, San Diego, United States) and the medium was replaced by prewarmed HEPES buffer. Imaging was carried out using the spinning disk microscope (Visitron Systems) at a constant temperature of 37 °C using an incubation chamber. The images were acquired over a time period of 450 s and an interval of 3 to 5 s. Kymographs were plotted using the MetaMorph 7.1 software.

3.2.11 Electron microscopy

Analysis by electron microscopy was carried out by the ZMNH core facility for morphology and electron microscopy led by Dr. Michaela Schweizer. Adult mice were anesthetized and fixed by transcardial perfusion with 4 % paraformaldehyde and 1 % glutaraldehyde in 0.1 M phosphate buffer at pH 7.4. The fixative was washed out with isotonic NaCl solution. 100 µm thick sections from wt and ko testes were cut with a vibratome (Leica VT 1000S). The sections were rinsed three times in 0.1 M sodium cacodylate buffer (pH 7.2–7.4) and osmicated using 1 % osmium tetroxide in cacodylate buffer. Following osmication, the sections were dehydrated with ascending ethanol concentration steps, followed by two rinses in propylene oxide. Infiltration of the embedding medium was performed by immersing the pieces in a 1:1 mixture of propylene oxide and Epon and finally in neat Epon and hardened at 60 °C. Semithin sections (0.5 µm) were prepared for light microscopy, mounted on glass slides and stained for 1 minute with 1 % Methylene blue. Ultrathin sections (60 nm) were examined in an EM902 (Zeiss). Pictures were taken with a MegaViewIII digital camera (Tröndle).

3.3 Molecular biology

3.3.1 Polymerase chain reaction

For the amplification of DNA fragments, sequence-specific oligonucleotides were used in a polymerase chain reaction (PCR) (Saiki, Gelfand et al. 1988). The oligonucleotides (Table 8) were designed such that the PCR product could be cloned into a vector either by the use of specific restriction sites or by the ligation of blunt ends.

For PCR products larger than 1 kb and in case of amplification of an insert for plasmid cloning, polymerases with a proofreading capacity such as Phusion Polymerase (New England Biolabs) or PfuTurbo-DNA-polymerase (Stratagene) were used following the supplier's instructions.

In Table 10, a generalized temperature cycling protocol is presented. Depending on the primer sequences, an annealing temperature between 55 °C and 65 °C was chosen. The elongation temperature was between 68 °C and 72 °C depending on the polymerase chosen and the amplicon.

Table 10: Temperature cycling programme of a typical PCR.

| Step # | Temperature | Time | Repeats | Purpose |
|--------|-------------|-----------|---------|----------------------|
| 1 | 98 °C | 1 min | - | Initial denaturation |
| 2 | 98 °C | 30 sec | 30 | Denaturation |
| 3 | 55-65 °C | 30 sec | | Annealing |
| 4 | 68-72 °C | 30 sec/kb | | Elongation |
| 5 | 68-72 °C | 10 min | - | Final elongation |
| 6 | 4 °C | ∞ | - | Cooling |

A basic PCR protocol from Table 11 was modified according to the specific requirements of the experiment.

Table 11: Standard reaction mixture for a PCR.

| Ingredients | Volume |
|---------------------------------|----------|
| 10 mM dNTPs | 1 µL |
| 10 x Buffer | 0.5 µL |
| Taq Polymerase | 0.5 µL |
| 10 µM Primer A + 10 µM Primer B | 2+2 µL |
| Template DNA | 0.5 µL |
| H ₂ O | ad 50 µL |

3.3.2 Genotyping of mouse-tail-tip biopsies

For genotyping of all spastin and katanin animals' tail biopsies, the QuickExtract DNA extraction solution (Biozym) was used. 25 µL of the extraction solution was added to the tail biopsies and then incubated at 65 °C for 5 min under constant shaking. After heat inactivation at 95 °C for 2 min, 2 µL of the DNA extracts were used for the genotyping PCR.

For genotyping, 1 U of DreamTaq DNA polymerase (Thermo Scientific, 0.2 µL per PCR reaction) was pipetted to the PCR mix. Finally, 1 µL of genomic DNA was added as the last component for genotyping PCRs. For all genotyping reactions, the touchdown PCR protocol was used (Don, Cox et al. 1991, Hecker and Roux 1996). The difference to a standard PCR consisted in the high annealing temperature in the first cycle (66 °C), followed by a constantly decreasing annealing temperature for each following cycle (-0.5 °C per cycle). Under touchdown PCR conditions, most DNA fragments can be amplified because the amplification of nonspecific DNA is prevented by the initially high annealing temperature, which competes out the amplification of non-specific PCR-products. Touchdown increases the specificity of the reaction at higher temperatures and increases the efficiency towards the end by lowering the annealing temperature. Table 12 summarizes the primer combinations for all genotyping PCR protocols used for this study.

Table 12: Overview of all primer combinations for all genotyping PCR protocols used in this study.

| Locus | Oligonucleotides | Possible bands |
|----------------------|------------------|--|
| FLP | P154 + P155 | 500 bp FLP ^{TG} |
| CamKII α -Cre | P83 + P84 | 250 bp CamKII α -Cre ^{TG} |
| Cre | P142 + P143 | 250 bp Cre ^{TG} |
| Katanin | P170 + P94 | 270 bp Katanin ^{WT} , 238 bp Katanin ^{KO-1st} , 238 bp Katanin ^{FL} |
| | P93 + P170 + P94 | 397 bp Katanin ^{KO} , 270 bp Katanin ^{WT} , 238 bp Katanin ^{FL} |
| | P88 + P170 + P94 | 374 bp Katanin ^{GT} |
| | P93 + P94 | 2190 bp Katanin ^{WT} , 2351 bp Katanin ^{FL} |
| Spastin | P169 + P89 | 223 bp Spastin ^{WT} , 270 bp Spastin ^{KO-1st} , 270 bp Spastin ^{FL} |
| | P41 + P169 + P89 | 432 bp Spastin ^{KO} , 270 bp Spastin ^{FL} , 223 bp Spastin ^{WT} |
| | P88 + P169 + P89 | 405 bp Spastin ^{GT} , 223 bp Spastin ^{WT} , 270 bp Spastin ^{KO-1st} |
| | P41 + P89 | 1256 bp Spastin ^{WT} , 1515 bp Spastin ^{FL} |

3.3.3 Cloning of DNA fragments

The DNA-sequence of interest was quantitatively restricted from the recombinant plasmid-DNA (see section 3.3.6). Afterward, the 5'-end from the target vector was dephosphorylated in order to prevent its recircularization (section 3.3.7). The DNA-sequences of interest and the target-vectors were then purified using agarose gel electrophoresis (section 3.3.9) and the DNA-bands with the sizes of interest were extracted from the gel. In order to determine the amount of DNA obtained, 2 μ L of the extracts were either used on a nanoquant or by reapplying the DNA on an agarose gel (section 3.3.5). Subsequently, the DNA could be used for ligation (section 3.3.11) and then for the transformation of *E. coli* (section 3.3.12). Positive clones were determined either using colony PCR (section 3.3.13) or by restriction analysis of the obtained plasmid DNA followed by DNA sequencing (section 3.3.14) using the automated Sanger dideoxy chain termination method.

3.3.4 Isolation of plasmid-DNA from bacteria

5 mL of bacterial overnight cultures containing the plasmid-DNA of interest were precipitated by centrifugation. Additionally, 50 μ L of the grown bacterial cells were stored in 50 % glycerol at -80 °C until further use. The plasmid-DNA was isolated using NucleoSpin[®] Plasmid QuickPure plasmid purification kit (Macherey-Nagel) following the manufacturer's instructions. The purified and plasmid DNA was finally eluted from the silica membrane with 100 μ L of pure-distilled H₂O.

In order to isolate plasmid-DNA from 250 mL overnight cultures, the QIAprep[®] Maxiprep Kit (Qiagen) was used after alkaline lysis and anion exchange columns following the supplier's instructions.

3.3.5 Determination of DNA-concentration and purity

The purity and the concentration of aqueous DNA-solutions were determined using either one or two of the following methods.

In the first method, comparing the signal intensities between ethidium bromide-stained DNA fragments separated by agarose gel electrophoresis and the ones of the DNA molecular weight marker Hyperladder I (Biolone) with predefined concentrations of the fragments allowed to determine the concentration and the quantity of DNA fragments. Spectrophotometric analysis

using the NanoQuant plate for Infinite 200 PRO NanoQuant (Tecan) additionally enabled judging the contamination with salts, proteins and RNA by measuring light absorption at the wavelengths of 230, 260 and 280 nm.

3.3.6 Restriction digestion

Plasmid-DNA was incubated with the restriction enzymes following the supplier's instructions and using the provided buffers. For a typical restriction digestion 1 U of enzyme was used per 1 µg of DNA. When multiple enzymes were to be used, the buffer that allowed the maximum activity of all the enzymes was chosen. When this was not possible, sequential restriction digestion was applied.

3.3.7 Dephosphorylation of DNA fragments

In order to prevent recircularization and religation of previously cut vectors, the 5'-ends were dephosphorylated using thermosensitive alkaline phosphatase (FastAP, Fermentas). Depending on the reaction volume, between 0.5 to 1 µL FastAP (10 U/µL) was used and incubated for 10 min at 37 °C.

3.3.8 Phosphorylation of DNA fragments

In case a blunt-end ligation was planned for PCR-fragments with no 3'-overhangs, the purified PCR products had to be phosphorylated in order to maximize the yield during ligation. T4 polynucleotide kinase (NEB) was added to the DNA-fragment solution with the provided buffer supplemented with ATP. The phosphorylation reaction was stopped by heat inactivation following manufacturer's instructions. The phosphorylated DNA fragments were then purified using the NucleoSpin® Gel and PCR Clean-up kit (Macherey-Nagel).

3.3.9 Agarose gel electrophoresis

Agarose gel electrophoresis could be applied in order to visualize the fragment sizes amplified in a PCR reaction (e. g. for genotyping or cloning), after a restriction digestion, or to determine the DNA concentration and the amount of different DNA-fragments.

Depending on the expected molecular weight of the target DNA-fragments, 0.6 to 4 % agarose (w/v) gels were used. For the preparation of the gels, the required weight of agarose was boiled in 1 x TAE buffer until dissolved. After cooling down, a gel was formed with a certain meshwork, thus enabling the optimal separation of the corresponding DNA-fragments.

For the electrophoresis, 1 x TAE buffer was used. After the DNA solutions were mixed with DNA loading buffer they were loaded onto the gel and separated in horizontal electrophoresis chambers by applying 7 to 10 V/cm gel length. Depending on the following steps, the agarose gel could either be poststained in an ethidium bromide staining solution (0.5 µg/mL ethidium bromide in 1 x TAE buffer) for 30 min or the ethidium bromide could directly be added to the hot agarose solution (dilution 1:50,000). After separation, the DNA fragments could be visualized by UV-light from a transilluminator (Intas). Hyperladder I (Bioline) was used as a molecular weight marker. The concentration of DNA could also be determined by comparison with the predetermined

concentration of the DNA fragments of the molecular weight marker.

3.3.10 Purification of DNA fragments from agarose gels

DNA fragments previously separated by agarose gel electrophoresis could be isolated directly from the gel by cutting them out of the agarose gel using a scalpel and visualization using UV-light. In order to obtain pure DNA solution in water, the gel extraction kit (Macherey-Nagel) was used following the manufacturer's instructions. The DNA was eluted from the columns using 15 μL H_2O and then used for concentration determination.

3.3.11 Ligation of DNA fragments

For the ligation of DNA fragments, the T4 DNA ligation kit (Thermo Fisher Scientific) was used. 50 ng of vector DNA and a threefold stoichiometric excess of insert (Crouse, Frischauf et al. 1983) were mixed and incubated overnight at 4 °C according to the manufacturer's instructions (5 μL , 20 μL reaction volume).

3.3.12 Transformation of chemically competent E. coli strains

In order to amplify plasmid DNA, either Escherichia coli XL1-Blue or DH5 α were transformed as described previously (Inoue, Nojima et al. 1990). 100 μL of chemocompetent E. coli were supplemented with 1.7 μL β -mercaptoethanol and thawed on ice for 10 min under occasional and careful shaking. Then either 10 μL of the ligation mixture or 50 ng of plasmid-DNA was added to the cells for further 30 min on ice, followed by a heat shock at 42 °C for 30 sec. After the addition of 900 μL of ice-cold LB-medium, the cells were incubated at 37 °C in a thermomixer for 45 min. Then, the cells were plated onto LB-Agar-plates containing the corresponding antibiotic at the required concentration (Table 13) and incubated at 37 °C overnight.

Table 13: Antibiotic concentration used for LB-Agar-plates.

| Antibiotic | Concentration |
|---------------|----------------------------|
| Ampicillin | 50 $\mu\text{g}/\text{mL}$ |
| Kanamycin | 20 $\mu\text{g}/\text{mL}$ |
| Cerbenicillin | 50 $\mu\text{g}/\text{mL}$ |

3.3.13 Colony-PCR

In order to identify bacterial colonies containing the DNA-insert of interest and in the correct orientation (e. g. after blunt-end cloning or when using only one restriction enzyme), colony PCR was applied. In this modified PCR protocol, instead of template-DNA, a single E. coli colony was picked with a pipette tip from the LB-agar-plate and directly added to the PCR mix. The first primer binds inside the vector sequence and the second one binds inside the DNA-fragment to be inserted. In that case, the presence of the right band-size after PCR and following agarose-gel electrophoresis sorts out false-positive clones. In this way, only the preselected clones were chosen for plasmid-DNA-isolation and DNA-sequencing.

3.3.14 Sequencing of DNA

The sequencing reactions for plasmid-DNA or DNA-fragments were performed by the ZMNH-sequencing-service group led by PD Dr. S. Hoffmeister-Ullerich applying Sanger's dideoxy chain termination method (Sanger, Nicklen et al. 1977). For the reaction, the ABI Prism 377 DNA-sequencer (Applied Biosystems) and the BigDye Terminator v1.1 Cycle Sequencing Kit (Applied Biosystems) were used. The results of the sequencing reactions were plotted into electropherograms using the EditView-Software Version 1.0.1 (ABI Prism, Applied Biosystems). The analysis and editing of the DNA-sequence trace files was done using the Macintosh-Software 4Peaks (nucleobytes.com) and the DNASTAR software (Lasergene).

3.3.15 Ethanol precipitation of DNA

In order to purify the targeting vector for spastin, 0.1 volume of 3 M sodium acetate (pH 5.2) to a final concentration of 0.3 M was added to the DNA-solution to be precipitated. Then 2 volumes of pure ice-cold ethanol (-20 °C) were added and the mixture was incubated for 30 min on ice. After a 15 min centrifugation step at >15,000 g and 4 °C, the supernatant was discarded. The pellet was then washed twice at room temperature using 70 % ethanol and vortexing for one minute followed by a 30-second centrifugation step. Finally, the pellet was air-dried and resuspended in 200 µL of H₂O.

3.3.16 Quantitative linearization of the targeting vector for spastin

For the electroporation into the embryonic stem cells, the purified spastin targeting vector was linearized using the unique restriction site AsiSI. 100 µL of the purified targeting vector (1 µg/µL) were supplemented with 126 µL H₂O and 25.66 µL 10 x Tango Buffer (Fermentas) and incubated with 5 µL AsiI (Fermentas) for 12 hours at 37 °C. The quantity of linearization was tested by agarose gel electrophoresis and comparison of band sizes between the original and the AsiSI treated vectors.

3.3.17 Phenol/chloroform extraction of DNA

In order to obtain the pure linearized targeting vector for the subsequent electroporation of embryonic stem cells, 1 volume of phenol:chloroform (Carl Roth) was added to the DNA-containing solution and mixed well under vortexing followed by a 10-minute centrifugation step at 12,000 g. The upper aqueous solution containing the DNA was carefully removed by pipetting. Next, the same 1 volume of TE buffer was added to the organic phase in order to extract the remaining DNA. Again, after mixing by vortexing, the centrifugation steps were repeated followed by pooling of the aqueous DNA-containing solutions. After the addition of 1 volume of chloroform and mixing by vortexing, the suspension was centrifuged at 12,000 g at room temperature. The upper aqueous phase was then used to precipitate the DNA following the ethanol precipitation method. The pellet was then dissolved in 40 µL H₂O and the concentration and quality of the obtained DNA was measured via agarose gel electrophoresis and photospectrometrically.

3.3.18 Electroporation of mouse embryonic stem cells

For the electroporation of mouse embryonic stem cells with the linearized spastin targeting vector, previously thawed C57BL/6N embryonic stem cells growing on a 1 cm cell culture dish were washed once with 10 mL PBS and incubated for 4 min with 3 mL of trypsin-EDTA at 37 °C in the cell culture hood. After that, the cells were resuspended carefully by 3 x 5 strokes using a glass Pasteur pipette. The cells were then transferred into a 15 mL tube containing 7 mL of prewarmed medium, resuspended shortly and then centrifuged for 4 min at 900 rpm. The supernatant was removed carefully with a Pasteur pipette in a rotary movement at the surface area touching the wall of the tube in order to remove the DNA originating from damaged cells, leaving the cell pellet with approximately 500 µL medium above. The cells were resuspended carefully by flipping 4 to 5 times against the tube and then washed with 10 mL PBS and centrifuged for 4 min at 900 rpm. The supernatant was removed again, this time leaving approximately 200 µL above the cell pellet. After resuspension by flipping against the tube, 800 µL of fresh PBS were added, and the cell suspension was transferred into an electroporation cuvette already containing 20 µL of linearized targeting vector DNA (20 µL x 1.45 µg) using a glass pipette. After 3 min, the cuvette was inserted into the electroporator using 250 V and a capacitance of 500. After the pulse and a short cooling time in the cuvette, the cells were transferred into a 15 mL conic tube containing 10 mL of the prewarmed medium and resuspended carefully with a 10 mL plastic pipette. The cell suspension was then evenly distributed onto 5 x 10 cm cell culture dishes already containing prewarmed and CO₂-enriched medium. After 24 hours in the incubator, positive selection was started by supplementing the medium with 100 µg/mL GM-418.

3.3.19 Generation of radiolabeled probes for Southern Blotting

In order to demonstrate the integration of the targeting vector at the correct genomic locus, a specific radiolabeled probe was generated for the usage in Southern Blotting. They were selected at the 5'- and at the 3'-ends of the putative integration site. Then, the corresponding DNA-fragment was amplified from genomic DNA purified from mouse tail biopsies using the polymerase chain reaction. After phosphorylation, the PCR fragment was cloned into an EcoRV-cut and dephosphorylated cloning vector (pBluescript II SK(+)). After the selection of the correct clones, the plasmid DNA with the correct insert was digested using flanking restriction sites. After separation using agarose gel electrophoresis, the correct DNA-fragment was extracted from the gel. The purified DNA was used for radiolabeling using the Megaprime DNA Labeling System kit (Amersham) following the manufacturer's instructions. Briefly, 5 µL of the extracted DNA (approximately 25 ng in total) were mixed with 5 µL random prime oligonucleotides, boiled at 95 °C for 5 min and then kept on ice. Then, 4 µL of each dNTPs was added with the exception of dATPs. After the addition of 5 µL reaction buffer, 5 µL of P32 labeled dATPs and 2 µL of the provided enzyme and 16 µL H₂O, the reaction mixture was incubated for 15 min at 37 °C.

After the addition of 40 μL TE-buffer, the radiolabeled probes were applied to the G50 columns and centrifuged for 5 min. The purified probes were transferred into new tubes and 1 μL was used for measuring the labeling efficiency in a counter (approximately 200,000 counts).

3.3.20 Southern Blotting (alkaline method)

After EcoRV-restriction digestion, the isolated DNA samples were separated on a 0.65 % agarose gel using TAE buffer. Being suitable for the detection of DNA-fragments larger than 2 kb, bromophenol blue was used in the DNA loading buffer. After separation, the agarose gel was acidified in 0.25 M HCl for approximately 10 min until the bromophenol blue turned yellow and then it was washed with deionized water. In the next step, 0.4 M NaOH was added for 15 min.

Then, the gel was placed onto a blotting bridge. It consisted of one long filter paper on a glass plate with two of its ends immersing a reservoir of 0.4 M NaOH solution and two additional filter papers on top. The area around the gel was covered with plastic wrap to ensure migration of the solution exclusively through the gel. In the next step, the XL-1 membrane (Amersham) was immersed shortly in deionized water and was then equilibrated with the label down in 0.4 M NaOH. Then it was placed onto the agarose gel. The membrane was covered then with two additional filter papers and a stack of dry paper towels. These were covered by a glass plate and weighed down with approximately 500 g using a bottle (Figure 15).

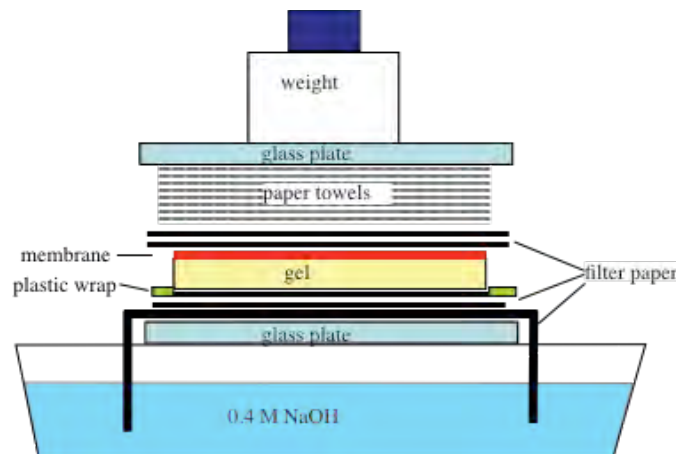


Figure 15: Experimental setup for Southern Blotting (alkaline method).

The next day, the weight and towels were removed and the membrane was floated with the writing down in 2 x SSC buffer for maximum 10 min. Then the membrane was baked for 2 h at 80 $^{\circ}\text{C}$ on a filter paper.

The membrane was blocked with prewarmed hybridization buffer containing denatured herring sperm DNA in a rolling oven at 65 $^{\circ}\text{C}$ for 3 h. Fresh hybridization buffer supplemented with the previously radiolabelled and denatured probe at a concentration of $2.5 \times 10^5 - 5 \times 10^5$ cpm/mL was then used for hybridization overnight at 65 $^{\circ}\text{C}$ in a rolling oven.

The next day, the membrane was repeatedly washed with prewarmed washing buffer A for 10 min each time and the activity of the discarded buffer was measured with a hand monitor. After no activity could be detected in the discarded buffer A, the washing procedure was continued with

washing buffer B. When the radioactivity signal became undetectable again, the membrane was wrapped in plastic wrap and exposed and developed using a phosphoimager setup (Fujix, BAS 2000, Raytest Isotopenmeßgeräte).

3.3.21 Long-range-PCR

Long-range PCR was established to confirm the correct insertion of the targeting vector at the 3' or at the 5' end of the homology arms of the targeted genes. The volumes of the ingredients are summarized in Table 14. A reaction volume of 25 µL was used for each reaction.

Table 14: Reaction mixture for a long-range PCR.

| ingredients | volume in µL |
|------------------|--------------|
| 10 x Buffer | 10 |
| 10 mM dNTPs | 2 |
| Primer A | 2 |
| Primer B | 2 |
| Template-DNA | 8 |
| H ₂ O | 75,5 |
| Taq polymerase | 0,5 |

The following primer combinations (for sequence information see **Table 8**) were used for the long-range PCR:

Table 15: Primer combinations and amplicon sizes for the long-range PCRs used during the study.

| | Primer A | Primer B | Amplicon size |
|------------|----------|----------|---------------|
| Spastin 3' | 23 | 61 | 5043 bp |
| Katanin 5' | 87 | 123 | 6226 bp |
| Katanin 3' | 86 | 122 | 3762 bp |

The cycling conditions for the individual long-range PCRs are summarized below:

Table 16: cycling conditions used for long-range PCR in this study. The individual annealing temperatures and extension times are highlighted in subcolumns.

| Cycling conditions | Temperature in °C | | | Time in min | | | repeats |
|----------------------|-------------------|------------|------------|-------------|------------|------------|---------|
| | Spastin 3' | Katanin 5' | Katanin 3' | Spastin 3' | Katanin 5' | Katanin 3' | |
| Initial denaturation | 95 | | | 0.5 | | | - |
| Denaturation | 95 | | | 0.5 | | | 40 |
| Annealing | 60 | 57 | 57 | 0.5 | | | |
| Extension | 70 | | | 4 | 5 | 3 | - |
| Final extension | 70 | | | 10 | | | |
| Cooling | 4 | | | ∞ | | | - |

3.4 Biochemistry

3.4.1 Protein extraction from HEK293-TN (or neuronal cell) lysates

Cultivated HEK293-TN-cells were harvested 8 to 24 hours after transfection. After removal of the medium, the cells were kept ice-cold. After washing with 5 to 10 mL 1x PBS the cells were removed from the dish using a cell scraper (Sarstedt) in HEK-cell-lysis buffer. For lysis, the

harvested cells were incubated for 30 min on ice under occasional vortexing and subsequently centrifuged at 1,000 g. The supernatant containing the soluble protein fraction was either used for immediate protein analysis or was directly frozen using liquid nitrogen and kept frozen at -80 °C.

After cultivation and transfection in culture dishes, the lysis of cells (primary neurons / HeLa cells) was performed on ice. The cells were washed with ice-cold 1x PBS. Then, an appropriate amount of cell lysis buffer was added to the cells, which were subsequently scraped off the dishes using a cell scraper. After optional sonication (duty cycle = 20 %, output control = 0.2) cells were rotated for 20 min at 4 °C to complete cell lysis. Cell debris was removed by centrifugation for 5 min at 4 °C at 10,000 g.

3.4.2 Preparation of cellular fractions from brain lysates by differential centrifugation

In order to obtain different cellular fractions, the differential centrifugation method was used (Table 17).

Table 17: Overview of the cell fractionation by differential centrifugation.

| Step | Centrifugation speed | Time | Rotor used | Pellet | Pellet components |
|------|----------------------|--------|--------------------------|--------|---|
| 1 | 1,000 x g | 10 min | JA 20 or JS 13.1 Beckman | P1 | cell-membrane debris, mitochondria and nuclei |
| 2 | 10,000 x g | 10 min | JA 20 or JS 13.1 Beckman | P2 | small cell-membrane debris, mitochondria, large vesicular cell organelles (like ER) and the plasma membrane |
| 3 | 100,000 x g | 60 min | SW40 Ti Ultra | P3 | Golgi, transport vesicles, microsomes etc. |
| 4 | 400,000 x g | 60 min | TLA 100, Ultra | P4 | small vesicles and protein complexes |

Initially, eight postnatal day 11 (P11) mice were sacrificed by decapitation. The brains were isolated, and put into 7.5 mL tubes supplemented with IMAC buffer (20 mM HEPES, 100 mM potassium acetate, 40 mM KCl, 5 mM EGTA, 5 mM MgCl₂, pH 7.2 freshly supplemented with protease inhibitor (Roche cOmplete), 2 mM Mg-ATP, 5 mM DTT and 1 mM PMSF). The brains were homogenized with 8 strokes at 900 rpm. The lysates were centrifuged for 10 min at 1,000 x g (JA 20 or JS 13.1, Beckman), and the supernatant S1 was transferred into a new tube. The pellet P1 containing cell-membrane debris, mitochondria and nuclei was put aside.

The supernatant S1 was then centrifuged for 10 min at 10,000 x g (JA 20 or JS 13.1 Beckman), and the resulting supernatant S2 was transferred into a new tube. The pellet P2 consisting of small cell-membrane debris, mitochondria, large vesicular cell organelles (like ER) and the plasma membrane was put aside.

The supernatant S2 was then centrifuged for 1 h at 100,000 x g (SW40 Ti Ultra), and the supernatant (S3) was transferred to a new tube. The pellet P3 consisting of Golgi, transport vesicles, microsomes was put aside for further usage.

After the centrifugation of the supernatant S3 for 1 h at 400,000 x g (TLA 100, Ultra), the supernatant S4 was transferred into a new tube. The pellet P4 contained small vesicles and protein complexes.

After the differential centrifugation, each pellet was resuspended in 2 mL IMAC buffer.

3.4.3 Preparation of synaptosomal fractions

Synaptosomes are artificial fusions of neuronal pre- and postsynaptic membranes. They form *in vitro* after homogenization of neuronal tissue following several centrifugation steps. This method allows to specifically enrich synaptic proteins for further analysis (Whittaker, Michaelson et al. 1964).

After sacrificing, mice were decapitated and their whole brains were transferred into 4 mL ice-cold sucrose buffer A each. For homogenization, 12 strokes at a rotation speed of 900 rpm were applied in a 15 mL potter S (B Braun). After 6 strokes, 4 mL of sucrose buffer A were added. Subsequently, the homogenate was centrifuged at 4 °C for 10 min and 1,400 x g ((12 mL centrifuge tubes (Greiner Bio-one); JA20 rotor). The pellet was resuspended in 4 mL of sucrose buffer A by applying 8 strokes at 900 rpm and centrifuged again for 10 min at 4 °C and 700 x g. The supernatants from both centrifugation steps were then pooled and centrifuged at 13,800 x g for 10 min.

The pellet was resuspended in 2 mL sucrose buffer B and applied on a sucrose gradient (3 mL of 1.2 M, 1.0 M and 0.85 M sucrose and with an increasing sucrose density from top to bottom) and centrifuged for 2 h at 82,500 x g (SW40Ti Rotor). The synaptosome-enriched interface between 1.2 M and 1 M as well as the other interfaces were then collected and used for further analyses (see Figure 16).

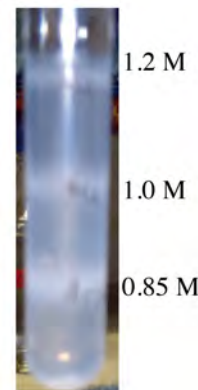


Figure 16: Exemplary picture of synaptosomal fractionation. A sucrose density gradient of 1.2 M, 1.0 M and 0.85 M sucrose was used. The separated fractions were used for further analysis.

3.4.4 Co-immunoprecipitation

For co-immunoprecipitation, 30 μ L slurry protein G coupled dynabeads (Dynal) were washed three times with 1 mL IP buffer using the Dynal magnetic particle concentrator (Dynal). Then 5 μ g of antibody were coupled to the washed beads in 800 μ L IP buffer overnight using an overhead shaker at 4 °C. Three washing steps with IP buffer were used to ensure the removal of unbound antibodies. Subsequently, the dynal beads with immobilized antibodies were incubated with cellular fractions obtained from differential centrifugation at 4 °C overnight using an overhead shaker. Then the dynal beads were washed again three times using IP buffer supplemented with 0.5 % Triton-X-100 and cOmplete protease inhibitor cocktail (Roche) for 5-10 min each time. The

dynabeads were then dissolved in 30-45 μL H_2O and supplemented with 10-15 μL 4 x SDS-sample buffer and boiled for 10 min at 95° to elute bound proteins. Finally, the samples were separated by SDS-PAGE followed by a Western Blotting analysis.

3.4.5 Determination of protein concentration (BCA Assay)

To normalize samples to total protein levels the BCA method (BCA Protein Assay kit from Thermo Scientific) was used. A standard curve was determined by using a BSA solution with a known concentration. The appropriate amount of BSA and 1 – 2 μL from each cell lysate was filled up to 25 μL with distilled water. Ice-cold BCA Protein Assay Reagent A was mixed with BCA Protein Assay Reagent B (ratio 50:1) and 200 μL of this solution was added on ice to each protein sample. The reactions run for 30 min at 37 °C. Afterward, the samples were allowed to cool down to room temperature for 5 min before the OD was measured at 562 nm with a SLT Rainbow Scanner (SLT Labinstruments). The concentration of each protein sample was determined with help of the calculated standard curve and adjusted to 1 $\mu\text{g}/\mu\text{L}$ with protein sample buffer and lysis buffer. Samples were stored at -20 °C until further usage.

3.4.6 SDS-PAGE

Proteins were separated by their molecular weight by using SDS-polyacrylamide gel electrophoresis (SDS-PAGE) with the Mini-Protean III system (Biorad). In order to prepare the gels, a 40 % (w/v) acrylamide-/bis-acrylamide solution (Carl Roth) was used (Sambrook, Fritsch et al. 1989). Depending on the target molecular weight, different final percentages of the acrylamide-/bis-acrylamide in the gel were selected. In the following table an exemplary composition of a typical SDS-PA gel is presented.

Table 18: Typical composition of SDS polyacrylamide gels.

| Components | Stacking gel 7.5 % | Separating gel 15 % |
|-----------------------------------|--------------------|---------------------|
| Acrylamide/Bisacrylamide (37.5:1) | 1.25 mL | 6 mL |
| 0.5 M Tris-HCl, pH 6.8 | 1.25 mL | - |
| 1 M Tris-HCl pH 8.8 | - | 3 mL |
| 10 % SDS (w/v) | 50 μL | 120 μL |
| H_2O (Millipore) | 2.45 mL | 2.75 mL |
| 10 % APS (w/v) | 50 μL | 120 μL |
| TEMED | 5 μL | 6 μL |

After mixing the protein solutions with 4 x SDS-loading buffer and boiling at 95 °C for 5 min, the samples were loaded onto the gel to separate the proteins. The electrophoresis was buffered in 1 x SDS-Running buffer. For the initial separation in the stacking gel, a voltage of 90 V was applied followed by a voltage of 120 V in the separating gel. The Precision Plus Protein

Standards Dual Color (Biorad) molecular weight marker was used to identify the region of the target molecular weight. After electrophoresis, the gel was either used for Coomassie staining or for Western Blotting.

3.4.7 Western Blotting

In order to detect proteins following separation by SDS-PAGE with specific antibodies, they had to be transferred from the SDS-PA-gel onto a PVDF-membrane (Hybond-P, pore size 0.45 μm , Amersham). The Wet-Blot Mini Trans-Blot Cell System (Biorad) was used for the transfer at 100 V for 75 min.

The PVDF-membrane was activated in Methanol for 15 to 30 s and then washed with transfer buffer. Then, the protein-containing gel was placed onto it. This so-called sandwich was then wrapped from both sides with two layers of filter paper soaked with transfer buffer each and one sponge (Biorad). The protein containing gel was facing the cathode and the PVDF- membrane was facing the anode so that the negatively charged proteins were transferred in the direction of the anode and fixed on the PVDF-membrane.

To identify the immobilized proteins on a PVDF membrane using specific antibodies, the membrane was incubated for 60 min in a 1 % BSA solution in TBST. This step was necessary to prevent nonspecific binding of the antibodies to the protein-free sites on the PVDF-membrane.

Next, the PVDF-membrane was incubated with a specific primary antibody diluted (Table 4) in the same 1 % BSA solution in TBST for 2 h at room temperature or at 4 °C overnight. Then, the membrane was washed three times with TBST for 10 min each time and then incubated with an HRP-conjugated secondary antibody diluted in 1 % BSA in TBST for 30 min at room temperature. After this incubation, the membrane was washed again three times using TBST and then used for the chemodetection of the specific protein bands using the Immobilon Western HRP substrate (Millipore) following the manufacturer's instructions.

The documentation of the results was done using the chemiluminescence reader Intas ChemoCam (Intas).

For the specific detection of additional protein bands from the same PVDF-membrane, previously used primary antibodies had to be removed. For that purpose, the membrane was incubated in stripping buffer for 30 min at room temperature and shaking. After two following washing steps using TBST, the membrane was again incubated with the HRP-conjugated secondary antibody to exclude remaining bound primary antibody. In case no remaining signal could be detected, the immunodetection protocol was used again starting with the blocking of the membrane with 1 % BSA in TBST.

3.5 Behavior analysis

3.5.1 Experimental animals and housing conditions

The housing of animals and the behavioral experiments were conducted in accordance with regulatory requirements and were approved by the responsible authority.

All behavioral experiments were done using adult female and male mice. The KO group consisted of homozygous floxed katanin animals with an additional *CamKII α* promoter-driven Cre transgene. The wild type group consisted of homozygous floxed littermates without the existence of a Cre transgene.

The animals were housed in a pathogen-free laboratory at the animal service facilities of the ZMNH, UKE. Three weeks after birth, the animals were weaned and separated by gender.

With approximately 2-3 months, the animals were transferred to the behavior laboratory section with an inversed light-dark cycle, and a light-phase from 7 pm to 7 am. The room temperature was about 22 °C and the air humidity averaged 55 %. The animals had direct access to food and water. All experiments were performed during the dark cycle. Prior to the behavioral experiments, the animals were habituated to the experimenter by handling each mouse for approximately 3 min each day two weeks before the actual experiment was performed.

The following established tests were used for an initial behavioral phenotyping of the mice. The tests were video-recorded and analyzed using the Software EthoVision and Observer (Noldus).

3.5.2 Exploration and anxiety behavior

3.5.2.1 Elevated plus maze

The elevated plus maze is based on the animal's natural tendency to stay in enclosed spaces and their unconditioned fear for open spaces and heights (Crawley 1985). It is one of the most used behavioral tests for spontaneous anxiety. The maze contains two open arms and two wall-sheltered, closed arms. Anxious animals tend to spend more time in the closed arms compared to less anxious animals.

The elevated plus maze was assembled of four arms (5 x 30 cm) and a central plate (5 x 5 cm). It was placed on an 80 cm high pedestal. Three 15 cm high walls surrounded two opposite arms and were called the closed arms. Each of the remaining opposite arms only had 3 mm high borders and were named the open arms. The maze was placed in a room with dim lighting (50 lux).

Each mouse was gently placed onto the central plate of the maze with the head pointing towards an open arm. The exploration activity was video-recorded for 5 min and then the mice were transferred back to their home cages. The traced path was used for automated analysis using the EthoVision software. Before the examination of the next mouse, the elevated plus maze was cleaned with 70 % ethanol and water.

3.5.2.2 Open field test

The open field is an empty square test arena, in which the animals' activity can be measured. It is based on an animal's unconditioned fear for open spaces and heights and the tendency for exploration (Crawley 1985). It is a well-established test to investigate anxiety-related and exploratory behavior of rodents as well as their horizontal locomotor activities (Denenberg 1969).

An anxiety-like response referred to as thigmotaxis can be measured as the amount of time spent close to the wall versus the amount of time spent in the inner zone of the arena. Additionally, the general locomotor behavior is often considered by measuring the total distance moved.

The open field consisted of four 50 x 50 x 50 cm arenas constructed from white forex plates. Each arena was illuminated with 50 lux, and four mice could be analyzed simultaneously (Figure 17). In the center of each arena, the center zone was defined as a square with 16 cm long sides. The outer zone close to the walls was 5 cm wide and the middle zone was 12 cm wide. Each mouse was placed in one corner of the corresponding arena and could move freely in the arena. Their behavior was documented with a video camera for either 30 or 60 min, the tracks were produced with the software EthoVision (Noldus).

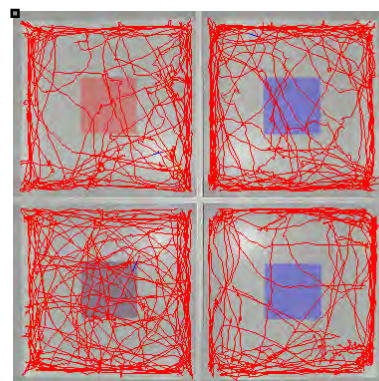


Figure 17: Top view of the open field apparatus. Representative tracks after a recording time of 5 min are shown in red. The center zones are highlighted.

Before the examination of the next mouse, the arena was cleaned with 70 % ethanol and water.

3.5.3 Learning and memory

3.5.3.1 Spontaneous alternation in a Y-maze

To measure short time spatial memory without positive or negative reinforcement, a Y-maze test was used. Here the mice were placed in the start arm of a weakly illuminated (10 lux) Y-maze (three identical arms of 39 cm x 9 cm x 16 cm placed 120 ° to each other) with white nontransparent walls. The total number of entries and the percentage of arm alternations were measured manually over a period of 10 min. An arm entry was defined as a situation when the mouse entered an arm with its fore and hind limbs.

3.5.3.2 Place recognition task in a Y-maze

The natural tendency of mice to explore a novel environment was used to investigate spatial learning and memory in the place recognition test in a Y-maze. The Y-maze had three identical arms with transparent walls that were placed 120 degrees to each other. The Y-maze was placed in the experimenting room with additional cues. Each individual mouse was assigned a start arm, a familiar arm and a novel arm. During the sample phase, the mice were placed onto the start arm and were free to explore the start and familiar arms for 5 min, whereas the entry to the novel

arm was blocked. After an inter-trial interval (ITI) of either 3 min or 24 hours, the mice were allowed to explore the full maze with all three arms unblocked for 5 min (test phase). In order to minimize the influence of experiences from the previous experiment (3 min ITI) on the performance in the following one (24 h ITI), the different experiments were conducted in different rooms with other cues and mulch bedding for the experiment with a 24 h ITI. The illumination was about 40 ± 3 lux in all three arms.

3.6 Quantification and statistics

Band intensities from immunodetections were determined using the ImageJ and Fiji software. The quantified signal intensities were normalized to the corresponding signal intensities of control proteins. Fluorescence intensities from immunocytochemistry were quantified as mean grey values per area using the ImageJ software. Acquired data was tested for normal distribution prior to further analysis. Prism (GraphPad) software was used for statistical analysis. Unless stated otherwise, all values are shown as mean \pm SEM. P values were determined either using a two-tailed Student's t-test for up to two groups or an analysis of variance (ANOVA) for more than two groups.

4 RESULTS

4.1 Gene targeting and breeding strategies

4.1.1 Knockout-first-allele targeting strategy

For the generation of all mouse models during this work, the EUCOMM/KOMP (European conditional mouse mutagenesis program/ knockout mouse project) “knockout-first allele” (KO-1st) targeting approach was used (Skarnes, Rosen et al. 2011). For both katanin and spastin, the targeting strategies relied on the identification of one or more critical exons that were common to all known transcript variants and which, when deleted, created a frameshift mutation.

In addition to the loxP-flanked exons determined for the excision with Cre recombinase and the two homology arms, this KO-first allele contained a gene-trapping cassette flanked by a FRT site at the 5' end and by a loxP site at the 3' end followed by a neomycin selection cassette which was flanked by an additional FRT site at its 3' end.

The gene-trapping cassette (Figure 18) consisted of a promoterless LacZ gene that was flanked by an upstream 3' En2 SA (engrailed-2 splice acceptor) site followed by an IRES (internal ribosomal entry site) sequence and a downstream transcriptional termination sequence (polyadenylation sequence; polyA).

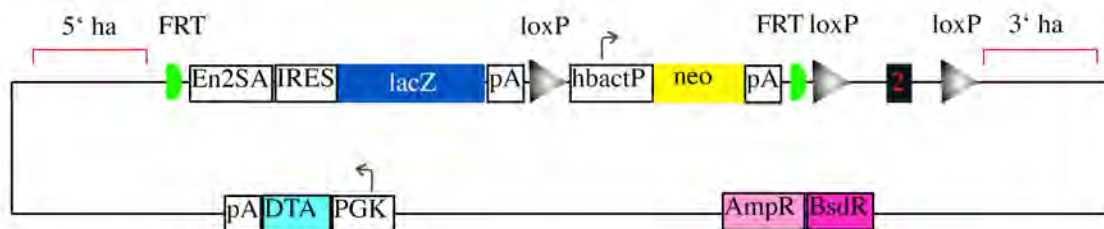


Figure 18: Example of a promoter-driven KO-first-allele targeting vector. Shown is an exon (black rectangle) to be targeted characteristically flanked by LacZ (β galactosidase cDNA), neo (neomycin phosphotransferase cDNA), 5' and 3' homology arms (5' ha and 3' ha), FRT recognition sites (green semicircles) and loxP recognition sites (grey triangles). En2SA: engrailed-2 splice acceptor; IRES: internal ribosomal entry site; pA: polyadenylation signal; hbactP: human β actin promoter; AmpR: ampicillin resistance; BsdR: blasticidin S deaminase resistance; PGK: phosphoglycerate kinase promoter; DTA: diphtheria toxin A.

This targeting strategy was chosen for reporting the endogenous promoter activity of the targeted gene because the gene-trapping cassette is transcribed from the endogenous promoter in the form of a fusion transcript, in which the exons upstream of the insertion site are spliced in frame to the reporter gene. The transcription is terminated prematurely at the polyadenylation site, and the processed fusion transcript encodes a truncated and non-functional version of the cellular protein and the reporter.

An autonomous hbactP (human β actin promoter) driven neomycin selection cassette allowed to enrich successfully recombined ESC clones after electroporation with the targeting vector. The

selection cassette could be removed via FRT sites or via loxP sites depending on the downstream experiments. Additionally, the plasmid backbone contained a PGK (phosphoglycerate kinase) promoter-driven DTA (diphtheria toxin A) cassette for negative selection and AmpR and BsdR for plasmid amplification before gene targeting.

4.1.2 Breeding strategy for katanin and spastin knockout mouse lines

The KO-first-allele can be used for multiple purposes and can produce reporter KOs, conditional KOs, and null-alleles depending on the sequence of exposure to the site-specific recombinases Flp and Cre (Figure 18). This required sequential breedings to different transgenic Cre and Flp driver lines. The embryonic stem cells for gene targeting of both katanin and spastin were derived from C57BL/6N mice (Pettitt, Liang et al. 2009) and the KO-1st animals obtained in filial generation 1 (F1) were backcrossed to the C57BL/6J genetic background in 5 filial generations. The breedings using Cre and FLP driver lines with following outcrossing of these transgenes further added to the backcrossing. Following the breeding scheme developed in Table 19, conditional KO mice were generated with an F5 backcrossed C57BL/6J background.

The C57BL/6N ES cells used for the generation of chimeric founder mice had an agouti locus leading to a brown fur in their offspring. Thus, brown chimeric animals were selected for the generation of F1 lines.

Table 19: Overview of the sequential breedings to generate mice containing KO-first (KO 1-st), floxed (FL), conditional KO, null (KO) and reporter alleles (GT) for the genes of interest (GOI, i. e. spastin or katanin) starting with chimeric mice in the F0 generation. F0-F5: filial generations with one additional breeding using a mouse line in the BL57/6J genetic background. For better orientation, the individual alleles are highlighted in different colors.

| | | | |
|----|--|--|--|
| F0 | GOI ^{WT/KO 1-st} chimera (C57BL/6N background) | | |
| F1 | GOI ^{WT/KO1-st} | | KO 1-ST ALLELES |
| F2 | GOI ^{WT/FL} /FLP ^{WT/TG} (after FLP mating) | | FLOXED ALLELES |
| F3 | GOI ^{WT/FL} /FLP ^{WT/WT} (after crossing out FLP) | | REPORTER ALLELES |
| F4 | GOI ^{WT/FL} /Cre ^{WT/CamKII-TG} | GOI ^{WT/FL} /Cre ^{WT/WT} | GOI ^{WT/KO} /Cre ^{WT/TG} |
| F5 | GOI ^{WT/WT} /Cre ^{WT/CamKII-TG} , GOI ^{WT/WT} /Cre ^{WT/WT} | GOI ^{WT/WT} /Cre ^{WT/WT} | GOI ^{WT/KO} /Cre ^{WT/WT} |
| | GOI ^{WT/FL} /Cre ^{WT/CamKII-TG} , GOI ^{WT/FL} /Cre ^{WT/WT} | GOI ^{WT/FL} /Cre ^{WT/WT} | GOI ^{KO/KO} /Cre ^{WT/WT} |
| | GOI ^{FL/FL} /Cre ^{WT/CamKII-TG} , GOI ^{FL/FL} /Cre ^{WT/WT} | GOI ^{FL/FL} /Cre ^{WT/WT} | |
| | CONDITIONAL KO ALLELES | | NULL-ALLELES |
| | | | REPORTER KOs |

4.1.3 Forebrain-specific Cre-driver lines

In order to generate postnatal and forebrain-specific KOs for spastin and katanin, CamKII α -Cre transgenic mice were used. Several transgenic CamKII α -Cre-driver lines were tested by using a ROSA26 knock-in reporter strain developed by Soriano et al. in order to test the expression and activity of Cre recombinase (Figure 19a). In this reporter strain, two loxP sites flank a STOP

codon upstream of a LacZ reporter cassette, preventing its expression in the absence of Cre-mediated recombination. Following Cre-mediated recombination, the stop codon is deleted and allows the expression of the reporter. LacZ staining of brains from offspring resulting from CamKII α -Cre and ROSA26 Cre reporter strain breedings at different developmental stages were done. For the transgenes originating from the transgenic lines developed by Casanova et al. and Minichiello et al., prenatal expression of CamKII α -Cre was already observed at different extent (Figure 19c). In contrast, the transgene reported by Tsien et al. showed no apparent LacZ activity until postnatal day 2, with a starting expression of Cre at postnatal day 8 and a full forebrain expression in adult mice (Figure 19c and b). In the cerebellum, no LacZ activity was observed as well as in the negative controls only containing the R26R reporter locus (data not shown).

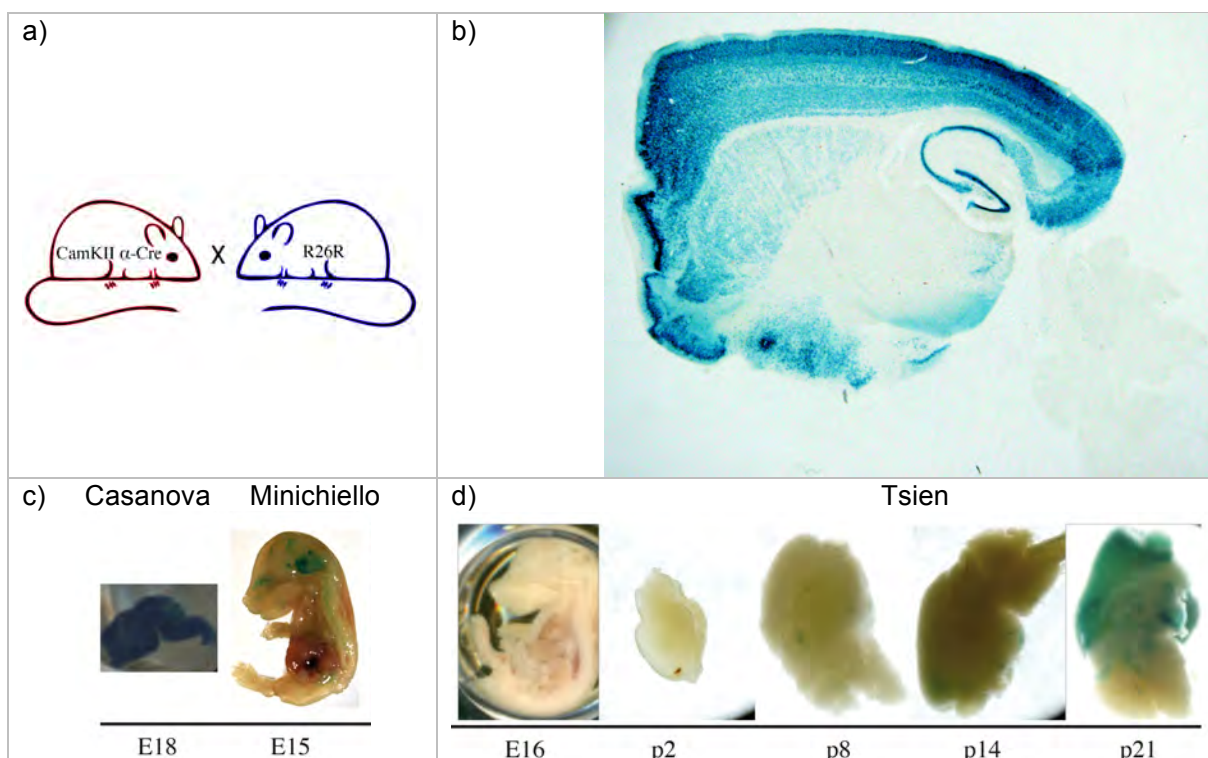


Figure 19: LacZ staining of tissues from offspring resulting from different CamKII α -Cre-driver lines (Casanova, Minichiello, Tsien) mated to the R26R reporter line (Soriano et al. 1999) to visualize Cre-mediated recombination. a) The CamKII α -Cre driver lines to be tested were bred to the ROSA26 Cre reporter line. b) Expression pattern of β -galactosidase in adult mouse brain resulting from a mating using the CamKII α -Cre driver line developed by Tsien et al.. c) Expression of β -galactosidase in prenatal mouse brains using CamKII α -Cre driver lines originating from Casanova et al. (E18) and Minichiello et al. (E15). d) β -galactosidase expression in brains isolated from offspring resulting from matings using the CamKII α -Cre driver line from Tsien et al. (E16, P2, P8, P14 and P21).

To rule out the possibility of occasional germline expression of Cre in conditional KO mouse lines, a PCR method was developed to control for this event using two primers outside and one primer inside the floxed region (Figure 20, bottom left). However, as can be concluded from the electropherogram in Figure 20, a band corresponding to the size of a null-allele could occasionally be observed using template-DNA extracted from tail-tip biopsies in theoretically forebrain-specific conditional-KO mouse lines containing the CamKII α -Cre transgene from the Tsien et al. origin (see lanes 2 and 4, Figure 20).

RESULTS

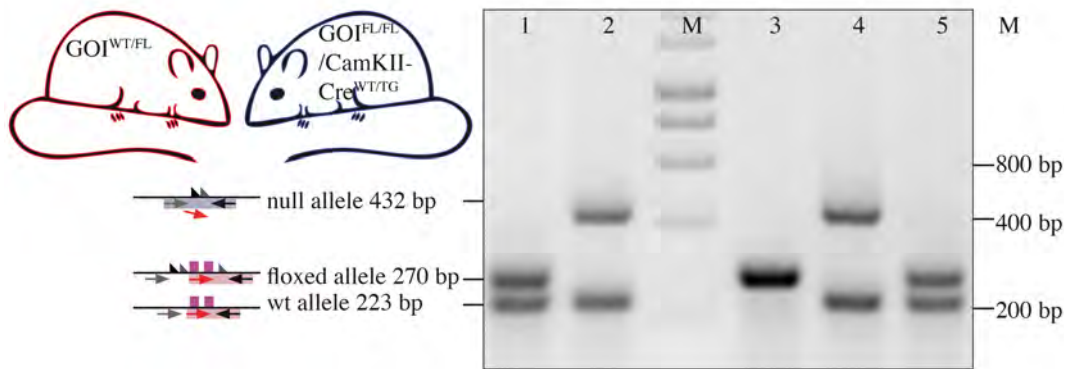


Figure 20: PCR method to control for CamKII α -Cre expression in germ cells. Genotyping PCR using tail-tip DNA extracts from offspring resulting from matings of GOI^{WT/FL} females (mouse shown in red) with GOI^{FL/FL}/CamKII-Cre^{WT/TG} males (mouse shown in blue). As shown by agarose gel electrophoresis, besides the expected band sizes for GOI^{WT/FL} and GOI^{FL/FL} mice also bands at the size of GOI^{WT/KO} mice (with a null-allele, lanes 2 and 4) were obtained. The results were obtained using samples from one litter. GOI: gene of interest. M: molecular weight marker.

4.2 Spastin

4.2.1 Spastin targeting strategy and confirmation

In mice, the *Spg4* gene is coded on chromosome 17 and comprises 17 exons (Figure 21a). Gene knockout aims to delete one or more exons that are critical for protein function. Since a major part of exon 1 is not present in all spastin isoforms, the exons 2 and 3 do not lead to a frameshift mutation and exon 4 is alternatively spliced, exon 5 was the first exon suitable for targeting (Figure 21, highlighted in red). In its absence, a frameshift mutation occurs, leading to a nonsense-mediated decay and the loss of protein function.

a) wild type allele (spastin^{WT}):



b) linearized targeting vector:



c) KO-first allele (spastin^{KO-1st}):



d) floxed allele after FLP recombination (spastin^{FL}):



e) frameshift allele after FLP recombination, followed by Cre recombination (spastin^{KO}):



f) reporter allele after Cre recombination only (spastin^{GT}):



Figure 21: Targeting strategy for the murine spastin gene. a) The spastin^{WT} allele is shown; the targeted exon 5 is highlighted in red. The genomic region targeted by homologous recombination is highlighted in pink. b) Linearized targeting vector used for targeting of the spastin^{WT} allele. Depending on the sequence of matings with Cre and Flp recombinases of the spastin^{KO-1st} animals (c), spastin^{FL} floxed (after FLP recombination (d)), spastin^{KO} frameshift (after Flp followed by Cre recombinations (e)) and Spastin^{GT} gene-trap reporter loci (after direct Cre excisions (f)) can be generated. The binding sites for the 5' Southern Blot probe and the 3' long-range PCR are indicated to demonstrate correct targeting. Grey arrows show the binding sites for the primers P169, P61, P23, P41 and P89.

A targeting vector with targeted exon 5 was obtained from KOMP also containing exons 6, 7 and 8 in the 3' homology region (Figure 21b). The correct *E. coli* clone containing the targeting vector was selected from *E. coli* bacteria obtained from KOMP after the confirmation of the correct sequence by restriction digestion and sequencing (for a detailed description of the used KOMP targeting vectors see section 4.1.1 and Figure 18). Using the restriction endonuclease *AsiSI*, the selected targeting vector was quantitatively linearized and used for electroporation of ES cells derived from C57BL/6NJMA8 mice (Figure 21b and Figure 22).

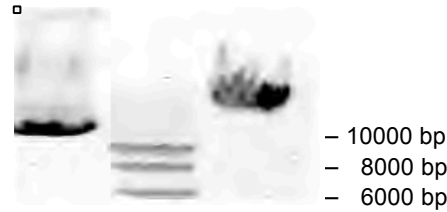


Figure 22: Agarose gel confirming the linearization of the spastin targeting vector using the restriction endonuclease *AsiSI*. Lane1: Spastin targeting vector before restriction digestion; Lane 2: molecular weight marker (HyperLadder I, Bioline); Lane 3: Spastin targeting vector after *AsiSI* digestion.

4.2.1.1 Southern Blotting

To confirm the correct insertion of the targeting vector at the 5' end of the homology arm, a probe for Southern Blotting (the binding sites are indicated in Figure 21a and c; for a detailed sequence information see chapter 7.5.3) was generated using the primers P20 and P21 (Table 8). After digestion using the restriction endonuclease *EcoRV*, the probe recognized a DNA-fragment of 18.5 kb in DNA extracts derived from wild type mice. Because the targeting vector contained an additional *EcoRV* restriction site, a 14.8 kb fragment could be observed in targeted *spastin*^{KO1-st^{WT}} ES cells and their progeny (see Figure 23a and b).

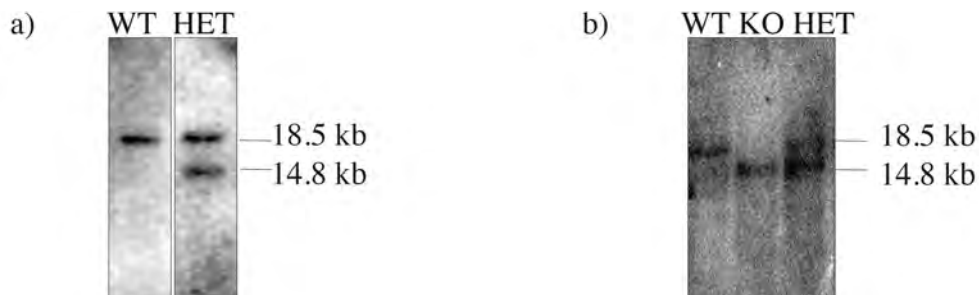


Figure 23: Confirmation of the correctly targeted murine spastin gene at the 5' homology arm via Southern Blotting. *EcoRV* digestion of wild type DNA leads to an 18.5 kb fragment between exons 2 and 6 of the spastin gene. The correct insertion of the targeting cassette introduces a new *EcoRV* restriction site leading to a shorter 14.8 kb fragment detectable by the 5' probe (see Figure 21 for strategy) in the KO-1st allele. a) The Southern Blot was performed using DNA extracts originating from ES-cell clone 1C11 (HET). b) The Southern Blot was done using DNA extracted from tail-tip biopsies from *spastin*^{KO-1st}-allele F2 generation littermates descending from ES-cell clone 1C11. WT: *Spastin*^{WT/WT}; KO: *Spastin*^{KO-1st/KO-1st}; HET: *Spastin*^{WT/KO-1st}.

4.2.1.2 Long-range PCR

Because the generation of a 3' probe for Southern Blotting did not lead to satisfactory results using DNA extracts derived from wild type mice (data not shown), a long-range PCR was established to confirm the correct insertion of the targeting vector at the 3' end. As can be

concluded from Figure 21c, the forward primer P61 binds close to the third loxP site in the targeted locus, which originates from the targeting vector, whereas the reverse primer P23 (Table 8) binds downstream of the targeting vector region, which should be present both in wild type and in targeted alleles. As expected, a 5043 bp band could be observed in *spastin*^{KO-1st}-allele ES cells as well as in their progeny (Figure 24).

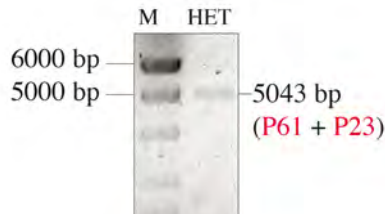


Figure 24: Agarose gel showing results from 3' long-range PCR to confirm correct targeting of *spastin*^{WT/KO-1st} in animals (HET) derived from ES cell clone 1C11. Primers P61 and P23 were used to amplify a long-range PCR product of 5043 bp. M: molecular weight marker (HyperLadder I, Bioline).

Mating of KO-first-allele mice to a Flp-recombinase driver line leads to the excision of the LacZ- and the neomycin-phosphotransferase cassettes resulting in a floxed allele that is flanked by one FRT site and two loxP sites (Figure 21d). The usage of primers P41 and P89 in polymerase chain reaction can detect the presence of the additional loxP and FRT sites by a slight band shift of the PCR product from 1256 bp for wild type and 1515 bp for floxed mice. The lack of the wild type PCR product in homozygous floxed animals was used to additionally prove the insertion of the targeting vector at the locus of purpose (Figure 25).



Figure 25: Confirmation of correct targeting of the *Spg4* gene in PCR using the primers P41 and P89. DNA extracts from *spastin*^{WT/WT} (+/+), *spastin*^{WT/FL} (+/FL) and *spastin*^{FL/FL} (FL/FL) animal tail-tip biopsies were used as template for the polymerase chain reaction.

4.2.1.3 Confirmation of spastin protein loss in brain lysates

To confirm the ultimate loss of spastin protein in spastin knockout mice, antibodies derived from mouse clone 6C6 (Table 4) were used. To confirm the specific binding of the antibodies to spastin, HEK293-TN cells were transfected with a pEGFP-spastin construct starting from methionine M85 (pEGFP-spastin- Δ M1; see Table 6). The proteins from the lysates were separated by SDS-PAGE and analyzed by Western Blotting using the 6C6 anti-spastin and anti-GFP antibodies (Figure 26).

In pEGFP-transfected HEK cells, a 30 kDa fragment was detected using the anti-GFP antibody and a band of approximately 50 kDa when using the spastin 6C6 antibody (lanes 1 and 5). In non-transfected control cells (lanes 2 and 6), no band could be observed using the GFP antibody and a band at the same molecular weight as in pEGFP-transfected-cells when using the anti-spastin antibody. Contrarily, in pEGFP-spastin- Δ M1-transfected cells, two fragments of 75 kDa

RESULTS

and approximately 50 kDa were detected for both the GFP and the spastin antibodies (lanes 3 and 7 respectively). The 75 kDa band approximately corresponds to the expected molecular weight of the GFP- Δ M1-spastin fusion protein. The 50 kDa band has approximately the molecular weight expected for spastin starting from methionine M85/87.

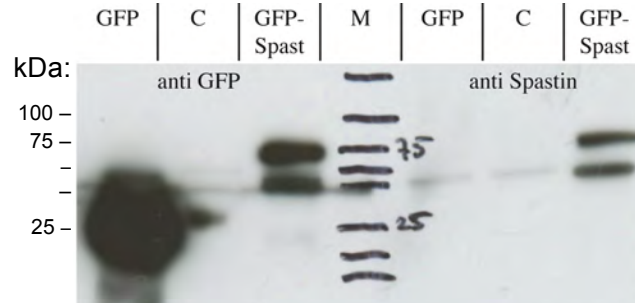


Figure 26: Western Blotting of pEGFP-transfected, untransfected, and pEGFP-Spastin- Δ M1-transfected HEK-cell lysates using the mouse monoclonal 6C6 anti-spastin antibody or the rabbit anti-GFP antibody (SIGMA). GFP: pEGFP-transfected cells, C: untransfected control cells, GFP-Spast: pEGFP-Spastin- Δ M1-transfected cells.

The latter antibody was subsequently used to determine the loss of spastin expression in Western Blotting using full-brain lysates derived from spastin^{KO 1-st/KO 1-st} and spastin^{KO/KO} mutant mice separated by SDS-PAGE. As can be seen in Figure 27a and b, the bands at the expected approximal molecular weights of spastin (approximately 50 and 60 kDa corresponding to the isoforms starting from methionine M85) can no longer be detected both in spastin^{KO 1-st/KO 1-st} and spastin^{KO/KO} mutants. The quantification of signal intensities from heterozygous spastin^{KO 1-st/WT} animals revealed a reduction of approximately 54 % (Figure 27a and c). A one-way ANOVA revealed that the means of the measured spastin signal intensities differed significantly for the three genotypes $F(2, 15) = 46.85, p < 0.0001$. Sidak's multiple comparisons test yielded that spastin levels were significantly reduced in both heterozygous mice ($t = 5.478, df = 15, p = 0.0001$) as well as in knockout mice compared to wild types ($t = 9.650, df = 15, p < 0.0001$).

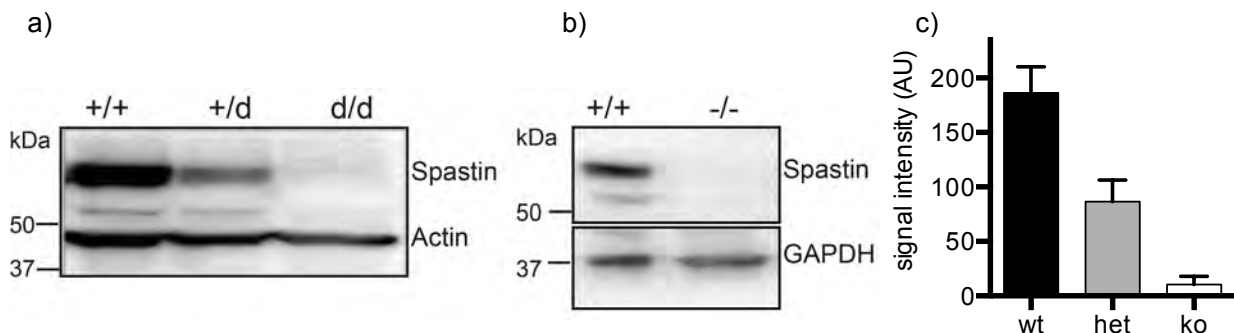


Figure 27: Reduced spastin protein levels in prenatal spastin KO mice as revealed by Western Blotting using the 6C6 anti-spastin antibody on whole brain lysates. a) Western Blotting analysis of lysates from spastin^{WT/WT} (+/+), spastin^{WT/KO-1st} (+/d) and spastin^{KO-1st/KO-1st} (d/d) littermates. A primary antibody directed against actin was used as a loading control. b) Western Blotting analysis of lysates derived from null-allele mutant spastin^{WT/WT} (+/+) and spastin^{KO/KO} (-/-) littermates. An antibody directed against GAPDH was used as a loading control. c) Quantification of spastin protein loss in prenatal spastin KO mice after normalization to the mean signal intensity of each tested group. The error bars represent the SEM.

The latter antibody was also used to determine the reduction of spastin protein levels in forebrain-specific spastin KO animals (spastin^{FL/FL}/CamKII α -Cre^{WT/TG}). Brains from 15-week-old mice were isolated and separated into olfactory bulb, cortex, hippocampus, midbrain and cerebellum. After SDS-PAGE of the brain lysates, the 6C6 anti-spastin antibody was used for Western Blotting analysis. The spastin-specific signal intensities were normalized to the ones for PAN-cadherin or for NSE, which were used as loading controls. In contrast to mice with full spastin knockout, conditional spastin KO animals only showed a reduction of signal intensity for the upper of the two bands detected by the anti-spastin antibody. Interestingly, there was no difference in the lower band intensities between spastin^{WT/WT}/CamKII α -Cre^{WT/TG} and spastin^{FL/FL}/CamKII α -Cre^{WT/TG} littermates (Figure 28a).

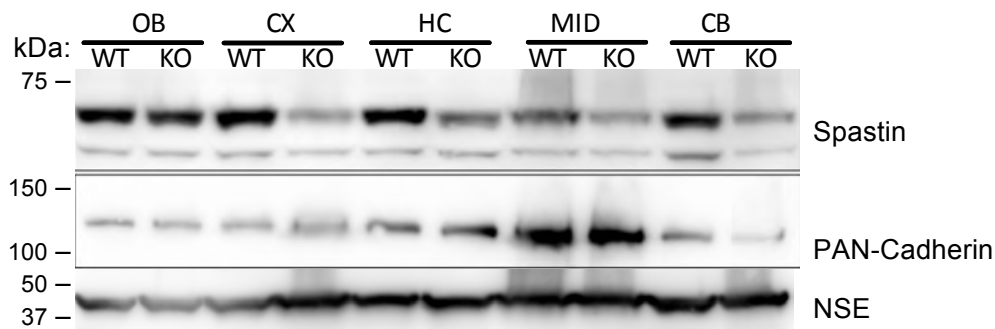


Figure 28: Conditional targeting of spastin. a) Western Blotting analysis of spastin expression in brain lysates obtained from 15 weeks spastin^{WT/WT}/CamKII α -Cre^{WT/TG} (termed WT) and spastin^{FL/FL}/CamKII-cre^{WT/TG} littermates (termed KO). The mouse anti-spastin antibody (clone 6C6) was used. PAN-cadherin and NSE were used as loading controls. *OB*: olfactory bulb; *CX*: cortex; *HC*: hippocampus; *MID*: midbrain; *CB*: cerebellum.

The Western Blotting upper band signal intensities using the 6C6 anti-spastin antibody revealed a mean reduction by 83 % for the cortex, 69 % for the hippocampus and by 80 % for the midbrain in adult spastin^{FL/FL}/CamKII α -Cre^{WT/TG} mice. The results could not be tested for significance due to a small sample size.

4.2.1.4 Confirmation of spastin protein loss in immunocytochemistry

Neurons were cultivated from hippocampi isolated from spastin^{WT/WT} animals and spastin^{KO/KO} littermates at postnatal day 0 to confirm spastin protein loss in the KOs. As can be seen in Figure 29a, the usage of the 6C6 primary antibodies followed by Alexa 488 anti-mouse secondary antibodies led to reduced fluorescence signal intensities as detected by confocal laser-scanning microscopy. A significant difference in the mean fluorescence intensities between the genotypes obtained from 4 different experiments could be confirmed with an ordinary one-way ANOVA: $F(2, 76)=79.13$, $p<0.0001$. A post hoc Tukey test showed that the means between WT vs. HET, WT vs. KO and HET vs. KO differed significantly ($p<0.0001$, <0.0001 and $p=0.0001$, respectively).

The mean fluorescence intensities were reduced by 41 % for HET and by 74 % for KO when compared to the mean fluorescence intensities from WT pointing to an intermediate reduction of spastin protein levels for heterozygous animals.

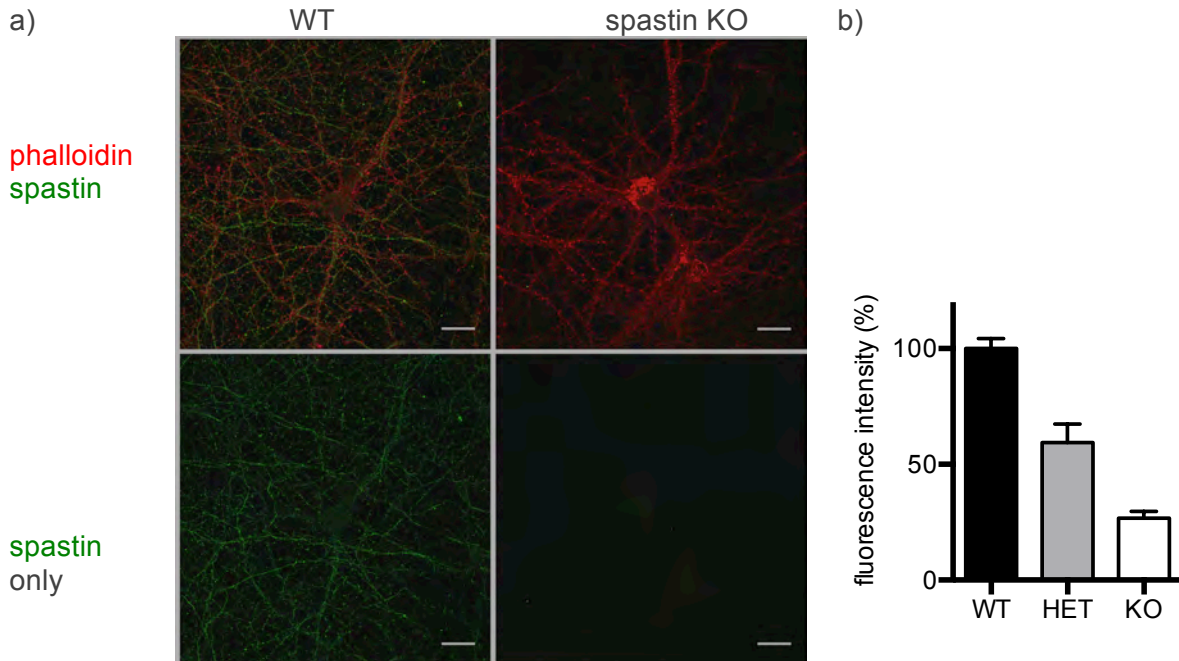


Figure 29: Immunocytochemistry using the spastin 6C6 antibody. A) Exemplary picture showing cultivated postnatal day 0 primary hippocampal neurons derived from spastin^{WT/WT} (termed WT) animals and spastin^{KO/KO} (termed KO) littermates that were stained using the monoclonal 6C6 anti-spastin antibody (green) and phalloidin (red). B) Quantification of the mean fluorescence intensities obtained from four independent experiments (with n=35 measurements for WT, n=15 for HET, and n=29 for KO). The measured fluorescence intensities were normalized to the mean fluorescence intensity from WT. Scale Bar: 20 μ m

4.2.2 General health of spastin depleted animals & reproduction

4.2.2.1 Litter sizes and genotype distribution for mouse lines with prenatally depleted spastin

To determine whether the general depletion of spastin affected litter size, parent animals with different genotype combinations (WT x HET vs. HET x HET vs. WT x KO) were mated and the number of pups per litter was analyzed. As shown in Figure 30, the litter sizes averaged approximately 6 pups per litter for both WT x HET vs. HET x HET matings (two-tailed t-test: $t=1.199$, $df=96$, $p=0.2334$). In contrast to that, no pups were obtained for WT x KO matings (4 KO females and 6 KO males were tested in total).

RESULTS

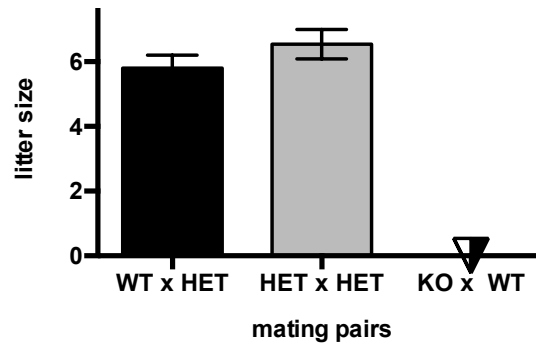


Figure 30: Litter sizes resulting from matings of prenatally depleted spastin KO mice. Heterozygous spastin-KO mice were mated with either WT (left column) or heterozygous spastin KO mice (right column). n=46 matings for WT x HET with a mean litter size of 5.80 ± 0.39 and n=52 matings for HET x HET with a mean litter size of 6.54 ± 0.46 were analyzed in total. Because both spastin^{KO-1st} and spastin^{KO} mice showed the same tendency, results from both mouse lines were combined. The graph represents the mean litter sizes \pm SEM.

In order to study how the defective spastin allele is inherited, mice with a prenatal spastin depletion (spastin^{KO-1st} alleles and spastin^{KO} alleles) were mated, and the genotypes from the resulting pups were determined for each litter. As shown for WT x HET matings (Figure 31a), there was a significant difference between the genotypes obtained per litter with 3.2 ± 0.3 for wild type pups versus 2.4 ± 0.2 for heterozygous pups (two-tailed t-test: $t = 2.655$, $df = 80$, $p = 0.001$).

The genotypes of 260 animals from 43 litters resulting from HET x HET matings were distributed as follows: 77 WT, 134 HET, 49 KO in comparison to the theoretically expected values of 65 WT, 130 HET, 65 KO (see Figure 31b). A Chi-square test yielded that the observed genotype distribution was significantly different from the expected one (Chi-square=6.277, $df = 2$, $p = 0.0433$). The mean numbers of pups per litter were 1.8 ± 0.22 for WT, 3.2 ± 0.35 for HET and 1.2 ± 0.19 for KO animals, respectively. There were significantly fewer pups obtained for KO than for WT (two-tailed t-test: $t = 2.308$, $df = 82$, $p = 0.0235$).

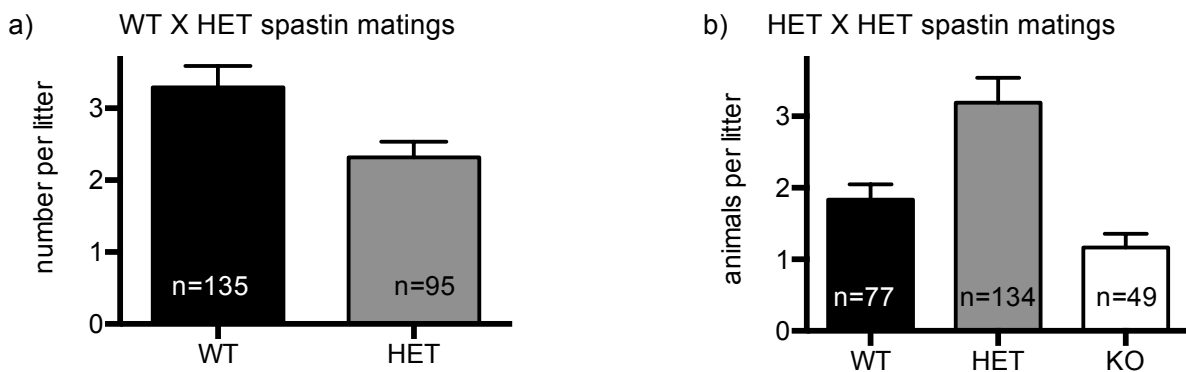


Figure 31: Genotype distribution of mouse lines with prenatally depleted spastin. The mean number of pups for each genotype (WT, HET, KO) per litter \pm SEM is shown for a) HET x WT and b) HET x HET matings. a) 42 litters with 230 animals and an average litter size of 5.6 were analyzed. b) 43 litters with 260 animals and an average litter size of 6.01 were analyzed.

To determine the causality of lacking offspring from WT x spastin KO matings, testicles from spastin^{KO-1st/KO1-st} males and their control littermates were isolated. An initial opening of WT testicles in buffer solution allowed the observation of sperm motility in the solution, but not for the testicles that were derived from spastin^{KO1-st/KO1-st} males (data not shown).

Also, methylene blue stainings to visualize DNA were done on semithin sections from testes (0.5 μm) isolated from adult spastin^{WT/WT} and spastin^{KO-1st/KO-1st} littermates (see section 3.2.11). In contrast to WT mice, no spermatocytes could be observed in homozygous KO mice (Figure 32 left). Additional electron micrographs of ultrastructural analysis of testicles failed to visualize mature and elongated spermatocytes for homozygous spastin KO mice in contrast to their WT littermates (Figure 32 right).

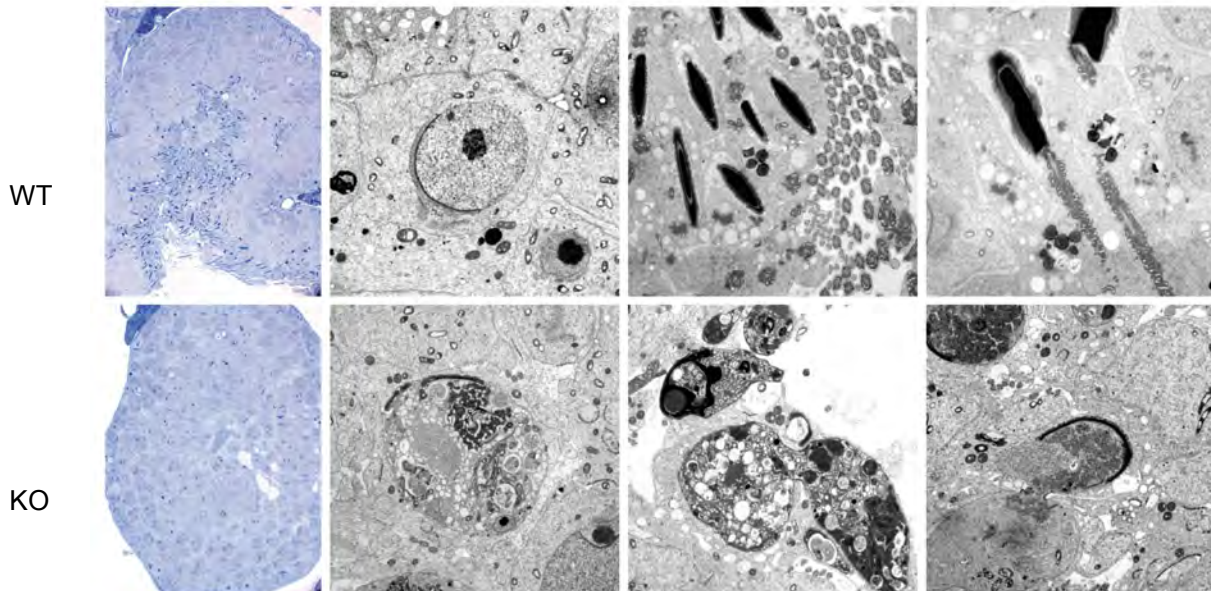


Figure 32: Sterility of homozygous spastin knockout mice. Testes derived from adult spastin^{WT/WT} (WT) and homozygous spastin^{KO-1st/KO-1st} (KO) littermates (n=1 for each genotype) were analyzed. Left: methylene blue-stained semithin sections of testes (0.5 μm). Right three pictures: electron micrographs of ultrathin sections from testes (60 nm). 3 representative electron micrographs are shown for each genotype.

4.2.2.2 Body weight of mice prenatally depleted for spastin

Spastin KO mice between 2 and 43 weeks of age were compared to their gender-matched littermates in terms of body weights (Figure 33). The body weights of homozygous spastin KO mice were significantly reduced by approximately 6.5 % in comparison to their gender and age-matched wild type littermates (Kruskal-Wallis-test (H=8.029, p=0.018); Dunn's multiple comparisons test (mean rank differences 7.117 for WT vs. HET and 14.13 for WT vs. KO)).

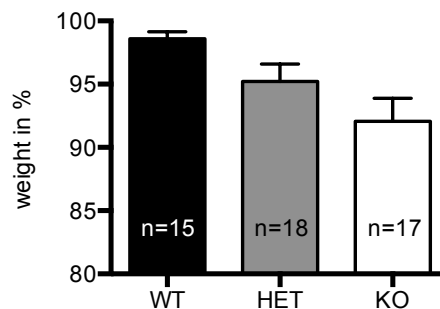


Figure 33: Gender and age-matched relative body weights of spastin WT, HET and KO animals. The body weights of 2-43 week old animals were normalized to the heaviest animal of the corresponding litter of the same gender and age. The graph shows mean values, the error bars representing \pm SEM. Mean relative body weights were 98.6 % for WT, 95.2 % for HET; and 92.1 % for KO mice. 15 WT, 18 HET and 17 KO animals were tested.

4.2.2.3 Motor function

Because spastin plays an important role in motor function and the available mouse models were reported to have gait abnormalities as well, mice were video-analyzed in their transparent homecages without bedding from a ventral view. The distance between their hind limbs during regular horizontal locomotor activity was measured for 5 min (Figure 34a). Compared to wild type mice, all mice with a prenatal depletion of spastin showed a larger stride length between their hind limbs compared to their control littermates: two-way ANOVA (age group x genotype): main effect for age group: $F(2, 609) = 60.59$, $p < 0.0001$; main effect for genotype: $F(1, 609) = 89.98$, $P < 0.0001$; interaction effect: $F(2, 609) = 20.66$, $P < 0.0001$ (Figure 34c). Sidak's multiple comparisons test resulted in significantly larger stride lengths for each knockout mouse compared to its wild type littermate ($t = 13.1$, $dF = 609$, $p < 0.0001$ for 4-month old mice; $t = 2.985$, $dF = 609$, $p = 0.0088$ for 6 month old mice; $t = 3.215$, $dF = 609$, $p = 0.0041$ for 9-month-old mice). However, the mean of the averaged step lengths for each subject tested did not yield any significantly different result between the two genotypes (two-tailed t-test: $t = 1.54$, $df = 4$, $p = 0.1985$).

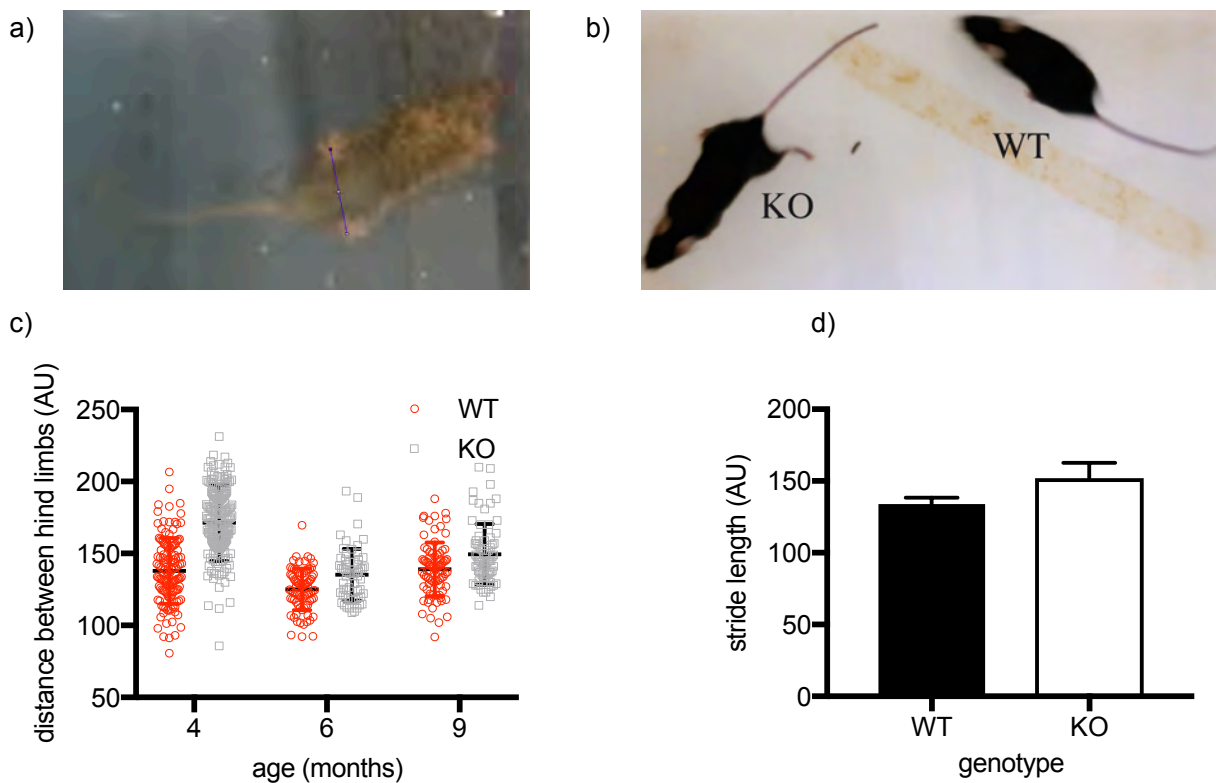


Figure 34: Altered gait parameters in adult spastin KO mice. 3 WT and 3 spastin-KO mice at 4, 6 and 9 months were video-analyzed during homecage activity and the stride length between their hind limbs was measured using the ImageJ software. a) Exemplary picture showing the measurements of stride length using the imageJ software. b) Exemplary picture showing the gait of a spastin^{WT/WT} and a spastin^{KO/KO} mouse. c) Representation of the individual step lengths in AU (normalized to the cage size) for gender and age-matched littermates with and without a prenatal spastin depletion (labeled KO and WT, respectively). For each age and genotype, one mouse (n=1) was tested. d) Mean stride length ± SEM in AU (values were normalized to the corresponding cage size) for wild type ($134 \pm 4,509$, n=3) and knockout ($152 \pm 10,79$, n=3) mice.

4.2.3 Spastin expression pattern

4.2.3.1 Endogenous spastin promoter activity in heterozygous reporter knockouts

By mating spastin^{KO-1st} animals with Cre-deleter lines, spastin^{WT/GT}/Cre^{WT/TG} offspring with a LacZ reporter cassette could be generated (see also Figure 21f). This allowed studying endogenous spastin promoter activity and expression in developing mice via LacZ stainings. For that purpose, postnatal day 8 and adult (13 weeks old) spastin^{WT/GT} littermates with a heterozygous reporter allele were used for LacZ staining of brain and organs (Figure 35 and Figure 36).

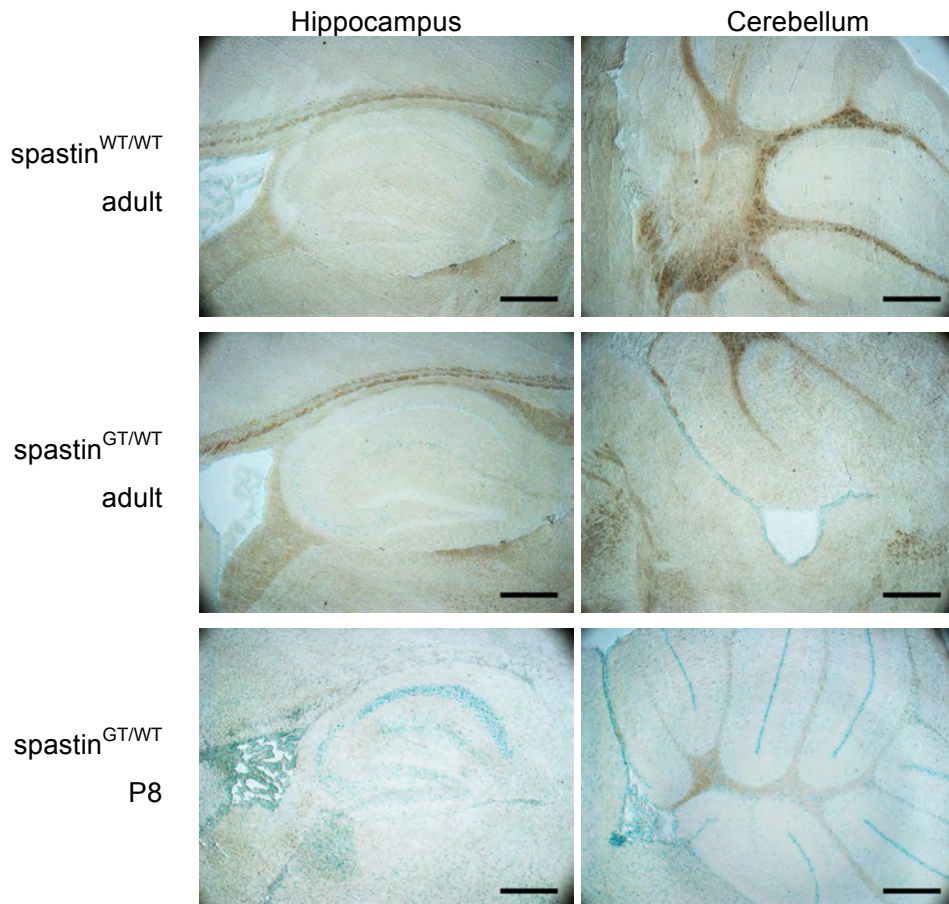


Figure 35: Assessment of endogenous spastin promoter activity in brains of heterozygous spastin reporter KO mice (spastin^{GT/WT}/Cre^{WT/TG}). LacZ stainings of hippocampi and cerebelli from adult and postnatal day 8 (P8) mice. A negative control of WT littermates is shown for adult mice. The experiment was repeated 3 times. Scale bar: 400 μ m.

In the brain, the strongest LacZ staining was observed at postnatal day 8 in the CA1 region of the hippocampus followed by the cerebellum and the CA3 and dentate gyrus of the hippocampus. Also, a scattered expression throughout the whole brain, including the frontal cortex was visible. The expression in the brain declined strongly in adult mice and was mainly confined to the CA1 and CA3 regions of the hippocampus and parts of the cerebellum. In the dentate gyrus, the LacZ staining was not detectable any longer.

In contrast, the LacZ signal was stronger in other organs (heart, stomach, kidney and lung), with the strongest expression in the pelvis of the kidney (Figure 36). With exception of lung tissue, the staining persisted at nearly the same strength through adulthood.

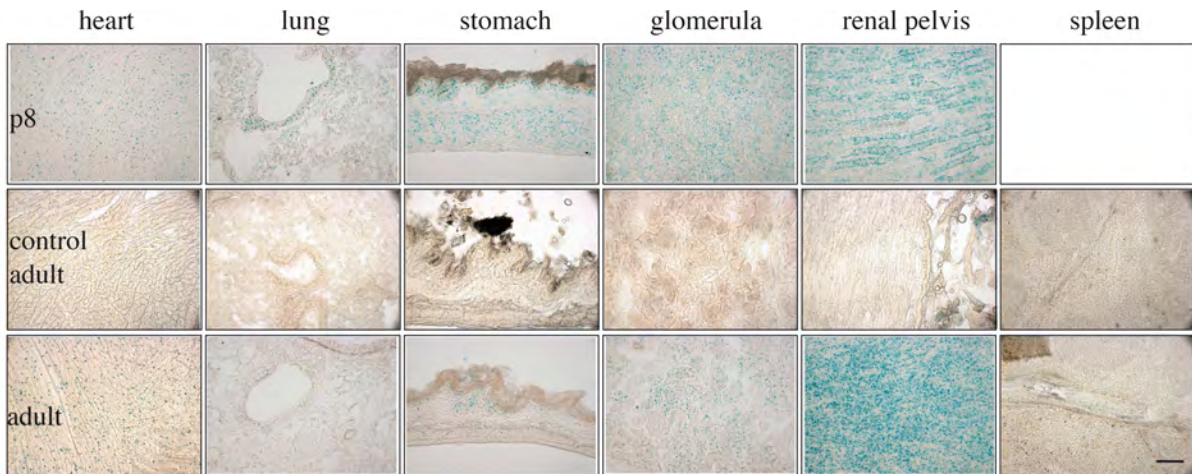


Figure 36: LacZ staining of cryosectioned heterozygous spastin reporter mouse ($spastin^{WT/GT}$) tissues to evaluate the endogenous expression pattern of spastin at postnatal day 8 and in adult mice. Tissue from the heart, stomach, kidney (pelvis and glomerula) and lung from postnatal day 8 (top row) and adult mice (13 weeks, bottom row) are shown. Scale bar (applies to all images): 100 μ m.

4.2.3.2 Spastin expression pattern in the brain at the protein level

The expression of spastin at the protein level was analyzed in Western Blotting using the 6C6 antibody on brain lysates, separated into olfactory bulb, cortex, hippocampus, midbrain and cerebellum isolated from wild type mice of different age (1 week, 6 weeks, 27 weeks).

As Figure 37 shows, spastin expression could be detected in all brain regions tested and at all ages using the anti-spastin (6C6) antibody with the strongest expression in the hippocampus of 1-week-old mice.

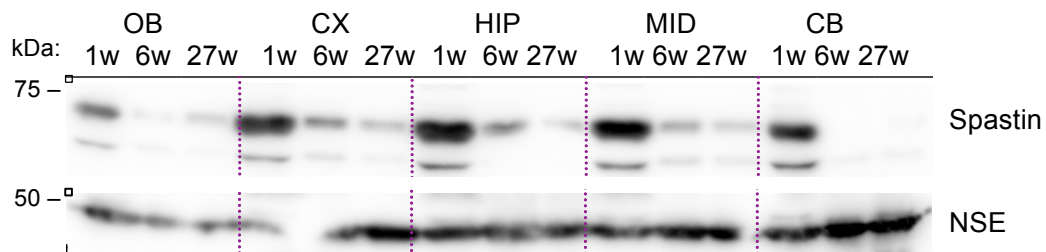


Figure 37: Western Blotting analysis of spastin expression in different brain regions in young, adolescent and adult mice. The lysates were derived from 1 week, 6 week and 27-week-old wild type mice. The brains were separated in olfactory bulb (OB), cortex (CX), hippocampus (HIP), midbrain (MID) and cerebellum (CB), respectively. The anti-spastin 6C6 antibody (1:500) and the anti-NSE control antibody were used.

The strongest expression was observed in the brains of one-week-old mice including cortex, hippocampus and midbrain. At 6 and 27 weeks, spastin expression decreases in all brain regions.

4.2.3.3 Subcellular location of spastin

The subcellular location of endogenous spastin was analyzed in immunocytochemistry using the anti-spastin 6C6 antibody on DIV7 cultivated hippocampal neurons derived from postnatal day 0 wild type mice. As shown in Figure 38, signals could be detected in the cell soma as well as in different compartments of the neurites, such as their tips, bifurcating growth cones (b), transport

vesicles (c), branching points, synaptic contacts (d), regions with strong curvature (e) and structures resembling neurite swellings (f and g).

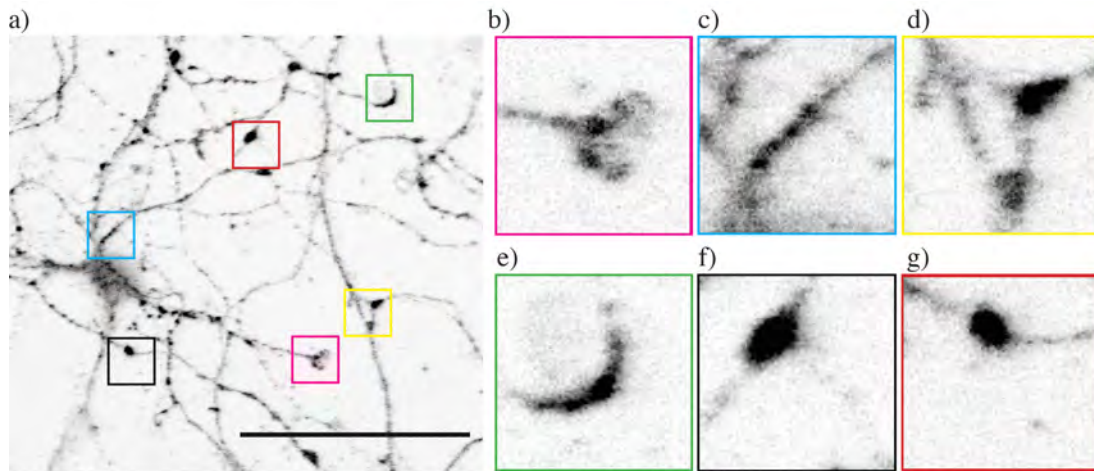


Figure 38: Localization of the anti-spastin 6C6 antibody signal in primary hippocampal neurons. a) Immunofluorescence of cultured mouse postnatal day 0 hippocampal neurons at DIV 7 using the monoclonal anti-spastin 6C6 antibody. The signal was detected in bifurcating growth cones (pink box, b), transport vesicles (blue box, c), neurite branching points and synapses (yellow box d), neurite bending/curvature points (green box, e) and neurite swellings (black and red boxes, f and g). Scale bar: 50 μm .

In addition, the distribution of ectopically expressed spastin was studied in neurons. At 10 days in vitro, overexpression of an EGFP-tagged spastin isoform starting from methionine M85 and retaining exon 4 in cultivated hippocampal neurons for 12 hours resulted mainly in a perinuclear location of the fusion protein and to a lesser extent in proximal neurites and branching points (Figure 39).

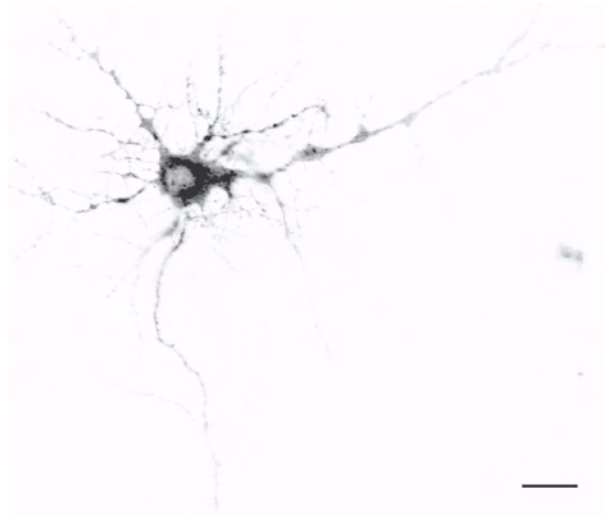


Figure 39: Overexpression of EGFP-spastin in neurons. Primary hippocampal neurons were transfected at DIV10 with pEGFP-spastin starting from methionine M85 for 12 hours. Excessive branching and neurite swelling was observed. No spastin-transfected neurons could be found 48 h after transfection, indicating that its overexpression into differentiated primary neurons is toxic. Scale bar: 20 μm .

In order to determine the expression of spastin and katanin at the subcellular level, differential centrifugation (as described in section 3.4.2) was performed using mouse whole brain homogenates at postnatal day 11. In addition to spastin and katanin, antibodies directed against

other neuronal proteins, e. g. GluN2B, Kif2a, GluR2 and PSD-95 were used in a Western Blotting analysis of the subcellular fractions (see Figure 40a).

The postsynaptic proteins GluN2B, PSD-95 and GluR2 were primarily found in pellets 1 through 3 including fractions corresponding to cell membrane debris, large vesicular cell organelles to microsomes and small transport vesicles (P1, P2, P3, S1 and S2). In contrast, the plus end depolymerase KIF2a and spastin were found in all subcellular fractions, including a weaker signal in the S4 fraction that corresponds to soluble proteins. Katanin was primarily detected in the P2 and P3 fractions but was also present in the remaining fractions at a low expression level.

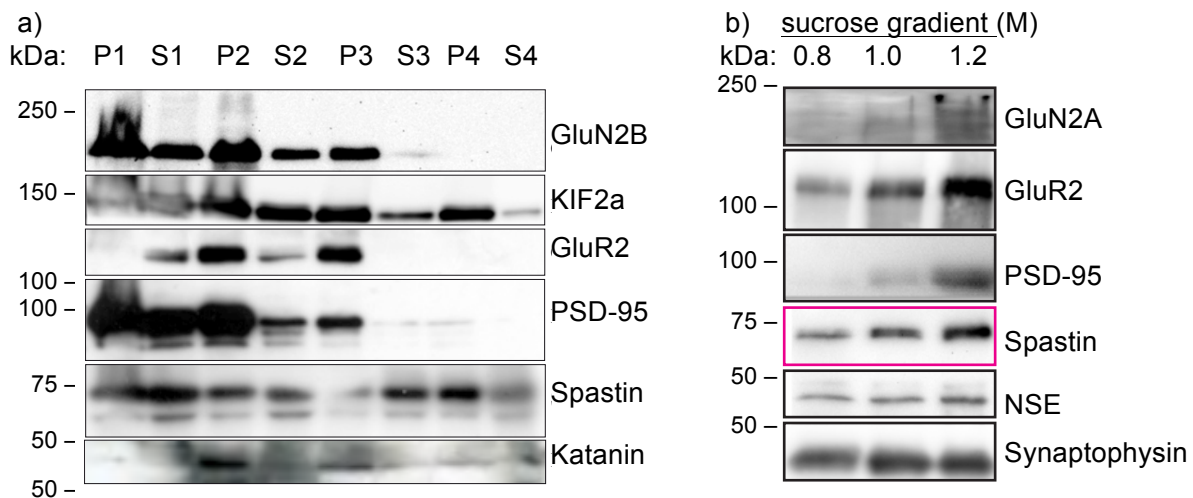


Figure 40: Spastin expression in different subcellular fractions. a) Subcellular fractions obtained from differential centrifugation of whole mouse brains at postnatal day 11. After SDS-PAGE, antibodies directed against GluN2B, KIF2a, GluR2, PSD-95, katanin and spastin were used for Western Blotting. P1-P4: pellets 1-4; S1-4: supernatants 1-4. P1: cell debris, mitochondria and nuclei. P2: small cell membrane debris, mitochondria, large vesicular cell organelles (e. g. ER), P3: Golgi, transport vesicles, microsomes etc. P4: small vesicles and protein complexes. B) Synaptosomal fractionation of whole brains from postnatal day 9 wild type mice were differentially fractionated using a sucrose gradient from 0.8 to 1.2 M sucrose. The obtained lysates were separated by SDS-PAGE followed by Western Blotting analysis. Antibodies directed against GluN2A, GluR2, PSD-95, NSE and synaptophysin were used as loading controls.

In addition, density gradient centrifugation was used to obtain fractions enriched in synaptic proteins (synaptosomes) from postnatal day 9 mouse whole brain homogenates (as described in 3.4.3). As shown in Figure 40b, the fractions with 1 M and 1.2 M sucrose were enriched in postsynaptic and presynaptic proteins such as GluN2A, GluR2, PSD-95 and synaptophysin, respectively. Spastin could be detected in all three fractions but was enriched in the synaptosomal fractions (1 M and 1.2 M sucrose).

4.2.4 Gross brain morphology of spastin KO-1st mice

Homozygous spastin^{KO-1st/KO-1st} mice and their WT littermates were sacrificed and their brains were used for the determination of the gross brain morphology using Nissl staining (as described in section 3.2.8).

As shown in Figure 41a, there were no apparent brain abnormalities in KO mice, compared to their WT littermates. However, a closer examination of the hippocampus pointed to a weaker density of the CA1 layer in KO mice (Figure 41b and c). Consequently, the CA1 regions of 11 WT, 6 HET and 11 KO mice between 2 and 43 weeks were measured and normalized to the thickest CA1 region of the corresponding litter (Figure 41d).

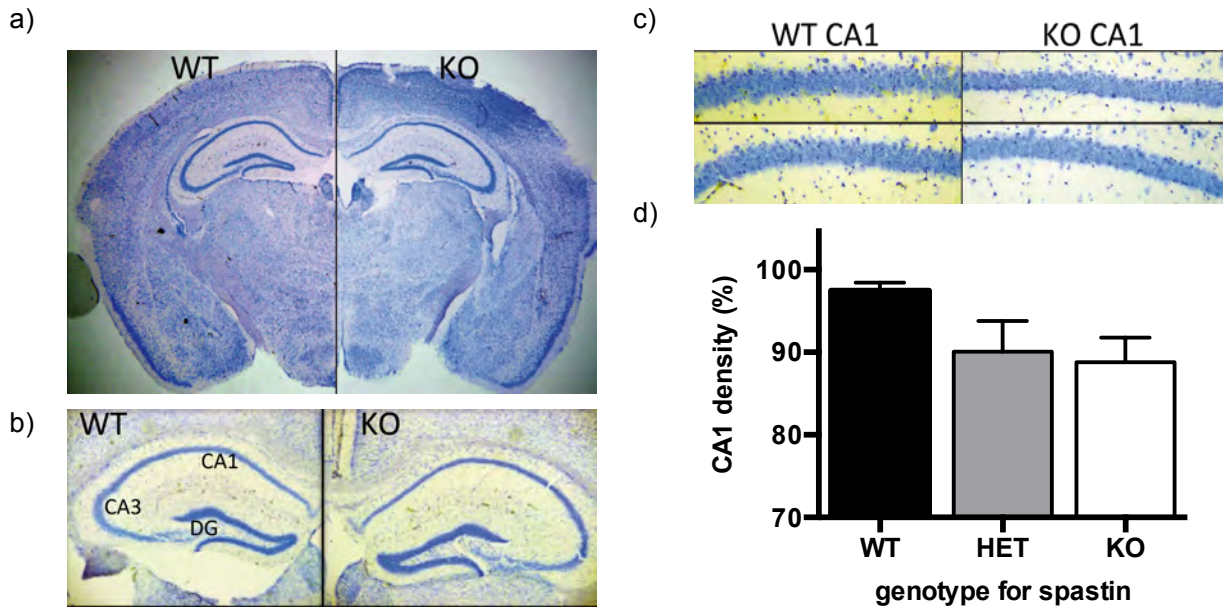


Figure 41: Nissl stainings of brain sections derived from wild type and spastin KO mice. a), b) and c) representative images of Nissl stained coronal brain sections from 8-week-old spastin^{WT/WT} and spastin^{KO1-st/KO1-st} littermates showing the gross brain morphology, the hippocampus and the magnified CA1 layers, respectively. d) Mean density of the CA1 layer in 2 to 43 week old spastin WT (97.46 ± 0.9913 %, n=11), HET (90.07 ± 3.711 %, n=6) and KO (88.81 ± 2.96 %, n=11) mice. The measured original values were normalized to the thickest CA1 region of the corresponding litter. The error bars represent the SEM.

A significant reduction in the CA1 layer density was detected for the knockouts compared to their WT littermates (unpaired t-test with Welch's correction: $t=2.760$, $df=12.19$, $p=0.0172$); the results for HET vs. WT were not significant (unpaired t-test with Welch's correction: $t=1.924$, $df=5.724$, $p=0.105$).

4.2.5 Microtubule modifications and AMPAR distribution in the hippocampus of spastin KO mice

Since polyglutamylated microtubules act as positive regulators of spastin's enzymatic activity (Lacroix, van Dijk et al. 2010), the polyglutamylation status of microtubules was tested in the CA1 dendrites of the hippocampus of WT versus KO mice using immunohistochemistry. As shown in Figure 42, increased polyglutamylation was observed in the proximal dendrites of the CA1 region of spastin^{KO-1st/KO-1st} mice. However, the results were not quantified due to the small sample size and time limitations.

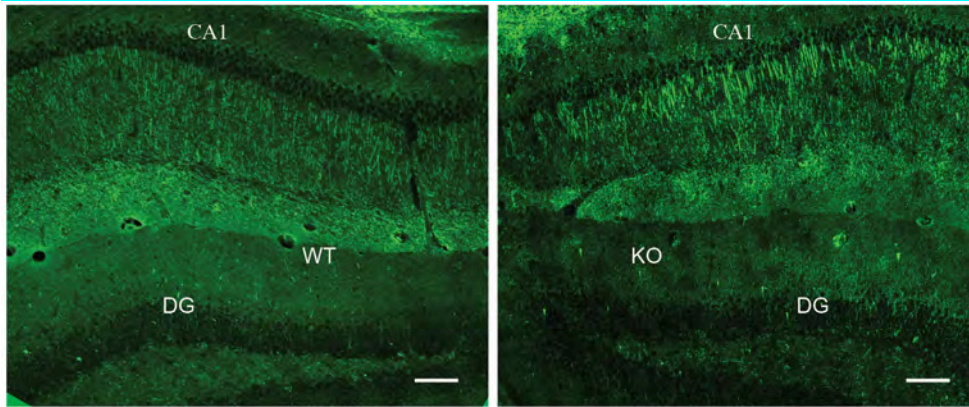


Figure 42: Immunohistochemistry analysis using coronal brain sections obtained from adult $spastin^{WT/WT}$ and $spastin^{KO-1st/KO-1st}$ littermates to study polyglutamylation of tubulin in spastin KO mice. The mouse anti-polyglutamylated tubulin antibodies (clone B3) were used. CA1: cornu ammoni 1; DG: gyrus dentatus. Scale bar: 100 μ m.

The analysis of whole brain lysates obtained from spastin knockout mice did not lead to significant results so far (not shown). Initial Western Blotting analysis of different brain regions using conditional spastin knockout mice ($spastin^{FL/FL}/CamKII\alpha-Cre^{TG/WT}$) and their control littermates using an antibody directed against polyglutamylated tubulin (clone B3) revealed the main expression of polyglutamylated tubulin in the cerebellum of $spastin^{WT/WT}/CamKII\alpha-Cre^{WT/TG}$ (termed WT) animals (Figure 43). In conditional knockout mice however, polyglutamylation levels of microtubules were only strongly increased in the hippocampus and not in the cortex where spastin levels were strongly reduced compared to the control littermates.

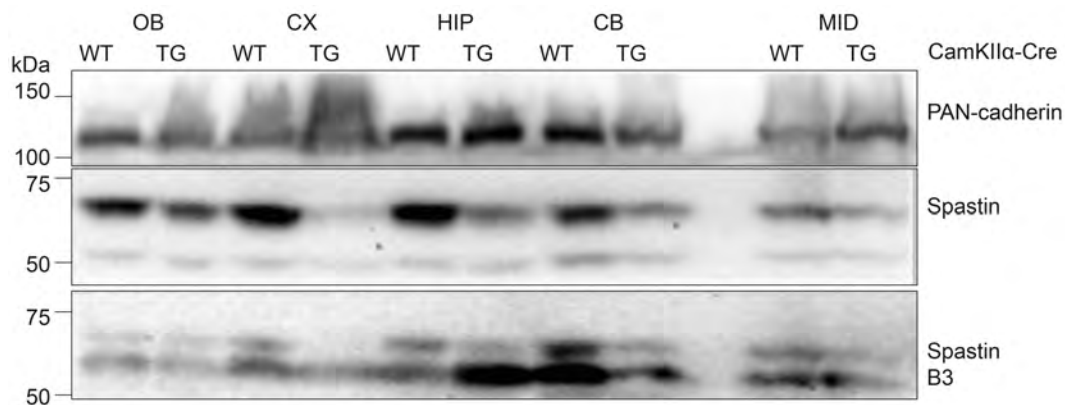


Figure 43: Western Blotting analysis using lysates obtained from different brain regions from $spastin^{WT/WT}/CamKII\alpha-Cre^{WT/TG}$ and $spastin^{FL/FL}/CamKII\alpha-Cre^{TG/WT}$ littermates. Anti-spastin and anti-PAN-cadherin antibodies were used as control proteins. Polyglutamylated tubulin (B3) was detected following the detection of spastin and washing with TBST. WT: $CamKII\alpha-Cre^{WT/WT}$; TG: $CamKII\alpha-Cre^{TG/WT}$. OB: olfactory bulb, CX: cortex, HIP: hippocampus, CB: cerebellum, MID: midbrain.

In line with the hypothesis of perturbed cargo delivery as a consequence of altered microtubule modification, the AMPA receptor subunit GluR2 was downregulated in immunohistochemistry analyses (Figure 44). The downregulation was not quantified further due to small sample size (n=1).

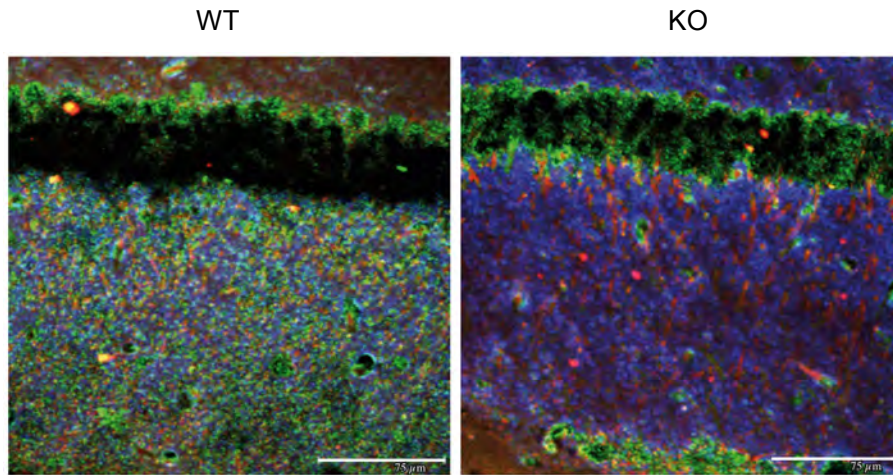


Figure 44: Immunohistochemistry analysis using coronal brain sections obtained from adult spastin^{WT/WT} and spastin^{KO-1st/KO-1st} littermates to study the expression levels of GluR2 (green), synaptophysin (blue) and the polyglutamylation of tubulin (red) in the stratum radiatum region of the CA1 in spastin KO mice. Scale bar: 75 μ m.

4.2.6 EB3 dynamics in dendritic spines of spastin knockout mice

Cultivated hippocampal neurons at DIV 16 derived from spastin^{WT/WT} and their spastin^{KO/KO} littermates were co-transfected with pEGFP-EB3 and pmRFP at postnatal day 7 (as described in section 3.2.6) and used for live cell imaging to visualize the mobility of intracellular GFP-EB3 comets (Figure 45a) (see section 3.2.10). The GFP-EB3 comets were observed both in WT and KO neurons (data not shown). mRFP was used as a volume marker and GFP-EB3 entry into spines could be visualized in neurons derived from KO mice, as shown in the kymograph in Figure 45b. The quantity of spine entry was not determined due to a small sample size.

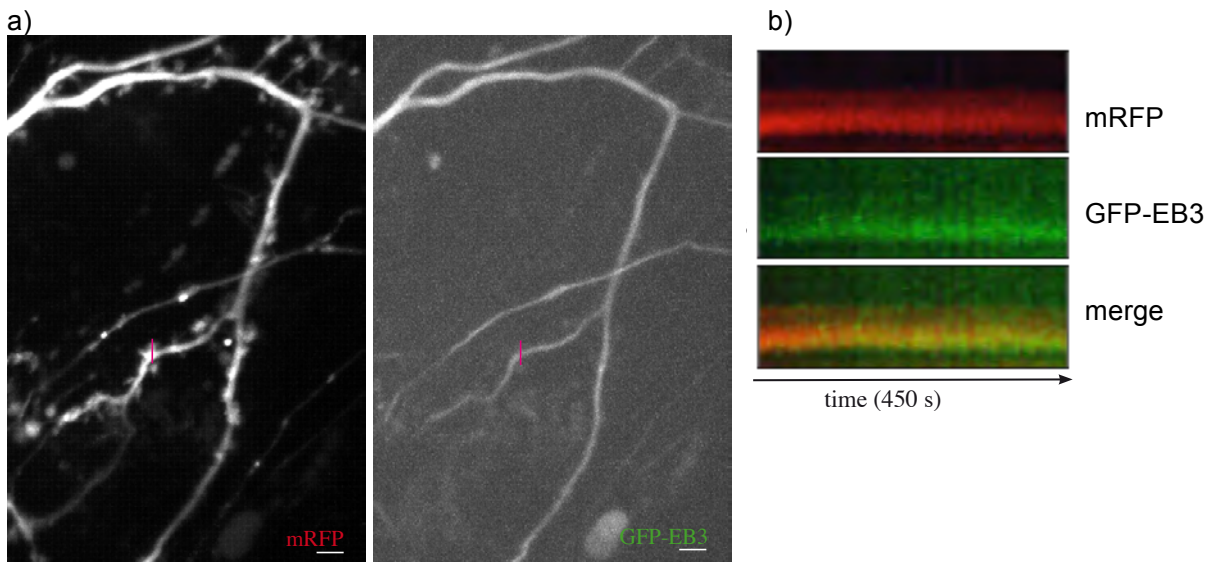


Figure 45: Live cell imaging of DIV 16 primary hippocampal neurons derived from spastin^{KO/KO} mice co-transfected with pmRFP and pEGFP-EB3 at DIV7. a) Z-stacks of a dendritic region, which has been video-recorded during 450 s (150 frames) to measure the spine entry of GFP-EB3. b) Kymograph from a selected dendritic spine (indicated with a pink line in a)) from a) during 450 s. Scale bar: 5 μ m.

Authors from one study using the EB3 protein found that MT dynamics in neurons were altered by the association of EB3 and the postsynaptic scaffolding protein PSD-95 (Sweet, Previterra et al. 2011). Interestingly, this association is assumed to influence dendritic arborization, but the exact

mechanism of action is unknown. To test whether MT severing enzymes play a direct or an indirect role in this complex, P2 and P3 fractions from mouse whole brain and antibodies directed against EB3 and PSD-95 were used for co-immunoprecipitations (section 3.4.4).

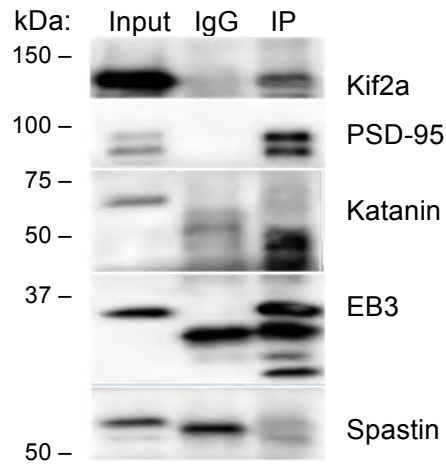


Figure 46: Immunoprecipitation using rat anti-EB3 antibodies on P2 fractions from mouse whole brain. Antibodies directed against kif2a, PSD-95, katanin, spastin and EB3 were used for Western Blotting.

As reported, EB3 and PSD-95 could co-immunoprecipitate each other (Figure 46, data only shown for the Immunoprecipitation using the anti EB3 antibodies). Also the M-type Kinesin Kin-13/KIF2a, mainly known to be involved in axonal branching, was reproducibly co-immunoprecipitated with EB3 and with PSD-95. In contrast, only faint bands were observed occasionally at the expected band size of spastin and katanin.

4.3 Katanin

4.3.1 Katanin targeting strategy and confirmation

In mice, the *Katna1* gene is coded on chromosome 10 and comprises 11 exons (Figure 47a). Exons 6 and 7 were the first suitable exons for targeting. In their absence, a frameshift mutation in the *Katna1* gene occurs, theoretically leading to a nonsense-mediated decay and the loss of protein function. The targeting strategy was analogous to the approach for spastin leading to KO-first-, floxed-, frameshift- and to reporter-alleles depending on the usage of Cre and Flp recombinases (Figure 47c-f).

Mouse embryonic C57BL/6NJMA8 stem cells with targeted exons 6 and 7 generated by KOMP using the KO-first-allele approach and a promoter-driven targeting vector (for details see section 4.1.1 and Figure 18) were injected into C57BL/6N blastocysts.

a) wild type allele (katanin^{WT}):



b) Linearized targeting vector:



c) KO-first allele (katanin^{KO-1st}):



d) floxed allele after FLP recombination (katanin^{FL}):



e) frameshift allele after FLP recombination, followed by Cre recombination (katanin^{KO}):



f) reporter allele after Cre recombination only (katanin^{GT}):



Figure 47: Targeting strategy for the murine katanin p60 gene to generate KO-first, floxed, classical frameshift, conditional-KO and reporter alleles. a) Targeted exons 6 and 7 of the WT *Katna1* gene are highlighted in red. The genomic region targeted by homologous recombination is highlighted in pink. b) The linearized targeting vector used for the generation of Katanin^{KO-first} alleles. c-f) Depending on the sequence of matings with Cre and Flp recombinases of the Katanin^{KO-1st} animals (c), Katanin^{FL} floxed (after FLP recombination (d)), Katanin^{KO} frameshift (after Flp followed by Cre recombinations (e)) and Katanin^{GT} gene-trap reporter loci (after direct Cre excisions (f)) can be generated. The amplicons for the 5' long-range PCR (P87 + P123) and the 3' long-range PCR (P86 + P122) are indicated to demonstrate correct targeting. Small grey arrows show the binding sites for the primers P93, P94, P170, P87, P123, P86 and P122. lacZ: β -galactosidase cDNA with a 3' En2SA site followed by an IRES sequence and a polyadenylation signal at the 3' end; neo: neomycin-phosphotransferase cDNA with a hbactP (human β actin promoter) and a polyadenylation signal at the 3' end; black triangles: FRT recognition sites; grey triangles: loxP recognition sites.

4.3.1.1 Long-range PCR for katanin

To confirm the correct insertion of the targeting vector at the 5' and the 3' ends of the homology regions, long-range PCRs were established. As can be concluded from Figure 47c, for the long-range PCR at the 5' end the forward primer P87 binds close to exon 5 of the *Katna1* gene and is not present in the targeting vector. The reverse primer P123 binds to a sequence upstream of the first FRT site originating from the targeting vector. In analogy to that, the long-range PCR at the 3' end of the *Katna1* targeted region has a binding site for the forward primer P86 close to the 3rd loxP site originating from the targeting vector and the reverse primer P122 binds to a sequence downstream of the targeting vector sequence present only in wild type and successfully targeted alleles. As expected for the 5' long-range PCR amplicon, a 6226 bp band and a 3762 bp band

corresponding to the 3' long-range PCR product could be observed in KO-first-allele ES cells for clone G09 (Figure 48a and b) as well as in their progeny (Figure 48c and d), respectively.

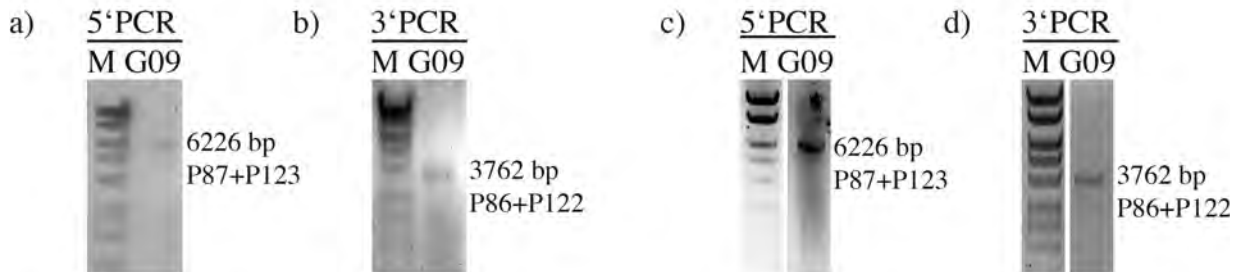


Figure 48: *Katna1* targeting confirmation both in ES cells and in F1 animals using long-range PCR. The correct insertion of the targeting vector into the *Katna1* locus was confirmed using the primer combinations P87+P123 for the 5' homology region and P87+P123 for the 3' homology region leading to 6226 bp and 3762 bp amplicons, respectively. In a) and b) DNA extracted from ES cell clone G09 used to generate *Katna1*^{KO1-st} mice was used as template DNA. In c) and d), DNA extracts from tail-tip-biopsies originating from heterozygous F1 generation animals (KO-first-allele) were used. G09: ESC-clone used to generate *Katna1*^{KO1-st} animals. M: molecular weight marker.

4.3.1.2 Loss of the wild type allele in homozygous floxed animals

Mating of *Katanin*^{KO1-st}-allele mice to a Flp-recombinase driver line leads to the excision of the LacZ- and the neomycin-phosphotransferase cassettes resulting in a floxed *Katna1* allele that is flanked by one FRT site and two loxP sites (Figure 47d). The primers P93 and P94 were used in polymerase chain reaction to detect the presence of the additional loxP and FRT sites by a slight band shift of the PCR product from 2190 bp for wild types and 2351 bp for floxed mice. The lack of the wild type PCR amplicon in homozygous floxed animals additionally proves the insertion of the targeting vector at the locus of purpose (Figure 49). The cloning and sequencing of the latter amplicon furthermore demonstrated the presence of the FRT and loxP sites (data not shown).

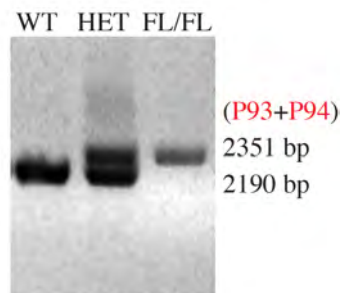


Figure 49: Confirmation of correct targeting of the *Katna1* gene in PCR using primers P93 and P94 in floxed animals (after breeding *Katna1*^{KO1-st/WT} animals to FLP-deleter mice). DNA extracts from *Katanin*^{WT/WT} (WT), heterozygous floxed *Katanin*^{WT/FL} (HET) and *Katanin*^{FL/FL} homozygous floxed (FL/FL) animal's tail-tip biopsies were used as template DNA for the polymerase chain reaction. In targeted homozygous floxed *Katanin*^{FL/FL} animals, the 2190 bp wild type band disappears.

4.3.1.3 Confirmation of katanin protein loss

To confirm the loss of katanin at the protein level in katanin KO mice, goat polyclonal M-13 antibodies directed against mouse katanin's C-terminal region (Table 4) were used. To confirm the specific binding of the antibodies to katanin, a pAcGFP-katanin full-length construct was generated and overexpressed in HEK293-TN cells (Figure 50a). The proteins from the obtained

RESULTS

lysates were then separated by SDS-PAGE and analyzed by Western Blotting using the anti-katanin and anti-GFP antibodies (Figure 50b).

In pAcGFP transfected HEK cells, a fragment of approximately 30 kDa was detected using the anti-GFP antibody and no band when using the anti-katanin antibody (lanes 4 and 1, Figure 50b). In non-transfected control cells (lanes 2 and 5), no band could be observed using the GFP antibody and a weak band at between 50 and 75 kDa when using the anti-katanin antibody. Contrarily, in pAcGFP-katanin transfected cells, two fragments of 75 kDa and approximately 50 kDa were detected for both the katanin and the anti-GFP antibodies (lanes 3 and 6, respectively). The 75 kDa band approximately corresponds to the expected molecular weight of the AcGFP-katanin fusion protein.

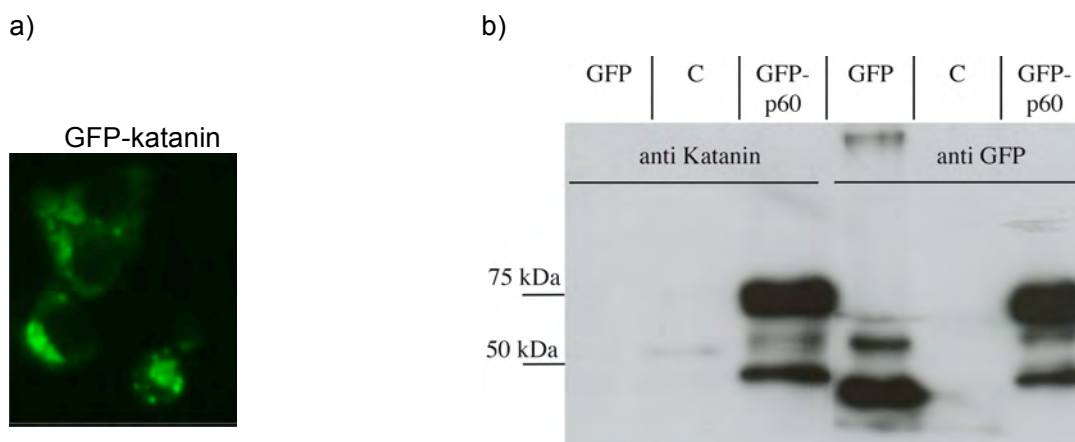


Figure 50: Usage of polyclonal goat anti-katanin antibodies for Western Blotting. a) HEK293-TN cells transfected with pAcGFP-katanin. b) Goat anti-katanin (polyclonal M-13) and rabbit anti-GFP antibodies were used for Western Blotting on lysates from HEK-cells either transfected with pAcGFP, untransfected or transfected with pAcGFP-katanin. GFP: green fluorescent protein; C: untransfected control cells; GFP-p60: cells overexpressing GFP-katanin.

Because no homozygous offspring were obtained for prenatally depleted (KO-first and null-allele) katanin mutants (see also Figure 53), the success of targeting could not be demonstrated at the protein level (i. e. Western Blotting or immunocytochemistry) using these mice. In the next step, mice with a floxed katanin allele (Figure 47d) were mated to the Nestin-promoter-driven Cre knock-in-mice (Tronche, Kellendonk et al. 1999) in order to generate neuron- and glial-specific mutants. Brain lysates obtained from homozygous floxed three weeks old mice and from their Nestin-Cre transgene positive littermates were compared in Western Blotting using the polyclonal goat anti-katanin antibody (clone M13). As can be seen in Figure 51, the signal detected using the anti-katanin antibody was slightly weaker for brain lysates from Nestin-Cre containing mutants. Normalization to the expression levels of PAN-cadherin (control protein) revealed an average reduction of katanin to 63 % in conditional KOs (quantification for 2 samples obtained from 1 animal for each genotype, data not shown).

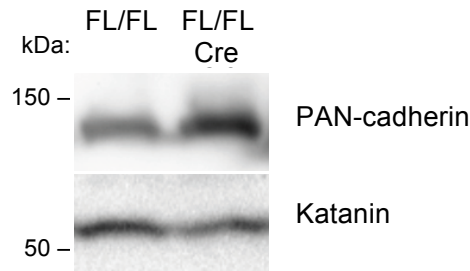


Figure 51: Katanin expression analysis in whole brain lysates from 9-week-old katanin^{FL/FL} mice (termed FL/FL) without or with the presence of the Nestin-Cre transgene. The goat anti-katanin (polyclonal M-13) and mouse anti-PAN-cadherin antibodies were used for Western Blotting.

Next, mice with a floxed katanin allele (Figure 47d) were mated to transgenic CamKII α -promoter-driven Cre mice (Tsien, Chen et al. 1996) in order to generate postnatal and forebrain-specific katanin KO mutants (see also Figure 19b and d).

Brains were isolated from adult homozygous floxed mice (termed WT) and from their CamKII α -Cre transgene positive littermates (termed KO) and separated into olfactory bulb (OB), cortex (CX), hippocampus (HC), midbrain (MID) and cerebellum (CB). Western Blotting using the polyclonal goat anti-katanin antibody (M13) showed the strongest signal intensity for hippocampal lysates originating from katanin WT mice (i. e. homozygous floxed). Several control antibodies were used to detect the expression levels of tau, acetylated tubulin (acTub), SNAP25 and actin in the corresponding brain regions.

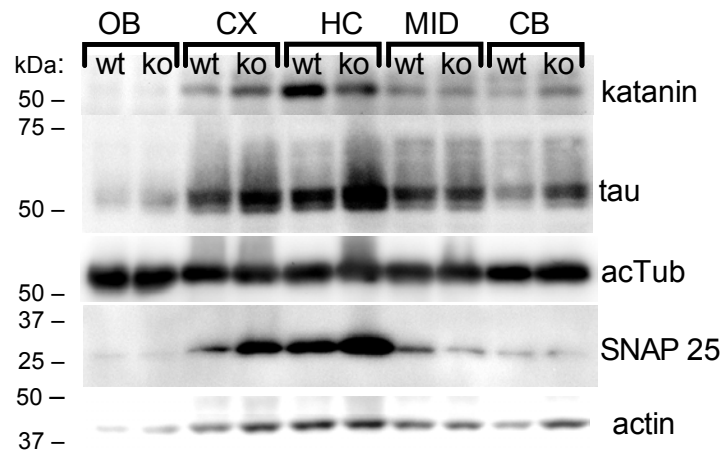


Figure 52: Postnatal and forebrain-specific targeting of katanin. Western Blotting using brain lysates from 6-month-old katanin^{FL/FL} (termed WT) and katanin^{FL/FL}/CamKII α -Cre^{TGWT} (termed KO) littermates using polyclonal goat anti-katanin, anti-tau, anti-acetylated tubulin (acTub), anti-SNAP25 and anti-actin antibodies. OB: olfactory bulb, CX: cortex, HC: hippocampus, MID: midbrain and CB: cerebellum. Three Western Blots from 2 WT and 2 KO animals were analyzed.

Katanin signal intensities were normalized to the average signal intensities of the control proteins (from 2 WT and 2 KO animals, data not shown). In summary, the relative katanin expression levels seem unaltered in the OB, MID and CB regions, slightly increased in the cortex and

reduced to approximately 42 % in the hippocampus of conditional KO mice (katanin^{FL/FL}/CamKII α -Cre^{TG/WT}).

4.3.2 General health of katanin depleted animals & reproduction

4.3.2.1 Litter sizes and genotype distribution

To determine whether the general depletion of katanin had an effect on litter size, parent animals with different genotype combinations for katanin (WT x HET vs. HET x HET) were mated and the number of pups per litter was analyzed. The litter sizes averaged approximately 6 pups per litter for WT x HET matings. In contrast to that, approximately 4.2 pups for HET x HET matings were obtained (Figure 53a). The comparison of the litter sizes for both mating pair combinations in an unpaired two-tailed t-test revealed a statistically significant reduction in the mean number of pups resulting from the HET x HET matings ($t=2.294$, $df=27$, $p=0.0298$). Because no homozygous KO animals for katanin were available, no matings using KO x WT or KO x HET were possible.

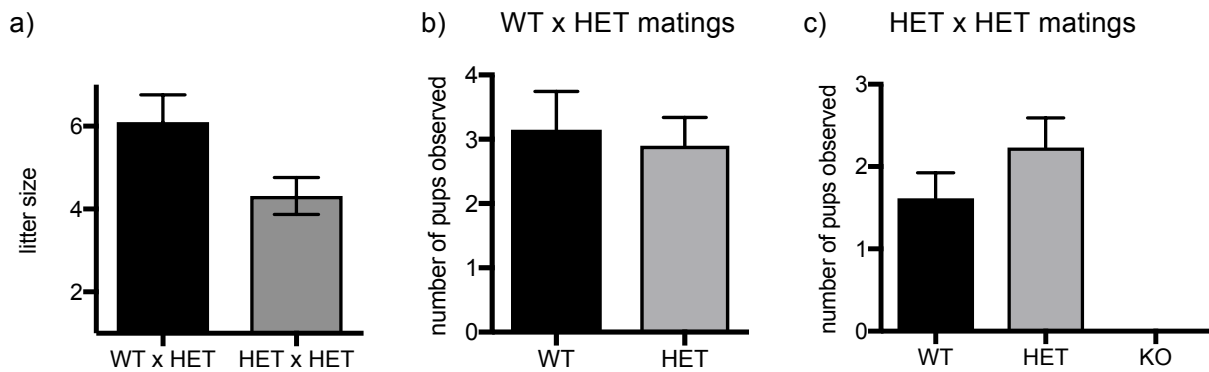


Figure 53: Litter sizes and genotype distribution for mouse lines with prenatally depleted katanin alleles.
a) Litter sizes resulting from matings HET (katanin^{KO1-st/WT} or katanin^{KO/WT}) with WT (katanin^{WT/WT}, black column) or HET mice (grey column). For WT x HET matings 61 pups from n=10 litters with a mean litter size of 6.1 ± 0.6574 were obtained. For HET x HET matings 82 pups from n=19 litters and a mean litter size of 4.316 ± 0.4462 were obtained. b) Mean animal numbers obtained per litter and genotype from WT x HET matings. 60 animals resulting from 10 WT x HET matings were analyzed with 3.15 ± 0.59 pups obtained for WT and 2.85 ± 0.46 for HET. c) Mean animal numbers obtained per litter and genotype from HET x HET matings. 50 animals resulting from 14 HET x HET matings were analyzed with 1.65 ± 0.3109 of pups for WT, 2.231 ± 0.3608 for HET and 0 for KO animals. Because mice with both the katanin-KO-1st and katanin KO-allele showed the same tendency, data from both mouse lines were combined in this graph for a better overview. Results for both genders were combined due to the same tendency for WT x HET matings. The graphs represent the mean values \pm SEM.

In order to characterize the genotype distribution of mice with prenatal katanin depletion, genotypes for different matings were determined for each litter. As shown in Figure 53b, there was no significant difference in the number of pups per litter resulting from ten WT x HET matings, with mean animal numbers of 3.15 for wild type versus 2.85 for heterozygous animals (two-tailed t-test: $t=0.3983$, $df=18$, $p=0.6951$).

The genotypes of 50 animals resulting from 13 litters from HET x HET matings were distributed as follows: 21 WT : 29 HET : 0 KO in comparison to the theoretically expected values of 12.5 WT : 25 HET : 12.5 KO (see Figure 53c). A Chi-square test yielded that the observed genotype distribution was significantly different from the expected one (Chi-square=18.92, $df=2$,

$p < 0.0001$). The mean numbers of pups per litter were 1.6 for WT and 2.3 for HET and 0 for KO animals. A Kruskal-Wallis test yielded that the difference in mean animal numbers obtained was significant ($H=22.6$, $p < 0.0001$). Dunn's multiple comparisons test resulted in a significant difference for WT vs. KO: $p=0.0012$ and for HET vs. KO: $p < 0.0001$. The difference between WT and HET was not significant ($p > 0.9999$).

4.3.2.2 Body weights

Heterozygous mice with one prenatally depleted katanin allele (either katanin^{KO1-st/WT} or katanin^{KO/WT}) did not show any obvious difference in size, nor was their body weight altered when compared to their wild type littermates (two-tailed t-test: $t=0.005091$, $df=30$, $p=0.996$; Figure 54a). In contrast, neuron-specific katanin^{WT/FL/Nestin-Cre^{WT/TG}} and katanin^{FL/FL/Nestin-Cre^{WT/TG}} littermates (termed KO and HET) displayed significantly reduced body weights in comparison to katanin^{FL/FL} (termed WT) littermates without the presence of the Nestin-Cre transgene (One-way ANOVA: $F(2, 8) = 5.194$, $p=0.0358$ followed by Tukey's multiple comparisons test ($p=0.0167$ for WT vs. HET and $p=0.037$ for WT vs. KO)) (Figure 54b). However, katanin^{WT/WT/Nestin-Cre^{WT/TG}} animals were not available to test for the effect of Nestin-Cre (two-tailed t-test: $t=3.356$, $df=9$, $p=0.0084$ for Nestin-Cre vs. wild types).

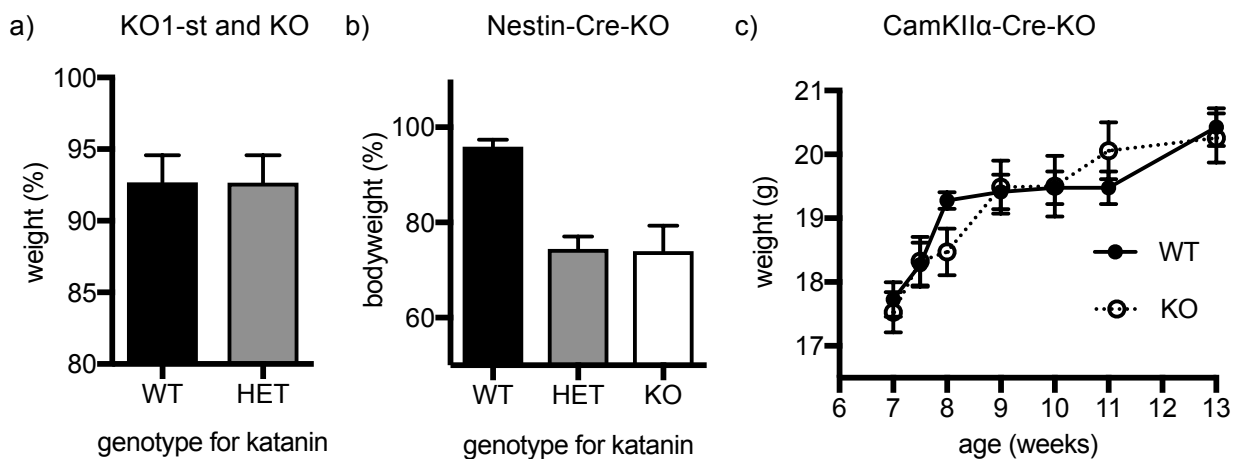


Figure 54: Body weight distribution in general and conditional katanin KO lines. a) Combined relative body weights of 18 WT (mean=92.68 % \pm 1.88) and 14 HET (mean=92.67 % \pm 1.916) animals with one KO-1st or null-allele for katanin. The body weights were normalized to the heaviest animal of each corresponding litter of the same age and gender. The actual body weights varied between 14.5 g and 63 g. b) Body weights of 3-week-old WT (katanin^{FL/FL/Nestin-Cre^{WT/WT}}, n=4), HET (katanin^{FL/WT/Nestin-Cre^{WT/TG}}, n=2) and KO (katanin^{FL/FL/Nestin-Cre^{WT/TG}}, n=4) animals. The graphs show mean values, the error bars representing \pm SEM. c) Weight distribution of katanin^{FL/FL/CamKII α -Cre^{TG/WT}} and katanin^{FL/FL/CamKII α -Cre^{WT/WT}} mice between 7 and 13 weeks. The animals were used for behavioral phenotyping. 8 wt (termed WT, black circles) and 7 ko (termed KO, open circles) age-matched females from the same cohort were used. The error bars represent the standard deviation.

To study the weight distribution of the forebrain-specific katanin knockout mouse line, 8 wt and 7 KO females born within the same week were weighed on a weekly basis between ages of 7 to 13 weeks (Figure 54c). In contrast to the katanin^{FL/FL/Nestin-Cre^{TG/WT}} mice, the katanin^{FL/FL/CamKII α -Cre^{TG/WT}} mice did not differ in means of their body weights compared to their katanin^{FL/FL} littermates (two-way ANOVA (genotype x age), main effect for genotype: $F(1, 13) = 0.02419$,

$p=0.8788$; main effect for age: $F(6, 78) = 46.12$, $p>0.0001$; interaction effect: $F(6, 78) = 2.331$, $p=0.042$).

4.3.3 Katanin expression pattern

4.3.3.1 Endogenous katanin promoter activity in heterozygous reporter knockouts

By mating katanin^{KO-1st} animals with Cre-deleter lines, katanin^{WT/GT}/Cre^{WT/TG} offspring with a LacZ reporter cassette could be generated (see also Figure 47f). This allowed studying endogenous katanin promoter activity and expression in developing mice via LacZ stainings. For that purpose embryonic day 17, postnatal day 8 and adult (10 weeks old) katanin^{WT/GT} littermates with a heterozygous reporter allele were used for LacZ staining of brain and organs (Figure 55 and Figure 56).

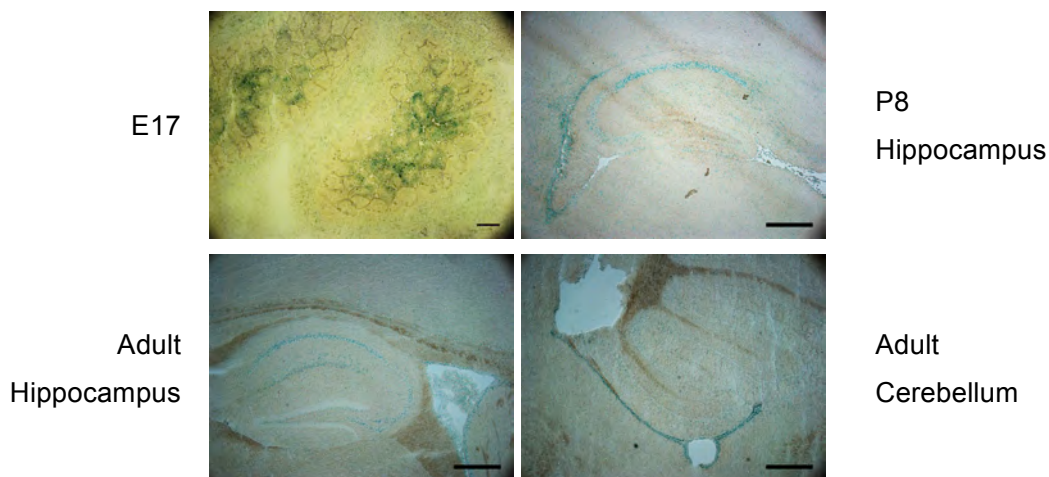


Figure 55: β -galactosidase staining of heterozygous katanin reporter mice (katanin^{WT/GT}/Cre^{WT/TG}) to assess the endogenous katanin promoter activity in the brain. LacZ stainings of brains from embryonic day 17, postnatal day 8 (P8) and adult mice are shown. A negative control was made in parallel (data not shown). Scale bar: 400 μ m.

A positive LacZ staining was obtained for the brains of embryonic day 17 (E17) mice, as well as for the hippocampi of postnatal day 8 (P8) and for the hippocampus and cerebellum of adult katanin mice (10 weeks) (Figure 55). Similar to the results for spastin in section 4.2.3.1 the lacZ expression was weak compared to the positive control (not shown) and declined even more in adult mice. The lacZ signal was strongest in the CA1 to CA3 regions of the hippocampus of postnatal day 8 mice and was barely detectable in the dentate gyrus. In 10 weeks old mice, the LacZ staining was much weaker and more confined to the CA1 and CA3 regions but not to the CA2 or dentate gyrus regions.

The LacZ signal was also detectable in other organs (heart, stomach, kidney, lung and thymus), with the strongest expression in the pelvis of the kidney and in the stomach (Figure 56). With exception of the stomach and renal pelvis tissue, the staining also declined in adult mice.

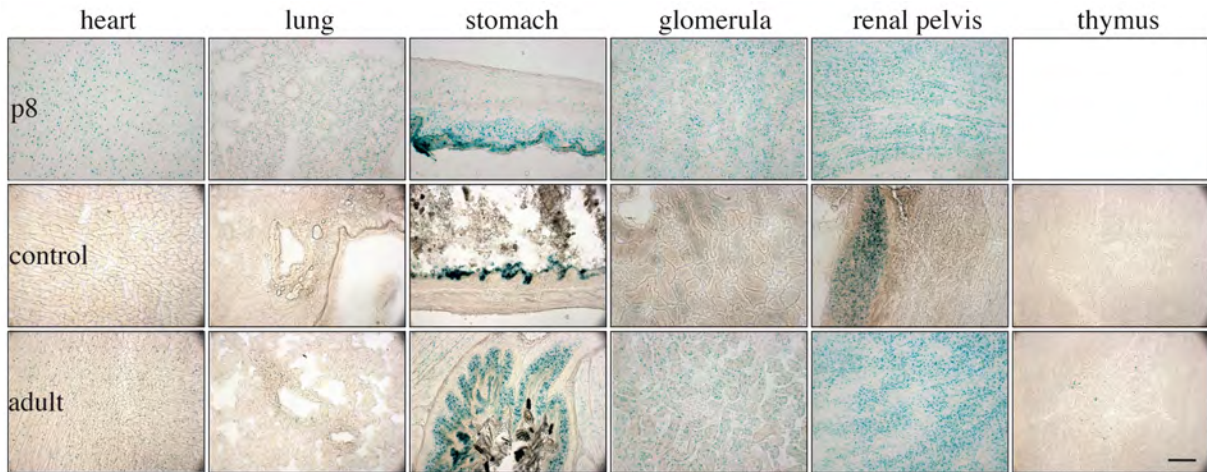


Figure 56: β -galactosidase staining of heterozygous katanin reporter mice ($\text{katanin}^{\text{WT/GT}/\text{Cre}^{\text{WT/TG}}}$) to assess the endogenous katanin promoter activity in organs. LacZ stainings of organs from adult and postnatal day 8 (P8) and adult mice are shown. A negative control of WT littermates is shown for adult mice. Scale bar (applies to all images): 0.1 mm.

4.3.3.2 Subcellular location of ectopically expressed katanin

In order to study katanin's subcellular location, katanin and its ATPase-defective mutant with a putative dominant negative function were cloned from a mouse cDNA library into the pAcGFP-C2 vector (AcGFP-katanin and AcGFP-dn-katanin, respectively). The vectors were used to ectopically express the fluorescently tagged proteins in HEK293 cells and in cultivated neurons.

Overexpression of AcGFP-katanin and AcGFP-dn-katanin mainly resulted in perinuclear expression in HEK293 cells (Figure 57a). In contrast to the expression of AcGFP only, the intracellular location of AcGFP-Katanin and AcGFP-dn-katanin was not diffuse but rather accumulated in a punctate pattern in the cell soma. In addition, AcGFP-dn-katanin aggregated more next to one side of the nucleus.

Overexpression into DIV10 neurons for 12 hours similarly resulted in a somatic location of AcGFP-katanin (Figure 57b). However, in contrast to HEK293 cells, its expression pattern was rather diffuse. The fusion protein could be detected in neurites and neurite tips negative for MAP2 (boxed excerpts in Figure 57b).

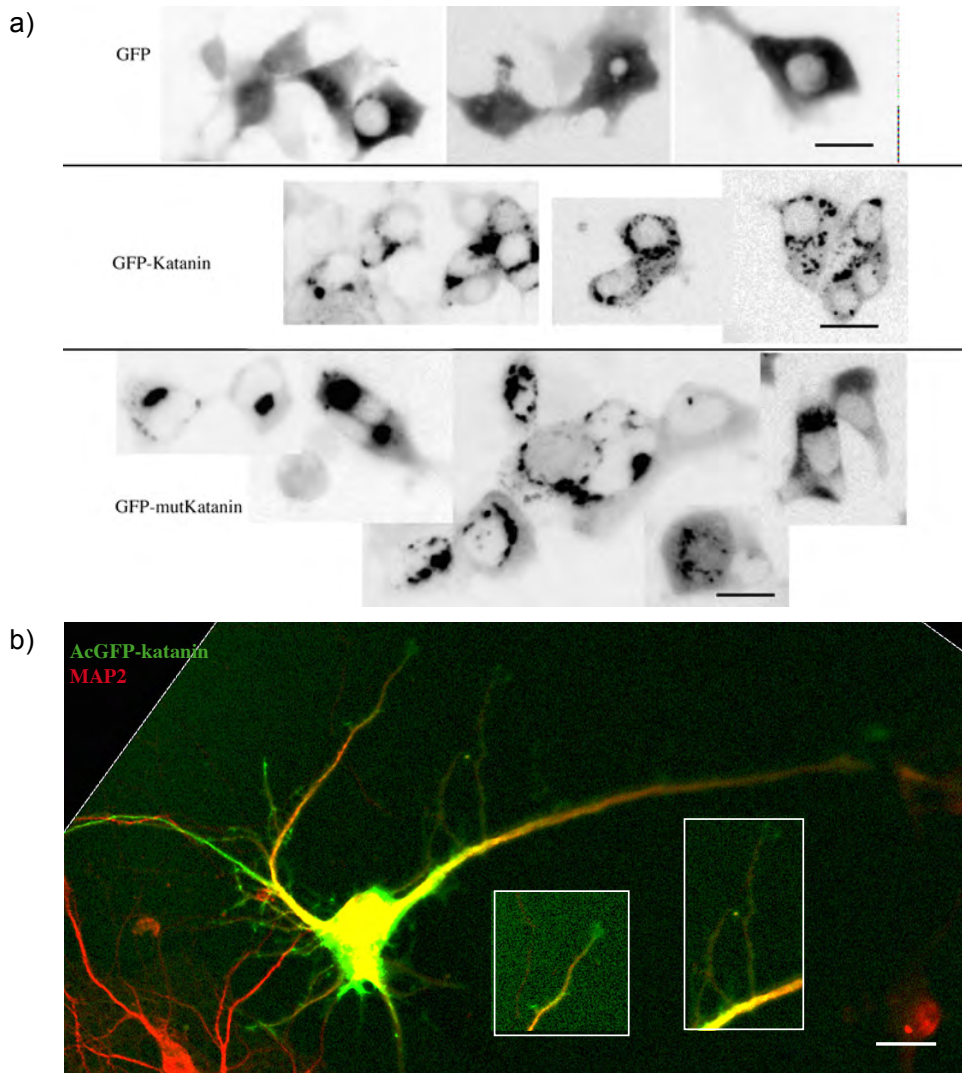


Figure 57: Ectopic expression of AcGFP-katanin. a) HEK293 cells transfected with AcGFP, AcGFP-katanin and AcGFP-dn-katanin. b) DIV10 hippocampal neurons transfected with AcGFP-katanin (green channel) for 12hours and then immunostained using the rabbit anti-MAP2 antibody (synaptic systems 1:2000, red channel). The boxed excerpts show a detailed view of selected distal neurites. Scale bar: 20 μ m.

4.3.4 Gross brain morphology of katanin knockout mice

4.3.4.1 Nissl staining of conditional katanin knockout using the Nestin-Cre promoter

As described in section 4.3.2.1, classical homozygous katanin knockout mice ($\text{katanin}^{\text{KO/KO}}$ and $\text{katanin}^{\text{KO1-st/KO1-st}}$) could not be generated during this study. To investigate whether prenatal katanin depletion in the brain affected viability as well, and to study gross brain morphology, $\text{katanin}^{\text{FL/FL}}$ mice were bred to the transgenic Nestin-Cre driver line. Homozygous $\text{katanin}^{\text{FL/FL/Nestin-Cre}^{\text{TG/WT}}}$ mice could be generated after two generations. The latter brain-specific katanin knockouts and their $\text{katanin}^{\text{FL/FL}}$ littermates were sacrificed at 36 weeks and their brains were used for Nissl staining (as described in section 3.2.8).

As shown in Figure 58a-c, there were no apparent brain abnormalities in homozygous $\text{katanin}^{\text{FL/FL/Nestin-Cre}^{\text{TG/WT}}}$ mice, compared to their $\text{katanin}^{\text{FL/FL}}$ littermates.

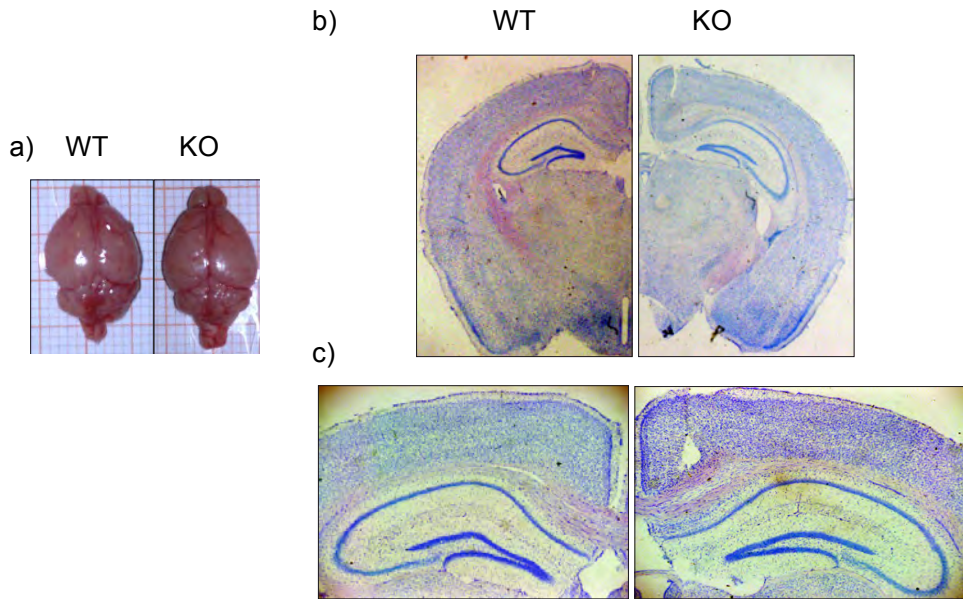


Figure 58: Gross brain morphology of brain-specific katanin knockout mice. a) Brains isolated from 36-week-old katanin^{FL/FL} (termed WT) and katanin^{FL/FL}/Nestin-Cre^{TG/WT} (termed KO) littermates. b) Nissl staining of coronal brain sections from a). c) Representative Nissl stainings from coronal brain sections showing hippocampi and cortex from katanin^{FL/FL} and katanin^{FL/FL}/Nestin-Cre^{TG/WT} littermates.

4.3.5 Behavioral phenotyping of forebrain-specific katanin knockout mice

As described in Figure 52, katanin's protein levels were reduced in the hippocampi of katanin^{FL/FL}/CamKII α -Cre^{TG/WT} (termed ko) adult mice compared to their katanin^{FL/FL}/CamKII α -Cre^{WT/WT} (termed wt) littermates. Next, these adult mice were used for initial behavioral phenotyping as described in section 3.5. Four control groups were pooled and were also termed the wild type group (katanin^{WT/WT}/CamKII α -Cre^{WT/WT}, katanin^{FL/WT}/CamKII α -Cre^{WT/WT}, katanin^{FL/FL}/CamKII α -Cre^{WT/WT} and katanin^{WT/WT}/CamKII α -Cre^{TG/WT}).

The mice were used for behavioral testing in two different cohorts: cohort 1 (11 WT and 8 KO females), and cohort 2 (9 wt and 8 ko females and 7 wt and 10 ko males) (Table 20).

Table 20: sequence and duration of experiments conducted with conditional katanin knockout cohort 1 (11 WT and 8 KO females) and cohort 2 (9 WT and 8 KO females; 7 WT and 10 KO males), and the age of mice at the time of the experiment.

| | Experiment | Duration | Age of animals |
|----------|--|----------|----------------|
| Cohort 1 | Open Field 30 min per mouse | 1 day | 13 weeks |
| | Elevated Plus Maze 5 min per mouse | 1 day | 14 weeks |
| | Place recognition 3 min delay | 1 day | 16 weeks |
| | Continuous Spontaneous Alternation 5 min per mouse | 1 day | 16 weeks |
| | Place recognition 24 h delay | 2 days | 17 weeks |
| Cohort 2 | Elevated Plus Maze 5 min per mouse | 1 day | 3-6 months |
| | Open Field 60 min per mouse | 2 days | 3-6 months |

4.3.5.1 Exploration and anxiety behavior

In order to test the $Katna^{FL/FL}/CamKII-Cre^{WT/TG}$ and their $Katna^{FL/FL}/CamKII-Cre^{WT/WT}$ littermates in their anxiety and exploration behavior as well as in their locomotor activities, the elevated plus maze and the open field tests were chosen.

Behavior in the Elevated Plus Maze

To analyze spontaneous anxiety, the elevated plus maze task was used (see section 3.5.2.1). The mice were placed onto the central plate of the maze with the head pointing towards an open arm and their exploration activity was video-recorded for 5 min. The traced paths were used for automated analysis of their horizontal locomotor activities and the percentage of time and frequency spent in the closed arms and open arms of the maze (Figure 59a-c).

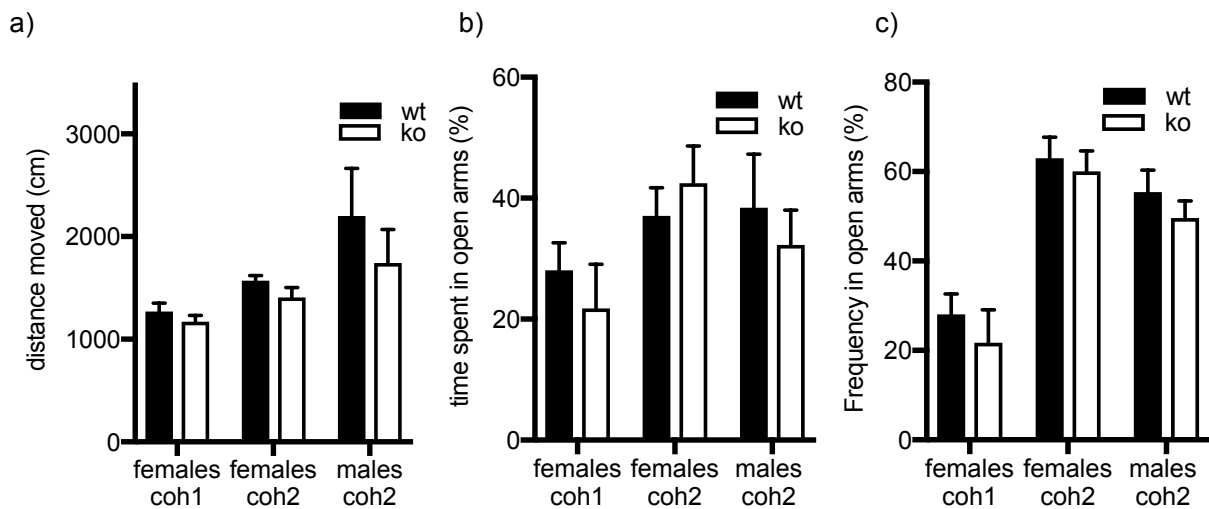


Figure 59: Behavior in the elevated plus maze. All graphs show the results for females from cohort 1 (11 wt and 8 ko), females from cohort 2 (9 wt and 8 ko) and males from cohort 2 (7 wt and 10 ko) during 5 min. Black bars: $Katna^{FL/FL}/CamKII-Cre^{WT/TG}$ (termed wt); white bars: $Katna^{FL/FL}/CamKII-Cre^{TG/WT}$ (termed ko). a) Total distance moved in cm. b) Percentage of time spent in the open arms. c) Percentage of entrance frequency into the open arms. All graphs represent mean values \pm SEM.

two-way ANOVA (cohort x genotype) analyses revealed that there was a difference between the females from both cohorts in terms of horizontal locomotor activity (main effect for cohort : $F(1, 32) = 12.55, P=0.0012$ but no main effect for genotype $F(1, 32) = 3.065, P=0.0896$), the percentage of time spent in the open arms (main effect for cohort: $F(1, 32) = 6.986, P=0.0126$ and no main effect for genotype: $F(1, 32) = 0.006715, P=0.9352$), and the percentage of entrance frequency into the open arms (main effect for cohort: $F(1, 32) = 47.32, P<0.0001$ and no main effect for genotype $F(1, 32) = 0.7555, P=0.3912$). two-way ANOVA (gender x genotype) analyses did not reveal any significant differences between both genders. Multiple t tests using the Holm-sidak method did not find any significant difference between the genotypes in any of the tested groups: females from cohort 1 (distance moved: $t = 0.3249, df=47, p=0.84$; percentage of time in the open arms: $t=0.7712, df=17, p=0.83$; percentage of entrance frequency into the open

arms: $t=0.7712$, $df=17$, $p=0.76$), males from cohort 2 (distance moved: $t=1.418$, $df=47$, $p=0.41$; percentage of time in the open arms: $t=0.6066$, $df=15$, $p=0.83$; percentage of entrance frequency into the open arms: $t=0.9121$, $df=15$, $p=0.78$) and females from cohort 2 (distance moved: $t=0.517$, $df=47$, $p=0.85$; percentage of time in the open arms: $t=0.7121$, $df=15$, $p=0.83$; percentage of entrance frequency into the open arms: $t=0.6066$, $df=15$, $p=0.83$).

Behavior in the open field test

The open field test was conducted with mice from cohort 1 and cohort 2. The mice were placed in one of the four arenas and their activity was video-recorded for 30 or 60 min (as described in section 3.5.2.2). Figure 60a shows the total distance the mice moved in 30 min. A two-way ANOVA (genotype x group) identified a significant main effect for the group tested ($F(2, 47) = 16.7$, $p < 0.0001$) but no main effect for genotype ($F(1, 47) = 3.156$, $p = 0.0821$). There was no significant difference in the total horizontal locomotor activity levels between both genders or genotypes from cohort 2 (two-way ANOVA, main effect for gender: $F(1, 30) = 0.2254$, $P = 0.6384$; main effect for genotype: $F(1, 30) = 2.188$, $P = 0.1495$; interaction: $F(1, 30) = 3.31$, $P = 0.0789$). In Figure 60b the distance moved is represented in twelve 5-minute bins for both genders from $Katna^{FL/FL}/CamKII-Cre^{WT/WT}$ (termed wt) and $Katna^{FL/FL}/CamKII-Cre^{TG/WT}$ (termed ko) mice from cohort 2. The distance moved decreased from approximately 3000 cm in the first 5 min to approximately 1100 cm in the last 5 min for both wt and ko females. For males it decreased from 2900-3200 (ko vs. wt) in the first 5 min to 970-1080 (ko vs. wt) in the last 5 min. There was no significant difference in the horizontal locomotor activity levels between both genotypes for females $F(1, 15) = 0.009613$, $P = 0.9232$ during the time of recording. For males, there was a marginally significant main effect for genotype $F(1, 15) = 3.271$, $P = 0.0906$. As shown in Figure 60c, the total distance moved in cm was not significantly different in the three zones of the arena (CZ: center zone, MZ: middle zone, OZ: outer zone) tested for females. For males however, there was a significant difference (two-way ANOVA, main effect for zones: $F(2, 45) = 240.1$, $p < 0.001$, main effect for genotype: $F(1, 45) = 4.123$, $p = 0.0482$, interaction effect: $F(2, 45) = 2.424$, $p = 0.1$. Bonferroni's multiple comparisons test revealed a significant reduction of the total distance moved in the outer zone for ko compared to wt males ($p = 0.0157$). In contrast to that, there was no apparent difference in the time spent in the individual zones of the arena (CZ, MZ and OZ) between the genotypes. Further analyses of the times the mice spent moving vs. not moving revealed that the knockout males spent significantly more time immobile (two-way ANOVA (zone x genotype): $F(1, 45) = 4.14$, $p = 0.0478$) throughout the experiment. However, Bonferroni's multiple comparisons test failed to find a significant result for a certain zone of the arena.

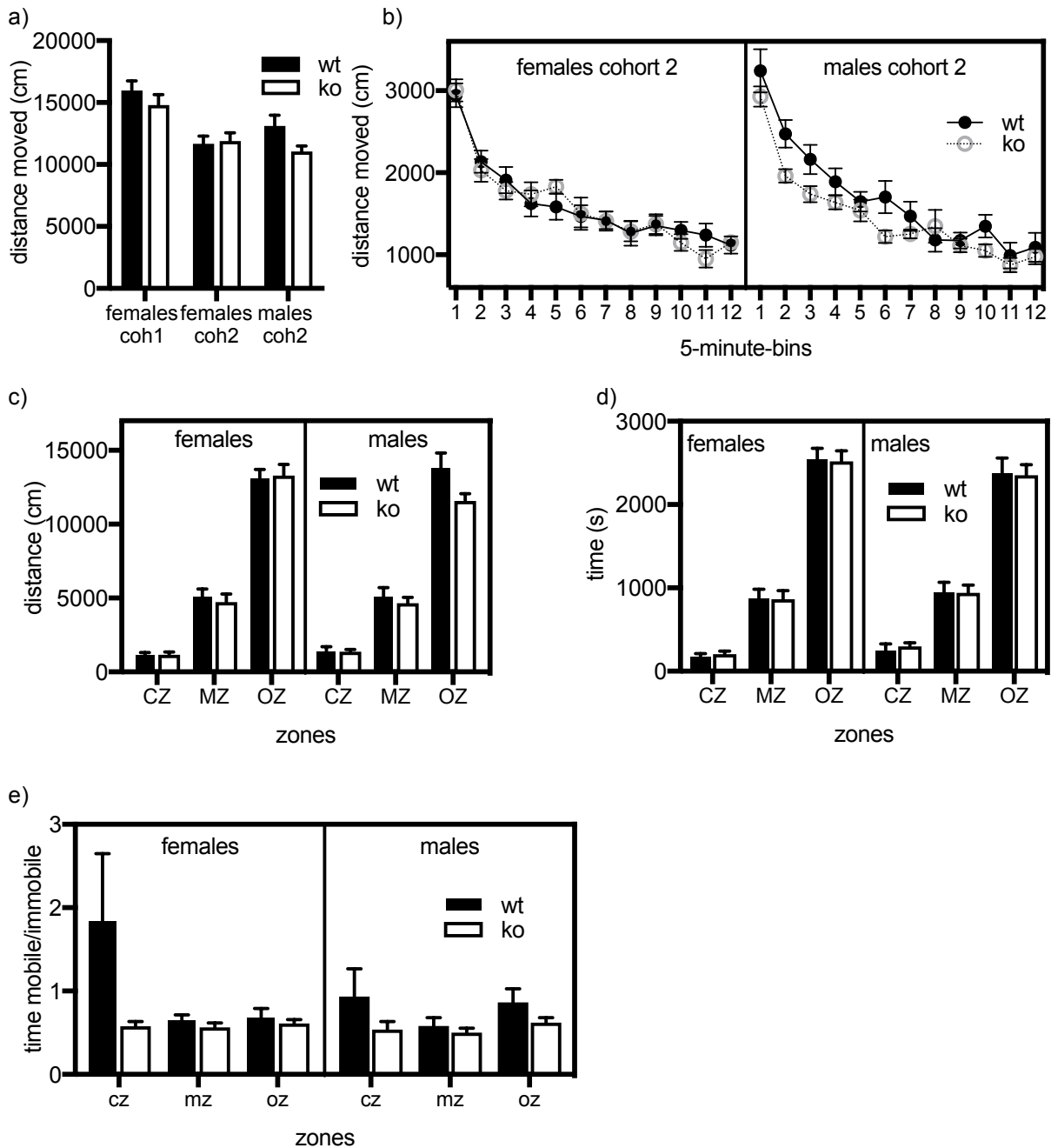


Figure 60: Behavior analysis of adult $Katna^{FL/FL}/CamKII-Cre^{WT/WT}$ (termed wt) and $Katna^{FL/FL}/CamKII-Cre^{TG/WT}$ (termed ko) mice in the open field test. a) Horizontal locomotor activity levels in mice from cohort 1 and cohort 2 measured as total distance moved in 30 min. b) The graphs represent the horizontal locomotor activity levels displayed as distance moved over 1 hour in 12 five-minute bins for cohort 2. c) Distance moved over 1 hour in the center zone, middle zone and in the outer zone of the arena. d) Total time spent in in the center zone, middle zone and in the outer zone of the arena in 1 hour. e) Fraction of time the mice spent moving vs. the time they spent not moving in the zones of the arena in 1 hour. All data represent mean values \pm SEM. Illumination: 50 lux. Black bars or black circles represent WT ($Katna^{FL/FL}/CamKII-Cre^{WT/WT}$) and white bars/grey circles represent KO ($Katna^{FL/FL}/CamKII-Cre^{TG/WT}$) mice. Cohort 1: 11 WT and 8 KO females. Cohort 2: 9 WT and 8 KO females; 7 WT and 10 KO males.

4.3.5.2 Learning and memory

To measure short time spatial memory without positive or negative reinforcement, a Y-maze test for spontaneous alternation was chosen (see section 3.5.3.1). Here the mice were placed in the start arm of a Y-maze with white nontransparent walls. The total number of entries and the

percentage of arm alternations were measured. As shown in Figure 61a, there was no significant difference in total arm entries between $Katna^{FL/FL}/CamKII-Cre^{WT/WT}$ (termed wt) and control (termed ko) mice (wt 29.0 ± 2.4 , $n=11$ and ko 26.5 ± 2.8 , $n=8$).

The mean percentage of alternation (Figure 61b) was slightly higher for knockouts but not significant (wt: 55.9 ± 3.9 , $n=11$ and ko: 61.0 ± 5.1 , $n=8$; two-tailed t-test: $t=0.8091$, $df=17$, $p=0.4296$).

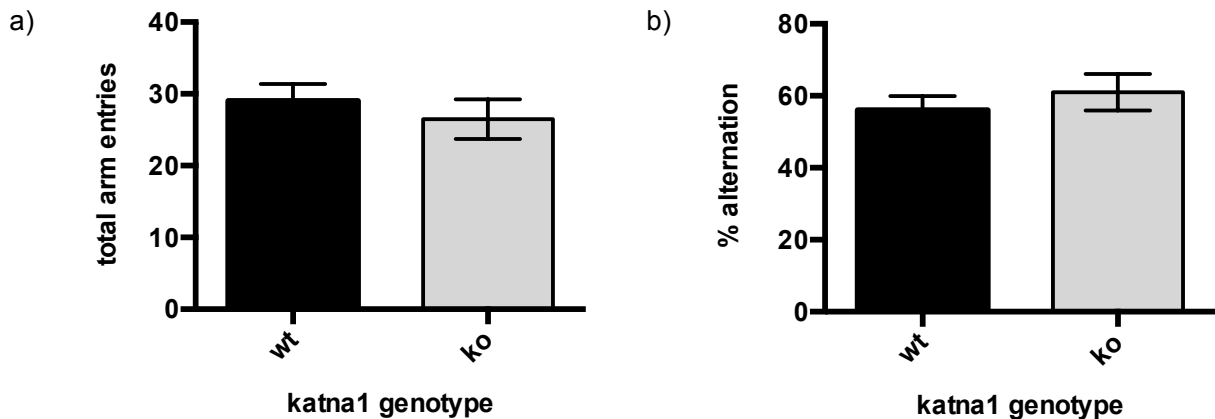


Figure 61: Continuous spontaneous alternation behavior in the Y-maze. 16-week-old forebrain-specific *Katna1* knockout mice (termed ko) and their control littermates (termed wt) were tested from cohort 1. A) total arm entries (wt 29.0 ± 2.4 , $n=11$ and ko 26.5 ± 2.8 , $n=8$). B) Percentage of alternation (wt: 55.9 ± 3.9 , $n=11$ F and ko: 61.0 ± 5.1 , $n=8$ F). The graphs represent mean values \pm SEM.

Additionally, mice from cohort 1 were tested in two place recognition tasks in a Y-maze (see section 3.5.3.2). As summarized in Figure 62a, both wt and ko mice showed a significant preference for the novel arm during the test phase after a 3-min inter-trial interval (two-way-ANOVA (arm x genotype): main effect for arm: $F(2, 51) = 30.35$; $p < 0.0001$; main effect for genotype: $F(1, 51) = 4.14e^{-14}$, $p > 0.9999$ followed by Tukey's multiple comparisons test for wt (start vs. other arm with $p < 0.05$; start arm vs. novel arm with $p < 0.01$; other arm vs. novel arm with $p < 0.0001$) and for ko (start vs. other arm with $p > 0.05$; start arm vs. novel arm with $p < 0.0001$; other arm vs. novel arm with $p < 0.001$). Contrarily, there was no preference for any of the arms during the sample phase (two-way ANOVA (arm x genotype), main effect for arm: $F(2, 32) = 1.704$, $p = 0.198$; main effect for genotype: $F(2, 32) = 0.8916$, $p = 0.8916$; interaction effect: $F(2, 32) = 6.888$, $p = 0.0033$). Sidak's multiple comparisons test did not find any significant preference of one arm over the other: arm A vs. arm B ($t = 0.1.768$, $df = 32$, $p = 0.2379$), arm A vs. arm C ($t = 0.9044$, $df = 32$, $p = 0.7529$), arm B vs. arm C ($t = 0.8296$, $df = 32$, $p = 0.7977$).

However, during the test phase after a 24 hour delay (Figure 62b), only the wild type mice showed a significant preference for the novel arm (two-way-ANOVA (arm x genotype) main effect for arm: $F(2, 51) = 7.836$; $p = 0.0011$; main effect for genotype: $F(1, 51) = 1.403e^{-13}$, $p > 0.9999$; interaction effect: $F(2, 51) = 5.785$, $p = 0.0054$; Tukey's multiple comparisons test for wt (start vs. other arm with $p > 0.05$; start arm vs. novel arm with $p < 0.0001$; other arm vs. novel arm with $p < 0.0001$) and for ko (start vs. other arm with $p > 0.05$; start arm vs. novel arm with $p > 0.05$; other

arm vs. novel arm with $p > 0.05$). One-sample t-tests against a chance level of 33.33 % resulted in a significant preference of the novel arm for wild types ($t = 3.762$, $df = 10$, $p = 0.0037$) and no arm preference for knockouts ($t = 0.2578$, $df = 7$, $p = 0.8$). Additional analysis revealed that the difference for the novel arm preference between wild types and knockouts was significant (two-tailed t-test: $t = 2.298$, $df = 17$, $p = 0.0345$).

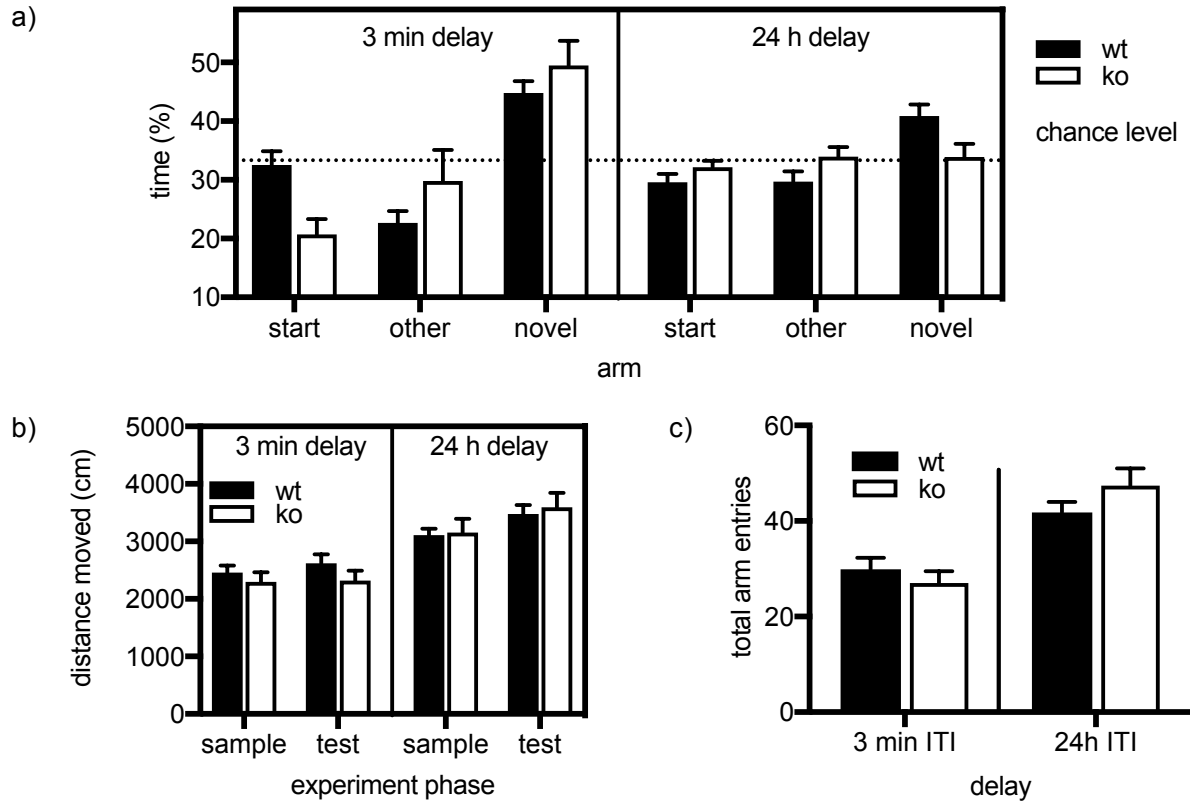


Figure 62: Summarized behavior in the place recognition task in the Y-maze. Forebrain-specific *Katna1* knockout mice (termed ko) and their control littermates (termed wt) were tested in two sequential experiments with different inter-trial intervals (3 min and 24 h) at ages of 16 and 17 weeks. A) The graph represents the percentage of time spent in the start, familiar or novel arm during the test phases. B) Distance moved in cm during the sample and the test phases. C) Total arm entries during the test phases. All graphs represent mean values \pm SEM. WT: $n = 11$ F, KO: $n = 8$ F.

As can be seen in Figure 62b and c, both genotypes showed similar horizontal locomotor activity levels as well as exploratory levels (as measured by total arm entries during the test phase) within one experiment.

5 DISCUSSION

5.1 Generation of spastin and katanin knockouts

5.1.1 Spastin

As has been shown in sections 4.2.1 and 4.2.2, the *spastin* gene was successfully targeted. KO-first, null-allele, gene-trap, floxed, as well as conditional forebrain-specific mutants could be obtained.

The correct targeting of the intended locus could be successfully demonstrated using Southern Blotting at the 5' homology region (Figure 23), whereas the probes generated for the 3' homology region produced multiple bands even in DNA extracts derived from wild type mice (data not shown). Thus, the correct targeting at the 3' homology region was demonstrated after the establishment of a long-range PCR protocol (Figure 24). Additionally, the insertion of the targeting vector at the intended locus is demonstrated by the fact, that in homozygously targeted animals (irrespective of whether it was a null-, a floxed-, or a different allele) the wild type band is absent in genotyping PCR reactions (e. g. Figure 25). An additional insertion of the targeting vector at other genomic regions than the intended one is highly unlikely, because the probability of multiple insertions into the genomic DNA is very low and in that case, the insertion would not have occurred via homologous recombination, leading to the expression of the cytotoxic DTA cassette in the ES cells.

At the protein level, homozygous spastin KO mutants with the KO-first as well as with the null-alleles displayed significant spastin loss as revealed by Western Blotting where the spastin signal intensity for knockout lysates was reduced to approximately 5 % when compared to wild type lysates (Figure 27). Besides, the significant reduction of spastin expression was demonstrated by fluorescence immunostainings using the anti-spastin antibody (clone 6C6) of hippocampal neurons derived from spastin knockout mice and their littermates (Figure 29). The remaining signal in knockout stainings are likely due to technical artefacts, since no secondary-only negative control was used for the experiment. In addition, the immunostaining conditions were improved from one experiment to the next leading to increasingly greater discrepancy between the WT and KO fluorescence signal intensities. However, also the data with less well-established results were included in the analysis. Nevertheless, both Western Blotting as well as immunocytochemistry results imply that spastin expression at the protein level was approximately reduced by half in heterozygous animals when compared to wild types.

It is noteworthy that two bands (approximately 60 and 55 kDa) were observed in Western Blotting using anti-spastin antibodies, which is consistent with previous reports, concluding that the most abundant isoform is the one starting from the second AUG and retaining exon 4. The possibility of a truncated version of spastin expressing the first 4 nontargeted exons was not tested in this

study. However, the authors from another study targeting spastin exons 5-7 report the absence of amino-terminal fragments, which suggests that they undergo nonsense-mediated decay due to the frameshift mutation (Fassier, Tarrade et al. 2013). The unlikely possibility exists that for KO-first mutants an N-terminal fragment- β -galactosidase fusion protein is expressed. In case of null-allele mutants, the preceding FLP-recombination step removes the gene-trapping cassette completely, thus excluding that possibility.

For forebrain-specific conditional spastin KOs using the CamKII α -Cre-driver line from Tsien et al., a strong reduction in spastin expression levels could be achieved, as shown in Figure 28. The strongest reduction was observed in the cerebral cortex, followed by the hippocampus and the midbrain as compared to homozygous floxed littermates, whereas no significant change was observed for the olfactory bulb and for the cerebellum. The remaining expression might be due to a scattered expression of the Cre transgene or because the remaining proteins were not degraded yet due to the postnatal expression of CamKII α -Cre. In order to study that, forebrain-specific spastin knockouts of an older should be tested for comparison.

Curiously, only the upper spastin band was reduced, whereas the lower band seemed unaffected. This contrasts the results observed for KO-1st and for null-allele mutants. One possibility is that another protein was detected at the expected size of the smaller spastin fragment due to decreased antibody specificity. In that case, a parallel lysate originating from spastin null-allele mutants would also show this band (however, this experiment was not done during that study). Another possibility is, that the different spastin isoforms are expressed in different cell types and the ones with the remaining smaller isoform do not express CamKII α -Cre. Another speculation would be, that exon 4 (not present in the smaller spastin fragment) regulates the stability of the protein, either already from the mRNA level or at the protein degradation level. The function of the 32 aa stretch coded by exon 4 has not been analyzed yet. In that case, this 32 aa stretch would lead to a faster degradation of the larger protein after the postnatal KO of spastin at the genomic level using CamKII α -Cre. However, the expression of CamKII α -Cre can be visualized from postnatal day 8 already, followed by considerable expression levels at postnatal day 21 (as shown in Figure 19); and the brain lysates for expression analysis were obtained from adult animals (15 weeks). Other indications, that spastin was targeted correctly include the observations of the gait phenotype for homozygous KO mice, pointing to a motor dysfunction as expected for models of HSP, and the sterility of both sexes, which matches the previous reports.

5.1.1.1 Usage of the pEGFP- Δ M1-spastinconstruct and 6C6 anti spastin antibodies

In order to prove the depletion of spastin at the protein level in future spastin knockout animals, a functional antibody had to be tested. For that purpose, the pEGFP- Δ M1-spastin construct was transfected into HEK293TN cells in addition to pEGFP-transfected and non-transfected cells. Antibodies directed against spastin (clone 6C6) and against GFP were used for the analysis of the three different protein extracts by Western Blotting. The results were as expected for GFP

transfected as well as for untransfected cells (Figure 26), meaning that neither the GFP antibody nor the spastin antibody bind to additional target proteins at a detectable extent. For pEGFP- Δ M1-spastin-transfected lysates however, two bands were observed at approximately 75 kDa (as expected for the fusion protein) and in addition at approximately 37-50 kDa for both the anti-GFP antibody as well as for the anti-spastin antibody. Given the quality of separation of the proteins from that SDS-PAGE gel it is not possible to judge whether the lower molecular weight bands are indeed the same molecular weight and thus, the same protein fragment. However it is highly likely, since the ratio between the upper and the lower bands are similar as well. In that case it would mean, that the overexpression of the pEGFP- Δ M1-spastin leads to a truncated protein besides the expected expected fusion protein. An explanation would be a mixture of plasmid DNAs, which unlikely since the plasmid DNA was amplified from a single colony and then successfully sequenced. The additional fragments could also be due to premature termination of translation or by intracellular or extracellular degradation processes. In fact, the pEGFP-construct has a very strong promoter leading to high expression levels of the target proteins, which are toxic to the cells. This is in line with multiple overexpression experiments in primary hippocampal neuronal cultures that resulted in very low transfection efficiency and non-healthy looking cells in comparison to pEGFP transfected cells or cells transfected with other GFP-tagged constructs (see also **Figure 39**). The toxicity might be due to aberrant MT severing inside the cells or due to intracellular aggregation due to misfolding of the fusion protein followed by intracellular degradation.

5.1.2 Katanin

As has been shown in sections 4.3.1 and 4.3.2, the katanin gene could be successfully targeted. KO-first, null-allele, gene-trap, floxed, as well as conditional forebrain-specific mutants were obtained. However, homozygous mutants were only obtained for floxed and conditional knockout alleles.

The correct insertion of the targeting vector into the mouse genome could not be demonstrated using Southern Blotting, due to non-specific binding of the probes generated for wild type DNA extracts (data not shown). The reason for this might be the combination of many repetitive sequences and the lack of restriction sites for well-established enzymes. However, long-range PCR also proves the correct targeting at both the 5' and the 3' homology regions in DNA extracts from both ESCs and tail-tip biopsies (Figure 48). Because homozygous katanin KOs did not seem to be viable, no ultimate proof could be achieved for the correct targeting using genotyping PCR of KO-first, gene-trap, and null-allele mutants, since in that case, the wild type band is always present and cannot exclude a random integration of the targeting vector. However, the ultimate proof of the correct targeting could be achieved indirectly through the viability of both homozygous floxed and homozygous conditional katanin KO mutants (see Figure 47d and e). In that case, the wild type band does disappear in genotyping PCRs (using the primers P93 and

P94, see Figure 49). In addition, the non-mendelian genotype distribution clearly points to embryonic lethality of homozygous katanin KO (see Figure 53c).

In contrast to the results for spastin, the loss-of-function at the protein level could not be demonstrated for katanin unambiguously. Although the goat polyclonal anti-katanin antibody was tested in HEK293 cells that were overexpressing GFP-tagged full-length katanin, it cannot be claimed that it was specific for katanin due to the lack of full KO lysates. To circumvent this problem, conditional katanin KO were generated using the Nestin- and CamkII α promoters to drive whole-brain and forebrain-specific expression of Cre, respectively. However, although the animals were conditional KO judging from genotyping results (they were homozygous floxed and had the respective Cre transgenes in their genomes), katanin expression at the protein level was only marginally reduced (to approximately 63 % for Nestin-Cre in the whole brain, see not shown). For the forebrain-specific katanin KO, a reduction of expression could only be assumed in the hippocampus (with an average reduction to 42 % Figure 52, quantification not shown due to small sample size). In contrast to conditional spastin KO, no reduction was seen in the cortex and in the midbrain fractions. One explanation could be, that katanin is primarily expressed in cells that are not targeted by Nestin-Cre and CamkII α -Cre, e. g. in glial cells. In addition, its expression in the brain is highest in the hippocampus but also drops in adult mice (Yu, Solowska et al. 2005), which might explain why only this region displayed a tendential reduction of katanin in KO.

Another challenge was the correct choice of control proteins for the judgment of the expression levels of katanin. Because MT-severing enzymes are likely to affect many cellular proteins related to cytoskeleton regulation, cargo transport and cell metabolism, it cannot be excluded that some of these well-established proteins might be up- or downregulated themselves, consequently masking the real expression levels of katanin after normalization. A determination of protein concentration in the lysates was hardly possible because of the presence of very small brain subregions (olfactory bulb and hippocampus), which would have excluded their further usage for Western Blotting. However, the volume of the lysis buffer used was adjusted to the weight of the subregions. As can be seen in Figure 52, the expression of the axonal MAP tau and the synaptosomal-associated protein 25 (SNAP-25) seem to be elevated in the hippocampus and eventually in the cortex of conditional katanin knockouts, whereas the levels of acetylated tubulin (acTub) rather seem to be inversely correlated. Because it is highly unlikely that all control proteins chosen were only up- or downregulated in knockouts, it seemed the most plausible solution to use their average expression levels to determine the relative katanin expression in the brain subregions of conditional katanin knockouts.

The usage of polyclonal antibodies increases the likelihood that a fraction can also bind to highly homologous AAA ATPases. An alternative might thus be to use a monoclonal anti-katanin antibody (Akkor and Karabay 2010).

In sum, it cannot be claimed that the katanin antibody used in this study was specific, due to the lack of confirmation using full knockout lysates. However, it can be assumed that there is a change in the hippocampus due to CamKII α -Cre mediated conditional katanin knockout either at the expression level of katanin or the expression level of tau and SNAP-25.

5.1.3 Targeting and breeding strategy

As described in Figure 18, the usage of the KO-first-allele permitted generating multiple alleles for different purposes. This required sequential breedings to different Cre and Flp driver lines.

The embryonic stem cells for gene targeting of both katanin and spastin were derived from C57BL/6N mice (Pettitt, Liang et al. 2009). However, several mutations have been reported for the C7BL/6N genetic background during the time of this work. For instance, the Rd8 mutation of the *Crb1* gene was reported (Mattapallil, Wawrousek et al. 2012), making it necessary to backcross to the C57BL/6J background and selecting the animals without that mutation by real-time PCR for further line expansion. Additionally, a slight chance exists for an unintended additional insertion of the targeting vector outside of the homology region. To rule out the inheritance of these unwanted mutations, an off-breeding strategy using C57BL/6J mice was required. In theory, the probability to inherit an unwanted mutation reduces by half with each off-breeding generation. This fact makes it necessary to backcross/outcross for five generations to have a less than 5 % probability of an unintended mutation.

In summary, the need to backcross for approximately five generations was rationalized by the possibility of additional mutations, the reported existence of mutations in the C57BL/6N mouse line, the availability of Flp and Cre-driver lines in that background and the suitability of the C57BL/6J background for behavioral experiments. In fact, the most extensively studied and described mice have a C57BL/6J background.

For the usage of conditional KO mice in behavioral experiments, the male mice contained the Cre transgene in the breeding pairs whereas the females had a homozygous floxed locus. This approach was chosen in order to prevent KO in female parent animals, eventually leading to unintended changes in maternal care.

5.1.4 Usage of conditional Cre-driver lines

5.1.4.1 CamKII α -Cre

Because the hippocampus is the most important brain structure to study learning and memory, a conditional KO of the two studied genes was aimed for. The CamKII α promoter was the most promising for the actual aim to study the role of MT-severing enzymes in synaptic plasticity, learning and memory because of its described postnatal and forebrain-specific expression (Burgin, Waxham et al. 1990, Mayford, Bach et al. 1996). Three different CamKII α -Cre-driver lines were tested during this work (developed by Cassanova, Minichiello, and Tonegawa) using LacZ stainings of mouse brains after breeding the specific CamKII α lines to the R26 reporter line

(Figure 19). As the other two tested transgenes resulted in prenatal Cre expression in different extents, the Cre-driver line developed by Tsien et al. was chosen for conditional targeting for spastin and katanin.

As can be concluded from Figure 20, even the most promising CamKII α -Cre-driver line shows occasional expression of Cre not only in the postnatal brain. In this specific case, also heterozygous prenatal-KO animals were obtained from the same litter besides the expected homozygous floxed and heterozygous floxed animals. An explanation for this phenomenon could be either a premature embryonic Cre-expression or expression of Cre in male germ cells. Indeed, there are several reports that Cre is expressed in germ cells sometimes, e. g. for the Nestin and GFAP promoters (Zhang, Dublin et al. 2013).

As a conclusion, CamKII α -Cre is a practical tool for postnatal and forebrain-specific KO of genes, but there is a need to continually control for germline transmission of Cre enlarging the complexity of genotyping. In line with that, a useful technique has been developed during this work enabling to control for germline expression of any promoter-driven Cre in a single PCR reaction (see Figure 20).

5.1.4.2 Nestin-Cre

The Nestin-Cre animals were not tested using the R26 reporter line for LacZ staining. Because the general homozygous KO for katanin was not viable, the rationale behind using this Cre-driver line was to achieve at least a close-to-full-KO in the nervous system. In this case, the usage of Nestin-Cre showed that generally, prenatal KO of katanin in the brain is viable.

The homozygous floxed animals containing the Nestin-Cre transgene were much smaller than the respective wild type animals (Figure 54b), but it cannot be ruled out that Nestin-Cre influenced the body weight itself. Katanin wild type animals containing the Nestin-Cre transgene were smaller in comparison to homozygous floxed or wild type animals without the Cre transgene, too. Indeed, it has been reported during the course of this work, that Nestin-Cre has several side effects independent of the presence of floxed alleles (Harno, Cottrell et al. 2013). In addition, it has been reported that Nestin-Cre does not entirely knock out genes of interest in the nervous system (Liang, Hippenmeyer et al. 2012). As a conclusion, it cannot be ruled out that the conditional katanin KOs generated by using Nestin-Cre-driver lines had a scattered genetic background in the brain. In line with that, Western Blotting using the polyclonal goat anti-katanin (M-13) antibody only showed a slight reduction of katanin levels in the brain (see Figure 51). The Western Blotting results could not be confirmed with more animals because in the following generations Nestin-Cre seemed to be expressed in germ cells (data was not shown), leading to the loss of the conditional allele and following time limitations.

Another possibility to conditionally knock out genes in the brain is by using the Emx-Cre-driver line. So far, Emx-Cre has been reported to be more brain-specific than Nestin-Cre and to have

fewer side effects. Thus, it should be a promising approach to study brain-specific katanin KO using this Cre-driver line.

Summarizing the results from all promoter-driven Cre lines, it can be concluded that for these conditional gene-targeting approaches many control littermates are necessary:

$$\begin{array}{cccc} \text{GOI}^{\text{FL/FL}} & & \text{GOI}^{\text{FL/FL}} & & \text{GOI}^{\text{WT/WT}} & & \text{GOI}^{\text{WT/WT}} \\ & & \text{Conditional-Cre}^{\text{WT/TG}} & & & & \text{Conditional-Cre}^{\text{WT/TG}} \end{array}$$

These genotype combinations can only be achieved by mating heterozygous floxed animals, with one of the mating partner additionally containing the Cre transgene, which significantly increases animal consumption. Alternatively, a prestudy has to be conducted where wild type animals are compared with those that express Cre in order to demonstrate that there is no Cre-effect for the specific question.

5.2 Expression analysis of spastin and katanin in mice

5.2.1 Expression analysis of spastin and katanin using gene-trap reporter alleles

Both the knockout-first and the reporter alleles are suitable to monitor the endogenous promoter activity of spastin and katanin because of the presence of a LacZ cassette that is spliced to the 5' upstream exons of the targeting site (see Figure 18). Thus, cells with active transcription of either spastin or katanin should turn blue following LacZ staining (see section 3.2.7). To monitor endogenous promoter activity, however, the animals from the KO-1st were not used, due to the possibility of an influence on the expression levels by the presence of the promoter-driven neomycin phosphotransferase cassette. Instead, these animals were mated to Cre-deleter mice to generate reporter alleles, followed by the outcrossing of the Cre transgene. Heterozygous reporter allele mice were then used for LacZ staining, assuming that the heterozygous loss of the respective proteins would not affect their development.

On the one hand, the mainly brain-specific and hippocampus-specific expression of β -galactosidase under the endogenous spastin and katanin promoters was expected. On the other hand, it was not expected to observe such a weak LacZ staining, standing for the activity of the two promoters. Technical problems of the LacZ staining procedure are unlikely since parallel LacZ staining of organs from the same mice and other β -galactosidase containing positive controls showed strong staining results (data not shown).

As can be concluded from the targeting strategies for spastin and katanin, the RNA sequence from the first 4 or 5 exons should be fused to the LacZ sequence respectively, leading to fusion transcripts (for comparison see Figure 21 and Figure 47). The presence of an IRES in the reporter-allele mice theoretically ensures that LacZ can be translated independently of the upstream sequences.

The possibility of an MIT- β -galactosidase fusion protein might inhibit LacZ enzymatic activity, either by targeting of the fusion proteins to special cellular compartments or by directly interfering with the folding process of β -galactosidase. Besides, the presence of a PEST sequence could lead to fast degradation of the putative N-terminal spastin- β -galactosidase fusion protein.

The quantity of LacZ expression does not allow concluding on the quantitative expression of spastin and katanin, because the translation of the N-terminal fragments of spastin or katanin should be independent of the translation of LacZ. Also, the enzymatic activity of LacZ should theoretically quantitatively convert the X-Gal substrate into its products galactose and 5-bromo-4-chloro-3-hydroxyindole, followed by the spontaneous dimerization and oxidation of the latter one to the blue-colored and insoluble end product 5,5'-dibromo-4,4'-dichloro-indigo. Thus, the weak lacZ staining observed in the spastin and katanin heterozygous reporter mice should be a result of a scattered expression of β -galactosidase restricted to very few cells in the hippocampus rather than merely the representation of a feeble β -galactosidase activity within the individual cells. Since such a sparse fraction of cells expressing katanin and spastin is unlikely and does not match the results observed in in-situ hybridizations (Ma, Chia et al. 2006), an alternative way to explain these phenomena might be the monoallelic transcription of the nontargeted alleles. In fact, recent studies indicate that in addition to imprinting, at least 1 % of all autosomal genes show monoallelic expression, including many genes expressed in the CNS (Wang, Valo et al. 2007). The mechanism of this selective gene expression frequently involves differences in DNA methylation and the modification of histones (Vu, Jirtle et al. 2006). It is hypothesized that it might play a role in certain genetic disorders that do not show standard Mendelian inheritance such as schizophrenia, bipolar disorder, epilepsy, and type I diabetes (Singer-Sam 2010). The compensation of deletions and other loss-of-function mutations both at the protein- and at the transcription-level are discussed to be a mechanism of the usual dominance of wild type alleles over mutant alleles. Besides, loss-of-function mutations are more likely to be fully recessive in genes coding for enzymes than in genes coding for other proteins (Fisher and Scambler 1994, Veitia 2002, Kondrashov and Koonin 2004) and for proteins that are less likely to form protein complexes (Papp, Pal et al. 2003).

5.2.2 Expression analysis of spastin and katanin in wild type mice

Western Blotting analysis using lysates from wild type mice revealed that spastin is expressed in all brain regions which is in line with the observations of other experiments reported by other groups (Ma, Chia et al. 2006). The highest levels were found in the hippocampus, followed by the cortex, the midbrain and the cerebellum of young mice, which is in line with the results of the gene-trap experiments. This expression level drops strongly in adult mice pointing to its importance during development.

For katanin, the expression in wildtype mice was not yet analyzed due to time limitations after the establishment of conditional katanin knockout mice. However, as shown in Figure 52, katanin

seems to be expressed in most brain regions of adult mice at the protein level but to a greater extent in the hippocampus.

5.2.3 Subcellular expression analysis of spastin and katanin

At the subcellular level, spastin's and katanin's expression could be studied using differential fractionation (Figure 40). Here spastin was found throughout all cell fractions including a weak signal for the soluble protein fraction S1 pointing to its ubiquitous intracellular functions. This is also in line with the results obtained from synaptosomal fractionation (Figure 40), where spastin was found to be enriched at synaptic sites. It also fits the observations from immunocytochemistry where spastin could be visualized in the cell soma as well as in different compartments of the neurites, such as their tips, bifurcating growth cones, transport vesicles, branching points, synaptic contacts, regions with a strong curvature and neurite swellings (Figure 38). In contrast to that, overexpression of a spastin isoform lacking the amino-terminal 85 amino acids into cultivated neurons resulted in a mainly perinuclear accumulation of the protein indicating that the amino terminus is responsible for the individual interaction with specific target molecules as well as the targeting to different compartments. Especially the hydrophobic stretch (called the TM domain) may be responsible for the targeting of spastin to membranous compartments.

In contrast to spastin, katanin was mainly found in the P2 and P3 fractions of whole brain lysates but was also detected in other fractions as well (Figure 40). Immunohistochemistry and immunocytochemistry experiments using the anti-katanin antibodies on samples derived from katanin^{FL/FL}/Nestin-Cre^{WT/TG} were not successful so far. Overexpression of AcGFP-tagged katanin, however, resulted in a diffuse expression pattern of the fusion protein. The fusion protein could be detected in neurites and neurite tips negative for MAP2 which is in line with previous reports.

5.3 General health of spastin depleted animals

5.3.1 Reduced body weight of spastin KO mice

As described in section 4.2.2 and shown in Figure 33, KO mice prenatally depleted of spastin (KO-1st and null-allele mutants) showed an 8 % reduction of their body weights in comparison to their wild type littermates. This reduction was primarily observed for adult animals, whereas newborn KO and forebrain-specific conditional spastin KOs (CamKII α -driven Cre) did not show any obvious difference (data were not shown).

Thus, a motor neuron disease-like mechanism is conceivable, where the onset of the disease is often associated with muscle wasting and a resulting body weight loss (Wong, Pardo et al. 1995). Mild muscle wasting in the lower limbs is also common in HSP patients who have had the disease for over a decade (Harding 1981, Durr, Brice et al. 1994). In line with the present results, young patients do not seem to be affected; for instance, a study carried out with HSP affected children did not find any significant difference in body weight or height compared to healthy

subjects (Cimolin, Piccinini et al. 2007). In rodent models of other HSP associated genes involved in endosomal trafficking (e. g. ZFYVE26/SPG15 and NIPA1/SPG6) a reduction of body weight was observed as well, especially with increasing age (Khundadze, Kollmann et al. 2013, Watanabe, Arnold et al. 2013). A recently described *SPG4* missense mutation model in mice also report a reduced body weight of older animals (Connell, Allison et al. 2016).

In sum, it is not likely that the reduced body weight is caused by a delayed embryonal development of spastin ko mice, but rather display a loss of tissue (atrophy) or decreased weight gain at later stages. However, it has not been examined further whether the decreased body weight is a result of muscle wasting, alterations in metabolism or in activity levels resulting in decreased body fat. In fact, spasticity results from a loss of inhibition of the lower motor neurons by the upper motor neurons leading to hypertonia and excessive muscle contraction. Thus, it is thinkable that all of the mechanisms mentioned above play a role in the loss of weight in spastin KOs.

5.3.2 Altered gait parameters in spastin KO mice

Since spastin's most prominent role is linked with motor function and because the available mutant mouse models developed gait abnormalities at different ages (Tarrade, Fassier et al. 2006, Kasher, De Vos et al. 2009, Connell, Allison et al. 2016), the question arose whether the prenatal spastin KO mice generated in this study were also affected. As it was not the main focus of this study to reproduce these results and due to time limitations only three gender-matched littermate pairs were video-analyzed in their home-cages from the ventral view to confirm the expected phenotype. As shown in Figure 34, mice aged between 4 and 9 months and with a prenatal depletion of spastin showed a larger stride length between their hind limbs when video-analyzed from the ventral view. This effect was significant for the mean stride length of each mouse compared to its littermate of the opposite genotype. However, the small sample size (n=3 for each genotype) and the variance of the age of the animals presumably have led to the non-significant result in a two-tailed t-test. Also, the measurement of the distance between the hind limbs might not have been the most sensitive test for altered gait parameters and should be repeated by established tests for motor function such as footprint assay, the grip strength test and the rotarod test.

At the first glance, a larger stride length of spastin knockout mice seemed unexpected, because a weakness of hind limbs associated with HSP rather implies that affected subjects should have a reduced step length. However, these results are also consistent with a recently published study in which the authors used an automated treadmill system to measure gait parameters (Connell, Allison et al. 2016). Thus, the observed increase in stride length could be a result of impaired balance due to altered skeletal muscle performance.

Interestingly, while most human HSP patients are severely affected by only one mutated spastin allele, homozygous mouse mutants only develop a mild gait phenotype. In contrast, a

homozygous mutation of spastin that is also observed in human HSP patients results in a very severe phenotype in cattle, while heterozygous animals seem unaffected at all. Also in heterozygous mutant spastin mouse models, no impairment of gait parameters is detectable (Connell, Allison et al. 2016). These discrepancies in the age of onset and the severity of the disease might be explained by the different lifespan and the length of the affected axons of these mammals. Thus, a higher dose of the mutated spastin allele might be needed due to the short lifespan of mice (Zoghbi and Botas 2002).

In summary, the gait phenotype reported for the different spastin mutant models could be confirmed partially for the age between four and nine months.

5.3.3 Sterility of homozygous spastin knockouts

As described in section 4.2.2.1, both male and female heterozygous spastin KOs (KO-1st and null-allele mutants) were fertile and reproduced at an average rate with approximately 6 pups per litter. In contrast, no pups could be obtained for homozygous KOs mated to wild types.

The sterility of homozygous spastin KOs has been reported in *Drosophila* and in mice for both sexes, but the causality has not been tested further (Sherwood, Sun et al. 2004, Tarrade, Fassier et al. 2006). Authors from another study discovered recently that spastin functions as a transcriptional corepressor of the homeobox gene HOXA10 in a human model cell line for endometrial epithelium (Daftary, Tetrault et al. 2011). HOXA10 is required for uterine development and its expression is driven by the steroid hormones estrogen and progesterone at the time of implantation (Taylor, Vanden Heuvel et al. 1997, Taylor, Arici et al. 1998, Daftary and Taylor 2006). Its mutation in mice led to severe fertility impairments due to a bilateral absence of testes, defective spermatogenesis and failure of embryo implantation (Satokata, Benson et al. 1995, Benson, Lim et al. 1996). HOXA10 functions as a transcriptional repressor of EMX2 (empty spiracles homeobox 2), which seems to be a negative regulator of fertility (Daftary and Taylor 2004) and whose mutation is also associated with embryonic lethality due to defective development of the urogenital tract (Miyamoto, Yoshida et al. 1997). Interestingly, HOXA10 only seems to inhibit EMX2 expression in association with spastin; in case spastin is missing, HOXA10 seems to have a contrary effect and promotes the expression of EMX2 (Daftary, Tetrault et al. 2011). Thus, the lack of spastin might enhance expression of EMX2 via the missing interaction with HOXA10 leading to decreased fertility.

To add complexity to the data observed in mice, *Drosophila* spastin lacks the amino-terminal region, which is claimed to cause nuclear translocation of human spastin. Thus, it should not be able to act as a transcriptional corepressor of the EMX2 orthologue in the nucleus by binding to HOXA10. Yet, spastin null mutants of *Drosophila* are also reported to be sterile. This implies that spastin might have pleiotropic effects in the control of fertility and that the mechanism of its loss is not only restricted to the control of EMX2 expression. Similar to katanin (see section 2.3.6.2), a role for spastin in the control of sperm flagella is imaginable because the MTs of these structures

display a high level of polyglutamylation, similar to the situation in the brain (Bobinnec, Marcaillou et al. 1999). Ciliated epithelia are equally crucial in females to guide the zygotes into the uterus or oviducts. Alternatively, severing by spastin might be needed to maintain MT dynamics in supportive cells, like it was concluded for Sertoli cells (SCs) from KATNAL1 KO mice (see section 2.3.6.1 and (Smith, Milne et al. 2012)). In *Drosophila*, the function of SCs is presumably taken over by head cyst cells, whose filopodia-like F-actin extensions are required to adhere to spermatid heads for their maturation and elongation (Desai, Shirolkar et al. 2009). Interestingly, the loss of spastin in *Drosophila* and its overexpression in neurons also resulted in filopodia-like protrusions in neurons (Sherwood, Sun et al. 2004, Yu, Qiang et al. 2008). In line with that, testes derived from spastin KO males also lack mature spermatozoa as shown by light microscopic and ultrastructural analysis (Figure 32). In Addition, the cells obtained from cauda epididymis were not motile in contrast to the ones obtained from wild type males.

In humans, there are only few male HSP patients known to be affected by mild sexual dysfunction with a late occurrence about a decade after the onset of the disease (McDermott, White et al. 2000). Nevertheless, with the obtained data and the data published so far, it is not possible to narrow down the mechanisms underlying the infertility of spastin KO mice. The involvement of MT-severing enzymes in so many processes ranging from mitosis, meiosis, cilia dynamics, transcriptional regulation during development and adulthood as well as MT- and actin-dynamics rather suggest a pleiotropic role involving more than one mechanism.

5.4 General health of katanin depleted animals

5.4.1 Embryonic lethality of homozygous katanin knockout mice

The fact that no homozygous general katanin KOs could be observed for offspring resulting from numerous heterozygous matings leads to the question of whether the targeting of the katanin locus was correct (particularly if the insertion of the targeting vector occurred at the intended genomic sequence; in this case, the wild type- band would be present during all genotyping reactions) or whether the homozygous general katanin KO is embryonic lethal. The targeting results, namely the results from long-range PCR (see Figure 48), the sequencing results and genotyping PCR indicate that the insertion of the targeting vector occurred at the correct genomic sequence. The fact that the wild type band did disappear for homozygous floxed animals (see Figure 49) mainly supports the second alternative.

In addition, the reduced offspring number resulting from heterozygous matings of both KO-first as well as classical KO lines in comparison to the ones from wild types and heterozygous animals (or of the floxed allele only) points to embryonic lethality (6.1 pups per litter for WT x HET matings vs. 4.3 for HET x HET matings, see Figure 53). Under consideration of Mendelian inheritance, the ratio of wild type, heterozygous and KO animals should be 1:2:1 or 25 %: 50 %: 25 %. In case of embryonic lethality this ratio shifts to 1:2:0 or 33.3 %: 66.6 %: 0 %, respectively. The latter ratio fits very well with the data obtained so far.

Another question arises concerning the reason for the non-viability of homozygous katanin KOs. It is unlikely that there is an impairment in the oocytes or spermatocytes of the heterozygous parent animals. The fact that no impairment was observed for the offspring from HET x WT matings, irrespective of the gender of the heterozygous parent animal, leads to the conclusion that the lethality is not caused by defects in male or female meiosis in heterozygous animals (see Figure 53). Moreover, although being KOs at the genetic level, the germ cells originating from heterozygous animals and containing the KO allele should still contain some remaining katanin protein expressed by the cells preceding meiotic chromosome segregation and reduction division.

The fact that the offspring number is reduced for HET x HET matings strongly supports the assumption that fertilization does happen initially, followed by lethality occurring at some point later during embryonic development. The litter sizes of the used C57BL/6J and C57BL/6N strain vary from 6-7 (Green and Witham 1991). The observed average litter size of 4.3 for prenatal HET x HET mutants supports the assumption of successful fertilization followed by the resorption of nonviable embryos. However, the timepoint of lethality could not be narrowed down further. These results are in contrast to the published observations for katanin's orthologue in *Caenorhabditis elegans* (Srayko, Buster et al. 2000). In *Caenorhabditis elegans*, katanin seems to be degraded by the end of meiosis and seems not to be important for mitosis (Lu and Mains 2007). For vertebrates, there is some evidence for katanin's role in the building of the mitotic spindle poles (Buster, Zhang et al. 2007, Sonbuchner, Rath et al. 2010).

5.4.2 Reduced body weight of Nestin-Cre conditional katanin knockouts

As has been shown in Figure 54b, katanin^{FL/FL}/Nestin-Cre^{WT/TG} animals had a reduced body weight compared to katanin^{FL/FL}/Nestin-Cre^{WT/WT} and katanin^{WT/WT}/Nestin-Cre^{WT/WT} littermates. However, it is very likely that this effect is mainly due to the presence of Nestin-Cre^{WT/TG}. Although only tested in one littermate, it has been observed that katanin^{WT/WT}/Nestin-Cre^{WT/TG} animals also displayed a similar reduction in body weight. Besides, it has been reported during the course of this work that Nestin-Cre has several side effects independent of the presence of floxed alleles (Harno, Cottrell et al. 2013). Thus, it cannot be claimed nor excluded from the data obtained during this study, that katanin influences body weight and size. As discussed in section 5.1.4.2, more appropriate control littermates will be necessary to answer that question.

5.5 Hippocampal CA1 cell loss in spastin KO mice

Mice prenatally depleted in spastin showed a reduced density of the hippocampal CA1 cell layer by approximately 8 % compared to their wild type littermates (Figure 41). Interestingly, heterozygous animals showed the same reduction in the CA1 layer like the homozygous animals. In contrast to the results from the body weight analysis (Figure 33), there is no intermediate phenotype for heterozygotes, indicating that in this case, the perturbation of spastin's dosage is responsible. However, only sic heterozygous animals were tested, in contrast to 11 animals for both wild type and knockout animals and this observed effect might be due to the small sample

size. Because pooled data from animals with ages ranging from 2 to 43 weeks were used for the quantification, only the relative thickness of the CA1 layer could be determined for each litter. The reduced CA1 cell layer in spastin knockouts could be a consequence of reduced cell number, either caused by reduced neurogenesis, by migratory defects or by neurodegenerative mechanisms. Another possibility could involve smaller cell bodies of the affected neurons. This should be analyzed further in the future, first by determining the cell number in the CA1 layer and then by determining the area of the cell bodies. Additionally, controls in other brain regions should be taken into account.

The consequences of this phenotype will have to be examined as well. Interestingly, decreased hippocampal volume and the dysfunction of neurons and synapses in the CA1 and in the entorhinal cortex correlate with memory deficits, a hallmark of Alzheimer's disease (Hyman, Van Hoesen et al. 1984, West, Kawas et al. 2000, Elgh, Lindqvist Astot et al. 2006, Kerchner, Hess et al. 2010). As already indicated in section 2.3.6.3, spastin indeed seems to play an executive role downstream of pathological tau mislocalization (Zempel, Luedtke et al. 2013) and its mutation has been linked to cognitive impairment in several cases (Heinzlef, Paternotte et al. 1998, Webb, Coleman et al. 1998, White, Ince et al. 2000, Mc Monagle, Byrne et al. 2001, Tallaksen, Guichart-Gomez et al. 2003, Murphy, Gorman et al. 2009, Guthrie, Pfeffer et al. 2013).

In case the reduced CA1 layer is due to cell loss, an interesting hypothesis would be that the latter one might be caused by hyperglutamylation of microtubules. Hyperglutamylated microtubules act as positive regulators of spastin's enzymatic activity (Lacroix, van Dijk et al. 2010). Thus, a spastin knockout might lead to the accumulation of microtubules with the latter post-translational modification leading to defects in microtubule dynamics and neuronal cargo delivery.

In fact, increased polyglutamylation was observed in the proximal dendrites of the CA1 region of spastin^{KO-1st/KO-1st} mice as shown by immunohistochemistry (Figure A). However, the results could not be tested for a significant difference between the genotypes due to the small sample size and time limitations.

Additional analysis of whole brain lysates obtained from spastin knockout mice did not lead to significant results yet (not shown), maybe because of the different distribution of this posttranslational modification in the brain or different compensation mechanisms for the loss of spastin. This hypothesis is underlined by the Western Blotting analysis of different brain regions using conditional spastin knockout mice (spastin^{FL/FL}/CamKII α -Cre^{TG/WT}) and their control littermates using an antibody directed against polyglutamylated tubulin (clone B3). Here, it seems that polyglutamylated tubulin in spastin^{WT/WT}/CamKII α -Cre^{WT/TG} (termed WT) animals is mainly found in the cerebellum. Whereas spastin expression is strongly reduced in the hippocampus and in the cortex, polyglutamylation levels only strongly rise in the hippocampus of conditional knockout mice (Figure 43).

In line with the hypothesis of perturbed cargo delivery as a consequence of altered microtubule modification, the AMPA receptor subunit GluR2 was downregulated in immunohistochemistry analyses (Figure 44). However, the downregulation was not quantified further due to small sample size (n=1).

5.6 Microtubule-severing and microtubule dynamics

As already indicated in sections 2.2.2, 2.2.3, 2.3.6.3 and 2.5, dynamic MTs seem to play an important role in dendritic spine function, as could be demonstrated in studies using the fluorescently-labeled protein EB3. Being a marker for the transitory presence of microtubules in dendritic spines, the latter protein seems to influence spine function itself (Figure 8). Because MT severing can generate short mobile MTs, the question arose whether the loss of spastin or katanin leads to altered MT dynamics in dendritic spines. Using live cell video-recordings of pmRFP and pEGFP-EB3 transfected hippocampal neurons derived from spastin^{KO-1st/KO-1st} mice, it could be excluded that spastin alone is needed for the spine entry of GFP-EB3 (see Figure 45). However, due to the small sample size, the EB3 entry into spines could not be quantified. In fact, the perturbation of spastin expression levels in motor-neuron like hybrid cells led to an altered EB3 assembly rate on MT and thus altered MT dynamics in another study (Riano, Martignoni et al. 2009). Thus, also spine related EB3 dynamics might be altered in spastin knockout mice. It is conceivable that the loss of one MT severing enzyme can at least be rescued by another related enzyme. Thus, it is unlikely to observe a complete abolishment of EB3 entry into spines in knockouts of only one MT severing enzyme, due to the fact that the mammalian genome codes for multiple MT severing enzymes, which are likely to at least partly rescue the phenotype.

Authors from one study using the EB3 protein found that MT dynamics in neurons were altered by the association of EB3 and the postsynaptic scaffolding protein PSD-95 (Sweet, Previtiera et al. 2011). Interestingly, this association is assumed to influence dendritic arborization, but the exact mechanism of action is unknown. Thus, it is imaginable that MT severing enzymes play a direct or an indirect role in this complex. However, immunoprecipitations using antibodies directed against EB3 and PSD-95 could co-precipitate neither spastin nor katanin undoubtedly (Figure 46). Although faint bands could be observed occasionally at the expected band size, the interpretation is difficult, because spastin and katanin have a molecular weight similar to the heavy chains of immunoglobulins.

Another possibility to circumvent this problem would be by using anti-spastin and anti-katanin antibodies for immunoprecipitations and to control for coprecipitation of EB3 and PSD-95 using Western Blotting. However, the self-precipitation of the MT severing enzymes was unsuccessful so far (data not shown). Additionally, the usage of nanobodies (Gibbs 2005) or of a heterologous expression system with tagged proteins (e. g. using the polyhistidine or the glutathione S transferase tags) would be possible but are very time-consuming.

Nevertheless, the M-type Kinesin Kin-13/KIF2a, mainly known to be involved in axonal branching, was reproducibly co-immunoprecipitated with EB3 and with PSD-95. Thus, KIF2a might be involved in the complex of EB3 and PSD-95 to control dendritic MT-dynamics and branching as well. However, to confirm whether the interaction between KIF2a and EB3 and PSD-95 is direct, additional experiments are necessary.

5.7 Behavior characterization of forebrain-specific katanin knockouts

Initial behavior characterization of forebrain-specific katanin knockouts did not reveal any major differences to their wild type littermates regarding horizontal locomotor activity and anxiety levels (open field test and elevated plus maze).

In the elevated plus maze, the mice were tested in two different cohorts, since cohort 1 only consisted of female mice. As two-way ANOVA analyses revealed, there was a significant difference between the two female groups from cohort 1 and cohort 2. This difference was especially apparent for the time and the entrance frequency in the open arms of the maze. This is likely due to the fact, that the females from cohort 2 were initially tested in the open field test in contrast to the mice from cohort 1, which might have had an impact on the anxiety levels (Table 20).

In the open field test, 2 cohorts were tested as well. As for the elevated plus maze test, there was a significant difference between the females from cohort 1 and cohort 2 concerning the total distance moved in the arena. In sum, the horizontal locomotor activity and anxiety levels seem to be impacted by previous experience leading to a stronger exploratory (i. e. distance moved) and a weaker anxiety-related behavior (i. e. time spent in the open arms of the EPM and in the CZ of the open field arena) with increasing amount of experiments. However, there was no apparent difference in the slope of the graphs e. g. when represented as the distance moved over time bins (not shown), leading to the assumption that the overall effect between the cohorts was the same for the two female groups. Nevertheless, the results from both cohorts were not combined for further analyses.

Taken together all the results from the EPM and OF tests, including the marginally significant reduction in distance moved for the males in the OF test, it is likely that the horizontal locomotor activity levels are slightly altered in the male forebrain-specific knockout group. This difference between the genotypes does not seem to be caused by a difference in speed but rather by increased immobile phases in the outer zone of the arena. This points to a psychological rather than a physiological causality of the marginally altered horizontal locomotor activity levels.

There was no evidence for altered anxiety levels, measured as the time and the entrance frequency in the open arms of the EPM and as the time spent in the center zone of the OF test.

Concerning initial learning and memory testing, the conditional knockouts did not show any impairment in the test phase after a short inter-trial interval (3 min delay) of the place recognition

task in a Y-maze (Figure 62). After a 24 h delay in the place recognition task, the knockout group did not show any significant preference of the novel arm. However, although there is a significant difference between the wild type and the knockout group in the place recognition test phase after a 24 h delay in terms of total time spent in the novel arm, the main difference seems to rise from the last two min of the test phase (not shown). As was shown in Figure 62b and c, both genotypes showed similar horizontal locomotor activity levels (measured as distance traveled) as well as exploratory levels (as measured by total arm entries during the test phase) within one experiment.

Taken together, the observations from behavioral results obtained so far indicate that the short time memory of forebrain-specific *Katna1* knockout mice is not impaired. Judging from the results including longer delays between the sample and the test phases, however, point to a possibly altered long-term memory. These results should be confirmed and widened out including tests with positive or negative reinforcement such as the fear conditioning test and the Morris water maze test.

5.7.1 Choice of the control group for behavioral analyses

For the initial behavioral characterization of conditional *Katna1* knockout mice, homozygous $Katna1^{FL/FL}/CamKII\alpha-Cre^{TG/WT}$ animals were compared to littermates that did not lead to any knockout of *Katna1*, i. e. $Katna1^{FL/FL}/CamKII\alpha-Cre^{WT/WT}$, $Katna1^{WT/FL}/CamKII\alpha-Cre^{WT/WT}$, $Katna1^{WT/WT}/CamKII\alpha-Cre^{WT/WT}$ and $Katna1^{WT/WT}/CamKII\alpha-Cre^{TG/WT}$. On the one hand this was due to the fact that the availability of animals was the limiting factor at that timepoint. On the other hand it is not definitely clear which of the above mentioned control groups was the appropriate one. In theory, all of them should be suitable. However, since the *CamKII α -Cre* mouse line is transgenic – with a random integration of a vector into the genome of the mouse – an impact of the transgene on behavior cannot be excluded. Nevertheless, the authors who developed the *CamKII α -Cre* mouse line state in their original publication that they didn't observe any gross behavioral phenotype, nor was there any report claiming the opposite since then.

On the other hand it was also important to control for the floxing of the *Katna1* gene itself meaning that it cannot be excluded that the minimal change in the *Katna1* gene might have led to an alternation of the expression of genes. This cannot be generally stated and must be considered separately for each behavioral experiment with conditional knockout mice.

Thus, the most suitable control group would consist of *CamKII α -Cre*^{TG/WT} animals that also have a floxed *Katna1* allele but without the excision of the gene, which does not exist. An approximation to this state would be the generation of a control group with mutated loxP sites, thereby preventing the excision by Cre recombinase. Another tool would be the usage of homozygous floxed animals and the injection of a Cre virus into the knockout group versus a non functional Cre virus in the control group. However, all of these techniques have their drawbacks

with individually tailored controls. Thus, for initial behavioral characterization it was considered the most suitable to combine all littermates without the loss of katanin into one control group. For future experiments however, the most suitable approach would consist in the usage of multiple control groups.

5.8 Conclusion and outlook

To summarize, both the *Katna1* and the *SPG4* genes could be successfully targeted in the mouse.

Spastin

For spastin, this could be successfully demonstrated at the genetic level (Southern Blotting, long-range PCR and partial sequencing), at the expression level (immunocytochemistry and Western Blotting) as well as by the initial characterization of the animals (gait abnormalities). In addition, it could be proven that both full knockouts, as well as forebrain-specific conditional knockouts, were viable. Furthermore, the full knockout lines were characterized in terms of genotype distribution and a deviation from Mendelian inheritance could be determined with less than the expected number of targeted alleles in the progeny. Additionally, the sterility of homozygous spastin knockout mice could be constated and slightly narrowed down to the germ cells. Also, the body weights of prenatally targeted animals were significantly reduced, the causality for which still has to be determined. In order to do so, more animals at different ages have to be analyzed and their activity levels as well as their food consumption levels have to be determined.

The expression of spastin was studied at different levels: promoter activity and indirectly the RNA expression were analyzed by LacZ stainings of targeted spastin^{GT/WT}-tissues, at the protein level by Western Blotting of different brain regions at different ages, as well as at the subcellular protein expression level (Western Blotting of subcellular and synaptosomal fractionations, immunocytochemistry and ectopic overexpression of pEGFP-tagged spastin into cultivated neurons). In summary, spastin expression was found in all brain regions including hippocampus and cerebellum as well as in most other organs. Its expression level in the brain dropped obviously with increasing age but did not change that much in other organs. Judging from immunostainings, subcellular fractionations and synaptosomal preparations, spastin is found throughout all subcellular locations, including the soluble protein fraction. To narrow down the organelles, additional colocalization experiments need to be done.

Nissl stainings of prenatal spastin knockout mice did not reveal any gross brain morphology abnormalities. However, the density of the CA1 region was reduced by approximately 10 %. One explanation might be cytotoxicity due to hyperpolyglutamylation of microtubules in that region. Nevertheless, it will be necessary to determine the causality for and the consequences of that reduction. Also, it should be tested whether the observed reduction is a temporary effect during development.

To further study general depletion of spastin the following experiments need to be done: quantification of excitatory and inhibitory synapses using primary neuronal cultures or by using isolated brain sections. In the next step, the activity-dependent change in spine quality and quantity should be studied either by using immunofluorescence or by surface biotinylations. Additionally, a possible alternation in LTP or LTD should be studied by electrophysiological measurements.

By EB3 imaging it was shown that EB3 comets still can enter spines in spastin knockouts. To further study microtubule-dependent spine dynamics, the EB3 spine entry should be quantified both under basal as well as under stimulating conditions.

For behavioral experiments, the full knockout animals should be used to initially test motor function (e. g. using the rotarod test) as well as the activity levels (e. g. using the open field test or the elevated plus maze test) in order to test whether the reduced body weight can be explained by an alternation in the latter ones. Additional behavioral experiments should be carried out using the conditional forebrain-specific knockout mouse line thus circumventing ambiguous interpretation of the results due to the differences in body weight and motor function.

Katanin

For katanin, the successful targeting could be demonstrated at the genetic level using long-range PCR, genotyping PCR and partial sequencing. Additionally, genotype distribution and litter sizes point to the correct targeting of the gene.

Targeting confirmation at the expression level (immunocytochemistry and Western Blotting) was not as straightforward as for spastin due to the apparent embryonic lethality of homozygous katanin knockout mice and the lack of corresponding negative controls. So far, no reduction in katanin levels could be observed for heterozygous knockouts but a partial reduction in whole brain lysates of conditional Nestin-Cre knockouts and in hippocampal lysates of CamKII α -Cre knockouts.

Homozygous depletion of katanin was lethal after fertilization. The lethality timepoint still has to be determined to identify katanin's critical function during embryogenesis. Additionally, although not significant yet, the data obtained so far imply that the heterozygous genotype is also disadvantaged compared to wild type.

Similar to spastin, katanin expression was detected in the hippocampus, the cerebellum as well as in most other organs using the Lac-Z genetrap method. The promoter activity decreased with increasing age. Due to the lack of a negative control, immunostainings for the study of endogenous intracellular katanin expression were not possible. However, homozygous floxed *Katna*^{FL/FL} neuronal cultures were already successfully cotransfected with mRFP and Cre vectors making it possible to optimize immunofluorescence conditions for studying katanin's endogenous

expression in future. Otherwise, hippocampal cells derived from conditional katanin knockouts can be used.

At the first glance, neither heterozygous prenatal katanin knockouts nor forebrain-specific conditional knockouts were impaired regarding general health including body weights, size and activity levels.

Initial behavioral characterization of forebrain-specific katanin knockouts and their wild type littermates was made. Both genotypes did not show any differences in their activity or anxiety levels and their short-time memory did not seem to be impaired. Experiments with longer inter-trial intervals already point to a possible impairment of long-term memory. This will have to be confirmed in future.

Although the initial characterization has been made, a big amount of work will be left to specify spastin's and katanin's role for microtubule dynamics and synaptic plasticity. As was shown for both genes, their targeting in a classical way leads to severe developmental phenotypes (e. g. the lethality of homozygous katanin knockout, different body weights and gait parameters for spastin) making it necessary to go for spatiotemporal control of the knockout. Thus, although a lot can be learned using the classical knockout approach, it will be necessary to use the conditional knockouts to learn more about adult synaptic plasticity.

6 REFERENCES

- Agostinho, P., A. Pliassova, C. R. Oliveira and R. A. Cunha (2015). "Localization and Trafficking of Amyloid-beta Protein Precursor and Secretases: Impact on Alzheimer's Disease." J Alzheimers Dis 45(2): 329-347.
- Akhmanova, A. and M. O. Steinmetz (2008). "Tracking the ends: a dynamic protein network controls the fate of microtubule tips." Nat Rev Mol Cell Biol 9(4): 309-322.
- Akkor, M. and A. Karabay (2010). "Production and characterization of a monoclonal antibody against P60-katanin." Hybridoma (Larchmt) 29(6): 531-537.
- Alvarez, V. A. and B. L. Sabatini (2007). "Anatomical and physiological plasticity of dendritic spines." Annu Rev Neurosci 30: 79-97.
- Amaral, D. G. and M. P. Witter (1989). "The three-dimensional organization of the hippocampal formation: a review of anatomical data." Neuroscience 31(3): 571-591.
- Anton, M. and F. L. Graham (1995). "Site-specific recombination mediated by an adenovirus vector expressing the Cre recombinase protein: a molecular switch for control of gene expression." J Virol 69(8): 4600-4606.
- Araque, A., V. Parpura, R. P. Sanzgiri and P. G. Haydon (1999). "Tripartite synapses: glia, the unacknowledged partner." Trends Neurosci 22(5): 208-215.
- Armstrong, C. M. and B. Hille (1998). "Voltage-gated ion channels and electrical excitability." Neuron 20(3): 371-380.
- Atkin, T. A., A. F. MacAskill, N. J. Brandon and J. T. Kittler (2011). "Disrupted in Schizophrenia-1 regulates intracellular trafficking of mitochondria in neurons." Mol Psychiatry 16(2): 122-124, 121.
- Ayala, R., T. Shu and L. H. Tsai (2007). "Trekking across the brain: the journey of neuronal migration." Cell 128(1): 29-43.
- Baas, P. W. (2002). "Neuronal polarity: microtubules strike back." Nat Cell Biol 4(8): E194-195.
- Baas, P. W. (2013). "Microtubule stability in the axon: new answers to an old mystery." Neuron 78(1): 3-5.
- Baas, P. W., M. M. Black and G. A. Banker (1989). "Changes in microtubule polarity orientation during the development of hippocampal neurons in culture." J Cell Biol 109(6 Pt 1): 3085-3094.
- Baas, P. W., J. S. Deitch, M. M. Black and G. A. Banker (1988). "Polarity orientation of microtubules in hippocampal neurons: uniformity in the axon and nonuniformity in the dendrite." Proc Natl Acad Sci U S A 85(21): 8335-8339.
- Baas, P. W., A. Karabay and L. Qiang (2005). "Microtubules cut and run." Trends Cell Biol 15(10): 518-524.
- Baas, P. W. and S. Lin (2011). "Hooks and comets: The story of microtubule polarity orientation in the neuron." Dev Neurobiol 71(6): 403-418.
- Baas, P. W. and L. Qiang (2005). "Neuronal microtubules: when the MAP is the roadblock." Trends Cell Biol 15(4): 183-187.
- Baas, P. W., C. Vidya Nadar and K. A. Myers (2006). "Axonal transport of microtubules: the long and short of it." Traffic 7(5): 490-498.

REFERENCES

- Babst, M., B. Wendland, E. J. Estepa and S. D. Emr (1998). "The Vps4p AAA ATPase regulates membrane association of a Vps protein complex required for normal endosome function." EMBO J 17(11): 2982-2993.
- Baloyannis, S. J. (2014). "Golgi apparatus and protein trafficking in Alzheimer's disease." J Alzheimers Dis 42 Suppl 3: S153-162.
- Barra, H. S., J. A. Rodriguez, C. A. Arce and R. Caputto (1973). "A soluble preparation from rat brain that incorporates into its own proteins (¹⁴ C)arginine by a ribonuclease-sensitive system and (¹⁴ C)tyrosine by a ribonuclease-insensitive system." J Neurochem 20(1): 97-108.
- Baxter, S. L., D. E. Allard, C. Crowl and N. T. Sherwood (2014). "Cold temperature improves mobility and survival in Drosophila models of autosomal-dominant hereditary spastic paraplegia (AD-HSP)." Dis Model Mech 7(8): 1005-1012.
- Beetz, C., M. Brodhun, K. Moutzouris, M. Kiehnopf, A. Berndt, D. Lehnert, T. Deufel, M. Bastmeyer and J. Schickel (2004). "Identification of nuclear localisation sequences in spastin (SPG4) using a novel Tetra-GFP reporter system." Biochem Biophys Res Commun 318(4): 1079-1084.
- Benson, G. V., H. Lim, B. C. Paria, I. Satokata, S. K. Dey and R. L. Maas (1996). "Mechanisms of reduced fertility in Hoxa-10 mutant mice: uterine homeosis and loss of maternal Hoxa-10 expression." Development 122(9): 2687-2696.
- Berg, J. M., J. L. Tymoczko and L. Stryer (2006). Biochemistry (6 th ed.). New York: W. H. Freeman, Sara Tenney.
- Bishop, N. and P. Woodman (2000). "ATPase-defective mammalian VPS4 localizes to aberrant endosomes and impairs cholesterol trafficking." Mol Biol Cell 11(1): 227-239.
- Blackstone, C. (2012). "Cellular pathways of hereditary spastic paraplegia." Annu Rev Neurosci 35: 25-47.
- Blagden, S. P. and D. M. Glover (2003). "Polar expeditions--provisioning the centrosome for mitosis." Nat Cell Biol 5(6): 505-511.
- Bliss, T. V. and G. L. Collingridge (1993). "A synaptic model of memory: long-term potentiation in the hippocampus." Nature 361(6407): 31-39.
- Bliss, T. V. and A. R. Gardner-Medwin (1973). "Long-lasting potentiation of synaptic transmission in the dentate area of the unanaesthetized rabbit following stimulation of the perforant path." J Physiol 232(2): 357-374.
- Bliss, T. V. and T. Lomo (1973). "Long-lasting potentiation of synaptic transmission in the dentate area of the anaesthetized rabbit following stimulation of the perforant path." J Physiol 232(2): 331-356.
- Bobinnec, Y., C. Marcaillou and A. Debec (1999). "Microtubule polyglutamylation in Drosophila melanogaster brain and testis." Eur J Cell Biol 78(9): 671-674.
- Bradley, A., M. Evans, M. H. Kaufman and E. Robertson (1984). "Formation of germ-line chimaeras from embryo-derived teratocarcinoma cell lines." Nature 309(5965): 255-256.
- Brady, S. T., M. Tytell and R. J. Lasek (1984). "Axonal tubulin and axonal microtubules: biochemical evidence for cold stability." J Cell Biol 99(5): 1716-1724.

REFERENCES

- Burgin, K. E., M. N. Waxham, S. Rickling, S. A. Westgate, W. C. Mobley and P. T. Kelly (1990). "In situ hybridization histochemistry of Ca²⁺/calmodulin-dependent protein kinase in developing rat brain." *J Neurosci* 10(6): 1788-1798.
- Burns, R. G. (1991). "Alpha-, beta-, and gamma-tubulins: sequence comparisons and structural constraints." *Cell Motil Cytoskeleton* 20(3): 181-189.
- Buster, D. W., D. Zhang and D. J. Sharp (2007). "Poleward tubulin flux in spindles: regulation and function in mitotic cells." *Mol Biol Cell* 18(8): 3094-3104.
- Cai, D., D. P. McEwen, J. R. Martens, E. Meyhofer and K. J. Verhey (2009). "Single molecule imaging reveals differences in microtubule track selection between Kinesin motors." *PLoS Biol* 7(10): e1000216.
- Cambray-Deakin, M. A. and R. D. Burgoyne (1987). "Acetylated and detyrosinated alpha-tubulins are co-localized in stable microtubules in rat meningeal fibroblasts." *Cell Motil Cytoskeleton* 8(3): 284-291.
- Capecchi, M. R. (1994). "Targeted gene replacement." *Sci Am* 270(3): 52-59.
- Caron, J. M. (1997). "Posttranslational modification of tubulin by palmitoylation: I. In vivo and cell-free studies." *Mol Biol Cell* 8(4): 621-636.
- Carroll, D. (2011). "Genome engineering with zinc-finger nucleases." *Genetics* 188(4): 773-782.
- Carter, T. C. and H. Gruneberg (1950). "Linkage between fidget and agouti in the house mouse." *Heredity (Edinb)* 4(3): 373-376.
- Casanova, E., S. Fehsenfeld, T. Mantamadiotis, T. Lemberger, E. Greiner, A. F. Stewart and G. Schutz (2001). "A CamKIIalpha iCre BAC allows brain-specific gene inactivation." *Genesis* 31(1): 37-42.
- Casanova, M., L. Crobu, C. Blaineau, N. Bourgeois, P. Bastien and M. Pages (2009). "Microtubule-severing proteins are involved in flagellar length control and mitosis in Trypanosomatids." *Mol Microbiol* 71(6): 1353-1370.
- Cassimeris, L. (2002). "The oncoprotein 18/stathmin family of microtubule destabilizers." *Curr Opin Cell Biol* 14(1): 18-24.
- Cermak, T., E. L. Doyle, M. Christian, L. Wang, Y. Zhang, C. Schmidt, J. A. Baller, N. V. Somia, A. J. Bogdanove and D. F. Voytas (2011). "Efficient design and assembly of custom TALEN and other TAL effector-based constructs for DNA targeting." *Nucleic Acids Res* 39(12): e82.
- Chang, F. L. and W. T. Greenough (1984). "Transient and enduring morphological correlates of synaptic activity and efficacy change in the rat hippocampal slice." *Brain Res* 309(1): 35-46.
- Cheung, K., S. Senese, J. Kuang, N. Bui, C. Ongpipattanakul, A. Gholkar, W. Cohn, J. Capri, J. P. Whitelegge and J. Z. Torres (2016). "Proteomic Analysis of the Mammalian Katanin Family of Microtubule-severing Enzymes Defines Katanin p80 subunit B-like 1 (KATNBL1) as a Regulator of Mammalian Katanin Microtubule-severing." *Mol Cell Proteomics* 15(5): 1658-1669.
- Chicurel, M. E. and K. M. Harris (1992). "Three-dimensional analysis of the structure and composition of CA3 branched dendritic spines and their synaptic relationships with mossy fiber boutons in the rat hippocampus." *J Comp Neurol* 325(2): 169-182.

REFERENCES

- Chinnery, P. F., S. M. Keers, M. J. Holden, V. Ramesh and A. Dalton (2004). "Infantile hereditary spastic paraparesis due to codominant mutations in the spastin gene." *Neurology* 63(4): 710-712.
- Ciccarelli, F. D., C. Proukakis, H. Patel, H. Cross, S. Azam, M. A. Patton, P. Bork and A. H. Crosby (2003). "The identification of a conserved domain in both spartin and spastin, mutated in hereditary spastic paraplegia." *Genomics* 81(4): 437-441.
- Cimolin, V., L. Piccinini, M. G. D'Angelo, A. C. Turconi, M. Berti, M. Crivellini, G. Albertini and M. Galli (2007). "Are patients with hereditary spastic paraplegia different from patients with spastic diplegia during walking? Gait evaluation using 3D gait analysis." *Funct Neurol* 22(1): 23-28.
- Cingolani, L. A. and Y. Goda (2008). "Actin in action: the interplay between the actin cytoskeleton and synaptic efficacy." *Nat Rev Neurosci* 9(5): 344-356.
- Cipolotti, L., T. Shallice, D. Chan, N. Fox, R. Scahill, G. Harrison, J. Stevens and P. Rudge (2001). "Long-term retrograde amnesia...the crucial role of the hippocampus." *Neuropsychologia* 39(2): 151-172.
- Citri, A. and R. C. Malenka (2008). "Synaptic plasticity: multiple forms, functions, and mechanisms." *Neuropsychopharmacology* 33(1): 18-41.
- Clandinin, T. R. and P. E. Mains (1993). "Genetic studies of mei-1 gene activity during the transition from meiosis to mitosis in *Caenorhabditis elegans*." *Genetics* 134(1): 199-210.
- Clark-Maguire, S. and P. E. Mains (1994). "Localization of the mei-1 gene product of *Caenorhabditis elegans*, a meiotic-specific spindle component." *J Cell Biol* 126(1): 199-209.
- Claudiani, P., E. Riano, A. Errico, G. Andolfi and E. I. Rugarli (2005). "Spastin subcellular localization is regulated through usage of different translation start sites and active export from the nucleus." *Exp Cell Res* 309(2): 358-369.
- Connell, J. W., R. Allison and E. Reid (2016). "Quantitative Gait Analysis Using a Motorized Treadmill System Sensitive Detects Motor Abnormalities in Mice Expressing ATPase Defective Spastin." *PLoS One* 11(3): e0152413.
- Connell, J. W., C. Lindon, J. P. Luzio and E. Reid (2009). "Spastin couples microtubule severing to membrane traffic in completion of cytokinesis and secretion." *Traffic* 10(1): 42-56.
- Cooper, J. A. (2013). "Cell biology in neuroscience: mechanisms of cell migration in the nervous system." *J Cell Biol* 202(5): 725-734.
- Cox, G. A., C. L. Mahaffey, A. Nystuen, V. A. Letts and W. N. Frankel (2000). "The mouse fidgetin gene defines a new role for AAA family proteins in mammalian development." *Nat Genet* 26(2): 198-202.
- Crawley, J. N. (1985). "Exploratory behavior models of anxiety in mice." *Neurosci Biobehav Rev* 9(1): 37-44.
- Crouse, G. F., A. Frischauf and H. Lehrach (1983). "An integrated and simplified approach to cloning into plasmids and single-stranded phages." *Methods Enzymol* 101: 78-89.
- Daftary, G. S. and H. S. Taylor (2004). "EMX2 gene expression in the female reproductive tract and aberrant expression in the endometrium of patients with endometriosis." *J Clin Endocrinol Metab* 89(5): 2390-2396.
- Daftary, G. S. and H. S. Taylor (2006). "Endocrine regulation of HOX genes." *Endocr Rev* 27(4): 331-355.

REFERENCES

- Daftary, G. S., A. M. Tetrault, E. M. Jorgensen, J. Sarno and H. S. Taylor (2011). "A novel role for the AAA ATPase spastin as a HOXA10 transcriptional corepressor in Ishikawa endometrial cells." Mol Endocrinol 25(9): 1539-1549.
- Davis, L. J., D. J. Odde, S. M. Block and S. P. Gross (2002). "The importance of lattice defects in katanin-mediated microtubule severing in vitro." Biophys J 82(6): 2916-2927.
- Deadwyler, S. A., T. Dunwiddie and G. Lynch (1987). "A critical level of protein synthesis is required for long-term potentiation." Synapse 1(1): 90-95.
- Denenberg, V. H. (1969). "Open-field behavior in the rat: what does it mean?" Ann N Y Acad Sci 159(3): 852-859.
- Dent, E. W. and P. W. Baas (2014). "Microtubules in neurons as information carriers." J Neurochem 129(2): 235-239.
- Dent, E. W., J. L. Callaway, G. Szebenyi, P. W. Baas and K. Kalil (1999). "Reorganization and movement of microtubules in axonal growth cones and developing interstitial branches." J Neurosci 19(20): 8894-8908.
- Dent, E. W. and F. B. Gertler (2003). "Cytoskeletal dynamics and transport in growth cone motility and axon guidance." Neuron 40(2): 209-227.
- Depienne, C., G. Stevanin, A. Brice and A. Durr (2007). "Hereditary spastic paraplegias: an update." Curr Opin Neurol 20(6): 674-680.
- Derkach, V. A., M. C. Oh, E. S. Guire and T. R. Soderling (2007). "Regulatory mechanisms of AMPA receptors in synaptic plasticity." Nat Rev Neurosci 8(2): 101-113.
- Desai, A. and T. J. Mitchison (1997). "Microtubule polymerization dynamics." Annu Rev Cell Dev Biol 13: 83-117.
- Desai, A., S. Verma, T. J. Mitchison and C. E. Walczak (1999). "Kin I kinesins are microtubule-destabilizing enzymes." Cell 96(1): 69-78.
- Desai, B. S., S. Shirolkar and K. Ray (2009). "F-actin-based extensions of the head cyst cell adhere to the maturing spermatids to maintain them in a tight bundle and prevent their premature release in *Drosophila* testis." BMC Biol 7: 19.
- Diaz-Valencia, J. D., M. M. Morelli, M. Bailey, D. Zhang, D. J. Sharp and J. L. Ross (2011). "*Drosophila* katanin-60 depolymerizes and severs at microtubule defects." Biophys J 100(10): 2440-2449.
- Dobyns, W. B. (1987). "Developmental aspects of lissencephaly and the lissencephaly syndromes." Birth Defects Orig Artic Ser 23(1): 225-241.
- Dobyns, W. B., O. Reiner, R. Carrozzo and D. H. Ledbetter (1993). "Lissencephaly. A human brain malformation associated with deletion of the LIS1 gene located at chromosome 17p13." JAMA 270(23): 2838-2842.
- Don, R. H., P. T. Cox, B. J. Wainwright, K. Baker and J. S. Mattick (1991). "'Touchdown' PCR to circumvent spurious priming during gene amplification." Nucleic Acids Res 19(14): 4008.
- Douglas, M. E. and M. Mishima (2010). "Still entangled: assembly of the central spindle by multiple microtubule modulators." Semin Cell Dev Biol 21(9): 899-908.
- Draberova, E., S. Vinopal, G. Morfini, P. S. Liu, V. Sladkova, T. Sulimenko, M. R. Burns, J. Solowska, K. Kulandaivel, J. P. de Chadarevian, A. Legido, S. J. Mork, J. Janacek, P. W. Baas,

REFERENCES

- P. Draber and C. D. Katsetos (2011). "Microtubule-severing ATPase spastin in glioblastoma: increased expression in human glioblastoma cell lines and inverse roles in cell motility and proliferation." *J Neuropathol Exp Neurol* 70(9): 811-826.
- Du, F., E. F. Ozdowski, I. K. Kotowski, D. A. Marchuk and N. T. Sherwood (2010). "Functional conservation of human Spastin in a *Drosophila* model of autosomal dominant-hereditary spastic paraplegia." *Hum Mol Genet* 19(10): 1883-1896.
- Durr, A., A. Brice, M. Serdaru, G. Rancurel, C. Derouesne, O. Lyon-Caen, Y. Agid and B. Fontaine (1994). "The phenotype of "pure" autosomal dominant spastic paraplegia." *Neurology* 44(7): 1274-1277.
- Dymecki, S. M. (1996). "Flp recombinase promotes site-specific DNA recombination in embryonic stem cells and transgenic mice." *Proc Natl Acad Sci U S A* 93(12): 6191-6196.
- Dymek, E. E., P. A. Lefebvre and E. F. Smith (2004). "PF15p is the chlamydomonas homologue of the Katanin p80 subunit and is required for assembly of flagellar central microtubules." *Eukaryot Cell* 3(4): 870-879.
- Edde, B., J. Rossier, J. P. Le Caer, E. Desbruyeres, F. Gros and P. Denoulet (1990). "Posttranslational glutamylation of alpha-tubulin." *Science* 247(4938): 83-85.
- Eipper, B. A. (1974). "Properties of rat brain tubulin." *J Biol Chem* 249(5): 1407-1416.
- Elgh, E., A. Lindqvist Astot, M. Fagerlund, S. Eriksson, T. Olsson and B. Nasman (2006). "Cognitive dysfunction, hippocampal atrophy and glucocorticoid feedback in Alzheimer's disease." *Biol Psychiatry* 59(2): 155-161.
- Epinat, J. C., S. Arnould, P. Chames, P. Rochaix, D. Desfontaines, C. Puzin, A. Patin, A. Zanghellini, F. Paques and E. Lacroix (2003). "A novel engineered meganuclease induces homologous recombination in yeast and mammalian cells." *Nucleic Acids Res* 31(11): 2952-2962.
- Erck, C., L. Peris, A. Andrieux, C. Meissirel, A. D. Gruber, M. Vernet, A. Schweitzer, Y. Saoudi, H. Pointu, C. Bosc, P. A. Salin, D. Job and J. Wehland (2005). "A vital role of tubulin-tyrosine-ligase for neuronal organization." *Proc Natl Acad Sci U S A* 102(22): 7853-7858.
- Errico, A., A. Ballabio and E. I. Rugarli (2002). "Spastin, the protein mutated in autosomal dominant hereditary spastic paraplegia, is involved in microtubule dynamics." *Hum Mol Genet* 11(2): 153-163.
- Errico, A., P. Claudiani, M. D'Addio and E. I. Rugarli (2004). "Spastin interacts with the centrosomal protein NA14, and is enriched in the spindle pole, the midbody and the distal axon." *Hum Mol Genet* 13(18): 2121-2132.
- Ersfeld, K., J. Wehland, U. Plessmann, H. Dodemont, V. Gerke and K. Weber (1993). "Characterization of the tubulin-tyrosine ligase." *J Cell Biol* 120(3): 725-732.
- Evans, K., C. Keller, K. Pavur, K. Glasgow, B. Conn and B. Lauring (2006). "Interaction of two hereditary spastic paraplegia gene products, spastin and atlastin, suggests a common pathway for axonal maintenance." *Proc Natl Acad Sci U S A* 103(28): 10666-10671.
- Evans, K. J., E. R. Gomes, S. M. Reisenweber, G. G. Gundersen and B. P. Lauring (2005). "Linking axonal degeneration to microtubule remodeling by Spastin-mediated microtubule severing." *J Cell Biol* 168(4): 599-606.
- Evans, M. J. and M. H. Kaufman (1981). "Establishment in culture of pluripotential cells from mouse embryos." *Nature* 292(5819): 154-156.

REFERENCES

- Fan, Y., G. Wali, R. Sutharsan, B. Bellette, D. I. Crane, C. M. Sue and A. Mackay-Sim (2014). "Low dose tubulin-binding drugs rescue peroxisome trafficking deficit in patient-derived stem cells in Hereditary Spastic Paraplegia." Biol Open 3(6): 494-502.
- Fassier, C., A. Tarrade, L. Peris, S. Courageot, P. Maily, C. Dalard, S. Delga, N. Roblot, J. Lefevre, D. Job, J. Hazan, P. A. Curmi and J. Melki (2013). "Microtubule-targeting drugs rescue axonal swellings in cortical neurons from spastin knockout mice." Dis Model Mech 6(1): 72-83.
- Feil, R., J. Wagner, D. Metzger and P. Chambon (1997). "Regulation of Cre recombinase activity by mutated estrogen receptor ligand-binding domains." Biochem Biophys Res Commun 237(3): 752-757.
- Feldman, D. E. (2009). "Synaptic mechanisms for plasticity in neocortex." Annu Rev Neurosci 32: 33-55.
- Ferrari-Toninelli, G., S. A. Bonini, P. Bettinsoli, D. Uberti and M. Memo (2008). "Microtubule stabilizing effect of notch activation in primary cortical neurons." Neuroscience 154(3): 946-952.
- Fiala, J. C., S. A. Kirov, M. D. Feinberg, L. J. Petrak, P. George, C. A. Goddard and K. M. Harris (2003). "Timing of neuronal and glial ultrastructure disruption during brain slice preparation and recovery in vitro." J Comp Neurol 465(1): 90-103.
- Fink, J. K. (2006). "Hereditary spastic paraplegia." Curr Neurol Neurosci Rep 6(1): 65-76.
- Fisher, E. and P. Scambler (1994). "Human haploinsufficiency--one for sorrow, two for joy." Nat Genet 7(1): 5-7.
- Frickey, T. and A. N. Lupas (2004). "Phylogenetic analysis of AAA proteins." J Struct Biol 146(1-2): 2-10.
- Gard, D. L. and M. W. Kirschner (1985). "A polymer-dependent increase in phosphorylation of beta-tubulin accompanies differentiation of a mouse neuroblastoma cell line." J Cell Biol 100(3): 764-774.
- Gibbs, W. W. (2005). "Nanobodies." Sci Am 293(2): 78-83.
- Glater, E. E., L. J. Megeath, R. S. Stowers and T. L. Schwarz (2006). "Axonal transport of mitochondria requires miltom to recruit kinesin heavy chain and is light chain independent." J Cell Biol 173(4): 545-557.
- Glotzer, M. (2001). "Animal cell cytokinesis." Annu Rev Cell Dev Biol 17: 351-386.
- Glotzer, M. (2009). "The 3Ms of central spindle assembly: microtubules, motors and MAPs." Nat Rev Mol Cell Biol 10(1): 9-20.
- Gouveia, S. M. and A. Akhmanova (2010). "Cell and molecular biology of microtubule plus end tracking proteins: end binding proteins and their partners." Int Rev Cell Mol Biol 285: 1-74.
- Green, M. C. and B. A. Witham (1991). "Handbook on Genetically Standardized JAX Mice." The Jackson Laboratory, Bar Harbor fourth edition.
- Grenningloh, G., S. Soehrman, P. Bondallaz, E. Ruchti and H. Cadas (2004). "Role of the microtubule destabilizing proteins SCG10 and stathmin in neuronal growth." J Neurobiol 58(1): 60-69.
- Gu, H., J. D. Marth, P. C. Orban, H. Mossmann and K. Rajewsky (1994). "Deletion of a DNA polymerase beta gene segment in T cells using cell type-specific gene targeting." Science 265(5168): 103-106.

REFERENCES

- Guthrie, G., G. Pfeffer, M. Bailie, K. Bradshaw, A. C. Browning, R. Horvath, P. F. Chinnery and P. Yu-Wai-Man (2013). "The neurological and ophthalmological manifestations of SPG4-related hereditary spastic paraplegia." *J Neurol* 260(3): 906-909.
- Hanson, P. I. and S. W. Whiteheart (2005). "AAA+ proteins: have engine, will work." *Nat Rev Mol Cell Biol* 6(7): 519-529.
- Harding, A. E. (1981). "Hereditary "pure" spastic paraplegia: a clinical and genetic study of 22 families." *J Neurol Neurosurg Psychiatry* 44(10): 871-883.
- Harno, E., E. C. Cottrell and A. White (2013). "Metabolic pitfalls of CNS Cre-based technology." *Cell Metab* 18(1): 21-28.
- Hartman, J. J., J. Mahr, K. McNally, K. Okawa, A. Iwamatsu, S. Thomas, S. Cheesman, J. Heuser, R. D. Vale and F. J. McNally (1998). "Katanin, a microtubule-severing protein, is a novel AAA ATPase that targets to the centrosome using a WD40-containing subunit." *Cell* 93(2): 277-287.
- Hartman, J. J. and R. D. Vale (1999). "Microtubule Disassembly by ATP-Dependent Oligomerization of the AAA Enzyme Katanin." *Science* 286(5440): 782-785.
- Hayashi, S. and A. P. McMahon (2002). "Efficient recombination in diverse tissues by a tamoxifen-inducible form of Cre: a tool for temporally regulated gene activation/inactivation in the mouse." *Dev Biol* 244(2): 305-318.
- Hazan, J., N. Fonknechten, D. Mavel, C. Paternotte, D. Samson, F. Artiguenave, C. S. Davoine, C. Cruaud, A. Durr, P. Wincker, P. Brottier, L. Cattolico, V. Barbe, J. M. Burgunder, J. F. Prud'homme, A. Brice, B. Fontaine, B. Heilig and J. Weissenbach (1999). "Spastin, a new AAA protein, is altered in the most frequent form of autosomal dominant spastic paraplegia." *Nat Genet* 23(3): 296-303.
- Hecker, K. H. and K. H. Roux (1996). "High and low annealing temperatures increase both specificity and yield in touchdown and stepdown PCR." *Biotechniques* 20(3): 478-485.
- Heinzlef, O., C. Paternotte, F. Mahieux, J. F. Prud'homme, J. Dien, M. Madigand, J. Pouget, J. Weissenbach, E. Roulet and J. Hazan (1998). "Mapping of a complicated familial spastic paraplegia to locus SPG4 on chromosome 2p." *J Med Genet* 35(2): 89-93.
- Hensch, T. K. (2004). "Critical period regulation." *Annu Rev Neurosci* 27: 549-579.
- Henson, B. J., W. Zhu, K. Hardaway, J. L. Wetzel, M. Stefan, K. M. Albers and R. D. Nicholls (2012). "Transcriptional and post-transcriptional regulation of SPAST, the gene most frequently mutated in hereditary spastic paraplegia." *PLoS One* 7(5): e36505.
- Herculano-Houzel, S. (2012). "The remarkable, yet not extraordinary, human brain as a scaled-up primate brain and its associated cost." *Proc Natl Acad Sci U S A* 109 Suppl 1: 10661-10668.
- Hernandez-Deviez, D., A. Mackay-Sim and J. M. Wilson (2007). "A Role for ARF6 and ARNO in the regulation of endosomal dynamics in neurons." *Traffic* 8(12): 1750-1764.
- Hirokawa, N. (1998). "Kinesin and dynein superfamily proteins and the mechanism of organelle transport." *Science* 279(5350): 519-526.
- Hirokawa, N., S. Niwa and Y. Tanaka (2010). "Molecular motors in neurons: transport mechanisms and roles in brain function, development, and disease." *Neuron* 68(4): 610-638.
- Hirokawa, N. and R. Takemura (2005). "Molecular motors and mechanisms of directional transport in neurons." *Nat Rev Neurosci* 6(3): 201-214.

REFERENCES

- Holtmaat, A. and K. Svoboda (2009). "Experience-dependent structural synaptic plasticity in the mammalian brain." *Nat Rev Neurosci* 10(9): 647-658.
- Hoogenraad, C. C. and A. Akhmanova (2010). "Dendritic spine plasticity: new regulatory roles of dynamic microtubules." *Neuroscientist* 16(6): 650-661.
- Hunn, B. H., S. J. Cragg, J. P. Bolam, M. G. Spillantini and R. Wade-Martins (2015). "Impaired intracellular trafficking defines early Parkinson's disease." *Trends Neurosci* 38(3): 178-188.
- Hyman, B. T., G. W. Van Hoesen, A. R. Damasio and C. L. Barnes (1984). "Alzheimer's disease: cell-specific pathology isolates the hippocampal formation." *Science* 225(4667): 1168-1170.
- Hyman, S. E. and R. C. Malenka (2001). "Addiction and the brain: the neurobiology of compulsion and its persistence." *Nat Rev Neurosci* 2(10): 695-703.
- Ikegami, K., R. L. Heier, M. Taruishi, H. Takagi, M. Mukai, S. Shimma, S. Taira, K. Hatanaka, N. Morone, I. Yao, P. K. Campbell, S. Yuasa, C. Janke, G. R. Macgregor and M. Setou (2007). "Loss of alpha-tubulin polyglutamylation in ROSA22 mice is associated with abnormal targeting of KIF1A and modulated synaptic function." *Proc Natl Acad Sci U S A* 104(9): 3213-3218.
- Inoue, H., H. Nojima and H. Okayama (1990). "High efficiency transformation of *Escherichia coli* with plasmids." *Gene* 96(1): 23-28.
- Inoue, S. and E. D. Salmon (1995). "Force generation by microtubule assembly/disassembly in mitosis and related movements." *Mol Biol Cell* 6(12): 1619-1640.
- Iredale, J. P. (1999). "Demystified ... gene knockouts." *Mol Pathol* 52(3): 111-116.
- Ishikawa, H., R. Bischoff and H. Holtzer (1968). "Mitosis and intermediate-sized filaments in developing skeletal muscle." *J Cell Biol* 38(3): 538-555.
- Iwasato, T., A. Datwani, A. M. Wolf, H. Nishiyama, Y. Taguchi, S. Tonegawa, T. Knopfel, R. S. Erzurumlu and S. Itohara (2000). "Cortex-restricted disruption of NMDAR1 impairs neuronal patterns in the barrel cortex." *Nature* 406(6797): 726-731.
- Iwaya, N., K. Akiyama, N. Goda, T. Tenno, Y. Fujiwara, D. Hamada, T. Ikura, M. Shirakawa and H. Hiroaki (2012). "Effect of Ca²⁺ on the microtubule-severing enzyme p60-katanin. Insight into the substrate-dependent activation mechanism." *FEBS J* 279(7): 1339-1352.
- Iyer, L. M., D. D. Leipe, E. V. Koonin and L. Aravind (2004). "Evolutionary history and higher order classification of AAA+ ATPases." *J Struct Biol* 146(1-2): 11-31.
- Janke, C. and J. C. Bulinski (2011). "Post-translational regulation of the microtubule cytoskeleton: mechanisms and functions." *Nat Rev Mol Cell Biol* 12(12): 773-786.
- Janke, C. and M. Kneussel (2010). "Tubulin post-translational modifications: encoding functions on the neuronal microtubule cytoskeleton." *Trends Neurosci* 33(8): 362-372.
- Janson, M. E. and M. Dogterom (2004). "A bending mode analysis for growing microtubules: evidence for a velocity-dependent rigidity." *Biophys J* 87(4): 2723-2736.
- Jaworski, J., L. C. Kapitein, S. M. Gouveia, B. R. Dortland, P. S. Wulf, I. Grigoriev, P. Camera, S. A. Spangler, P. Di Stefano, J. Demmers, H. Krugers, P. Defilippi, A. Akhmanova and C. C. Hoogenraad (2009). "Dynamic microtubules regulate dendritic spine morphology and synaptic plasticity." *Neuron* 61(1): 85-100.

- Jinushi-Nakao, S., R. Arvind, R. Amikura, E. Kinameri, A. W. Liu and A. W. Moore (2007). "Knot/Collier and cut control different aspects of dendrite cytoskeleton and synergize to define final arbor shape." *Neuron* 56(6): 963-978.
- Johjima, A., K. Noi, S. Nishikori, H. Ogi, M. Esaki and T. Ogura (2015). "Microtubule severing by katanin p60 AAA+ ATPase requires the C-terminal acidic tails of both alpha- and beta-tubulins and basic amino acid residues in the AAA+ ring pore." *J Biol Chem* 290(18): 11762-11770.
- Jourdain, L., P. Curmi, A. Sobel, D. Pantaloni and M. F. Carlier (1997). "Stathmin: a tubulin-sequestering protein which forms a ternary T2S complex with two tubulin molecules." *Biochemistry* 36(36): 10817-10821.
- Kammermeier, L., J. Spring, M. Stierwald, J. M. Burgunder and H. Reichert (2003). "Identification of the *Drosophila melanogaster* homolog of the human spastin gene." *Dev Genes Evol* 213(8): 412-415.
- Kanai, Y., N. Dohmae and N. Hirokawa (2004). "Kinesin transports RNA: isolation and characterization of an RNA-transporting granule." *Neuron* 43(4): 513-525.
- Kandel, E. R., J. H. Schwartz and T. M. Jessell (2000). *Principles of Neural Science*.
- Kapitein, L. C. and C. C. Hoogenraad (2011). "Which way to go? Cytoskeletal organization and polarized transport in neurons." *Mol Cell Neurosci* 46(1): 9-20.
- Kapitein, L. C., K. W. Yau, S. M. Gouveia, W. A. van der Zwan, P. S. Wulf, N. Keijzer, J. Demmers, J. Jaworski, A. Akhmanova and C. C. Hoogenraad (2011). "NMDA receptor activation suppresses microtubule growth and spine entry." *J Neurosci* 31(22): 8194-8209.
- Karabay, A., W. Yu, J. M. Solowska, D. H. Baird and P. W. Baas (2004). "Axonal growth is sensitive to the levels of katanin, a protein that severs microtubules." *J Neurosci* 24(25): 5778-5788.
- Karachot, L., Y. Shirai, R. Vigot, T. Yamamori and M. Ito (2001). "Induction of long-term depression in cerebellar Purkinje cells requires a rapidly turned over protein." *J Neurophysiol* 86(1): 280-289.
- Karsenti, E. and I. Vernos (2001). "The mitotic spindle: a self-made machine." *Science* 294(5542): 543-547.
- Kasher, P. R., K. J. De Vos, S. B. Wharton, C. Manser, E. J. Bennett, M. Bingley, J. D. Wood, R. Milner, C. J. McDermott, C. C. Miller, P. J. Shaw and A. J. Grierson (2009). "Direct evidence for axonal transport defects in a novel mouse model of mutant spastin-induced hereditary spastic paraplegia (HSP) and human HSP patients." *J Neurochem* 110(1): 34-44.
- Kawamoto, S., H. Niwa, F. Tashiro, S. Sano, G. Kondoh, J. Takeda, K. Tabayashi and J. Miyazaki (2000). "A novel reporter mouse strain that expresses enhanced green fluorescent protein upon Cre-mediated recombination." *FEBS Lett* 470(3): 263-268.
- Kerchner, G. A., C. P. Hess, K. E. Hammond-Rosenbluth, D. Xu, G. D. Rabinovici, D. A. Kelley, D. B. Vigneron, S. J. Nelson and B. L. Miller (2010). "Hippocampal CA1 apical neuropil atrophy in mild Alzheimer disease visualized with 7-T MRI." *Neurology* 75(15): 1381-1387.
- Keshishian, H., K. Brodie, A. Chiba and M. Bate (1996). "The *Drosophila* neuromuscular junction: a model system for studying synaptic development and function." *Annu Rev Neurosci* 19: 545-575.

- Khawaja, S., G. G. Gundersen and J. C. Bulinski (1988). "Enhanced stability of microtubules enriched in detyrosinated tubulin is not a direct function of detyrosination level." J Cell Biol 106(1): 141-149.
- Khundadze, M., K. Kollmann, N. Koch, C. Biskup, S. Nietzsche, G. Zimmer, J. C. Hennings, A. K. Huebner, J. Symmank, A. Jahic, E. I. Ilina, K. Karle, L. Schols, M. Kessels, T. Bräulke, B. Qualmann, I. Kurth, C. Beetz and C. A. Hubner (2013). "A hereditary spastic paraplegia mouse model supports a role of ZFYVE26/SPASTIZIN for the endolysosomal system." PLoS Genet 9(12): e1003988.
- Kimura, Y., N. Kurabe, K. Ikegami, K. Tsutsumi, Y. Konishi, O. I. Kaplan, H. Kunitomo, Y. Iino, O. E. Blacque and M. Setou (2010). "Identification of tubulin deglutamylase among *Caenorhabditis elegans* and mammalian cytosolic carboxypeptidases (CCPs)." J Biol Chem 285(30): 22936-22941.
- Klimpe, S., A. Zibat, U. Zechner, B. Wellek, M. Shoukier, S. M. Sauter, D. V. Pantakani and A. U. Mannan (2011). "Evaluating the effect of spastin splice mutations by quantitative allele-specific expression assay." Eur J Neuro 18(1): 99-105.
- Koh, Y. H., L. S. Gramates and V. Budnik (2000). "Drosophila larval neuromuscular junction: molecular components and mechanisms underlying synaptic plasticity." Microsc Res Tech 49(1): 14-25.
- Komarova, Y., C. O. De Groot, I. Grigoriev, S. M. Gouveia, E. L. Munteanu, J. M. Schober, S. Honnappa, R. M. Buey, C. C. Hoogenraad, M. Dogterom, G. G. Borisy, M. O. Steinmetz and A. Akhmanova (2009). "Mammalian end binding proteins control persistent microtubule growth." J Cell Biol 184(5): 691-706.
- Kondrashov, F. A. and E. V. Koonin (2004). "A common framework for understanding the origin of genetic dominance and evolutionary fates of gene duplications." Trends Genet 20(7): 287-290.
- Konkel, A. and N. J. Cohen (2009). "Relational memory and the hippocampus: representations and methods." Front Neurosci 3(2): 166-174.
- Korulu, S. and A. Karabay (2011). "IGF-1 participates differently in regulation of severing activity of katanin and spastin." Cell Mol Neurobiol 31(4): 497-501.
- Kranz, A., J. Fu, K. Duerschke, S. Weidlich, R. Naumann, A. F. Stewart and K. Anastassiadis (2010). "An improved Flp deleter mouse in C57Bl/6 based on Flpo recombinase." Genesis 48(8): 512-520.
- Krug, M., B. Lossner and T. Ott (1984). "Anisomycin blocks the late phase of long-term potentiation in the dentate gyrus of freely moving rats." Brain Res Bull 13(1): 39-42.
- Kurup, N., D. Yan, A. Goncharov and Y. Jin (2015). "Dynamic microtubules drive circuit rewiring in the absence of neurite remodeling." Curr Biol 25(12): 1594-1605.
- Lacroix, B., J. van Dijk, N. D. Gold, J. Guizzetti, G. Aldrian-Herrada, K. Rogowski, D. W. Gerlich and C. Janke (2010). "Tubulin polyglutamylation stimulates spastin-mediated microtubule severing." J Cell Biol 189(6): 945-954.
- Lakemper, S. and E. Meyhofer (2005). "The E-hook of tubulin interacts with kinesin's head to increase processivity and speed." Biophys J 89(5): 3223-3234.
- Lee, H. H., L. Y. Jan and Y. N. Jan (2009). "Drosophila IKK-related kinase Ik2 and Katanin p60-like 1 regulate dendrite pruning of sensory neuron during metamorphosis." Proc Natl Acad Sci U S A 106(15): 6363-6368.

REFERENCES

- Lee, H. K., M. Barbarosie, K. Kameyama, M. F. Bear and R. L. Huganir (2000). "Regulation of distinct AMPA receptor phosphorylation sites during bidirectional synaptic plasticity." Nature 405(6789): 955-959.
- Lee, K. S., F. Schottler, M. Oliver and G. Lynch (1980). "Brief bursts of high-frequency stimulation produce two types of structural change in rat hippocampus." J Neurophysiol 44(2): 247-258.
- Li, W., L. R. DeBella, T. Guven-Ozkan, R. Lin and L. S. Rose (2009). "An eIF4E-binding protein regulates katanin protein levels in *C. elegans* embryos." J Cell Biol 187(1): 33-42.
- Li, X. J., A. L. Orr and S. Li (2010). "Impaired mitochondrial trafficking in Huntington's disease." Biochim Biophys Acta 1802(1): 62-65.
- Liang, H., S. Hippenmeyer and H. T. Ghashghaei (2012). "A Nestin-cre transgenic mouse is insufficient for recombination in early embryonic neural progenitors." Biol Open 1(12): 1200-1203.
- Lin, F. L. and N. Sternberg (1984). "Homologous recombination between overlapping thymidine kinase gene fragments stably inserted into a mouse cell genome." Mol Cell Biol 4(5): 852-861.
- Lledo, P. M. and G. Gheusi (2006). "[Adult neurogenesis: from basic research to clinical applications]." Bull Acad Natl Med 190(2): 385-400; discussion 400-382.
- Lohret, T. A., L. Zhao and L. M. Quarmby (1999). "Cloning of *Chlamydomonas* p60 katanin and localization to the site of outer doublet severing during deflagellation." Cell Motil Cytoskeleton 43(3): 221-231.
- Lu, C. and P. E. Mains (2007). "The *C. elegans* anaphase promoting complex and MBK-2/DYRK kinase act redundantly with CUL-3/MEL-26 ubiquitin ligase to degrade MEI-1 microtubule-severing activity after meiosis." Dev Biol 302(2): 438-447.
- Ludueno, R. F. (1998). "Multiple forms of tubulin: different gene products and covalent modifications." Int Rev Cytol 178: 207-275.
- Lynch, G., J. Larson, S. Kelso, G. Barrionuevo and F. Schottler (1983). "Intracellular injections of EGTA block induction of hippocampal long-term potentiation." Nature 305(5936): 719-721.
- Ma, D. L., S. C. Chia, Y. C. Tang, M. L. Chang, A. Probst, J. M. Burgunder and F. R. Tang (2006). "Spastin in the human and mouse central nervous system with special reference to its expression in the hippocampus of mouse pilocarpine model of status epilepticus and temporal lobe epilepsy." Neurochem Int 49(7): 651-664.
- Maas, C., D. Belgardt, H. K. Lee, F. F. Heisler, C. Lappe-Siefke, M. M. Magiera, J. van Dijk, T. J. Hausrat, C. Janke and M. Kneussel (2009). "Synaptic activation modifies microtubules underlying transport of postsynaptic cargo." Proc Natl Acad Sci U S A 106(21): 8731-8736.
- Mains, P. E., K. J. Kemphues, S. A. Sprunger, I. A. Sulston and W. B. Wood (1990). "Mutations affecting the meiotic and mitotic divisions of the early *Caenorhabditis elegans* embryo." Genetics 126(3): 593-605.
- Malenka, R. C. (1991). "The role of postsynaptic calcium in the induction of long-term potentiation." Mol Neurobiol 5(2-4): 289-295.
- Malenka, R. C. and M. F. Bear (2004). "LTP and LTD: an embarrassment of riches." Neuron 44(1): 5-21.
- Malenka, R. C., B. Lancaster and R. S. Zucker (1992). "Temporal limits on the rise in postsynaptic calcium required for the induction of long-term potentiation." Neuron 9(1): 121-128.

REFERENCES

- Malenka, R. C. and R. A. Nicoll (1993). "NMDA-receptor-dependent synaptic plasticity: multiple forms and mechanisms." Trends Neurosci 16(12): 521-527.
- Mancuso, G. and E. I. Rugarli (2008). "A cryptic promoter in the first exon of the SPG4 gene directs the synthesis of the 60-kDa spastin isoform." BMC Biol 6: 31.
- Marin, O. and J. L. Rubenstein (2003). "Cell migration in the forebrain." Annu Rev Neurosci 26: 441-483.
- Marrus, S. B., S. L. Portman, M. J. Allen, K. G. Moffat and A. DiAntonio (2004). "Differential localization of glutamate receptor subunits at the *Drosophila* neuromuscular junction." J Neurosci 24(6): 1406-1415.
- Mattapallil, M. J., E. F. Wawrousek, C. C. Chan, H. Zhao, J. Roychoudhury, T. A. Ferguson and R. R. Caspi (2012). "The Rd8 mutation of the *Crb1* gene is present in vendor lines of C57BL/6N mice and embryonic stem cells, and confounds ocular induced mutant phenotypes." Invest Ophthalmol Vis Sci 53(6): 2921-2927.
- Matus, A. (1994). "Stiff microtubules and neuronal morphology." Trends Neurosci 17(1): 19-22.
- Matus, A. (2000). "Actin-based plasticity in dendritic spines." Science 290(5492): 754-758.
- Mayer, M. L., G. L. Westbrook and P. B. Guthrie (1984). "Voltage-dependent block by Mg²⁺ of NMDA responses in spinal cord neurones." Nature 309(5965): 261-263.
- Mayford, M., M. E. Bach, Y. Y. Huang, L. Wang, R. D. Hawkins and E. R. Kandel (1996). "Control of memory formation through regulated expression of a CaMKII transgene." Science 274(5293): 1678-1683.
- Mayford, M., S. A. Siegelbaum and E. R. Kandel (2012). "Synapses and memory storage." Cold Spring Harb Perspect Biol 4(6).
- Mc Monagle, P., P. Byrne, T. Burke, N. Parfrey and M. Hutchinson (2001). "Clinical and pathologic findings in hereditary spastic paraparesis with spastin mutation." Neurology 56(1): 139.
- McDermott, C., K. White, K. Bushby and P. Shaw (2000). "Hereditary spastic paraparesis: a review of new developments." J Neurol Neurosurg Psychiatry 69(2): 150-160.
- McDermott, C. J., C. E. Burness, J. Kirby, L. E. Cox, D. G. Rao, C. Hewamadduma, B. Sharrack, M. Hadjivassiliou, P. F. Chinnery, A. Dalton, P. J. Shaw, Uk and H. S. P. C. Irish (2006). "Clinical features of hereditary spastic paraplegia due to spastin mutation." Neurology 67(1): 45-51.
- McIntosh, J. R., E. L. Grishchuk and R. R. West (2002). "Chromosome-microtubule interactions during mitosis." Annu Rev Cell Dev Biol 18: 193-219.
- McMonagle, P., S. Webb and M. Hutchinson (2002). "The prevalence of "pure" autosomal dominant hereditary spastic paraparesis in the island of Ireland." J Neurol Neurosurg Psychiatry 72(1): 43-46.
- McNally, F. J., Okawa, Iwamatsu and R. D. Vale (1996). "Katanin, the microtubule-severing ATPase, is concentrated at centrosomes." Journal of Cell Science.
- McNally, F. J. and S. Thomas (1998). "Katanin Is Responsible for the M-Phase Microtubule-severing Activity in *Xenopus* Eggs." Molecular Biology of The Cell 9.
- McNally, F. J. and R. D. Vale (1993). "Identification of katanin, an ATPase that severs and disassembles stable microtubules." Cell 75.

REFERENCES

- McNally, K., A. Audhya, K. Oegema and F. J. McNally (2006). "Katanin controls mitotic and meiotic spindle length." *J Cell Biol* 175(6): 881-891.
- McNally, K. P., O. A. Bazirgan and F. J. McNally (2000). "Two domains of p80 katanin regulate microtubule severing and spindle pole targeting by p60 katanin." *J Cell Sci* 113 (Pt 9): 1623-1633.
- McNally, K. P., D. Buster and F. J. McNally (2002). "Katanin-mediated microtubule severing can be regulated by multiple mechanisms." *Cell Motil Cytoskeleton* 53(4): 337-349.
- McNally, K. P. and F. J. McNally (2011). "The spindle assembly function of *Caenorhabditis elegans* katanin does not require microtubule-severing activity." *Mol Biol Cell* 22(9): 1550-1560.
- Melton, D. W. (2002). "Gene-targeting strategies." *Methods Mol Biol* 180: 151-173.
- Merriam, E. B., D. C. Lumbard, C. Viesselmann, J. Ballweg, M. Stevenson, L. Pietila, X. Hu and E. W. Dent (2011). "Dynamic microtubules promote synaptic NMDA receptor-dependent spine enlargement." *PLoS One* 6(11): e27688.
- Milner, B. and L. B. Taylor (1970). "Somesthetic thresholds after commissural section in man." *Neurology* 20(4): 378.
- Minichiello, L., M. Korte, D. Wolfner, R. Kuhn, K. Unsicker, V. Cestari, C. Rossi-Arnaud, H. P. Lipp, T. Bonhoeffer and R. Klein (1999). "Essential role for TrkB receptors in hippocampus-mediated learning." *Neuron* 24(2): 401-414.
- Mishra-Gorur, K., A. O. Caglayan, A. E. Schaffer, C. Chabu, O. Henegariu, F. Vonhoff, G. T. Akgumus, S. Nishimura, W. Han, S. Tu, B. Baran, H. Gumus, C. Dilber, M. S. Zaki, H. A. Hossni, J. B. Riviere, H. Kayserili, E. G. Spencer, R. O. Rosti, J. Schroth, H. Per, C. Caglar, C. Caglar, D. Dolen, J. F. Baranoski, S. Kumandas, F. J. Minja, E. Z. Erson-Omay, S. M. Mane, R. P. Lifton, T. Xu, H. Keshishian, W. B. Dobyns, N. C. Chi, N. Sestan, A. Louvi, K. Bilguvar, K. Yasuno, J. G. Gleeson and M. Gunel (2014). "Mutations in KATNB1 cause complex cerebral malformations by disrupting asymmetrically dividing neural progenitors." *Neuron* 84(6): 1226-1239.
- Mitchison, T. and M. Kirschner (1984). "Dynamic instability of microtubule growth." *Nature* 312(5991): 237-242.
- Miyamoto, N., M. Yoshida, S. Kuratani, I. Matsuo and S. Aizawa (1997). "Defects of urogenital development in mice lacking *Emx2*." *Development* 124(9): 1653-1664.
- Moritz, M., M. B. Braunfeld, V. Guenebaut, J. Heuser and D. A. Agard (2000). "Structure of the gamma-tubulin ring complex: a template for microtubule nucleation." *Nat Cell Biol* 2(6): 365-370.
- Mukherjee, S., J. D. Diaz Valencia, S. Stewman, J. Metz, S. Monnier, U. Rath, A. B. Asenjo, R. A. Charafeddine, H. J. Sosa, J. L. Ross, A. Ma and D. J. Sharp (2012). "Human Fidgetin is a microtubule severing the enzyme and minus-end depolymerase that regulates mitosis." *Cell Cycle* 11(12): 2359-2366.
- Mullins, J. M. and J. R. McIntosh (1982). "Isolation and initial characterization of the mammalian midbody." *J Cell Biol* 94(3): 654-661.
- Murphy, S., G. Gorman, C. Beetz, P. Byrne, M. Dytko, P. McMonagle, K. Kinsella, M. Farrell and M. Hutchinson (2009). "Dementia in SPG4 hereditary spastic paraplegia: clinical, genetic, and neuropathologic evidence." *Neurology* 73(5): 378-384.
- Neely, M. D. and K. Boekelheide (1988). "Sertoli cell processes have axoplasmic features: an ordered microtubule distribution and an abundant high molecular weight microtubule-associated protein (cytoplasmic dynein)." *J Cell Biol* 107(5): 1767-1776.

REFERENCES

- Neves, G., S. F. Cooke and T. V. Bliss (2008). "Synaptic plasticity, memory and the hippocampus: a neural network approach to causality." *Nat Rev Neurosci* 9(1): 65-75.
- Nissl (1984). "Ueber eine neue Untersuchungsmethode des Centralorgans zur Feststellung der Localisation der Nervenzellen." *Neurologisches Centralblatt* 13: 507-508.
- Nogales, E. (2001). "Structural insight into microtubule function." *Annu Rev Biophys Biomol Struct* 30: 397-420.
- Nogales, E., S. G. Wolf and K. H. Downing (1998). "Structure of the alpha beta tubulin dimer by electron crystallography." *Nature* 391(6663): 199-203.
- Nowak, L., P. Bregestovski, P. Ascher, A. Herbet and A. Prochiantz (1984). "Magnesium gates glutamate-activated channels in mouse central neurones." *Nature* 307(5950): 462-465.
- O'Donnell, L., D. Rhodes, S. J. Smith, D. J. Merriner, B. J. Clark, C. Borg, B. Whittle, A. E. O'Connor, L. B. Smith, F. J. McNally, D. M. de Kretser, C. C. Goodnow, C. J. Ormandy, D. Jamsai and M. K. O'Bryan (2012). "An essential role for katanin p80 and microtubule severing in male gamete production." *PLoS Genet* 8(5): e1002698.
- Odde, D. J., L. Ma, A. H. Briggs, A. DeMarco and M. W. Kirschner (1999). "Microtubule bending and breaking in living fibroblast cells." *J Cell Sci* 112 (Pt 19): 3283-3288.
- Okada, Y., H. Yamazaki, Y. Sekine-Aizawa and N. Hirokawa (1995). "The neuron-specific kinesin superfamily protein KIF1A is a unique monomeric motor for anterograde axonal transport of synaptic vesicle precursors." *Cell* 81(5): 769-780.
- Ozdowski, E. F., S. Gayle, H. Bao, B. Zhang and N. T. Sherwood "Loss of *Drosophila melanogaster* p21-activated kinase 3 (pak3) suppresses defects in synapse structure and function caused by spastin mutations." *Genetics*.
- Ozols, J. and J. M. Caron (1997). "Posttranslational modification of tubulin by palmitoylation: II. Identification of sites of palmitoylation." *Mol Biol Cell* 8(4): 637-645.
- Palazzo, A., B. Ackerman and G. G. Gundersen (2003). "Cell biology: Tubulin acetylation and cell motility." *Nature* 421(6920): 230.
- Papp, B., C. Pal and L. D. Hurst (2003). "Dosage sensitivity and the evolution of gene families in yeast." *Nature* 424(6945): 194-197.
- Paturle, L., J. Wehland, R. L. Margolis and D. Job (1989). "Complete separation of tyrosinated, detyrosinated, and nontyrosinatable brain tubulin subpopulations using affinity chromatography." *Biochemistry* 28(6): 2698-2704.
- Paturle-Lafanechere, L., B. Edde, P. Denoulet, A. Van Dorselaer, H. Mazarguil, J. P. Le Caer, J. Wehland and D. Job (1991). "Characterization of a major brain tubulin variant which cannot be tyrosinated." *Biochemistry* 30(43): 10523-10528.
- Penzes, P., D. P. Srivastava and K. M. Woolfrey (2009). "Not just actin? A role for dynamic microtubules in dendritic spines." *Neuron* 61(1): 3-5.
- Peris, L., M. Wagenbach, L. Lafanechere, J. Brocard, A. T. Moore, F. Kozielski, D. Job, L. Wordeman and A. Andrieux (2009). "Motor-dependent microtubule disassembly driven by tubulin tyrosination." *J Cell Biol* 185(7): 1159-1166.
- Perrot, R., R. Berges, A. Bocquet and J. Eyer (2008). "Review of the multiple aspects of neurofilament functions, and their possible contribution to neurodegeneration." *Mol Neurobiol* 38(1): 27-65.

REFERENCES

- Petersen, S. A., R. D. Fetter, J. N. Noordermeer, C. S. Goodman and A. DiAntonio (1997). "Genetic analysis of glutamate receptors in *Drosophila* reveals a retrograde signal regulating presynaptic transmitter release." *Neuron* 19(6): 1237-1248.
- Pettitt, S. J., Q. Liang, X. Y. Rairdan, J. L. Moran, H. M. Prosser, D. R. Beier, K. C. Lloyd, A. Bradley and W. C. Skarnes (2009). "Agouti C57BL/6N embryonic stem cells for mouse genetic resources." *Nat Methods* 6(7): 493-495.
- Qiang, L., W. Yu, A. Andreadis, M. Luo and P. W. Baas (2006). "Tau protects microtubules in the axon from severing by katanin." *J Neurosci* 26(12): 3120-3129.
- Qiang, L., W. Yu, M. Liu, J. M. Solowska and P. W. Baas (2010). "Basic fibroblast growth factor elicits formation of interstitial axonal branches via enhanced severing of microtubules." *Mol Biol Cell* 21(2): 334-344.
- Rasi (2009). "Katanin Knockdown Supports a Role for Microtubule Severing in Release of Basal Bodies before Mitosis in *Chlamydomonas*."
- Redeker, V., N. Levilliers, J. M. Schmitter, J. P. Le Caer, J. Rossier, A. Adoutte and M. H. Bre (1994). "Polyglycylation of tubulin: a posttranslational modification in axonemal microtubules." *Science* 266(5191): 1688-1691.
- Regnard, C., S. Audebert, Desbruyeres, P. Denoulet and B. Edde (1998). "Tubulin polyglutamylase: partial purification and enzymatic properties." *Biochemistry* 37(23): 8395-8404.
- Regnard, C., E. Desbruyeres, P. Denoulet and B. Edde (1999). "Tubulin polyglutamylase: isozymic variants and regulation during the cell cycle in HeLa cells." *J Cell Sci* 112 (Pt 23): 4281-4289.
- Reymann, K. G. and J. U. Frey (2007). "The late maintenance of hippocampal LTP: requirements, phases, 'synaptic tagging', 'late-associativity' and implications." *Neuropharmacology* 52(1): 24-40.
- Riano, E., M. Martignoni, G. Mancuso, D. Cartelli, F. Crippa, I. Toldo, G. Siciliano, D. Di Bella, F. Taroni, M. T. Bassi, G. Cappelletti and E. I. Rugarli (2009). "Pleiotropic effects of spastin on neurite growth depending on expression levels." *J Neurochem* 108(5): 1277-1288.
- Rogers, S., R. Wells and M. Rechsteiner (1986). "Amino acid sequences common to rapidly degraded proteins: the PEST hypothesis." *Science* 234(4774): 364-368.
- Rogowski, K., J. van Dijk, M. M. Magiera, C. Bosc, J. C. Deloulme, A. Bosson, L. Peris, N. D. Gold, B. Lacroix, M. Bosch Grau, N. Bec, C. Larroque, S. Desagher, M. Holzer, A. Andrieux, M. J. Moutin and C. Janke (2010). "A family of protein-deglutamylating enzymes associated with neurodegeneration." *Cell* 143(4): 564-578.
- Roll-Mecak, A. and F. J. McNally (2010). "Microtubule-severing enzymes." *Curr Opin Cell Biol* 22(1): 96-103.
- Roll-Mecak, A. and R. D. Vale (2005). "The *Drosophila* homologue of the hereditary spastic paraplegia protein, spastin, severs and disassembles microtubules." *Curr Biol* 15(7): 650-655.
- Roll-Mecak, A. and R. D. Vale (2006). "Making more microtubules by severing: a common theme of noncentrosomal microtubule arrays?" *J Cell Biol* 175(6): 849-851.
- Roll-Mecak, A. and R. D. Vale (2008). "Structural basis of microtubule severing by the hereditary spastic paraplegia protein spastin." *Nature* 451(7176): 363-367.

REFERENCES

- Ross, J. L., M. Y. Ali and D. M. Warshaw (2008). "Cargo transport: molecular motors navigate a complex cytoskeleton." Curr Opin Cell Biol 20(1): 41-47.
- Saiki, R. K., D. H. Gelfand, S. Stoffel, S. J. Scharf, R. Higuchi, G. T. Horn, K. B. Mullis and H. A. Erlich (1988). "Primer-directed enzymatic amplification of DNA with a thermostable DNA polymerase." Science 239(4839): 487-491.
- Salinas, S., R. E. Carazo-Salas, C. Proukakis, J. M. Cooper, A. E. Weston, G. Schiavo and T. T. Warner (2005). "Human spastin has multiple microtubule-related functions." J Neurochem 95(5): 1411-1420.
- Sambrook, J., E. F. Fritsch and M. T. (1989). Molecular Cloning: A Laboratory Manual, Cold Spring Harbor Laboratory Press.
- Sanger, F., S. Nicklen and A. R. Coulson (1977). "DNA sequencing with chain-terminating inhibitors." Proc Natl Acad Sci U S A 74(12): 5463-5467.
- Satokata, I., G. Benson and R. Maas (1995). "Sexually dimorphic sterility phenotypes in Hoxa10-deficient mice." Nature 374(6521): 460-463.
- Sauer, B. (1998). "Inducible gene targeting in mice using the Cre/lox system." Methods 14(4): 381-392.
- Schickel, J., T. Pamminger, A. Ehrsam, S. Munch, X. Huang, T. Klopstock, G. Kurlemann, P. Hemmerich, W. Dubiel, T. Deufel and C. Beetz (2007). "Isoform-specific increase of spastin stability by N-terminal missense variants including intragenic modifiers of SPG4 hereditary spastic paraplegia." Eur J Neurol 14(12): 1322-1328.
- Schindelin, J., I. Arganda-Carreras, E. Frise, V. Kaynig, M. Longair, T. Pietzsch, S. Preibisch, C. Rueden, S. Saalfeld, B. Schmid, J. Y. Tinevez, D. J. White, V. Hartenstein, K. Eliceiri, P. Tomancak and A. Cardona (2012). "Fiji: an open-source platform for biological-image analysis." Nat Methods 9(7): 676-682.
- Schlager, M. A. and C. C. Hoogenraad (2009). "Basic mechanisms for recognition and transport of synaptic cargos." Mol Brain 2: 25.
- Schneider, C. A., W. S. Rasband and K. W. Eliceiri (2012). "NIH Image to ImageJ: 25 years of image analysis." Nat Methods 9(7): 671-675.
- Scholey, J. M. (2003). "Intraflagellar transport." Annu Rev Cell Dev Biol 19: 423-443.
- Schreij, A. M., E. A. Fon and P. S. McPherson (2016). "Endocytic membrane trafficking and neurodegenerative disease." Cell Mol Life Sci 73(8): 1529-1545.
- Schulze, E., D. J. Asai, J. C. Bulinski and M. Kirschner (1987). "Posttranslational modification and microtubule stability." J Cell Biol 105(5): 2167-2177.
- Schuster, C. M., A. Ultsch, P. Schloss, J. A. Cox, B. Schmitt and H. Betz (1991). "Molecular cloning of an invertebrate glutamate receptor subunit expressed in *Drosophila* muscle." Science 254(5028): 112-114.
- Schuyler, S. C. and D. Pellman (2001). "Microtubule "plus-end-tracking proteins": The end is just the beginning." Cell 105(4): 421-424.
- Schwenk, F., U. Baron and K. Rajewsky (1995). "A cre-transgenic mouse strain for the ubiquitous deletion of loxP-flanked gene segments including deletion in germ cells." Nucleic Acids Res 23(24): 5080-5081.

- Scoville, W. B. and B. Milner (1957). "Loss of recent memory after bilateral hippocampal lesions." J Neurol Neurosurg Psychiatry 20(1): 11-21.
- Sedel, F., B. Fontaine, J. M. Saudubray and O. Lyon-Caen (2007). "Hereditary spastic paraparesis in adults associated with inborn errors of metabolism: a diagnostic approach." J Inherit Metab Dis 30(6): 855-864.
- Setou, M., T. Nakagawa, D. H. Seog and N. Hirokawa (2000). "Kinesin superfamily motor protein KIF17 and mLin-10 in NMDA receptor-containing vesicle transport." Science 288(5472): 1796-1802.
- Sharma, N., J. Bryant, D. Wloga, R. Donaldson, R. C. Davis, M. Jerka-Dziadosz and J. Gaertig (2007). "Katanin regulates dynamics of microtubules and biogenesis of motile cilia." J Cell Biol 178(6): 1065-1079.
- Sharp, D. J. and J. L. Ross (2012). "Microtubule-severing enzymes at the cutting edge." J Cell Sci 125(Pt 11): 2561-2569.
- Sherwood, N. T., Q. Sun, M. Xue, B. Zhang and K. Zinn (2004). "Drosophila spastin regulates synaptic microtubule networks and is required for normal motor function." PLoS Biol 2(12): e429.
- Siddiqui, S. M., R. T. Sauer and T. A. Baker (2004). "Role of the processing pore of the ClpX AAA+ ATPase in the recognition and engagement of specific protein substrates." Genes Dev 18(4): 369-374.
- Silva, I., L. E. Mello, E. Freymuller, M. A. Haidar and E. C. Baracat (2000). "Estrogen, progesterone and tamoxifen increase synaptic density of the hippocampus of ovariectomized rats." Neurosci Lett 291(3): 183-186.
- Singer-Sam, J. (2010). "Monoallelic Expression." Nature Education 3(3): 1.
- Skarnes, W. C., B. Rosen, A. P. West, M. Koutsourakis, W. Bushell, V. Iyer, A. O. Mujica, M. Thomas, J. Harrow, T. Cox, D. Jackson, J. Severin, P. Biggs, J. Fu, M. Nefedov, P. J. de Jong, A. F. Stewart and A. Bradley (2011). "A conditional knockout resource for the genome-wide study of mouse gene function." Nature 474(7351): 337-342.
- Smith, L. B., L. Milne, N. Nelson, S. Eddie, P. Brown, N. Atanassova, M. K. O'Bryan, L. O'Donnell, D. Rhodes, S. Wells, D. Napper, P. Nolan, Z. Lalanne, M. Cheeseman and J. Peters (2012). "KATNAL1 regulation of sertoli cell microtubule dynamics is essential for spermiogenesis and male fertility." PLoS Genet 8(5): e1002697.
- Smithies, O., R. G. Gregg, S. S. Boggs, M. A. Koralewski and R. S. Kucherlapati (1985). "Insertion of DNA sequences into the human chromosomal beta-globin locus by homologous recombination." Nature 317(6034): 230-234.
- Soderling, T. R. and V. A. Derkach (2000). "Postsynaptic protein phosphorylation and LTP." Trends Neurosci 23(2): 75-80.
- Solowska, J. M., G. Morfini, A. Falnikar, B. T. Himes, S. T. Brady, D. Huang and P. W. Baas (2008). "Quantitative and functional analyses of spastin in the nervous system: implications for hereditary spastic paraplegia." J Neurosci 28(9): 2147-2157.
- Sonbuchner, T. M., U. Rath and D. J. Sharp (2010). "KL1 is a novel microtubule severing enzyme that regulates mitotic spindle architecture." Cell Cycle 9(12): 2403-2411.
- Song, Y., L. L. Kirkpatrick, A. B. Schilling, D. L. Helseth, N. Chabot, J. W. Keillor, G. V. Johnson and S. T. Brady (2013). "Transglutaminase and polyamination of tubulin: posttranslational modification for stabilizing axonal microtubules." Neuron 78(1): 109-123.

REFERENCES

- Soriano, P. (1999). "Generalized lacZ expression with the ROSA26 Cre reporter strain." Nat Genet 21(1): 70-71.
- Squire, L. R. and S. H. Barondes (1972). "Variable decay of memory and its recovery in cycloheximide-treated mice." Proc Natl Acad Sci U S A 69(6): 1416-1420.
- Srayko, M., D. W. Buster, O. A. Bazirgan, F. J. McNally and P. E. Mains (2000). "MEI-1/MEI-2 katanin-like microtubule severing activity is required for *Caenorhabditis elegans* meiosis." Genes Dev 14(9): 1072-1084.
- Srayko, M., T. O'Toole E, A. A. Hyman and T. Muller-Reichert (2006). "Katanin disrupts the microtubule lattice and increases polymer number in *C. elegans* meiosis." Curr Biol 16(19): 1944-1949.
- Staff, N. P., H. Y. Jung, T. Thiagarajan, M. Yao and N. Spruston (2000). "Resting and active properties of pyramidal neurons in subiculum and CA1 of rat hippocampus." J Neurophysiol 84(5): 2398-2408.
- Stanton, P. K. and J. M. Sarvey (1984). "Blockade of long-term potentiation in rat hippocampal CA1 region by inhibitors of protein synthesis." J Neurosci 4(12): 3080-3088.
- Stent, G. S. (1973). "A physiological mechanism for Hebb's postulate of learning." Proc Natl Acad Sci U S A 70(4): 997-1001.
- Stepanova, T., J. Slemmer, C. C. Hoogenraad, G. Lansbergen, B. Dortland, C. I. De Zeeuw, F. Grosveld, G. van Cappellen, A. Akhmanova and N. Galjart (2003). "Visualization of microtubule growth in cultured neurons via the use of EB3-GFP (end-binding protein 3-green fluorescent protein)." J Neurosci 23(7): 2655-2664.
- Sternberg, N. and D. Hamilton (1981). "Bacteriophage P1 site-specific recombination. I. Recombination between loxP sites." J Mol Biol 150(4): 467-486.
- Stewart, A., A. Tsubouchi, M. M. Rolls, W. D. Tracey and N. T. Sherwood (2012). "Katanin p60-like1 promotes microtubule growth and terminal dendrite stability in the larval class IV sensory neurons of *Drosophila*." J Neurosci 32(34): 11631-11642.
- Stiess, M., N. Maghelli, L. C. Kapitein, S. Gomis-Ruth, M. Wilsch-Brauninger, C. C. Hoogenraad, I. M. Tolic-Norrelykke and F. Bradke (2010). "Axon extension occurs independently of centrosomal microtubule nucleation." Science 327(5966): 704-707.
- Storm, J. F. (1987). "Action potential repolarization and a fast after-hyperpolarization in rat hippocampal pyramidal cells." J Physiol 385: 733-759.
- Sudo, H. and P. W. Baas (2010). "Acetylation of microtubules influences their sensitivity to severing by katanin in neurons and fibroblasts." J Neurosci 30(21): 7215-7226.
- Sudo, H. and P. W. Baas (2011). "Strategies for diminishing katanin-based loss of microtubules in tauopathic neurodegenerative diseases." Hum Mol Genet 20(4): 763-778.
- Sudo, H. and Y. Maru (2008). "LAPSER1/LZTS2: a pluripotent tumor suppressor linked to the inhibition of katanin-mediated microtubule severing." Hum Mol Genet 17(16): 2524-2540.
- Svenson, I. K., A. E. Ashley-Koch, P. C. Gaskell, T. J. Riney, W. J. Cumming, H. M. Kingston, E. L. Hogan, R. M. Boustany, J. M. Vance, M. A. Nance, M. A. Pericak-Vance and D. A. Marchuk (2001). "Identification and expression analysis of spastin gene mutations in hereditary spastic paraplegia." Am J Hum Genet 68(5): 1077-1085.

REFERENCES

- Sweet, E. S., M. L. Previtiera, J. R. Fernandez, E. I. Charych, C. Y. Tseng, M. Kwon, V. Starovoytov, J. Q. Zheng and B. L. Firestein (2011). "PSD-95 alters microtubule dynamics via an association with EB3." *J Neurosci* 31(3): 1038-1047.
- Tada, T. and M. Sheng (2006). "Molecular mechanisms of dendritic spine morphogenesis." *Curr Opin Neurobiol* 16(1): 95-101.
- Tallaksen, C. M., E. Guichart-Gomez, P. Verpillat, V. Hahn-Barma, M. Ruberg, B. Fontaine, A. Brice, B. Dubois and A. Durr (2003). "Subtle cognitive impairment but no dementia in patients with spastin mutations." *Arch Neurol* 60(8): 1113-1118.
- Tarrade, A., C. Fassier, S. Courageot, D. Charvin, J. Vitte, L. Peris, A. Thorel, E. Mouisel, N. Fonknechten, N. Roblot, D. Seilhean, A. Dierich, J. J. Hauw and J. Melki (2006). "A mutation of spastin is responsible for swellings and impairment of transport in a region of axon characterized by changes in microtubule composition." *Hum Mol Genet* 15(24): 3544-3558.
- Taylor, H. S., A. Arici, D. Olive and P. Igarashi (1998). "HOXA10 is expressed in response to sex steroids at the time of implantation in the human endometrium." *J Clin Invest* 101(7): 1379-1384.
- Taylor, H. S., G. B. Vanden Heuvel and P. Igarashi (1997). "A conserved Hox axis in the mouse and human female reproductive system: late establishment and persistent adult expression of the Hoxa cluster genes." *Biol Reprod* 57(6): 1338-1345.
- Thomsen, B., P. H. Nissen, J. S. Agerholm and C. Bendixen (2010). "Congenital bovine spinal dysmyelination is caused by a missense mutation in the SPAST gene." *Neurogenetics* 11(2): 175-183.
- Tokuraku, K., K. Matsushima, T. Matui, H. Nakagawa, M. Katsuki, R. Majima and S. Kotani (2003). "The number of repeat sequences in microtubule-associated protein 4 affects the microtubule surface properties." *J Biol Chem* 278(32): 29609-29618.
- Toyo-Oka, K., S. Sasaki, Y. Yano, D. Mori, T. Kobayashi, Y. Y. Toyoshima, S. M. Tokuoka, S. Ishii, T. Shimizu, M. Muramatsu, N. Hiraiwa, A. Yoshiki, A. Wynshaw-Boris and S. Hirotsune (2005). "Recruitment of katanin p60 by phosphorylated NDEL1, an LIS1 interacting protein, is essential for mitotic cell division and neuronal migration." *Hum Mol Genet* 14(21): 3113-3128.
- Tronche, F., C. Kellendonk, O. Kretz, P. Gass, K. Anlag, P. C. Orban, R. Bock, R. Klein and G. Schutz (1999). "Disruption of the glucocorticoid receptor gene in the nervous system results in reduced anxiety." *Nat Genet* 23(1): 99-103.
- Trotta, N., G. Orso, M. G. Rossetto, A. Daga and K. Broadie (2004). "The hereditary spastic paraplegia gene, spastin, regulates microtubule stability to modulate synaptic structure and function." *Curr Biol* 14(13): 1135-1147.
- Tsai, L. H. and J. G. Gleeson (2005). "Nucleokinesis in neuronal migration." *Neuron* 46(3): 383-388.
- Tsien, J. Z., D. F. Chen, D. Gerber, C. Tom, E. H. Mercer, D. J. Anderson, M. Mayford, E. R. Kandel and S. Tonegawa (1996). "Subregion- and cell type-restricted gene knockout in mouse brain." *Cell* 87(7): 1317-1326.
- Uchida, S., G. Martel, A. Pavlowsky, S. Takizawa, C. Hevi, Y. Watanabe, E. R. Kandel, J. M. Alarcon and G. P. Shumyatsky (2014). "Learning-induced and stathmin-dependent changes in microtubule stability are critical for memory and disrupted in ageing." *Nat Commun* 5: 4389.
- Utomo, A. R., A. Y. Nikitin and W. H. Lee (1999). "Temporal, spatial, and cell type-specific control of Cre-mediated DNA recombination in transgenic mice." *Nat Biotechnol* 17(11): 1091-1096.

REFERENCES

- Vale, R. D. (1991). "Severing of stable microtubules by a mitotically activated protein in *Xenopus* egg extracts." Cell 64(4): 827-839.
- Vale, R. D. (2003). "The molecular motor toolbox for intracellular transport." Cell 112(4): 467-480.
- Valenstein, M. L. and A. Roll-Mecak (2016). "Graded Control of Microtubule Severing by Tubulin Glutamylation." Cell 164(5): 911-921.
- Vallee, R. B. (1982). "A taxol-dependent procedure for the isolation of microtubules and microtubule-associated proteins (MAPs)." J Cell Biol 92(2): 435-442.
- van Dijk, J., J. Miro, J. M. Strub, B. Lacroix, A. van Dorsselaer, B. Edde and C. Janke (2008). "Polyglutamylation is a post-translational modification with a broad range of substrates." J Biol Chem 283(7): 3915-3922.
- Veitia, R. A. (2002). "Exploring the etiology of haploinsufficiency." Bioessays 24(2): 175-184.
- Verhey, K. J. and J. Gaertig (2007). "The tubulin code." Cell Cycle 6(17): 2152-2160.
- Vu, T. H., R. L. Jirtle and A. R. Hoffman (2006). "Cross-species clues of an epigenetic imprinting regulatory code for the IGF2R gene." Cytogenet Genome Res 113(1-4): 202-208.
- Wallace, M. E. (1950). "Locus of the gene 'fidget' in the house mouse." Nature 166(4218): 407.
- Wang, H., H. Yang, C. S. Shivalila, M. M. Dawlaty, A. W. Cheng, F. Zhang and R. Jaenisch (2013). "One-step generation of mice carrying mutations in multiple genes by CRISPR/Cas-mediated genome engineering." Cell 153(4): 910-918.
- Wang, J., Z. Valo, D. Smith and J. Singer-Sam (2007). "Monoallelic expression of multiple genes in the CNS." PLoS One 2(12): e1293.
- Wang, L. and A. Brown (2002). "Rapid movement of microtubules in axons." Curr Biol 12(17): 1496-1501.
- Wang, Z. and M. P. Sheetz (2000). "The C-terminus of tubulin increases cytoplasmic dynein and kinesin processivity." Biophys J 78(4): 1955-1964.
- Watanabe, F., W. D. Arnold, R. E. Hammer, O. Ghodsizadeh, H. Moti, M. Schumer, A. Hashmi, A. Hernandez, A. Sneh, Z. Sahenk and Y. Y. Kisanuki (2013). "Pathogenesis of autosomal dominant hereditary spastic paraplegia (SPG6) revealed by a rat model." J Neuropathol Exp Neurol 72(11): 1016-1028.
- Watanabe, T., J. Noritake and K. Kaibuchi (2005). "Regulation of microtubules in cell migration." Trends Cell Biol 15(2): 76-83.
- Webb, S., D. Coleman, P. Byrne, N. Parfrey, T. Burke, J. Hutchinson and M. Hutchinson (1998). "Autosomal dominant hereditary spastic paraparesis with cognitive loss linked to chromosome 2p." Brain 121 (Pt 4): 601-609.
- Wegner, A. (1976). "Head to tail polymerization of actin." J Mol Biol 108(1): 139-150.
- Welte, M. A. (2004). "Bidirectional transport along microtubules." Curr Biol 14(13): R525-537.
- West, M. J., C. H. Kawas, L. J. Martin and J. C. Troncoso (2000). "The CA1 region of the human hippocampus is a hot spot in Alzheimer's disease." Ann N Y Acad Sci 908: 255-259.
- Westermann, S. and K. Weber (2003). "Post-translational modifications regulate microtubule function." Nat Rev Mol Cell Biol 4(12): 938-947.

REFERENCES

- Wharton, S. B., C. J. McDermott, A. J. Grierson, J. D. Wood, C. Gelsthorpe, P. G. Ince and P. J. Shaw (2003). "The cellular and molecular pathology of the motor system in hereditary spastic paraparesis due to mutation of the spastin gene." *J Neuropathol Exp Neurol* 62(11): 1166-1177.
- White, K. D., P. G. Ince, M. Lusher, J. Lindsey, M. Cookson, R. Bashir, P. J. Shaw and K. M. Bushby (2000). "Clinical and pathologic findings in hereditary spastic paraparesis with spastin mutation." *Neurology* 55(1): 89-94.
- White, S. R., K. J. Evans, J. Lary, J. L. Cole and B. Lauring (2007). "Recognition of C-terminal amino acids in tubulin by pore loops in Spastin is important for microtubule severing." *J Cell Biol* 176(7): 995-1005.
- White, S. R. and B. Lauring (2007). "AAA+ ATPases: achieving diversity of function with conserved machinery." *Traffic* 8(12): 1657-1667.
- Whiteheart, S. W., T. Schraw and E. A. Matveeva (2001). "N-ethylmaleimide sensitive factor (NSF) structure and function." *Int Rev Cytol* 207: 71-112.
- Whitlock, J. R., A. J. Heynen, M. G. Shuler and M. F. Bear (2006). "Learning induces long-term potentiation in the hippocampus." *Science* 313(5790): 1093-1097.
- Whittaker, V. P., I. A. Michaelson and R. J. Kirkland (1964). "The separation of synaptic vesicles from nerve-ending particles ('synaptosomes')." *Biochem J* 90(2): 293-303.
- Wiese, C. and Y. Zheng (2000). "A new function for the gamma-tubulin ring complex as a microtubule minus-end cap." *Nat Cell Biol* 2(6): 358-364.
- Wittmann, T. and C. M. Waterman-Storer (2001). "Cell motility: can Rho GTPases and microtubules point the way?" *J Cell Sci* 114(Pt 21): 3795-3803.
- Wong, P. C., C. A. Pardo, D. R. Borchelt, M. K. Lee, N. G. Copeland, N. A. Jenkins, S. S. Sisodia, D. W. Cleveland and D. L. Price (1995). "An adverse property of a familial ALS-linked SOD1 mutation causes motor neuron disease characterized by vacuolar degeneration of mitochondria." *Neuron* 14(6): 1105-1116.
- Wood, J. D., J. A. Landers, M. Bingley, C. J. McDermott, V. Thomas-McArthur, L. J. Gleadall, P. J. Shaw and V. T. Cunliffe (2006). "The microtubule-severing protein Spastin is essential for axon outgrowth in the zebrafish embryo." *Hum Mol Genet* 15(18): 2763-2771.
- Woolley, C. S. (1998). "Estrogen-mediated structural and functional synaptic plasticity in the female rat hippocampus." *Horm Behav* 34(2): 140-148.
- Yamada-Inagawa, T., T. Okuno, K. Karata, K. Yamanaka and T. Ogura (2003). "Conserved pore residues in the AAA protease FtsH are important for proteolysis and its coupling to ATP hydrolysis." *J Biol Chem* 278(50): 50182-50187.
- Yang, Y., C. L. Mahaffey, N. Berube and W. N. Frankel (2006). "Interaction between fidgetin and protein kinase A-anchoring protein AKAP95 is critical for palatogenesis in the mouse." *J Biol Chem* 281(31): 22352-22359.
- Ye, B., J. H. Kim, L. Yang, I. McLachlan, S. Younger, L. Y. Jan and Y. N. Jan (2011). "Differential regulation of dendritic and axonal development by the novel Kruppel-like factor Dar1." *J Neurosci* 31(9): 3309-3319.
- Ye, X., Y. C. Lee, M. Choueiri, K. Chu, C. F. Huang, W. W. Tsai, R. Kobayashi, C. J. Logothetis, L. Y. Yu-Lee and S. H. Lin (2012). "Aberrant expression of katanin p60 in prostate cancer bone metastasis." *Prostate* 72(3): 291-300.

- Yeckel, M. F. and T. W. Berger (1990). "Feedforward excitation of the hippocampus by afferents from the entorhinal cortex: redefinition of the role of the trisynaptic pathway." Proc Natl Acad Sci U S A 87(15): 5832-5836.
- Yoshimori, T., F. Yamagata, A. Yamamoto, N. Mizushima, Y. Kabeya, A. Nara, I. Miwako, M. Ohashi, M. Ohsumi and Y. Ohsumi (2000). "The mouse SKD1, a homologue of yeast Vps4p, is required for normal endosomal trafficking and morphology in mammalian cells." Mol Biol Cell 11(2): 747-763.
- Yu, W., L. Qiang, J. M. Solowska, A. Karabay, S. Korulu and P. W. Baas (2008). "The microtubule-severing proteins spastin and katanin participate differently in the formation of axonal branches." Mol Biol Cell 19(4): 1485-1498.
- Yu, W., J. M. Solowska, L. Qiang, A. Karabay, D. Baird and P. W. Baas (2005). "Regulation of microtubule severing by katanin subunits during neuronal development." J Neurosci 25(23): 5573-5583.
- Yuste, R. and T. Bonhoeffer (2001). "Morphological changes in dendritic spines associated with long-term synaptic plasticity." Annu Rev Neurosci 24: 1071-1089.
- Zakharenko, S. and S. Popov (1998). "Dynamics of axonal microtubules regulate the topology of new membrane insertion into the growing neurites." J Cell Biol 143(4): 1077-1086.
- Zambito, A. M. and J. Wolff (1997). "Palmitoylation of tubulin." Biochem Biophys Res Commun 239(3): 650-654.
- Zempel, H., J. Luedtke, Y. Kumar, J. Biernat, H. Dawson, E. Mandelkow and E. M. Mandelkow (2013). "Amyloid-beta oligomers induce synaptic damage via Tau-dependent microtubule severing by TTL6 and spastin." EMBO J 32(22): 2920-2937.
- Zhang, D., K. D. Grode, S. F. Stewman, J. D. Diaz-Valencia, E. Liebling, U. Rath, T. Riera, J. D. Currie, D. W. Buster, A. B. Asenjo, H. J. Sosa, J. L. Ross, A. Ma, S. L. Rogers and D. J. Sharp (2011). "Drosophila katanin is a microtubule depolymerase that regulates cortical-microtubule plus-end interactions and cell migration." Nat Cell Biol 13(4): 361-370.
- Zhang, D., G. C. Rogers, D. W. Buster and D. J. Sharp (2007). "Three microtubule severing enzymes contribute to the "Pacman-flux" machinery that moves chromosomes." J Cell Biol 177(2): 231-242.
- Zhang, J., P. Dublin, S. Griemsmann, A. Klein, R. Brehm, P. Bedner, B. K. Fleischmann, C. Steinhauser and M. Theis (2013). "Germ-line recombination activity of the widely used hGFAP-Cre and nestin-Cre transgenes." PLoS One 8(12): e82818.
- Zoghbi, H. Y. and J. Botas (2002). "Mouse and fly models of neurodegeneration." Trends Genet 18(9): 463-471.
- Zola-Morgan, S., L. R. Squire and D. G. Amaral (1986). "Human amnesia and the medial temporal region: enduring memory impairment following a bilateral lesion limited to field CA1 of the hippocampus." J Neurosci 6(10): 2950-2967.

7 APPENDIX

7.1 Abbreviations

| | | | |
|-----------------|--|--------------------|---|
| AAA | ATPases associated with various cellular activities | EM | electron microscopy |
| ADP | adenosine diphosphate | En2 SA | Engrailed 2 Splice acceptor |
| AMPA | α -amino-3-hydroxy-5-methyl-4-isoxazolepropionic acid | EUCOMM | European Conditional Mouse Mutagenesis Program |
| AmpR | ampicillin resistance | ES cell | embryonic stem cell |
| APS | ammoniumpersulfate | FCS | fetal calf serum |
| APV | (2R)-amino-5-phosphonovaleric acid; (2R)-amino-5-phosphonopentanoate | FL | floxed allele |
| ATP | adenosine tris phosphate | FRT | Flippase recognition target |
| AU | Arbitrary Units | g | gravity |
| B-27 | | GABA | gamma amino butyric acid |
| BAC | bacterial artificial chromosome | GAPDH | glycerate aldehyde phosphate dehydrogenase |
| BCA | bicichinonic acid | GDP | guanosinediphosphate |
| BSA | bovine serum albumin | GFP | green fluorescent protein |
| BsdR | blasticidin S deaminase Resistance | GluR | Glutamate receptor |
| CAMKII α | Calcium/calmodulin-dependent protein kinase type II alpha chain | GOI | gene of interest |
| CA1/CA3 | Cornu ammonis 1/3 | GRIA | glutamate ionotropic receptor AMPA type |
| CCD | charge-coupled device | GRIN | glutamate ionotropic receptor NMDA type |
| cDNA | complementary DNA | GT | gene-trap |
| CNS | central nervous system | GTP | guanosine triphosphate |
| cpm | counts per minute | hBactP | human β actin promoter |
| DG | dentate gyrus | HBS | Hank's balanced salts |
| DIV | days in vitro | HEK | human embryonic kidney |
| D-MEM | Dulbecco's modified eagle medium | HEPES | 4-(2-hydroxyethyl)-1-piperazineethanesulfonic acid |
| DMSO | dimethylsulfoxide | HPSF | high purity salt-free |
| DNA | desoxyribonucleic acid | HRP | horseradish peroxidase |
| dNTP | 2'-desoxyribonucleoside-5'-triphosphate | HSP | hereditary spastic paraplegia or heat shock protein |
| DTA | diphtheria toxin A | ICC | immunocytochemistry |
| DTT | Dithiothreitol | i. e. | id est |
| dNTP | desoxynucleotide-triphosphate | IPTG | Isopropyl- β -D1-thiogalactopyranosid |
| EB-3 | end-binding protein 3 | IRES | internal ribosomal entry site |
| EDTA | ethylenediaminetetraacetic acid | KATNAL | Katanin catalytic subunit A1 like |
| e. g. | exempli gratia | kDa | kilodalton |
| EGTA | ethylene glycol tetraacetic acid | KO 1 st | knockout first |
| | | KOMP | knockout mouse project |
| | | LB | Lurial Bertani |
| | | loxP | Lox site derived from bacteriophage P1/ locus of x-ing over |

| | | | |
|--------|---|--------|--|
| LTD | long-term depression | PVDF | polyvinylidene fluoride |
| LTP | long-term potentiation | rcf | relative centrifugal force |
| MAP | microtubule associated protein | RIPA | radioimmunoprecipitation assay buffer |
| min | minutes | RFP | red fluorescent protein |
| MIT | microtubule interacting and trafficking | RNA | ribonucleic acid |
| MT | microtubule | rpm | rounds per minute |
| MTBD | microtubule binding domain | s | seconds |
| MTOC | microtubule organizing center | SDS | sodium dodecyl sulfate |
| mRNA | messenger RNA | SEM | standard error of the mean |
| N/A | numerical aperture | SNAP25 | Synaptosomal-associated protein 25 |
| NBD | nucleotide binding domain | SOC | super optimal broth with catabolite repression |
| NES | nuclear export sequence | SPG4 | Spastin |
| NIH | National Institutes of Health | SSC | saline-sodium citrate |
| NLS | nuclear localization sequence | TAE | Tris acetic acid EDTA |
| NMDA | N-methyl-D-aspartate | TBE | TRIS-borate-EDTA |
| nt | nucleotide | TBS | Tris buffered saline |
| NSE | neuron-specific enolase | TBST | Tris buffered saline + Tween |
| OD | optical density | TEMED | tetramethylethylenediamine |
| o/n | overnight | TG | transgene |
| PAGE | polyacrylamide gel electrophoresis | +TIP | plus tip interacting protein |
| PBS | phosphate buffered saline | Tris | Tris (hydroxymethyl) aminoethane |
| PCR | polymerase chain reaction | TTL | tubulin tyrosine ligase-like unit |
| PGK | phosphoglycerate kinase | U | unit |
| pH | potentia hydrogenii | v/v | volume per volume |
| PMSF | phenylmethylsulfonyl fluoride | WB | Western Blot |
| PNS | peripheral nervous system | w/v | weight per volume |
| PSD-95 | postsynaptic density protein 95 | ZMNH | center for molecular biology Hamburg |
| PTM | post-translational modifications | | |

7.2 Figures

| | |
|---|----|
| Figure 1: Model of a neuron. | 3 |
| Figure 2: Schematic representation of an excitatory chemical synapse.. | 5 |
| Figure 3: Magnesium blockade of the NMDA receptor. | 6 |
| Figure 4: Synaptic plasticity is NMDA-receptor dependent. | 8 |
| Figure 5: Schematic representation of the information flow in the hippocampal formation. | 9 |
| Figure 6: Schematic representation of microtubules. | 10 |
| Figure 7: Schematic representation of cytoskeletal associated motor proteins. | 11 |
| Figure 8: Proposed functions of dynamic MT entrance into spines. | 13 |
| Figure 9: Schematic representation of the $\alpha\beta$ -tubulin dimer and its associated modifications. | 14 |
| Figure 10: Schematic representation of the murine spastin protein sequence. | 18 |
| Figure 11: Domain architecture of the three KATNA1, KATNAL1, KATNAL2 catalytic subunits and the two KATNB1 and KATNBL1 regulatory subunits.. | 20 |

| | |
|--|----|
| Figure 12: Proposed model of microtubule-severing by the MT-severing enzyme spastin..... | 22 |
| Figure 13: Summarizing overview of the multiple neuronal functions of MT-severing enzymes..... | 26 |
| Figure 14: Mechanism of the Cre/loxP recombination system..... | 31 |
| Figure 15: Experimental setup for Southern Blotting (alkaline method)..... | 53 |
| Figure 16: Exemplary picture of synaptosomal fractionation.. | 56 |
| Figure 17: Top view of the open field apparatus.. | 60 |
| Figure 18: Example of a promoter-driven KO-first-allele targeting vector. | 62 |
| Figure 19: LacZ staining of tissues from offspring resulting from different CamKII α -Cre-driver lines mated to the R26R reporter line to visualize Cre-mediated recombination..... | 64 |
| Figure 20: PCR method to control for CamKII α -Cre expression in germ cells..... | 65 |
| Figure 21: Targeting strategy for the murine spastin gene. | 66 |
| Figure 22: Agarose gel confirming the linearization of the spastin targeting vector using the restriction endonuclease AsiSI..... | 67 |
| Figure 23: Confirmation of the correctly targeted murine spastin gene at the 5' homology arm via Southern Blotting..... | 67 |
| Figure 24: Agarose gel showing results from 3' long-range PCR to confirm correct targeting of spastin ^{WT/KO-1st} in animals (HET) derived from ES cell clone 1C11. | 68 |
| Figure 25: Confirmation of correct targeting of the <i>Spg4</i> gene in PCR..... | 68 |
| Figure 26: Western Blotting of pEGFP-transfected, untransfected, and pEGFP-Spastin- Δ M1- transfected HEK-cell lysates using the mouse monoclonal 6C6 anti-spastin antibody or the rabbit anti-GFP antibody (SIGMA). | 69 |
| Figure 27: Reduced spastin protein levels in prenatal spastin KO mice as revealed by Western Blotting using the 6C6 anti-spastin antibody on whole brain lysates..... | 69 |
| Figure 28: Conditional targeting of spastin..... | 70 |
| Figure 29: Immunocytochemistry using the spastin 6C6 antibody..... | 71 |
| Figure 30: Litter sizes resulting from matings of prenatally depleted spastin KO mice..... | 72 |
| Figure 31: Genotype distribution of mouse lines with prenatally depleted spastin..... | 72 |
| Figure 32: Sterility of homozygous spastin knockout mice. | 73 |
| Figure 33: Gender and age-matched relative body weights of spastin WT, HET and KO animals..... | 73 |
| Figure 34: Altered gait parameters in adult spastin KO mice. | 74 |
| Figure 35: Assessment of endogenous spastin promoter activity in brains of heterozygous spastin reporter KO mice (spastin ^{GT/WT} /Cre ^{WT/TG}). | 75 |
| Figure 36: LacZ staining of cryosectioned heterozygous spastin reporter mouse (spastin ^{WT/GT}) tissues to evaluate the endogenous expression pattern of spastin at postnatal day 8 and in adult mice. | 76 |
| Figure 37: Western Blotting analysis of spastin expression in different brain regions in young, adolescent and adult mice..... | 76 |
| Figure 38: Localization of the anti-spastin 6C6 antibody signal in primary hippocampal neurons..... | 77 |
| Figure 39: Overexpression of EGFP-spastin in neurons..... | 77 |
| Figure 40: Spastin expression in different subcellular fractions. | 78 |
| Figure 41: Nissl stainings of brain sections derived from wild type and spastin KO mice..... | 79 |

Figure 42: Immunohistochemistry analysis using coronal brain sections obtained from adult spastin^{WT/WT} and spastin^{KO-1st/KO-1st} littermates to study polyglutamylation of tubulin in spastin KO mice..... 80

Figure 43: Western Blotting analysis using lysates obtained different brain regions from spastin^{WT/WT}/CamKII α -Cre^{WT/TG} and spastin^{FL/FL}/CamKII α -Cre^{TG/WT} littermates..... 80

Figure 44: Immunohistochemistry analysis using coronal brain sections obtained from adult spastin^{WT/WT} and spastin^{KO-1st/KO-1st} littermates to study the expression levels of GluR2 (green), synaptophysin (blue) and the polyglutamylation of tubulin (red) in the stratum radiatum region of the CA1 in spastin KO mice. 81

Figure 45: Live cell imaging of DIV 16 primary hippocampal neurons derived from spastin^{KO/KO} mice co-transfected with pmRFP and pEGFP-EB3 at DIV7 81

Figure 46: Immunoprecipitation using rat anti-EB3 antibodies on p2 fractions from mouse whole brain. 82

Figure 47: Targeting strategy for the murine katanin p60 gene to generate KO-first, floxed, classical frameshift, conditional-KO and reporter alleles. 83

Figure 48: Katna1 targeting confirmation both in ES cells and in F1 animals using long-range PCR. .84

Figure 49: Confirmation of correct targeting of the Katna1 gene in PCR using primers P93 and P94 in floxed animals (after breeding Katna1^{KO1-st/WT} animals to FLP-deleter mice)..... 84

Figure 50: Usage of polyclonal goat anti-katanin antibodies for Western Blotting. 85

Figure 51: Katanin expression analysis in whole brain lysates from 9-week-old katanin^{FL/FL} mice without or with the presence of the Nestin-Cre transgene. 86

Figure 52: Postnatal and forebrain-specific targeting of katanin..... 86

Figure 53: Litter sizes and genotype distribution for mouse lines with prenatally depleted Katna1 alleles..... 87

Figure 54: Body weight distribution in general and conditional katanin KO lines..... 88

Figure 55: β -galactosidase staining of heterozygous katanin reporter mice (katanin^{WT/GT}/Cre^{WT/TG}) to assess the endogenous katanin promoter activity in the brain..... 89

Figure 56: β -galactosidase staining of heterozygous katanin reporter mice (katanin^{WT/GT}/Cre^{WT/TG}) to assess the endogenous katanin promoter activity in organs..... 90

Figure 57: Ectopic expression of AcGFP-katanin. 91

Figure 58: Gross brain morphology of brain-specific katanin knockout mice..... 92

Figure 59: Behavior in the elevated plus maze. 93

Figure 60: Behavior analysis of adult katna^{FL/FL}/CamKII-Cre^{WT/WT} and katna^{FL/FL}/CamKII-Cre^{TG/WT} mice in the open field test. 95

Figure 61: Continuous spontaneous alternation behavior in the Y-maze. 96

Figure 62: Summarized behavior in the place recognition task in the Y-maze. 97

7.3 Tables

| | |
|--|-----|
| Table 1: Summarizing overview of the known regulators of the MT-severing enzymes katanin and spastin. | 23 |
| Table 2: Enzymes used in this thesis and their suppliers. | 34 |
| Table 3: Software used in this thesis. | 35 |
| Table 4: Primary antibodies used for Western Blotting (WB), immunohistochemistry (IHC), immunoprecipitations (IP) and immunocytochemistry (ICC) including host species, dilution and source company. | 36 |
| Table 5: Secondary antibodies used for Western Blotting (WB) and immunocytochemistry (ICC) experiments in this thesis including conjugation, host species, dilution and source company. | 36 |
| Table 6: Vectors and constructs used in this study. | 37 |
| Table 7: Bacterial strains used for this study. | 37 |
| Table 8: Oligonucleotides used for this thesis. | 42 |
| Table 9: sequence of bath solutions used for Nissl staining. | 45 |
| Table 10: Temperature cycling programme of a typical PCR. | 47 |
| Table 11: Standard reaction mixture for a PCR. | 47 |
| Table 12: Overview of all primer combinations for all genotyping PCR protocols used in this study. | 48 |
| Table 13: Antibiotic concentration used for LB-Agar-Plates. | 50 |
| Table 14: Reaction mixture for a long-range PCR. | 54 |
| Table 15: Primer combinations and amplicon sizes for the long-range PCRs used during the study. | 54 |
| Table 16: cycling conditions used for long-range PCR in this study. | 54 |
| Table 17: Overview of the cell fractionation by differential centrifugation. | 55 |
| Table 18: Typical composition of SDS polyacrylamide gels. | 57 |
| Table 19: Overview of the sequential breedings to generate mice containing KO-first (KO 1-st), floxed (FL), conditional KO, null (KO) and reporter alleles (GT) for the genes of interest (GOI, i. e. spastin or katanin) starting with chimeric mice in the F0 generation. | 63 |
| Table 20: sequence and duration of experiments conducted with conditional katanin knockout cohort 1 (11 WT and 8 KO females) and cohort 2 (9 WT and 8 KO females; 7 WT and 10 KO males), and the age of mice at the time of the experiment. | 92 |
| Table 21: List of suppliers. | 146 |

7.4 Suppliers

Table 21: List of suppliers.

| Company | Address | Material purchased |
|-------------------------|------------------------------|--|
| Abcam | Cambridge, UK | Antibodies |
| ABR | Golden, USA | Antibodies |
| Agilent | Santa Clara, USA | Cloning vectors |
| AppliChem | Darmstadt, Germany | Chemicals |
| Applied Biosystems | Darmstadt, Germany | Sequencer and EditView-Software |
| ATCC | Manassas | HEK293-TN cells |
| Baker Company | Sanford, USA | Cell culture sterile hood |
| B Braun Melsungen AG | Melsungen, Germany | Potter |
| Beckman Coulter | Krefeld, Germany | Centrifuges, rotors |
| Biometra | Göttingen, Germany | PCR cyclers |
| Bioline | Luckenwalde, Germany | DNA molecular weight marker |
| Biorad | München, Germany | Protein molecular weight standards, power supplies, chambers for SDS-PAGE and western blotting |
| BD Biosciences | San José, USA | Antibodies, Falcon tubes |
| Biozym Scientific GmbH | Hessisch Oldendorf, Germany | DNA extraction solution, Histo-Clear |
| Carl Roth GmbH & Co. KG | Karlsruhe, Germany | Chemicals |
| Clontech | Heidelberg, Germany | Vectors |
| Dianova | Hamburg, Germany | Antibodies |
| Dynal | Oslo, Norway | Beads for immunoprecipitation |
| Edmund Bühler GmbH | Hechingen, Germany | Platform shaker |
| Epicentre | Madison, USA | QuickExtract solution |
| epitomics | Burlingame, USA | Antibodies |
| Eppendorf | Hamburg, Germany | Centrifuges, thermomixer, pipettes and plasticware |
| Fermentas | St. Leon-Rot | Restriction enzymes, alkaline phosphatase |
| Fröber Labortechnik | Lindau, Germany | Overhead shaker |
| FujiFilm | Staubenhardt, Germany | Fluorescent image analyser, phosphoimager setup |
| GFL | Burgwedel, Germany | Water bath |
| Gilson | Limburg-Offheim, Germany | Pipettes |
| GraphPad | La Jolla, USA | Statistical software |
| Greiner Bio-one | Frickenhäuser, Germany | Plasticware |
| Heidolph Instruments | Kelheim, Germany | Platform shaker, vortex |
| IDL GmbH & Co. KG | Nidderau, Germany | Rolling incubator |
| Intas | Göttingen, Germany | Chemiluminescence imager, UV-light transilluminator, Western Blot chemiluminescence reader |
| Invitrogen | Carlsbad, USA | Bacterial strains, cell culture media, trypsin |
| KOMP | USA | Targeting vectors, embryonic stem cells |
| Leica Microsystems | Heidelberg, Wetzlar, Germany | Confocal microscope and proprietary imaging software, cryostat, vibratome |
| Liebherr | Ochsenhausen, Germany | Freezer, refrigerator |
| LifeTechnologies | Darmstadt, Germany | Enzymes, cell culture media |

APPENDIX

| | | |
|--------------------------|---------------------------------|---|
| Lonza | Verviers, Belgium | Cell culture media |
| Macherey-Nagel | Düren, Germany | DNA and RNA purification kits |
| Merck | Darmstadt, Germany | Chemicals |
| Mettler-Toledo | Giessen, Germany | Laboratory scales, pH meter |
| Millipore Corporation | Schwalbach am Taunus, Germany | Antibodies, water purification system, filter tips, Immobilon Western HRP substrate |
| MJ Research | Waltham, USA | PCR machines |
| MWG Biotech | Ebersberg, Germany | Desoxyoligonucleotides |
| New Brunswick Scientific | Nürtingen, Germany | Bacterial culture incubator |
| Noldus | Wageningen, The Netherlands | automated mouse behavior analysis |
| Novus Biologicals | Littleton, USA | Antibodies |
| Olympus | Heidelberg and Hamburg, Germany | Confocal microscope and imaging software |
| Polysciences | Warrington, USA | Aqua-polymount |
| Promega | Mannheim, Germany | Cloning vectors |
| Qiagen | Hilden, Germany | Maxiprep kit |
| Roche | Mannheim, Germany | Enzymes and chemicals |
| Santa Cruz Biotechnology | Dallas, USA | Antibodies |
| Sanyo | Osaka, Japan | Ultra low temperature freezer |
| Sarstedt | Nümbrecht | Plasticware, centrifuges |
| Sartorius | Göttingen, Germany | Homogenizer and laboratory scales |
| SCIE-PLAS | Cambridge, UK | Semi-dry blotter |
| SIGMA | Taufkirchen, Germany | Antibodies, chemicals, sera, Whatman filter Paper |
| SLT Labinstruments | Markham, Canada | SLT rainbow scanner |
| Stratagene | La Jolla, USA | DNA polymerases, bacterial strains |
| Synaptic Systems | Göttingen, Germany | Antibodies |
| Tecan | Männedorf, Switzerland | Microtiter plate reader and spectrophotometer |
| Tröndle | Moorenweis, Germany | MegaViewIII digital camera |
| Thermo Fisher Scientific | Asheville, USA | Agarose gel electrophoresis system, cell culture incubators, microscope slides, plasticware, high fidelity polymerase, ECL kit, antibodies, T4 DNA ligation kit |
| Universal Imaging | Downingtown, USA | Metamorph software |
| Visitron Systems | Puchheim, Germany | Spinning disk microscope, imaging software MeaVue |
| VWR | Darmstadt, Germany | Chemicals |
| Zeiss | Jena, Germany | Epifluorescent microscope, transmission microscope, imaging software, electron microscope |

7.5 Sequences

7.5.1 Katna1 p60 amino acid sequence

Sequence 1: Amino acid sequence for the catalytic p60 subunit of katanin. The upper sequence represents the mouse and the lower sequence represents the human p60 katanin respectively. Bold letters represent the AAA ATPase domain; strikethrough amino acids represent the targeted amino acids for the murine katanin corresponding to exons 6 and 7. Amino acid differences between the human and mouse orthologues are highlighted.

| | | | | |
|--------------------------------------|-------------------------------------|-------------------------|--------------------------------------|---|
| 10 | 20 | 30 | 40 | 50 |
| MSLQMI V ENV | KLAREYALLG | NYDSAMVYYQ | GVLDQMNKYL | YSVKDTHLRQ |
| MSLLMI S ENV | KLAREYALLG | NYDSAMVYYQ | GVLDQMNKYL | YSVKD T YL Q Q |
| 60 | 70 | 80 | 90 | 100 |
| KWQQVWQ E IN | VEAKQVKDIM | KTLESFKLDI | TSLQAAQHEL | PAAEGEVWSL |
| KWQQVWQ E IN | VEAK H VKDIM | KTLESFKLDS | T PLKAAQ H DL | PA S E E GEVWSM |
| 110 | 120 | 130 | 140 | 150 |
| PVPVERRPLP | GPRKRQSSQH | SDPKPHSNRP | STVVR A HRPS | PQNLHND R RGK |
| PVPVERR P SP | GPRKRQSSQ Y | SDPKSHGNRP | STTVR V HR S S | A QNV H ND R RGK |
| 160 | 170 | 180 | 190 | 200 |
| AVRSREKKEQ | SKGREEKNKL | PAAVTEPEAN | KFD G TGYDKD | LVEALERDII |
| AVR C REKKEQ | N KGREEKN K S | PAAVTEPETN | KFD S TGYDKD | LVEALERDII |
| 210 | 220 | 230 | 240 | 250 |
| SQNP NVRW Y D | IADL VEAKKL | LQEA VVLPMW | MPEFF KGIRR | PWKG VLMVGP |
| SQNP N VRW D D | IADLVEAKKL | L K EAVVLPMW | MPEFFKGIRR | PWKGVLMVGP |
| 260 | 270 | 280 | 290 | 300 |
| PGT GKTLLAK | AVATE CKTTF | FNVSS STLTS | KYRGE SEKLV | RLL FEMARFY |
| PGTGKTLLAK | AVATECKTTF | FNVSSSTLTS | KYRGESEKLV | RLLFEMARFY |
| 310 | 320 | 330 | 340 | 350 |
| SPATIFIDEI | DSICSRRGTS | EEHEASRMK | AELLVQMDGV | GGASENDDPS |
| SPATIFIDEI | DSICSRRGTS | EEHEASRR V K | AELLVQMDGV | GG T SENDDPS |
| 360 | 370 | 380 | 390 | 400 |
| KMVMVLAATN | FPWDIDEALR | RRLEKRIYIP | LPSAKGREEL | LRISLRELEL |
| KMVMVLAATN | FPWDIDEALR | RRLEKRIYIP | LPSAKGREEL | LRISLRELEL |
| 410 | 420 | 430 | 440 | 450 |
| ADDVNLASIA | ENMEGYSGAD | ITNVCRDASL | MAMRRRIEGL | TPEEIRNLSR |
| ADDV N LASIA | ENMEGYSGAD | ITNVCRDASL | MAMRRRIEGL | TPEEIRNLS K |
| 460 | 470 | 480 | 490 | |
| EAMHMPTTME | DFEMALKKIS | KSVSAADIER | YEKWIVEFGS | C |
| EEMHMPTTME | DFEMALKK V S | KSVSAADIER | YEKWIV E FGS | C |

7.5.2 Spastin amino acid sequence

Sequence 2: Amino acid sequence for the full-length spastin protein. The upper sequence represents the mouse and the lower sequence represents the human spastin respectively. Strikethrough amino acids represent the targeted amino acids for the murine spastin corresponding to exon 5. Amino acid differences between the human and mouse orthologues are highlighted. Boxed: tm sequence. Phosphothreonine and phosphoserine sites are highlighted in grey. Aa 4-11: NLS. The NES is highlighted in yellow. The ATP binding site is highlighted in green. Exon 4 is highlighted by grey letters

```

      10          20          30          40          50
MSSPAGRRKK KGSGGASPAP ARPPPPAAVP APAAGPAPAA GSPPKRNPSS
MNSPGGRGKK KGSGGASNPV PPRPPPCLA PAPPAGPAP PPESPHKRNLYY
      60          70          80          90          100
FSSPLVVGFA LLRL LACHLG LLFAWLCQRF SRALMAAKRS SGTAPAPASP
FSYPLLFVGFA LLRLVAFHLG LLFVWLCQRF SRALMAAKRS SGAPAPASA
      110         120         130         140         150
SPPEPGPGGE AESVRVFHKQ AFEYISIALR IDEEEKAGQK EQAVEWYKKG
SAPAPVPGGE AERVRVFHKQ AFEYISIALR IDEDEKAGQK EQAVEWYKKG
      160         170         180         190         200
IEELEKGIIV IVTGQGEQYE RARRLOAKMM TNLVMAKDRL QLEKLOPVL
IEELEKGIIV IVTGQGEQCE RARRLOAKMM TNLVMAKDRL QLEKLOPVL
      210         220         230         240         250
QFSKSQTDVY NESTNLTCRN GHLQSESGAV PKRKDPLTHA SNSLPRSKTV
PFSKSQTDVY NESTNLTCRN GHLQSESGAV PKRKDPLTHA SNSLPRSKTV
      260         270         280         290         300
LKSGSAGLSG HHRAPSCSGL SMVSGARPGP GPAATTHKGT PKPNRTNKPS
MKTGSAGLSG HHRAPSYSGL SMVSGVKQGS GPAPTTHKGT PKTNRTNKPS
      310         320         330         340         350
TPTTAVRKKK DLKNFRNVDS NLANLIMNEI VDNGTAVKFD DIAGQELAKQ
TPTTATRRKKK DLKNFRNVDS NLANLIMNEI VDNGTAVKFD DIAGQDLAKQ
      360         370         380         390         400
ALQEIVILPS LRPELFTGLR APARGLLLF G PPGNGKTMLA KAVAAESNAT
ALQEIVILPS LRPELFTGLR APARGLLLF G PPGNGKTMLA KAVAAESNAT
      410         420         430         440         450
FFNISAASLT SKYVGEGEKL VRALFAVARE LQPSIIFIDE VDSLLCERRE
FFNISAASLT SKYVGEGEKL VRALFAVARE LQPSIIFIDE VDSLLCERRE
      460         470         480         490         500
GEHDASRRLK TEFLIEFDGV QSAGDDRVLV MGATNRPQEL DEAVLRRFIK
GEHDASRRLK TEFLIEFDGV QSAGDDRVLV MGATNRPQEL DEAVLRRFIK
      510         520         530         540         550
RVYVSLPNEE TRLLLLKNLL CKQGSPLTQK ELAQLARMTD GYSGSDLTAL
RVYVSLPNEE TRLLLLKNLL CKQGSPLTQK ELAQLARMTD GYSGSDLTAL
      560         570         580         590         600
AKDAALGPIR ELKPEQVKNM SASEMRNIRL SDFTESLKKI KRSVSPQTL
AKDAALGPIR ELKPEQVKNM SASEMRNIRL SDFTESLKKI KRSVSPQTL
      610
AYIRWNKDFG DTTV
AYIRWNKDFG DTTV

```

7.5.3 Sequence of the 5' southern probe for spastin.

Sequence 3: Desoxynucleotide sequence of the probe for southern blotting in order to confirm the correct targeting of spastin at the 5' homology region.

```
5'AGCTTTACATTCCAAGAAGATACATTTTAATAGTGTCATTACTATGAAGTAAATCTGCATTGT
AACTTTTGCTTACTACTCTGATTAAATACATAAGAAAAGAAAGAATTCAAAGCCTTGGCTTTGT
TCTGGTGAAGAACTTCATATTTTAGGCTTCCTGTGTCTCAGTTGGTTTTTGTGGGTTTG
GTATGAGTTTTGCCCAAGCCTTTAGACTACAAGGTAGTTTGCTTGGTTGCTGGTTTTGTTTTG
TTACTTTTTCAACAGTAGTTTCATGTCCAGGGCTATTGGTTGAGGTTTTCTGAGACAGTGTTT
TCACCTCTAGCTGGAAGTTACTCAGCAGCTAAGGCTCAAGTGATTCTCCTATCTGACTCCTG
AACAACTCATCACCCCACTTTACCCAGGTTTGTACTTAAATTTTATTATAGTAAATATAACTT
CAAATTGTAGGGAATAAACTTTAGATTAGACTATGAAGTAGCTGCTGGTTTTTATTCATTTATA
GGAAGCAAATTTGAAAGTTTACTTCTTAATTTTATTTAGTTTTTTGAGTACTAGGGAAGTCAAC
CAATGCCTGAAACATGCTACTCAAGACTCTGACACTGTGATAGATCCCTGGGCCAAAGATGA
AGGAAGGATCTAT3'
```

7.6 Acknowledgements

This thesis has been an important period of my life. That's why I would like to say thank you to all the people who supported me during this time in all possible ways.

First of all I would like to acknowledge Professor Dr. Matthias Kneussel for giving me the opportunity and trust to work on this challenging project and his constant support. Also, I would like to thank him for his patience in supervising and correcting this work.

Secondly, I would also like to thank Professor Dr. Christian Lohr for the co-supervision of this project and for the collaboration in the electrophysiological characterization of the spastin KO-mice with the support of his master student Janet.

I would like to thank Professor Dr. Hans Jürgen Kreienkamp for co-supervising my project at the graduate research group GRK1459 and for his honest and helpful comments. Generally, I enjoyed very much the friendly atmosphere and especially the scientific programme of the GRK including seminars, speakers, symposia, retreats and practical courses.

I would like to mention PD Dr. Irm Hermanns-Borgmeyer and Sarah Homann, PD Dr. Sabine Hoffmeister Ulrich, Dr. Michaela Schweizer and Dr. Susanne Fehr from the service facilities and to thank them for their expertise, friendly help and support. Especially to Irm, for expert help and advice at the initial phases of gene targeting, help with ES cell culture, blastocyst injections and Southern Blotting and later on, for help to identify the origin of germline defects of the spastin KO mouse line. The animal-care-takers Silvana Deutsch, Maria Kuschel and Ulrike Wolters: thank you very much for taking care well of the animals.

My special thanks go to the current and past Kneussel lab members for the friendly and familiar working atmosphere. Especially Dr. Mary Wanjiku Muhia for sharing your passion for the possibilities of animal behavior, Dr. Kira Brune for great ideas at the microscope and Edda Thies for her expertise in almost all possible fields. Of course, I will never forget my roomie Party-Petra and her constant spreading of good mood!

I would like to thank my friends for distracting me from the laboratory life and the salsa-guys for making mi vida un carnaval, the guys from the third floor for the funny after-work sushi and burger sessions and for the small coffee and ice cream distractions during the weekends in the lab!

Last but not least I thank my family for their trust, love and for making so much possible. Ole, Emma and Maja, thank you for being there for me all the time!

7.7 Curriculum Vitae

entfällt aus datenschutzrechtlichen Gründen

7.8 Publications

Brill, M. S., et al. (2016). "Branch-Specific Microtubule Destabilization Mediates Axon Branch Loss during Neuromuscular Synapse Elimination." Neuron 92(4): 845-856.

Heisler, F. F., et al. (2014). "GRIP1 interlinks N-cadherin and AMPA receptors at vesicles to promote combined cargo transport into dendrites." Proc Natl Acad Sci U S A 111(13): 5030-5035.

7.9 Statement of contribution

Animal breeding and caring was provided by Silvana Deutsch. Dr. Irm Hermans-Borgmeyer and Sarah Homann performed cultivation and injection of embryonic stem cells. Yvonne Pechmann kindly provided mouse cDNA libraries and competent bacteria used for molecular cloning. Perfusions were carried out under the supervision of Dr. Michaela Schweizer. The LacZ stainings related to endogenous spastin and katanin expression were carried out with Dr. Susanne Fehr. EM analyses were done by Dr. Michaela Schweizer. Dr. Sabine Hoffmeister-Ullerich performed the Rd8 mutation screen and sequencing of DNA.

7.10 Erklärung

Hiermit versichere ich eidesstattlich, dass ich die vorliegende Arbeit selbstständig und ohne fremde Hilfe verfasst habe. Ich habe keine anderen als die angegebenen Hilfsmittel und Quellen benutzt und habe die entnommenen Stellen als solche kenntlich gemacht.

Diese Arbeit ist zuvor keiner Prüfungsbehörde, weder in dieser noch in abgewandelter Form, zum Erwerb des Doktorgrades vorgelegt worden. Auch mit keiner anderen Arbeit habe ich mich zuvor um den Erwerb des Doktorgrades bemüht.

Hamburg, 2018